The roles of HSP20 in cardiac hypertrophy

A thesis submitted in fulfillment of the requirements for the Degree of

Doctor of Philosophy

in

Molecular Functions in Disease

College of Medicine, Veterinary and Life Sciences, University of Glasgow,
United Kingdom

Yuan Yan (Angie) Sin

2012

THIS THESIS IS DEDICATED TO MY MOST LOVING PARENTS,

HUSBAND AND ONE VERY SPECIAL LITTLE GIRL,

MY DAUGHTER, EILIDH HONG.

TABLE OF CONTENTS

Abstract ……...….i

Author's declaration ……..iii

Acknowledgements ……iv

List of figures ……...…v

List of tables ……vii

Abbreviations ……...……viii

Publications/Conferences ……..ix

Chapter 1: Introduction

1.1. Heat shock protein 1

1.1.1. Background 1

1.1.2. Functions 2

1.1.3. Synthesis of heat shock protein 3

1.1.4. Families of heat shock protein 3

1.1.5. Structure of heat shock protein 4

1.2. Heat shock protein 20 5

1.2.1. HSP20 phosphorylation 6

1.3. HSP20 in cardiovascular system 8

1.3.1. Ischaemia/reperfusion injury 8

1.3.2. Apoptosis 10

1.3.3. Hypertrophy 13

1.4. HSP20 in other diseases 15

1.5. Cardiac cell-based model 16

1.6. Aims of research 17

Chapter 2: Materials and methods

2.1 Materials 18

2.2 Expression and purification of recombinant proteins 18

2.2.1 Histidine (His) fusion protein 18

2.2.2 Glutathione-S-Transferase (GST) fusion proteins 19

2.3 Plasmid DNA 19

2.3.1 Transformation of competent cells 19

2.3.2 Isolation of plasmids DNAs 20

2.3.3 Storage of plasmid DNA 20

2.3.4 Analysis of plasmid DNA 21

2.3.5 Quantification of DNA concentration 21

2.4 Mammalian cell culture 21

2.4.1 Primary culture of cardiomyocytes 22

2.4.2 HEK293 cells 23

2.4.3 Transfection of plasmid DNA 23

2.4.4 siRNA-mediated gene knockdown in cardiomyocytes 24

2.5 Preparation of cell lysates 24

2.5.1 Whole cell lysate 24

2.5.2 Subcellular fractionation of cardiomyocytes 25

2.6 Protein analysis 26

2.6.1 SDS-PAGE 26

2.6.2 Coomassie staining 26

2.6.3 Western immunoblotting 26

2.7 Protein-protein interactions 29

2.7.1 ProtoArray 29

2.7.2 *In vitro* pull-down assay 31

2.7.3 Co-immunoprecipitation 31

2.7.4 SPOT synthesis of peptides and overlay experiments 32

2.8 *In vitro* phosphorylation assays 34

2.8.1 *In vitro* kinase assay 34

2.8.2 *In vitro* phosphorylation of peptide array 34

2.9 Cell-based experiments 34
2.9.1 Manual measurements of cell size 34
2.9.2 Real-time xCELLigence measurements 35
2.9.3 Measurement of protein content 36
2.9.4 Disruptor peptide synthesis 36

2.10 Quantitative real-time PCR analysis of fetal gene expression 37
2.10.1 RNA extraction 37
2.10.2 Reverse transcription of PCR 37
2.10.3 TaqMan real-time PCR 38
2.10.4 qPCR data analysis 39

2.11 Microscopic analyses 40
2.11.1 Differential interference contrast microscopy (DIC) 40
2.11.2 Immunostaining and confocal microscopy 41
2.11.3 Phalloidin staining of actin 41
2.11.4 Duolink™ proximity ligation assay (PLA) 42

2.12 Statistical analysis 42

Chapter 3: Disruption of cAMP PDE4D5-HSP20 complex attenuates *β*-agonist induced hypertrophic response in cardiomyocytes

3.1 Introduction 44
3.1.1 cAMP signalling and compartmentalisation 44
3.1.2 PDE family 47
3.1.3 PDE4 structure and isoforms 48
3.1.4 cAMP-signalling modulation in the heart 50

3.2 Aims 54

3.3 Results 55
3.3.1 Characterisation of neonatal rat cardiomyocytes 55
3.3.2 Regulation of PKA-mediated HSP20 phosphorylation by PDE4 57
3.3.3 HSP20 interacts directly with PDE4 isoforms 60
3.3.4 Mapping interaction sites between HSP20 and PDE4D5 64
3.3.5 Peptide disruption of PDE4D5-HSP20 complex 67
3.3.6 The effect of PDE4D5-HSP20 interaction on HSP20 phosphorylation 67

3.3.7 The role of PDE4D5-HSP20 complex in hypertrophy 70
3.3.7.1 Measurement of cell size 70
3.3.7.2 Measurement of protein content 71
3.3.7.3 Expression of ANF mRNA and protein expression 74

3.4 Discussion.....76
3.4.1 Background 76
3.4.2 PDE4 modulates PKA-mediated HSP20 phosphorylation upon ISO stimulation.....76
3.4.3 PDE4 isoforms associate directly with HSP20 77
3.4.4 HSP20 binds to the conserved catalytic region of PDE4.....78
3.4.5 Disruption of PDE4D5-HSP20 complex protects against hypertrophy.....79
3.4.6 Conclusions.....80
3.4.7 Small molecules therapies for heart disease.....81

Chapter 4: ProtoArray analysis identifies protein kinase D1 (PKD1) as an interactor of HSP20

4.1 Introduction.....82
4.1.1 The study of protein-protein interaction 82
4.1.2 Background and project aim 82

4.2 Results 83
4.2.1 ProtoArray identified 21 HSP20 interactors 83
4.2.2 Validation of the interaction between HSP20 and PKD1 89
4.2.3 Mapping binding region of HSP20 on PKD1 92
4.2.4 Protein structure prediction of PKD1 catalytic domain 94

4.3 Discussion.....98

Chapter 5: The role of the PKD1-HSP20 complex in hypertrophy signalling

5.1 Introduction.....103
5.1.1 Background and structure of PKD 103
5.1.2 PKD1 phosphorylation.....105
5.1.3 PKD1 substrates in heart.....105
5.1.4 Subcellular distribution of PKD1.....106

5.1.5. The roles of PKD1 in hypertrophy.....107
5.1.6. Aims of Chapter 5 110

5.2 Results 111
5.2.1 Disruption of PKD1-HSP20 interaction.....111
5.2.2 Peptide disruption of PKD1-HSP20 complex protects against hypertrophy in cardiomyocytes 113
5.2.2.1 Measurement of cell size.....113
5.2.2.2 Effect on cell morphology and actin cytoskeleton dynamics 114
5.2.2.3 Measurement of protein content 118
5.2.2.4 Quantification of fetal gene expression 119
5.2.3 Mapping binding region of PKD1 on HSP20 121
5.2.4 Identification of PKD1 phosphorylation site on HSP20 123
5.2.5 The effect of PKD1 activation on HSP20 phosphorylation 126
5.2.6 The effect of PKD1-HSP20 interaction on HSP20 phosphorylation 128
5.2.7 Use of a novel PLA to assess PKD1 association with HSP20.....130
5.2.8 Cell fractionation shows PKD1 and HSP20 localisation.....131
5.2.9 HSP20 phosphorylation: PKA vs PKD1.....134

5.3 Discussion.....136
5.3.1 PKD1-HSP20 interaction in hypertrophic response 136
5.3.2 PKD1 regulates HSP20 phosphorylation 137
5.3.3 HSP20 is the ‘molecular escort’ of PKD1 139
5.3.4 Conclusions.....142

5.4 Further work 143

Chapter 6: Final discussion

6.1 Background.....150
6.2 The association of PDE4D and HSP20.....150
6.3 The association of PKD1 and HSP20 151
6.4 Antagonistic actions of PKA and PKD1 on HSP20.....152
6.5 Conclusions.....154
6.6. Future directions.....155
6.7. Limitations of this work 156

REFERENCES.....157

ABSTRACT

Cardiac hypertrophy often develops to compensate for hemodynamic overload and is associated with heart failure. Recent studies have revealed that overexpression and PKA-mediated phosphorylation of heat shock protein 20 (HSP20) at Ser16 can attenuate hypertrophic growth of cardiomyocytes and trigger cardioprotective functions following sustained β-adrenergic stimulation (Fan *et al*., 2004, 2005, 2006). However, the molecular mechanism of HSP20 induced cardioprotection remains to be fully elucidated. In order to gain insight into the protective mode of action of HSP20, I attempted to (1) investigate the spatiotemporal control of PKA-mediated phosphorylation of HSP20, as well as (2) identifying novel protein binding partners for HSP20 utilising cutting edge ProtoArray technology.

Initially, I set up an *in vitro* hypertrophy model using sustained isoprenaline (ISO)-stimulated neonatal rat cardiomyocytes. Cell size, protein synthesis and fetal gene expression were assessed as parameters of hypertrophic growth. In the first section of my studies, members of the cAMP-specific PDE4 family were shown to form signalling complexes with HSP20, and that the PKA-mediated phosphorylation of HSP20 could be modulated by PDE4. Based on peptide array data, a cell-permeable peptide 'bs906' was developed to inhibit the interaction of PDE4 with HSP20. Interestingly, the disruption of the PDE4-HSP20 complex was shown to induce PKA-mediated phosphorylation of HSP20 and trigger cardioprotection against the hypertrophic response measured in neonatal cardiomyocytes upon chronic β-adrenergic stimulation.

In the second part of my studies, protein kinase D1 (PKD1) was identified as one interacting partner that robustly associated with HSP20. This interaction was confirmed by biochemical and immunocytochemical means. Using similar approaches to those used for the PDE4-HSP20 interaction, a cell-permeable peptide 'HJL09' was generated to promote disruption of the PKD1-HSP20 complex. Experimentation using the peptide concluded that the disruption of the PKD1-HSP20 complex reduced HSP20 phosphorylation and attenuated the hypertrophic response in cultured cardiomyocytes as shown by reduced increases in cell size, protein content and actin reorganisation. In undertaking this work, I also defined a novel PKD phosphorylation site (Ser16) on HSP20 that conforms to the

PKD phosphorylation motif of RxxS (also a PKA site). My biochemical data suggested that PKD1 may regulate the cardioprotective function of HSP20 via phosphorylation at Ser16. *In situ* proximity ligation assay (PLA) further revealed a role of HSP20 as 'molecular escort' in targeting the nuclear translocation of PKD1. This function, in part, may be responsible for the induction of fetal gene reexpression as selective disruption of PKD1-HSP20 complex using 'HJL09' hindered the nuclear influx of the complex, thereby attenuating hypertrophic signalling.

In summary, these studies describe some exciting findings which provide further insight into novel signalling mechanism of cardiac hypertrophy in neonatal rat cardiomyocytes. I have shown that PKA and PKD1 exhibiting opposite functions despite sharing the phosphorylation site on HSP20. In this regard, HSP20 functions as a molecular nexus for the opposing actions of the PKA and PKD1 signalling pathways in hypertrophy, suggesting that crosstalk may occur between anti-hypertrophic and pro-hypertrophic pathways. The identification and characterisation of these complexes should help to build a better understanding of the hypertrophic signalling pathway, and may provide novel therapeutic strategies for the treatment of cardiac hypertrophy.

Keywords: HSP20, hypertrophy, phosphodiesterase, cAMP-dependent PKA, PKD1, phosphorylation

DECLARATION

I hereby declare that the work presented in this thesis has been carried out by me unless otherwise cited or acknowledged. The work is entirely of my own composition and has not been submitted, in whole or in part, for any other degree at the University of Glasgow or any other institution.

Yuan Yan (Angie) Sin

April 2012

ACKNOWLEDGEMENTS

First of all, I would like to express my sincere gratitude and appreciation to my supervisor, Dr George Baillie, for all his guidance, continued support and enthusiasm during the entire project. I am happy that George offered me a placement in his lab during my first year and am truly glad to choose his lab for my PhD project. This work has been a pleasant experience filled with excitements of discoveries.

I would also like to thank Prof Miles Houslay and Prof Manuela Zaccolo for giving me their valuable insights and constructive advices to improve my work. Also, thanks to all the present and former members of the Gardiner laboratory for offering their technical expertise and generous assistance, in particular, Dr Elaine Huston, Dr Shelley Li, Dr Hannah Murdoch, Dr Frank Christian and Dr Allan Dunlop. Also, many thanks to Dave, Louisa, Krishna, Jon and Diana for their timely encouragements and jokes to cheer me up.

Moreover, I would like to thank Dr Ekaterina McKenna and Dr Kit-Yee Tan who helped me with ProtoArray, Dr Andreas Koschinski and John McAbney for their assistances in using DIC and Nikon Eclipse microscope, respectively.

I am truly privileged and grateful to the Wellcome Trust four-year PhD studentship and ORSAS for funding my PhD. Special thanks and appreciation goes to the program coordinators, Bill, Darren and Olwyn, for their kind advices and tremendous support throughout my PhD years.

Most of all, I want to thank my family for their continual support and unwavering faith in me over the years. To my most supportive and loving husband, MY, thank you so much for all your words of encouragement, great patience and understanding. To my wonderful daughter, Eilidh, thank you for giving me the strength and motivation to strive further. You never fail to put a smile in my heart. I am so blessed to have you in my life. ♥

LIST OF FIGURES

Figure 1.1	HSP20 and its cardioprotective roles.	12
Figure 2.1	Schematic diagram showing experimental procedure used for HSP20 interactors identification on ProtoArray.	30
Figure 2.2	Schematic diagram showing SPOT synthesis of peptide.	33
Figure 2.3	Schematic diagram of *in situ* PLA.	43
Figure 3.1	The cAMP signalling cascade.	46
Figure 3.2	Structure and encoding of PDE4 isoforms.	49
Figure 3.3	Schematic diagram showing multidimensional outline of βARs signalling.	53
Figure 3.4	Primary culture of neonatal rat cardiomyocytes.	56
Figure 3.5	PDE4 involved in the modulation of HSP20 phosphorylation at Ser16 in cardiomyocytes.	58
Figure 3.6	The phosphorylation of HSP20 at Ser16 is modulated by PKA.	59
Figure 3.7	HSP20 forms a complex with PDE4D isoforms.	61
Figure 3.8.	HSP20 interacts directly with PDE4 isoforms.	62
Figure 3.9.	HSP20 colocalises with PDE4D.	63
Figure 3.10	Mapping the site of HSP20 interaction on PDE4D5.	65
Figure 3.11	Mapping the site of PDE4D5 interaction on HSP20.	66
Figure 3.12	Disruption of PDE4D5-HSP20 interaction.	68
Figure 3.13	Disruption of PDE4D5-HSP20 interaction promotes PKA phosphorylation on Ser16.	69
Figure 3.14	Disruption of PDE4D5-HSP20 complex inhibits cardiomyocyte enlargement.	72
Figure 3.15	Disruption of PDE4D5-HSP20 complex inhibits protein synthesis.	73
Figure 3.16	Disruption of PDE4D5-HSP20 complex enhanced transcriptional activation of hypertrophy response gene.	74-75

Figure 4.1	Native purification of His-tagged HSP20.	84
Figure 4.2	The His-tagged HSP20-specific probe utilised for ProtoArray analysis.	85
Figure 4.3	Identification of PKD1 on ProtoArray.	88
Figure 4.4	Immunoblots showing *in vitro* and *in vivo* association of HSP20 and PKD1.	90
Figure 4.5	PKD1 colocalises with HSP20.	91
Figure 4.6	Identification of HSP20-PKD1 interaction sites.	93
Figure 4.7	Amino acid alignment of PKD1 catalytic domain with template 2c30 protein on Phyre2 web server.	95
Figure 4.8	Predicted structure of PKD1 catalytic domain and location of residues implicated in HSP20 binding.	96-97
Figure 5.1	Functional domains and conserved phosphorylation sites of PKD1.	104
Figure 5.2	Schematic diagram depicting the hypertrophic signalling cascades.	109
Figure 5.3	Disruption of PKD1-HSP20 interaction.	112
Figure 5.4	The effect of PKD1-HSP20 interaction on cell size.	115
Figure 5.5	The effect of PKD1-HSP20 interaction on cell morphology.	116
Figure 5.6	The effect of PKD1-HSP20 interaction on actin organisation.	117
Figure 5.7	The effect of PKD1-HSP20 interaction on protein synthesis.	118
Figure 5.8	The effect of PKD1-HSP20 interaction on fetal gene expression.	120
Figure 5.9	Identification of PKD1-HSP20 interaction sites.	122
Figure 5.10	Predicted phosphorylation site of HSP20 by PKD1.	124
Figure 5.11	PKD1 phosphorylates HSP20 at Ser16.	124
Figure 5.12	Ser16 is the site phosphorylated on HSP20 by PKD1.	125
Figure 5.13	The effect of PKD1 activity on HSP20 phosphorylation.	126
Figure 5.14	siRNA-mediated knockdown of PKD1 blunt phosphorylation of HSP20.	127

Figure 5.15	The effect of PKD-disruptor peptide 'HJL09' on HSP20 phosphorylation.	128
Figure 5.16	The effect of PKD-disruptor peptide 'HJL09' on HSP20 phosphorylation in ISO-induced hypertrophic cardiomyocytes.	129
Figure 5.17	The effect of PKD-disruptor peptide 'HJL09' on subcellular distribution of PKD1-HSP20 complex.	132
Figure 5.18	Cell fractionation experiments showing PKD1 and HSP20 localisations.	133
Figure 5.19	PKA and PKD1 modulate HSP20 phosphorylation under prolonged β-adrenergic stimulation.	135
Figure 5.20	Proposed models for the role of HSP20 in PKD1 nuclear translocation.	141
Figure 5.21	Simultaneous detection of PKD1 and PDE4D5 interactions on HSP20.	147
Figure 5.22	Predicted structure of HSP20 and location of binding sites with PKD1 and PDE4D5.	148
Figure 5.23	Optimisation of peptide length and substitutional analysis.	149

LIST OF TABLES

Table 2.1	List of primary antibodies used.	28
Table 2.2	Synthesised peptides used in this study.	36
Table 2.3	Sequences of oligonucleotide primer-probe sets used in quantitative real-time PCR assay.	39
Table 4.1	The list of HSP20 interactors identified by ProtoArray.	86-87
Table 4.2	Sequence alignment of G^{606}-E^{630} of PKD1.	102
Table 4.3	Amino acid homology showing comparison of G^{606}-E^{630} between species.	102

ABBREVIATIONS

AKAP	A-kinase-anchoring protein
***β*AR**	*β*-adrenergic receptor
cAMP	3’,5’-cyclic adenosine monophosphate
DMSO	dimethly sulfoxide
GPCR	G-protein-coupled receptor
HDAC5	histone deacetylase 5
HEK	human embryonic kidney
HSP20	heat shock protein 20
ISO	isoprenaline
MEF2	myocyte enhance factor 2
PDE	phosphodiesterase
PKA	protein kinase A
PKC	protein kinase C
PKD1	protein kinase D1
PKG	protein kinase G
PLA	Proximity ligation assay
siRNA	small interfering RNA
WT	wild-type

PUBLICATIONS

Sin, Y.Y. and Baillie, G.S. (2012) Protein Kinase D in the hypertrophy pathway. *Biochem Soc Trans*. **40**: 287-289.

Sin, Y.Y., Edwards, H.V., Li, X., Day, J.P., Christian, F., Dunlop, A.J., Adams, D.R., Zaccolo, M., Houslay, M.D., Baillie, G.S. (2011) Disruption of the cyclic AMP phosphodiesterase-4 (PDE4)–HSP20 complex attenuates the *β*-agonist induced hypertrophic response in cardiac myocytes. *J Mol Cell Cardiol.* **50**: 872-883.

Sin, Y.Y., Anthony, D.F., Vadrevu, S., Advant, N., Day, J.P., Byrne, A.M., Lynch, M.J., Milligan, G., Houslay, M.D., Baillie, G.S. (2011) β-Arrestin 1 inhibits the GTPase-activating protein function of ARHGAP21, promoting activation of RhoA following angiotensin II type 1A receptor stimulation. *Mol Cell Biol.* **31**: 1066-75.

ABSTRACTS AND POSTERS

- Molecular Chaperone Club Meeting, London, UK. (December 2011)
- Cell Signaling Networks 2011, Merida, Yucatan, Mexico. (October 2011)
- Signalling 2011: A Biochemical Society centenary celebration, Edinburgh, UK. (June 2011)
- Peptide arrays as tools for study of protein interaction, London, UK. (March 2011)
- FEBS Workshop 17th Protein Kinase Meeting 'Spatiotemporal Dynamics of Cell Signalling', Oslo, Norway. (September 2010)
- Wellcome Trust 4-year PhD Annual Scientific Retreat (2007, 2008, 2010)

Chapter 1

Introduction

1.1 Heat shock protein

Heat shock proteins (HSPs) are ubiquitously found in both prokaryotic and eukaryotic cells under normal or stressful conditions. These proteins are currently under investigation by researchers from many different scientific fields due to their remarkable properties. Besides being a chaperone for proteins, HSPs have also been described as key mediators of cytoprotection in response to various stimuli. Several recent advances in our understanding of HSPs have provided important insights into their roles in pathophysiologic conditions. This chapter will briefly review the current understanding of the structure and functions of HSPs in eukaryotic cells. In particular, the protective roles of HSP20 in heart will be highlighted here.

1.1.1 Background

The heat response in cells was first discovered by an Italian investigator, Ferruccio Ritossa (1962) during a study of elevated temperature effects on the salivary glands of fruit fly *Drosophila* embryos. He reported that an unusual gene expression had occurred which rapidly induced the synthesis of a new set of proteins in response to the heat stress (elevation of approximately 5^{o} above normal growth temperature). Subsequently, a dramatic change in the flies' polytene chromosomal puffing patterns was observed under light microscopic examination. It was later discovered by Tissieres and his co-workers (1974) that the puffs were sites of messenger RNA (mRNA) transcription leading to enhanced synthesis of a group of proteins which he named them HSPs. Initially, it was believed that these proteins were only found in fruit flies. However, Schlesinger (1986) later demonstrated that there were also identical heat responses in avian and mammalian tissue culture cells. With similar discoveries from other scientists in prokaryotes like *E. coli* (Yamamori *et al*., 1978) and *Tetrahymena* (Fink and Zeuther, 1978), the heat shock response appeared to be a universal response in all living organisms. Accordingly, Schlesinger (1986) believed that virtually all organisms from prokaryotes to eukaryotes might have a set of special proteins to enhance their survival ability and help the cells to recover from stress when favourable conditions pertain.

1.1.2 Functions

Heat shock proteins (HSPs) form a multigenic family of proteins that are ubiquitously expressed in all major subcellular compartments. It is believed that this protein family perform protective functions across the whole biological spectrum. HSPs are able to maintain cell stability and protect cells from severe damage. They are synthesised in organisms in response to unfavourable conditions such as heat, pH changes and oxidative injury, which can alter protein functions and lead to deleterious effects in cells (Visick and Clarke, 1995; reviewed in Benjamin and McMillan, 1998). Despite also being named as stress proteins, HSPs have critical roles during unstressed conditions (Hartl, 1996). As these proteins play such an indispensable role in regulation of intracellular homeostasis, they have been highly conserved in structure through evolution among widely divergent organisms from bacteria to mammals (Lindquist, 1986; Benjamin and McMillan, 1998).

Previous research has provided evidence about the different functional properties of HSPs. For some time, their function as molecular chaperones for other proteins has been known. For example, they have been involved in various intra-cellular processes and protein-protein interactions such as protein biosynthesis, transport to mitochondria or endoplasmic reticulum, cell signalling, assembly of multi-subunit complexes, and degradation of toxic metabolites through ubiquitination and proteasome lysis (Chiang *et al*., 1989; Hightower, 1991; Hendrick and Hartl, 1993; Becker and Craig, 1994). Most of the HSPs facilitate proper *de novo* folding, assembly and disassembly of proteins by recognising hydrophobic features of misfolded or partially unfolded substrate polypeptides (Gething and Sambrook, 1992; Hartl, 1996). Via the action of HSPs, the distorted proteins can be restored to their native conformation and stabilised to prevent unwanted aggregation of denatured proteins. Enzymatic repair mechanism for methionine oxidation, proline isomerisation and formation of isoaspartyl residues may also stem from the reversal of a particular form of protein damage (Visick and Clarke, 1995). Additionally, HSPs also assist in the maintenance of proper protein structure during intracellular trafficking, denatured protein repair and direction of unsaveable proteins to intracellular “garbage disposal machines” (proteasome) for protein degradation (Hightower, 1991).

1.1.3 Synthesis of heat shock proteins

Increases in HSPs synthesis is a key part of heat shock response against cell insults such as elevated temperatures, physiological or chemical stresses. Although there is a beneficial impact of HSPs upon stressful stimulation (increased HSPs level for cell survival), too much HSPs or prolonged exposure to HSPs can also be destructive. This can be explained by the cell adaptation mechanism. For example, when the temperature has been elevated for some time, the cellular conditions have probably adjusted to the temperature increase so that no further proteins are denatured, meaning that high concentrations of free HSPs could be lethal. This happens when the synthesis of more HSPs deplete the cell's energy and nutrient stores, thus interfering with ongoing process in the cell. As HSPs can have both a positive and a negative impact on fitness, natural selection may have acted to balance these impacts in regulating the level of HSP expression (Feder and Hofmann, 1999). Indeed, the heat shock gene expression is transcriptionally regulated by heat shock factors (HSF1-4), in particular HSF-1 in vertebrates, which is normally present in latent state under normal cellular conditions (McMillan *et al*., 1998). In resting cells, HSFs are bound to various HSPs in the cytosol. After stress, damaged proteins become abundant and there is a reduction of free HSPs, hence resulting in dissociation of HSFs from the HSPs. The stress signal then induces HSFs formation of monomers to homotrimers and initiates the translocation of HSFs from the cytosolic to the nuclear compartment. In the nucleus, HSFs transcriptional activity is activated upon phosphorylation and high-affinity DNA binding to an upstream promoter, sequence-specific heat shock element (HSE) which is located in the TATA-box-proximal 5'-flanking regions of heat shock genes (Amin *et al*., 1988). As a result, the expression of new HSPs is increased. Upon cell recovery, HSF is dephosphorylated and most of the HSP exits the nucleus and return to the cytoplasm. In short, heat stress response actually depends on *de novo* synthesis of the HSPs (Fishelson *et al*. 2001).

1.1.4 Families of heat shock proteins

Traditionally, HSPs are classified into six major families: HSP40, HSP60, HSP70, HSP90, HSP100, and small HSPs (sHSPs) where the monomer size typically ranges between 12- to 30-kDa proteins (Kappe *et al*., 2003). In addition, the subfamily of sHSPs in mammalian

system consists of 10 members (HSPB1-HSPB10) that can be further classified into two major categories (Class I and II) according to their subcellular or tissue distribution, gene expression patterns and transcriptional regulation (Taylor and Benjamin, 2005). In fact, HSPs are named mainly according to their structure and molecular weights which is expressed in kilodalton (kDa) (Rakonczay *et al*., 2003). For instance, the most widely-studied HSP70 and HSP90 refer to HSPs of 70 and 90 kDa in size, respectively, although sizes may vary slightly among different organisms. Interestingly, the small 8-kDa protein ubiquitin which is responsible for heat- or stress-damaged protein degradation, also shares similar properties as HSPs (Raboy *et al*., 1991).

1.1.5 Structure of heat shock proteins

Although HSP families are genetically and biochemically different, there are significant homologies present in members from the same HSP family. For instance, all of the related HSP70 proteins have two distinct functional domains: a highly conserved N-terminal nucleotide binding domain which is responsible for ATPase activity, and a C-terminal domain substrate binding domain (Rudiger *et al*., 1997). Recently, it is shown that these two domains are connected by an adjacent exposed linker, which is important for mediating interdomain communication and chaperone function (Jiang, *et al*., 2005).

As for sHSPs, their structures mainly consist of a poorly conserved N-terminal domain which is involved in chaperone activity and oligomerisation, followed by a highly flexible, variable C-terminal extension that shares similar polarity and hydrophobicity which is responsible for stabilising quaternary structure (de Jong *et al*., 1993; Kappe *et al*., 2003). Although the sizes of sHSPs vary considerably, all members of sHSPs share a highly conserved, homologous α-crystallin domain at the C-terminal with signature amino acid motif that is about 80-100 residues long (Casper *et al*., 1995). Excitingly, the crystal structure of rat HSP20 α-crystallin domain was solved recently, revealing two pockets and a shared groove interface at the C-terminal extension that are associated with homodimerisation (Bagneris *et al*., 2009). Notably, the interface is more extended compared to other sHSPs, thereby resulting in a less compact dimer which contributes to the versatility of HSP20 binding nature.

In addition, unlike other HSPs of higher molecular weight which contain ATP/ADP binding site, sHSPs promote proper refolding of denatured proteins by preventing aggregation in an ATP-independent fashion. Nevertheless, there is evidence showing that ATP hydrolysis is required for the interactions between sHSPs and other ATP-dependent chaperones, suggesting a cooperative relationship exists among these proteins (Wang and Spector, 2001).

1.2 Heat shock protein 20

Heat shock protein 20 (HSP20), also referred to as P20 or HSPB6 represents a prominent example of the sHSPs family. With apparent molecular mass of 20 kDa, HSP20 was first discovered in extracts of rat and human skeletal muscle when co-purified with HSP27 and αB-crystallin, suggesting similar functional properties for all three proteins (Kato *et al*., 1994). HSP20 may exist as monomers or larger oligomeric structures, but has stronger tendency to form disulfide-linked dimers in a concentration-dependent manner (van de Klundert *et al*., 1998). Further experiments have demonstrated that HSP20 is active in the dimer form at low concentrations, whereas its activity is weakened when forming large oligomers at high concentration (Lee *et al*., 2005). In addition, size exclusion chromatography (SEC) has shown that subunits of HSP20 can be readily exchanged and interconverted for different sHSPs in complexes, to form heterooligomeric complexes that confer distinct biochemical properties (Bukach *et al*., 2004). Notably, the phosphorylation status of HSP20 is associated with its structural organisation which presents different aggregation patterns with respect to its functional role (van de Klundert *et al*., 1998). It was demonstrated that HSP20 phosphorylation at Ser16 altered its ability to aggregate thereby, triggering its protective effect, which is in agreement with earlier notion that the N-terminal domain is essential for oligomerisation. Conversely, non-phosphorylatable HSP20 favoured the formation of larger aggregates which ultimately resulted in loss of cardioprotection (Qian *et al*., 2009). On the other hand, there were studies reported that the phosphorylation of HSP20 is regulated by its formation of heterooligomeric complexes with other sHSPs. For example, HSP27 forms heterooligomeric complexes with HSP20 and inhibits the rate of HSP20 phosphorylation by cAMP-dependent protein kinase (Bukach *et al*., 2009). Taken together, it is accepted that the different oligomerisation patterns of sHSPs is likely to affect their cytoprotective ability during cellular stress.

Moreover, intracellular concentration and cellular distribution of HSP20 tend to change in response to different cellular conditions. At basal level, HSP20 is primarily found in the cytosol but a subpopulation may translocate into the nuclear compartment in response to stress signals (Fan *et al*., 2005). Because HSP20 is ubiquitously expressed in almost all tissues, it is no surprise that numerous studies have focused on the functions of HSP20 in a variety of cellular processes, notably apoptosis and actin cytoskeletal rearrangements. In addition, as HSP20 presents at high levels especially in heart, skeletal and smooth muscle (reviewed in Fan *et al*., 2011), extensive work has also been carried out to examine the potential roles of HSP20 in cardiovascular disease (discussed later in Section 1.3.).

1.2.1 HSP20 phosphorylation

HSP20 is inactive or partially active under physiological conditions and converts to an active phosphorylated state upon modulation by stress-kinases. The phosphorylation of HSP20 normally occurs in response to increased levels of cyclic nucleotide second messengers that activate such upstream kinases. There are several phosphorylation sites identified to date, which play important roles in the functioning of HSP20. Serine 16, which is phosphorylated by cAMP-dependent protein kinase A (PKA) and cGMP-dependent protein kinase G (PKG), has roles in mediating cyclic nucleotide-dependent smooth muscle relaxation and rate of relaxation in cardiomyocytes (Beall *et al*., 1997; Woodrum *et al*., 1999; Rembold *et al*., 2000; Pipkin *et al*., 2003; Chu *et al*., 2004). There is evidence showing that phosphorylation of HSP20 could be induced by sodium nitroprusside, a nitric oxide donor (Pipkin *et al*., 2003). Moreover, it was found that agonist-induced muscle contraction was inhibited by the introduction of phosphopeptide analogues of HSP20. It was thought that the phosphorylated HSP20 increased shortening and lengthening rates in rat cardiomyocytes through rapid uptake of calcium. In addition, HSP20 has been shown to localise in sarcomeric transverse bands, suggesting a role in regulating cytoskeletal or contractile dynamics of cardiomyocytes (Pipkin *et al*., 2003). Indeed, previous mechanistic studies have highlighted dynamic interactions between HSP20 and the cytoskeletal element, actin, as well as actin-binding protein α-actinin (Brophy *et al*., 1999; Tessier *et al*., 2003). Treatment of cells with ISO results in HSP20 redistribution to the cytoskeleton and colocalisation with actin and this dynamic transition is most likely a phosphorylation-dependent reaction (Fan *et al*., 2004). Notably, non-phosphorylated HSP20 associates with filamentous actin (F-actin), whereas

phosphorylated HSP20 binds to globular actin (G-actin). The actin-binding region spanning residues 110-121 of HSP20 shares sequence homology with the myofilament protein cardiac troponin I, a key regulator of cardiac contraction and relaxation (Rembold *et al*., 2000; Layland *et al*., 2005; Solaro *et al*., 2008). Clearly, this binding region is important to inhibit crossbridge formation via direct interaction with contractile elements, resulting in relaxation of smooth muscle. Indeed, Dreiza *et al*. (2005) showed that the phosphopeptide motif of HSP20 could modulate actin cytoskeletal dynamics by preventing the association of cofilin, an actin-depolymerising protein to the scaffold protein 14-3-3 through a competitive binding mechanism.

Other phosphorylation sites include serine 59 which is phosphorylated by protein kinase C (PKC) and serine 157 which is phosphorylated by insulin stimulation (Wang *et al*., 1999; Chu *et al*., 2004). Serine 157 phosphorylation site is not conserved in human HSP20 and the physiological significance of serine 59 phosphorylation is unclear. To date, most assumptions about the significance of HSP20 phosphorylation have been made around serine 16, which is located within the sequence motif (RRXS), a characteristic consensus motif for PKA/PKG (Fan and Kranias, 2005). More interestingly, HSP20 is the only sHSPs that possesses this target motif despite sharing considerable sequence homology with HSP27 and αB-crystallin (Kato *et al*., 1994).

The phosphorylation of HSP20 is thought to be a critical aspect of neurohormonal regulation. Indeed, increasing evidence has suggested that HSP20 phosphorylation is an important event in the β-adrenergic signalling cascade in the myocardium, pointing to its potential role as a mediator in cardiac responses. This is supported by previous findings which showed that HSP20 expression was increased and its phosphorylation was specifically induced by the β-adrenergic agonist, ISO in cardiomyocytes (Chu *et al*., 2004). Similar observations were also obtained in post-infarcted animal hearts, pinpointing a compensatory role of HSP20 phosphorylation in the pathophysiology of heart (Fan *et al*., 2005; Qian *et al*., 2009).

1.3 HSP20 in the cardiovascular system

There has been a rapid increase in the prevalence of cardiovascular disease in recent years. Despite therapeutic advances, heart diseases which are often caused by the malfunction of cardiac cell homeostasis remain as leading causes of death in industrialised nations. Because HSPs are normally up-regulated in response to stress stimuli in order to modulate cellular homeostasis, the many emerging roles of sHSPs in a cardiac setting may suggest potential therapeutic avenues for intervention in heart diseases (Ghayour-Mobarhan *et al*., 2009). Numerous studies have been carried out to define the roles of HSP20 in cellular protection systems, in particular, its protective capabilities against myocardial dysfunction. In short, the roles of HSP20 in heart can be broadly divided into three areas, i.e. ischaemia/reperfusion injury, apoptosis and hypertrophy.

1.3.1 Ischaemia/reperfusion injury

In the heart, ischaemia is often accompanied by reperfusion and induces apoptosis, which may ultimately lead to myocardial defects (Eefting *et al*., 2004). Because HSPs synthesis tends to increase as a response to protect cell after stress stimuli, much research has also been carried out to investigate the contribution of HSP20 to protect cells during ischaemia and reperfusion injury. Using transgenic mice with cardiac-specific overexpression of HSP20, it is reported that the expression of total HSP20 was upregulated by ischaemic/reperfusion insult. This in turn promoted protection against ischaemia/reperfusion-induced injury by reducing myocardial infarction size in HSP20 transgenic hearts *in vivo* and improving their cardiac function during reperfusion, as compared with wild-type mice (Fan *et al*., 2005). Correspondingly, blockade of HSP20 phosphorylation by expression of a phospho-null HSP20 (S16A) mutant in hearts increased susceptibility to ex vivo ischaemia/reperfusion-induced cellular disruptions such as necrosis and apoptosis (Qian *et al*., 2009). Interestingly, autophagy, a process which degrades damaged or non-functional cytoplasmic organelles, was activated in wild-type but not in S16A hearts. Notably, further investigation revealed that S16A hearts pre-treated with rapamycin, an activator of autophagy, led to improvement of functional recovery compared to untreated control. Hence, it was proposed that HSP20 protects against ischaemia/reperfusion injury via its phosphorylation which increases autophagy activity

and decreases cell death. In contrast, HSP20 suppresses autophagy activity when HSP20 phosphorylation of Ser16 is blocked, thereby increasing cell death and lead to cardiac injury (Qian *et al*., 2009). Clearly, the phosphorylation status of HSP20 and corresponding level of autophagy are likely to determine the fate of the heart in response to ischaemia/reperfusion insult. More recently, HSP20 phosphorylation at Ser16 was shown to be associated with an autophagy marker, Beclin 1, to promote cardiac autophagy, thereby inducing cardioprotection (Zhu *et al*., 2011).

In addition, similar salutary effects were also reported in chronic doxorubicin (DOX)-triggered cardiac toxicity in HSP20 transgenic mice (Fan *et al*., 2008). The overexpression of HSP20 in the heart attenuated doxorubicin (DOX)-induced ischemia/reperfusion injury and inhibited cardiac apoptosis via Akt phosphorylation. Evidence also exists delineating the relationship between HSP20 and microRNA, a small non-coding RNA which regulate gene expression via RNA destruction or RNA-induced silencing complexes (Latronico *et al*., 2007). It was reported that overexpression of microRNA-320 promotes apoptosis and cell death in cultured adult rat cardiomyocytes and transgenic mice during ischaemia/reperfusion injury, whereas cytoprotection was initiated in knockdown model via negative regulation of HSP20 (Ren *et al*., 2009). In addition, gene transfer of HSP20 in rat hearts *in vivo* displayed better functional recovery and reduced myocardial necrosis and apoptosis upon ischaemia/reperfusion injury (Zhu *et al*., 2005). Collectively, these observations underscore the adaptive protective response of HSP20 in the heart upon physiological and pathophysiological stress. These HSP20-mediated processes are exceptionally important in reducing injury from ischemia/reperfusion, which is often manifested during heart diseases, organ transplantation and post-operatively.

1.3.2 Apoptosis

Apoptosis is defined as programmed cell death that does not involve an inflammatory reaction. It can also be induced when cells are exposed to non-physiological conditions such as stress insult. Previous work has shown that prolonged stimulation with ISO induces cardiac apoptosis, resulting in the decompensation of hypertrophic myocardium and the progression of end-stage heart failure (Tevaearai and Koch, 2004). Because apoptosis can directly lead to cardiomyopathy without undergoing cell replacement (Bishopric *et al*., 2001), it has been regarded to be an important prognostic indicator in patient with ischaemic heart disease and heart failure. Hence, special attention has been given to investigations of the induction of cytoprotective mechanisms in apoptotic signalling pathways.

Recent studies utilising adenovirally expressed HSP20 have shown that the overexpression of HSP20 confers cellular protection against ISO-mediated apoptosis in cardiomyocytes, as indicated by reduced pyknotic nuclei (Fan *et al*., 2004, 2006). It is clear from this report, that the alteration of HSP20 expression levels triggers an adaptive response to adrenergic stress. Further studies using loss-of-function and gain-of-function cardiomyocyte models verified that the HSP20 phosphorylation state correlates with its anti-apoptotic function. In fact, using non-phosphorylatable HSP20 (S16A) and constitutively phosphorylated HSP20 (S16D) forms, it was further proven that S16D overexpression conferred greater anti-apoptotic effect than wild-type through the inhibition of caspase-3 activation (Fan *et al*., 2004). However, the protective effect was abrogated in S16A mutant. In view of these findings, it is likely that, HSP20 phosphorylation at Ser16 promotes its anti-apoptotic function.

To date, possible downstream targets of HSP20 in cardiac survival/apoptosis pathways activated by the cAMP-PKA pathway include actin and Bax. HSP20 association with these targets results in stabilisation of cytoskeletal architecture and inhibition of apoptosis, respectively (Fan *et al*., 2004; 2005) (Fig. 1.1). The cascade begins with phosphorylation of HSP20 by a stress-kinase, followed by oligomer dissociation and conformational change of HSP20 to promote binding to the targets. Here, HSP20 is shown to translocate to the actin filaments and stabilise the microfilament assembly. Anti-apoptotic effects were achieved via the binding of HSP20 to Bax, thereby preventing the translocation of Bax from the cytosol into the mitochondria. As a result, the integrity of mitochondria was maintained, inhibiting the release of cytochrome C and repressing caspase-3 activity.

Furthermore, Wang *et al*. (2009) found that overexpression of HSP20 could improve contractility and cell viability in response to endotoxin-induced myocardial dysfunction and apoptosis. These protective effects appear to be mediated through suppression of nuclear factor–κB (NF-κB) activation which reduced proinflammatory cytokine production such as tumour necrosis factor-α (TNF-α) and interleukin-1β (IL-1β) production, and inhibition of caspase-3 activity.

It is also noteworthy that there are opposing effects of *β*-adrenoceptor subtypes on apoptosis in cardiomyocytes. Pharmacological studies have reported that stimulation of β_1-adrenoceptors leads to cardiac apoptosis, whereas stimulation of β_2-adrenoceptors confers protection against apoptosis (Zaugg *et al*., 2000). Nevertheless, it is conceivable that HSP20 is a negative regulator of apoptosis as it could prevent the effector steps of apoptotic cell death. This special ability of HSP20 is essential to confer cardioprotection during heart failure as this complication is often accompanied by apoptosis.

Other studies have utilised mutational analyses to reveal a single nucleotide base mutation of C59T, changing a highly conserved proline residue to leucine at position 20 (P20L) in human HSP20. This mutation was shown to affect HSP20 phosphorylation at Ser16 and abrogate its cytoprotective effects (Nicolaou *et al*., 2008). This mutation conferred no protection against apoptosis as shown by Hoechst staining and DNA fragmentation. It was further confirmed that the impaired ability was due to diminished phosphorylation at Ser16, reaffirming its critical role in cardioprotection.

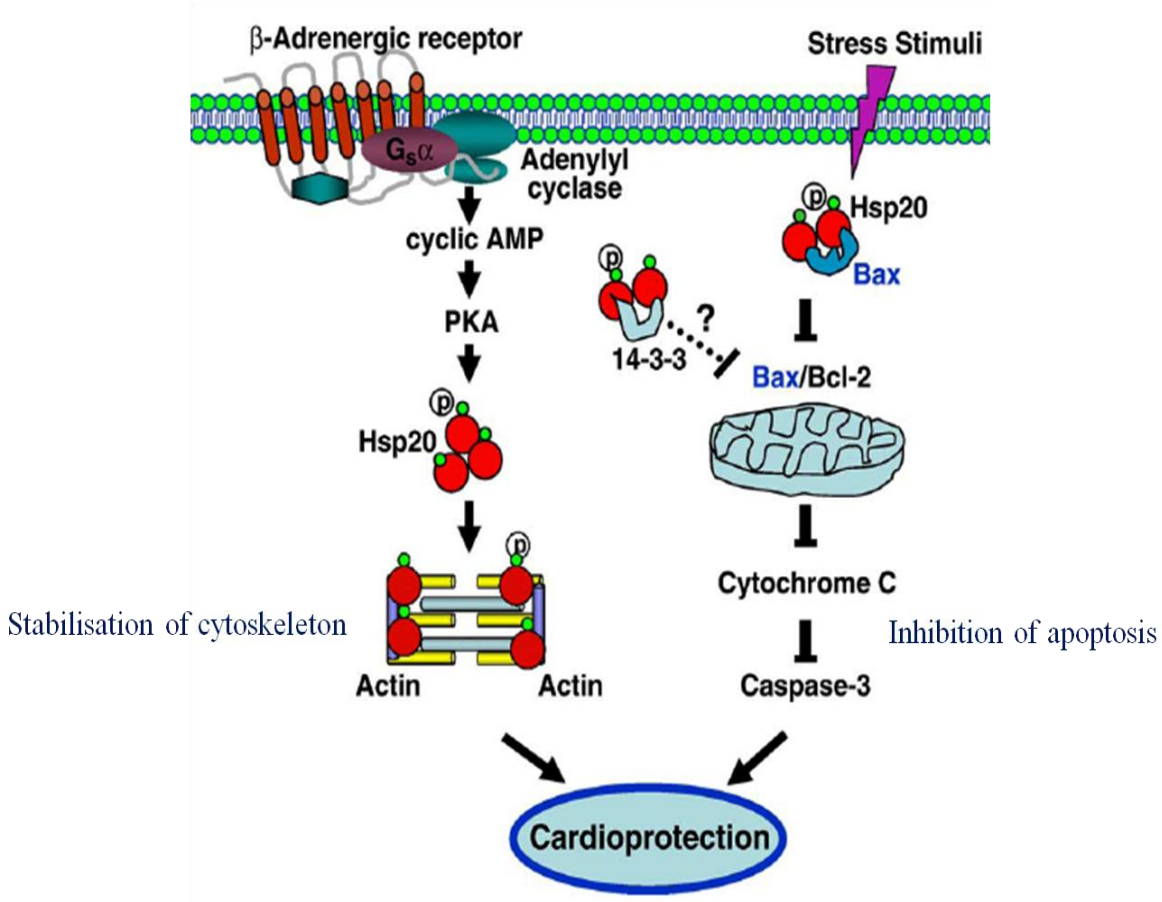

Figure 1.1 HSP20 and its cardioprotective roles. Schematic diagram showing the roles of HSP20 and its phosphorylation in regulation of actin reorganisation and apoptosis activity upon *β*-adrenergic stimulation. (Adapted from Fan *et al*., 2005)

1.3.3 Hypertrophy

Besides having well-establised roles in cardiac injury and apoptosis, there is also emerging evidence to suggest a role for HSP20 in the physiological adaptation during cardiac hypertrophy. The development of the heart is differentially regulated depending on different stages of morphogenesis. Cardiomyocytes actively proliferate at embryonic and fetal stages, but gradually lose their capacity for cell division during the early post-natal period. After birth, any growth of the myocardium is primarily due to hypertrophic growth (Ahuja *et al*., 2007).

Cardiac hypertrophy involves ventricular enlargement, remodeling and generally presents as an increase in cell size without cell division or any increase in cell number. It often develops in response to long-term excessive hemodynamic stress such as pressure and volume overload in response to various intrinsic and extrinsic stimuli, including neurohormones, growth factor and mechanical stress (Sugden, 1999). The process of hypertrophy can be mainly divided into two stages of development: the compensatory hypertrophy stage and decompensatory stage which potentially leads to heart failure. Cardiac hypertrophy may initially be an adaptive physiological process that normalises wall stress and compensates for the lost contractile performance in the short term. Such a phenotype of heart enlargement is reversible and is regarded as a physiological phenomenon, normally seen during chronic exercise or pregnancy. However, due to ancillary changes such as fibrosis, reduced contractility and chamber dilatation, prolonged hypertrophy can be maladaptive and detrimental, often accompanied by irreversible damage. Consequently, it may eventually impair cardiac function, resulting in reduced pump function and invariably leading to the progression of catastrophic heart failure (Frey and Olson, 2003).

The development of cardiac hypertrophy is also accompanied by phenotypic modifications. The typical cellular features of pathological hypertrophy promote cardiac remodelling which is associated with an increase in cardiomyocyte size, enhanced protein synthesis and reorganisation of actin filament (reviewed in Frey and Olson, 2003). In addition, there are also alterations in gene expression which can be divided into three phases. Initially, immediate-early gene expression including *c-fos*, *c-jun* and *Egf*, which are involved in regulation of myofibrillar proteins are rapidly increased (Izumo *et al*., 1988). This is followed by the re-expression of fetal genes such as natriuretic peptide hormones [atrial natriuretic factor (ANF) and brain natriuretic factor (BNF)] and embryonic contractile

proteins [β-myosin heavy chain (β-MHC) and skeletal muscle α-actin]. This fetal gene expression normally occurs during 12 to 24 h. After 24 h, other constitutive contractile protein genes like cardiac muscle α-actin and ventricular myosin light chain 2 (vMLC2) are re-expressed (Chien *et al*., 1991; Rosenzweig and Seidman, 1991). As such, these genes are regarded as molecular markers of cardiac hypertrophy.

Interestingly, there are different pathways activated in response to different durations of hypertrophic stimuli during the hypertrophy signaling process. Short-term exposure to β-adrenergic stimulation is particularly important in mediating heart contractility upon fight-or-flight response. However, chronic stimulation of β-adrenergic agonists has been shown to have deleterious effects in animal models and human subjects, resulting in pathological cardiac remodeling and the progression of heart failure. Recent studies have revealed that sustained ISO stimulation results in the over-expression and phosphorylation of the small heat shock protein 20 (HSP20). Together, these actions combine to attenuate the hypertrophic growth of cardiomyocytes by triggering cardioprotective functions (Fan *et al*., 2005). In addition, it has become apparent that apoptosis signal-regulating kinase 1 (ASK1) is involved in the regulation of stress-activated protein kinases, such as c-Jun N-terminal kinase (JNK) and p38 mitogen-activated protein kinase (MAPK), which are implicated in the onset of cardiac hypertrophy (Hirotani *et al*., 2002). Further work has revealed an association between increased HSP20 expression and the downregulation of ASK1 in mice infused with prolonged ISO (Fan *et al*., 2006). After treatment, transgenic mice overexpressing HSP20 exhibited minimal heart enlargement and smaller increases in cross-sectional area of cardiomyocytes, as well as downregulation of fetal gene expression. It was deduced that both the overexpression and phosphorylation of HSP20 were involved in the downregulation of ASK1-JNK/p38 signalling. Consequently, this led to the attenuation of cardiac remodeling and inhibition of ISO-triggered apoptosis *in vivo* and *in vitro*, thereby hindering ISO-mediated hypertrophy and the downstream progression of heart failure. Nevertheless, the molecular mechanism of HSP20 induced cardioprotection is not yet clearly defined. Not much is known about the regulation of HSP20 and if other signalling pathways are also involved.

1.4 HSP20 in other diseases

With ever-increasing interest on the function of HSP20 in cardiovascular system, it is also apparent that HSP20 is implicated in many other pathological processes. Besides the aforementioned examples, HSP20 can also be found in blood and was found at lower level in injured arteries. Subsequently, the release of HSP20 is induced from the arterial walls into the circulation as an immediate response to endothelial injury and thus affects platelet functions (Kozawa *et al*., 2002). It has been shown that HSP20 suppresses platelet aggregation by binding to platelets at its N-terminal platelet aggregation inhibitory domain via protease activated receptor-1 (PAR-1) and platelet glycoprotein complex (GPIb/V/IX-von Willebrand factor axis), which may be beneficial in myocardial infarction (Matsuno *et al*., 2003; Fan *et al*., 2005). There have also been studies examining the role of HSP20 in the mediation of PKA-dependent airway smooth muscle (ASM) relaxation (Komalavilas *et al*., 2008). Using human airway smooth muscle (HASM) cell lines, the PKA-mediated phosphorylation of HSP20 has been shown to lead to relaxation of ASM, which is associated with the disruption of actin stress fibers. In contrast, inhibition of this pathway prevents alterations in stress fiber morphology and focal adhesion complex formation which favour bronchospasm in asthma. Because phosphorylation of HSP20 is associated with dephosphorylation of cofilin to disrupt actin in ASM, it is suggested that HSP20 mediates ASM relaxation through its direct regulation of actin filament assembly.

In addition, HSP20 is also implicated in the prevention of *β*-amyloid (A*β*) fibril formation in senile plaques in the brain, a pathological hallmark of neurodegenerative diseases such as Alzheimer's disease (Lee *et al*., 2005, 2006). It is known that Aβ deposits readily *in vitro* and *in vivo*, and forms toxic fibrils and protofibrils upon aggregation. Interestingly, HSP20 was shown to reduce A*β*-mediated cytotoxicity by interacting with A*β* and preventing its aggregation, thereby resulting in the solubilisation and clearance of toxic A*β* oligomers in neuronal cells (Lee *et al*., 2005, 2006). This suggests a potential role of HSP20 as an antagonist of the biological action of A*β*, in particular the formation of A*β* aggregates.

Recent studies have also highlighted possible roles of HSP20 in carcinogenesis. It was reported that HSP20 expression decreases with tumour growth in patients with hepatocellular carcinoma (HCC), pinpointing a suppressive effect of HSP20 on the progression of human HCC (Noda *et al*., 2007). Accordingly, HSP20 expression was inversely correlated with tumour stage by TNM (Tumour, Node, Metastasis) classification,

degree of metastasis and tumour size. Further investigations on the role of HSP20 in HCC proliferation revealed that overexpression of HSP20 inhibited the growth of HCC via the suppression of MAPKs and AKT signalling pathways (Matsushima-Nishiwaki *et al*., 2011). Seemingly, HSP20 negatively regulate MAPK/ERK kinase (MEK) [mitogen-activated protein kinase (MAPK)/ extracellular signal-regulated kinase (ERK)], c-jun N-terminal kinase (JNK) and PDK1 (3-phosphoinositide-dependent protein kinase-1), leading to the downregulation of cyclin D1 expression, thereby hindering neoplastic transformation and growth. In contrast, the decrease in HSP20 expression promotes proliferation of HCC, hence contribute to tumour progression.

Taken all together, it is clear that HSP20 shows versatile functions, being implicated in a wide range of biological roles. It is purported that the versatility of HSP20 is partly due to its interaction with 14-3-3, resulting in the displacement of many other 14-3-3 binding partners from their complexes with 14-3-3 (Seit-Nebi and Gusev, 2010). Moreover, HSP20 is regulated by various protein kinases which are key regulators of many cellular functions (Fan *et al*., 2006, 2008). Undoubtedly, the multifunctional nature of HSP20 makes it a particular attractive molecular target for future therapeutic interventions.

1.5 Cardiac cell-based model

The use of relevant models for cardiovascular research is essential to provide valuable information to reflect the physiological condition of heart tissue, as well as to unravelling mechanisms of the pathogenesis of cardiovascular diseases. To date, the most commonly used experimental models include intact whole heart and primary culture of cardiomyocytes. Amongst those models, neonatal and adult rat cardiomyocytes have been used extensively for decades as tools to study and understand the morphological, biochemical and electrophysiological characteristics of the heart under controlled conditions. These models have also been used to evaluate cardiac toxicity and identify candidate molecules for testing in animals. Because rats share a high degree of genetic homology to humans, it is anticipated that the experimental findings will be of relevance to human biology.

In view of previous studies which have documented that cardiac hypertrophy can be induced by sustained adrenergic stimulation (Morisco *et al*. 2001; Zhang *et al*., 2002), animal models of chronic agonist administration have been considered as a suitable experimental setting to study the effect of sympathetic overactivation on myocardial function. Hence, in the present study, neonatal rat cardiomyocytes were mainly utilised as an *in vitro* cardiac cell system to study the cellular and molecular aspects of cardiac function, particularly hypertrophic signalling in response to prolonged β-adrenergic stimulation. Importantly, it is economical, readily available, versatile, manageable and labour-saving, as compared to the calcium-sensitive adult rat cardiomyocytes model, which is more prone to cellular disintegration, hence requiring more stringent protocols. Moreover, previous studies have shown that the phenotype of cultured neonatal cardiomyocytes is very stable. Their contractile profiles correspond to the hearts *in situ* and hypertrophic growth is quite similar to the adult myocardium, thereby allowing better functional evaluation of hearts (Yamashita *et al*., 1994).

1.6 Aims of research

On the basis of the aforementioned findings, it is evident that HSP20 is a multifaceted protein which plays many pivotal roles in cardioprotection. My PhD project aims to further elucidate the molecular mechanisms that underpin HSP20's unique ability in this regard. My thesis focuses on induced cardioprotection against cardiac dysfunction, in particular hypertrophy, as there is a great paucity of information on this subject regarding HSP20.

This study is divided into three parts:

(1) neonatal rat cardiomyocytes as a model system to study hypertrophy signalling

(2) investigations into the role(s) of the PDE4-HSP20 complex in hypertrophy;

(3) identification of novel signalling complexes containing HSP20 and characterisation of their possible mechanisms of action

It is anticipated that my findings may enhance our current knowledge about the functions of HSP20 and provide direction towards a novel treatment for hypertrophy.

Chapter 2

Materials and Methods

2.1 Materials

The chemicals used in this study were of analytical grade. All chemicals were supplied by Sigma-Aldrich unless otherwise indicated. Isoprenaline (ISO) and disruptor peptides were dissolved in dimethly sulfoxide (DMSO) and added to cell media at a final concentration of 0.001% of DMSO. The water used in all experiments was purified by a water purification system with automatic sanitization module (Millipore, France).

2.2 Expression and Purification of Recombinant Proteins

2.2.1 Histidine (His) Fusion Protein

Ultimate™ ORF clone IOH57317 (Invitrogen), containing the open reading frame (ORF) of human HSP20 in pENTR221 vector, was used to generate an N-terminal His-tagged protein by Gateway cloning technology into pDEST-17 vector (Invitrogen). *Escherichia Coli* (*E. Coli*) cells containing the plasmid were inoculated into 10 ml of Luria-Bertani (LB) medium supplemented with 100 µg/ml ampicillin and grown overnight in an orbital shaker at 37 ^{o}C. The overnight culture was then added to 500 ml of LB medium supplemented with 100 µg/ml ampicillin and grown for a further 2.5 h. The density of the cell growth was monitored at regular intervals. Once the cell density reached $OD_{600} \approx 0.6$-0.7 indicating that the culture was in the logarithmic phase, the exponentially growing cells were then subjected to 1 mM of isopropyl-*β*-D-thiogalactopyranoside (IPTG) to induce protein expression. Cells were grown for a further 3 h at 37 ^{o}C and subsequently pelleted by centrifugation at 6000 x g for 10 min at 4 ^{o}C. The cell pellets were resuspended in 10 ml of lysis buffer (50 mM Tris-HCl; pH 8.0, 300 mM NaCl, 10 mM imidazole) supplemented with protease cocktail inhibitor tablet (Roche) and frozen at -80 ^{o}C overnight. Imidazole was added to the lysis buffer to increase purity by minimising binding of untagged and contaminating proteins. Frozen cells were thawed on ice the following day and subjected to sonication (40-60 kHz; Sonicator, Jencons, England) for 10 min (seven cycles of 30 sec each with a one-min pause for cooling after every treatment) to ensure sufficient cell lysis occurred. Following lysis, cell lysates were centrifuged at 13000 rpm for 15 min at 4 ^{o}C to collect the soluble fractions and remove cell debris. The cell supernatants were then incubated end-over-end with pre-equilibrated nickel-nitrilotriacetic acid (Ni-NTA) resins (Qiagen) for 1 h at 4 ^{o}C with gentle agitation for binding of expressed fusion protein. The resins with bound protein was then transferred to a disposable column and washed

extensively with wash buffer (50 mM Tris-HCl, 300 mM NaCl; pH 8.0) containing 10 mM imidazole to reduce background contaminants. The fusion protein was then eluted from the Ni-NTA resins with elution buffer (50 mM Tris-HCl, 300 mM NaCl, pH 8.0) containing linearly increasing concentrations of imidazole (25-250 mM) to increase purity of recombinant fusion protein.

40 µl samples from each step were collected for analysis by SDS-PAGE and Coomassie staining as described in Section 2.6.1 and 2.6.2. The most pure eluted fractions (indicated by single band on a gel) were then pooled and subjected to ultrafiltration using a Vivaspin device (Sartorius Stedim Biotech) containing dialysis buffer (5% glycerol (v/v), 50 mM Tris-HCl; 100 mM NaCl, pH 8.0) for buffer exchange and sample concentration. After obtaining the desired concentration, the purified recombinant fusion protein was frozen on dry ice and stored as aliquots at -80 ^{o}C until further use.

2.2.2 Glutathione-S-Transferase (GST) Fusion Proteins

Full–length human PDE4D5 was expressed as an N-terminal GST-fusion protein using pGEX-6P1 vector (Invitrogen). Culture were grown, induced, harvested and lysed as described above. Purification of GST fusion proteins were carried out using glutathione sepharose resin (Amersham Biosciences) and elution buffer composed of 10 mM reduced glutathione, 50 mM Tris-HCl; pH 8.0. The subsequent procedures were similar to the purification of His protein as described above in Section 2.2.1.

2.3 Plasmid DNA

All plasmid work was carried out in a sterile environment and all buffers were autoclaved prior to use.

2.3.1 Transformation of competent cells

BL21 competent cells (Invitrogen) were stored at -80 ^{o}C and thawed on ice prior to use. 1-10 ng of DNA was added to 50 µl of competent cells and incubated on ice for 15 mins. The cells were then heat shocked at 42 ^{o}C for 45 sec then placed on ice for 2 mins. The solution

was added to 450 µl Luria Broth (LB) media (1% (w/v) bacto-tryptone, 0.5% (w/v) bacto-yeast extract and 170 mM NaCl) containing 100 µg/ml ampicillin and incubated at 37 ^{o}C for 1 h with shaking. 50-250 µl of transformation mix was then spread on 100 mm petri dishes containing LB media, 1.5% (w/v) agar and 100 µg/ml ampicillin, and incubated overnight at 37 ^{o}C. The growth of bacterial colonies indicated successful cell transformation.

2.3.2 Isolation of Plasmids DNAs

Single colonies were picked and grown overnight in 5 ml LB media containing 100 µg/ml ampicillin in an orbital shaker at 37 ^{o}C. QIAprep Miniprep Kit (Qiagen) was used to isolate smaller amounts of plasmid DNA. Alternatively, for a larger volume of bacterial culture, the 5 ml overnight bacterial culture was added onto a 500 ml LB media supplemented with 100 µg/ml ampicillin and incubated a further 12-16 h. The large amounts of plasmid DNA was extracted using QIAprep Maxiprep Kit (Qiagen) according to the manufacturer's instructions. The purified DNA was then eluted with either sterile H_20 or TE buffer (10 mM Tris-Cl, 1 mM EDTA; pH 7.5) and stored at -20 ^{o}C.

2.3.3 Storage of plasmid DNA

For plasmid storage, 1 ml of overnight culture was removed and mixed with 500 µl sterilised glycerol in a sterile cryovial. The glycerol stock was then snap-frozen on dry ice and stored at -80 ^{o}C until required.

Glycerol stocks could also be used to inoculate culture media by scraping the frozen stock with a sterile pipette tip and then transferred into 5 ml LB media containing 100 µg/ml ampicillin. The plasmid isolation was then performed as described in Section 2.3.2.

2.3.4 Analysis of plasmid DNA

Agarose gel electrophoresis was used to separate DNA by molecular weight. Negatively charged DNA samples will migrate from the cathode toward the anode during electrophoresis. The DNA was resolved on a 1 % agarose gel dissolved in Tris-acetate acid-EDTA (TAE) buffer containing 40 mM Tris-Cl; pH 8.5, 0.114% (v/v) glacial acetic acid and 2 mM EDTA. The solution was allowed to cool slightly before adding 0.5 µg/ml ethidium bromide. For gel casting, the solution was poured into the Bio-Rad Mini-Sub Cell GT agarose gel system with comb inserted to create wells and allowed to set at room temperature. Once set, the comb was removed and the gel was placed in a gel tank containing TAE buffer. DNA samples were diluted 1:6 in loading buffer (0.25% (w/v) bromophenol blue, 0.25% (w/v) xylene cyanol FF and 40% (w/v) sucrose). 1kb DNA ladder (Promega) was used as a molecular size marker. The gel was run at 100 V until the first dye front (bromophenol blue) has migrated about 2/3 of the gel. The gel was then removed from the tank and visualised on an ultraviolet transilluminator (Gel Doc XR+ System, Bio-Rad).

2.3.5 Quantification of DNA concentration

The concentration of purified DNA was determined by Nanodrop 3300 spectrophotometer (Thermo Scientific). Absorbance wavelength was set at 260 nm and 280 nm. The A_{260}:A_{280} ratio determines the purity of DNA where a value of 1.8 is indicative of highly purified DNA. The DNA concentration was calculated using the Beer-Lambert law, where an A_{260} reading of 1.0 optical density (OD) unit is equivalent to 50 µg/ml double-stranded DNA (Sambrook *et al*., 1989).

2.4 Mammalian cell culture

All cell culture procedures were carried out in a Class II hoods using standard aseptic techniques and sterile instruments. All culture reagents were supplied by Sigma. The tissue culture flasks, dishes and pipettes were supplied by Corning. All cultures were examined regularly under a phase contrast inverted microscope (Leitz Diavert, Germany) to confirm the healthy status of the cells and the absence of contamination.

2.4.1 Primary culture of cardiomyocytes

The preparation of neonatal rat cardiomyocytes was based on a modification of the methods described by Bogoyevitch *et al.* (1995) and Chlopeikova *et al.* (2001). Cardiomyocytes were dissociated from the ventricles of neonatal Sprague-Dawley rat hearts (1-3 days old) by serial digestion with 0.3 mg/ml Type 2 collagenase (Worthington) and 0.6 mg/ml pancreatin (Sigma) in a balanced salt solution containing 120 mM NaCl, 20 mM HEPES, 5.5 mM glucose, 5.4 mM KCl, 1 mM NaH_2PO_4 and 0.8 mM $MgSO_4$ (pH 7.4). The first digestion supernatant (5 min at 130 cycles/min in a shaking water bath at 37 ^oC) was removed and discarded. The digestion step was repeated 3-5 times till tissue was digested completely (20 min each at 160 cycles/min shaking). Cell suspensions from every digestion were collected and centrifuged at 1250 rpm for 5 min. Each cell pellet was then resuspended in 2 ml of newborn calf serum and kept at 37 °C in a humidified incubator with an atmosphere of 95% air and 5% carbon dioxide. After the final digestion, the cell suspensions were pooled and centrifuged at 1250 rpm for 5 min before being resuspended in plating medium containing Dulbecco's modified Eagle's medium (DMEM)/M199 [4:1 (v/v)], supplemented with 10% horse serum, 5% fetal calf serum, 100 units/ml penicillin-streptomycin). Since non-myocardiomyocytes attach to the substrate more readily than cardiomyocytes, the cells were pre-plated on non-coated T-75 flask (Corning) for 2 h to allow differential attachment of non-myocardial cells. The non-adherent cardiomyocytes were then collected and centrifuged at 1250 rpm for 5 min. After counting, the cells were plated at a density of 2 x 103 cells/mm^2 on culture dishes pre-coated with sterile 1% (w/v) gelatin (Sigma-Aldrich). The purity of cardiomyocytes culture was determined by immunocytochemistry with an anti-α-sarcomeric actinin mouse antibody, a well-known protein marker in the cytosol of cardiomyocytes (See Section 2.11.2).

For hypertrophy induction, plating medium was removed after 24 h and cells were cultured in serum-free maintenance medium containing DMEM/M199 [4:1 (v/v)] and 100 units/ml penicillin and streptomycin. After 48 h of culture in the serum-free medium, cardiomyocytes were stimulated by 10 μM of ISO for 24 h.

Alternatively, for microscopic experiments, cardiomyocytes were plated at a density of 1.4 x 10^3 cells/mm^2 on slides pre-coated with laminin (BD Biosciences). Where appropriate, cardiomyocytes were pretreated with compounds before being stimulated for 24 h with 10 μM isoprenaline for hypertrophy induction. Cells derived from the same primary culture

were used for each set of experimental comparisons (n=1). All experiments were performed at least 3 times with different primary cell isolates.

2.4.2 HEK293 cells

The human embryonic kidney 293 (HEK293) cells were cultured in 75 cm^2 culture flasks at 37 ^oC in a humidified atmosphere of 5% CO_2 and 95% air. Cells were maintained in growth media containing DMEM supplemented with 10% fetal bovine serum, 2 mM L-glutamine, 100 U/µg penicillin-streptomycin in a humidified atmosphere containing 5% CO_2. For routine cultures, the media were replenished every 2-3 days. The cells were passaged when reaching approximately 80% confluency to improve cell growth. To passage, growth medium was removed and the cells were gently washed in sterile pre-warmed phosphate buffer saline (PBS) to remove traces of serum. The PBS was then discarded and the cells were treated with 2 ml of trypsin-EDTA solution per 75 cm^2 culture flask of cells to dissociate cells in the monolayer. 8 ml of growth medium was then added to inactivate the trypsin-EDTA solution and cells were collected by centrifugation at 12,000 rpm for 3 min at room temperature. The supernatant was removed and the cell pellet was resuspended in fresh growth media. The volume of PBS, trypsin-EDTA and growth media were adjusted according to the size of the culture flask. When cells were harvested for long term storage, the cells were resuspended in 10% dimethyl sulfoxide (DMSO) containing growth medium and stored at -80 ^oC.

2.4.3 Transfection of plasmid DNA

DNA plasmid constructs used for transfection included V5-HSP20 in pDEST vector and GFP-PKD in pEF-BOS vector. For transient expression, HEK293 cells were plated at a density of 4 x 10^5 cells per 100 mm dish. Transfections were performed at 50–70% confluence with 8 µg of circular plasmid DNA using Polyfect transfection reagent (Qiagen) according to the manufacturer's instructions. Briefly, the cells were plated at a density of 4 x 10^5 cells per 100 mm dish. After 24 h transfection, the medium was replaced with fresh prewarmed culture medium and was further incubated for 24 h prior to experiments. This assay was scaled down for smaller culture dishes. For microscopic experiments, cells were

plated out onto poly(L-lysine)-treated slides at approximate 40% confluence. 24 h after transfection, cells were fixed and permeabilised before immunostaining.

2.4.4 siRNA-mediated gene knockdown in cardiomyocytes

Small interfering RNA (siRNA) knockdown was carried out to access gene function of PKD1 protein. Cardiomyocytes were plated at a density of 2 x 10^5 cells/ well in 6-well plates. The cells were cultured in antibiotic-free normal growth media supplemented with FBS prior to transfection. A siRNA transfection kits containing siRNA specific for rat PKD1 (sc-36260), control siRNA-A (sc-37007) and siRNA transfection reagent (sc-29528) were purchased from Santa Cruz Biotechnology. The cells were transfected with control siRNA or PKD1 siRNA at a final concentration of 80 pmols according to the manufacturer's protocol. The siRNA duplex solution was added directly to the transfection reagent and incubated for 30 min at room temperature before adding drop-wise onto the cells. The cells were incubated for 5-7 h at 37 ^{o}C in a CO_2 incubator. At the end of the incubation, normal growth medium containing 2 times the normal serum and antibiotics concentration was added to the culture and incubated for an additional 24 h. The medium was then removed and replace with fresh 1x normal growth medium. Effect of PKD1 siRNA on phospho-HSP20 expression was determined 48 h post-transfection.

2.5 Preparation of cell lysates

2.5.1 Whole cell lysates

Protein extracts were prepared from cardiomyocytes and HEK293 cells. The culture media was removed and the cells were washed thrice in ice cold sterile PBS. The culture plates were drained thoroughly before adding 3T3 cell lysis buffer (50 mM NaCl, 50 mM NaF, 25 mM HEPES, 5 mM EDTA, 30 mM sodium pyrophosphate, 10% glycerol, 1% Triton X-100; pH 7.5) supplemented with protease cocktail inhibitor tablet (Roche). The cell lysates were collected using a sterile scraper and transferred into 1.5 ml Eppendorf tubes kept on ice. The tubes were placed on a rotating wheel for 30 min at 4 ^{o}C before centrifuging at 2000 x g for 10 min at 4 ^{o}C. The lysate supernatant was then snap frozen in dry ice and stored at -80 ^{o}C until required.

2.5.2 Subcellular fractionation of cardiomyocytes

Cardiomyocytes were harvested and washed twice with ice-cold phosphate-buffered saline (PBS). Subsequently, cells were fractionated into cytosolic, membrane and nuclear fractions using FractionPrepTM (BioVision, Mountain View, CA) following the manufacturer's protocol. Equal amounts of each cell lysate were used for Western blot analysis. To assess the purity of fractionation, cytoplasmic, membrane and nuclear fractions were confirmed by immunoblotting using anti-HSP90 as cytoplasmic marker, anti-GM130 as membrane marker and anti-Lamin A/C as nuclear marker, respectively. To assess subcellular distribution of a specific protein in each fraction, lysates from each fraction were subjected to SDS-PAGE and Western-immunoblotting as described in Section 2.6.4 and 2.6.5.

2.5.3 Determination of protein concentration

The protein concentration of purified recombinant proteins and cell lysates were determined according to the Bradford dye-binding method (Bradford, 1976) using dye reagent from Bio-Rad (Hampstead, U.K.). The quantification is based on the colour change of Coomassie Blue G-250 in response to various concentrations of protein. Briefly, Bradford reagent was prepared by diluting 1 part of concentrated Bio-Rad dye reagent with 4 parts of sterile water. A range of bovine serum albumin (BSA) concentrations (0-5 µg/µl) were prepared as protein standards. The protein samples were assayed in triplicates at various dilutions (1:10, 1:50) in 96-well microtitre plates followed by 200 µl of Bradford reagent added to each well. The 96-well plate was then analysed at 595 nm using an MRX microplate reader (Dynex Technologies, UK). A standard graph of absorbance against BSA concentration was plotted using least squared regression analysis to provide a relative measurement of protein concentration. The concentration of protein samples was then adjusted to account for any dilution factor.

2.6 Protein analysis

2.6.1 SDS-PAGE

Sodium dodecyl sulfate polyacrylamide (SDS-PAGE) gel electrophoresis was carried out to separate proteins according to their molecular weight. Briefly, equal concentration of protein samples were denatured and reduced in 5x SDS-PAGE sample buffer (10% SDS, 300 mM Tris-Cl; pH 6.8, 0.05% bromophenol blue, 50% glycerol, 10% β-mercaptoethanol) followed by boiling for 5 min. After brief centrifugation, protein samples were resolved on precast polyacrylamide gels (4-12% NuPAGE Novex Bis-Tris gel, Invitrogen) immersed in MOPS or MES SDS running buffer according to nature of the samples and different protein separation range. Pre-stained protein marker (Bio-Rad) was loaded to the first well of the gel while the protein samples were loaded to the subsequent wells. The gel was then run for 1 h at 200 V.

2.6.2 Coomassie staining

For direct protein visualisation, gels were removed from the precast gel cassette and stained with Coomassie blue (1.25 g Coomassie Brilliant Blue, 44% methanol [v/v], 6 % acetic acid [v/v]) and incubated for 20 min at room temperature with gentle agitation. Residual Coomassie background stain was then removed using destain solution (10% methanol [v/v], 10% acetic acid [v/v]) and incubated for 5-6 h at room temperature with gentle agitation to give clearly visible bands. The gel was washed in sterile water with 10% glycerol to prevent gel cracking following drying. The molecular weight of proteins was estimated by referring to the protein marker.

2.6.3 Western immunoblotting

For Western blotting, resolved proteins were electrotransferred onto nitrocellulose membranes (0.45 µm pore, Protran, Whatman GmbH) using X-Cell II blotting modular (Invitrogen) in Nu-PAGE transfer buffer containing 20% methanol for 2 h at 25V or overnight at 10V. Successful transfer was indicated by full transfer of the prestained molecular weight markers onto the nitrocellulose membrane. The membrane was then

blocked in 5% (w/v) non-fat dry milk (Marvel) or PhosphoBLOCKER blocking reagent (Cell Biolabs, Inc.) in TBST (20 mM Tris-Cl; pH 7.6, 150 mM NaCl, 0.1% Tween 20) for 1 h at room temperature with gentle agitation. Membranes were then probed with specific primary antibodies (Table 2.1) diluted in 1% milk/TBST solution and incubated overnight at 4 ^{o}C. The membranes were washed thrice for 10 mins each in TBST before adding appropriate horseradish peroxidise (HRP) conjugated anti-immunoglobulin G (IgG) secondary antibody diluted 1:5000 in 1% milk/TBST solution. After secondary antibody incubation, membranes were washed and detected by enhance chemiluminescence (ECL) Western Blotting Substrate (Thermo Scientific) and autoradiography. Chemiluminescent images of immunodetected bands were recorded on blue-light sensitive autoradiography X-ray films (Kodak BioMax MS, Carestream Health, Inc.) which were then developed using the Kodak® X-Omat Model 2000 processor. Immunoblots intensities were quantitatively analysed using Quantity One software (Bio-Rad) and averaged from at least three independent experiments.

Alternatively, blots could also be scanned using the Odyssey Infrared Imaging System (LI-COR Biosciences, UK) for fluorescence detection of the secondary antibodies. Fluorescence signal intensity could then be quantified using the Odyssey application software (LI-COR Biosciences, UK).

Table 2.1. List of primary antibodies used.

Antibody	Supplier	Catalogue No.	Host	Dilution	Applications
α-Actinin (sarcomeric)	Sigma	A7811	Mouse	1:800	ICC
ANP (FL-153)	Santa Cruz	sc-20158	Rabbit	1:1000	WB
α-tubulin	Abcam	ab-18251	Rabbit	1:20k	WB
GFP	Abcam	ab290	Rabbit	1:1000, 1 µl/0.4 µg	WB IP
GM130	Abcam	ab-52649	Rabbit	1:2000	WB
GST (1E5)	Santa Cruz	sc-53909	Mouse	1:1000	WB
His	Sigma	H 1029	Mouse	1:2000	WB
HSP20	Upstate	07-490	Rabbit	1:2000 1:400 1 µl/0.4 µg	WB ICC IP
HSP20	Santa Cruz	sc-51955	Mouse	1:400	ICC
HSP90	Abcam	ab13495	Rabbit	1:10k	WB
Lamin A/C	Santa Cruz	sc-56140	Mouse	1:100	WB
PDE4D5	In-house		Rabbit	1:10k	WB
Pan-PDE4D	Scottish Antibody Production Unit (SAPU)		Sheep	1:5000	WB
Phospho-HSP20 (Ser 16)	Abcam	ab58522	Rabbit	1:2000 1:400	WB ICC
Phospho-PKD (Ser 916)	Cell Signaling	2051	Rabbit	1:1000	WB
PKCµ (C-20)	Santa Cruz	sc-639	Rabbit	1:1000	WB
PKD/PKCµ	Cell Signaling	2052	Rabbit	1:1000	WB
PRKD1	Abnova	H00005587-A01	Mouse	1:400	ICC
V5	Sigma	V8137	Rabbit	1:2000 1 µl/0.4 µg	WB IP

Application key: WB=Western blot; ICC=immunocytochemistry; IP=Immunoprecipitation.

For ECL and film detection, the mouse (Amersham) and rabbit (Sigma) secondary antibodies were used at a 1:5000 concentration.

2.7 Protein-protein interactions

2.7.1 ProtoArray

ProtoArray® Human Protein Microarray v4.0 (Invitrogen) is a powerful tool to identify novel protein-protein interactions without previous knowledge of potential interactions using one common protocol. ProtoArray chips containing more than 8000 recombinant N-terminal glutathione S-transferase (GST)-tagged human proteins were used for protein interaction screening. The target proteins were expressed using a baculovirus expression system and purified under native conditions. They cover a wide range of biologically important proteins, including kinases, membrane proteins, cell signaling proteins and metabolic proteins. All proteins (including internal standard controls to verify the reliability and accuracy of the detection) are spotted in duplicates on a nitrocellulose-coated glass slide in an arrangement of 4 x 12 subarrays and 20 x 20 spots in each subarray. To compensate inter-lot variations among arrays, each microarray has a barcode for acquiring ProtoArray Lot Specific information from the ProtoArray Central Portal website (http://tools.invitrogen.com/content.cfm?pageid=10356).

To prepare the probe for ProtoArray analysis, Ultimate™ ORF clone IOH57317 (Invitrogen), containing the open reading frame (ORF) of HSP20 in pENTR221 vector, was used to generate N-terminal His-fusion protein by Gateway cloning technology into pDEST-17 vector (Invitrogen). The His-tagged HSP20 protein was expressed in *E.coli* and purified by Ni-NTA Superflow resin (Qiagen). The purity and specificity of the probe were verified by Coomassie Blue staining and Western blot with mouse monoclonal anti-His antibody (Sigma) and rabbit polyclonal anti-HSP20 antibody (Upstate-Millipore).

Briefly, the array was incubated in blocking buffer (1xPBS, 1% BSA and 0.1% Tween 20) for 1 h at 4 ^{o}C with gentle shaking to block non-specific binding. The array was then probed with 10 µM (200 µg/ml) of His-HSP20 protein in probing buffer (1xPBS, 5 mM $MgCl_2$, 0.5 mM dithiothreitol (DTT), 0.05% Triton X-100, 5% glycerol, 1% BSA) for 1.5 h at 4 ^{o}C. After washing, the array was incubated at 4 ^{o}C with mouse monoclonal anti-His antibody (Sigma) and Alexa Fluor 647 goat anti-mouse IgG (H+L) (Molecular Probes, Invitrogen) diluted 1:2000 in probing buffer for 45 min and 30 min, respectively. After washing and drying, the array was scanned by ScanArray Express Microarray Scanner (Packard Bioscience Biochip Technology, PerkinElmer) at a wavelength of 633 nm (Fig. 2.1). The results were analysed using BlueFuse for Microarrays software (BlueGnome,

Cambridge), following acquisition of the ProtoArray Lot Specific information. The Confidence Flags were used to indicate the degree of confidence showing potential interactions. A control array was also included in parallel to determine probe-specific interactions and exclude any non-specific interactions.

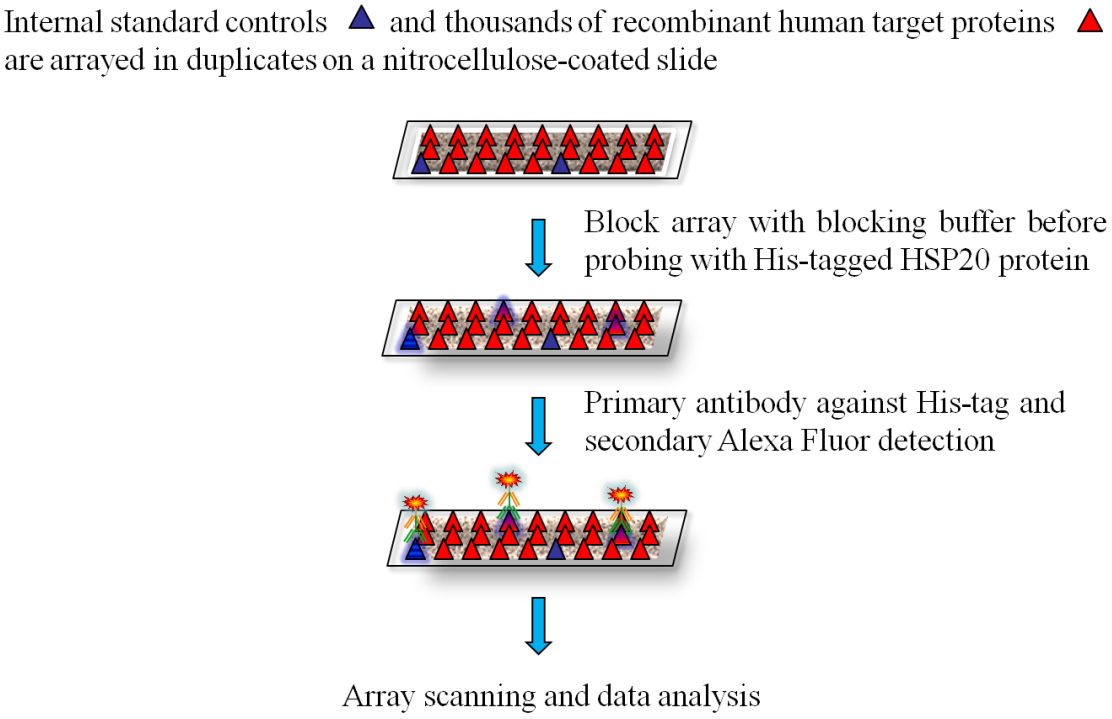

Figure 2.1. Schematic diagram showing experimental procedure used for HSP20 interactors identification on ProtoArray.

2.7.2 *In vitro* pull-down assay

In vitro pull-down assays were carried out to validate direct interactions between two or more proteins. One of the proteins of interest is expressed with an affinity tag allowing binding on a solid support while the other protein is immunolabelled for the detection of interaction. Briefly, equal molar concentrations of purified recombinant His (negative control) or His-HSP20 and PKD1 (Abcam) were mixed in 3T3 lysis buffer and incubated end-on-end with gentle agitation for 1 hour at 4 ^{o}C. Pre-equilibrated Ni-NTA Superflow resin (Qiagen) was then added to the protein cocktail and incubated with gentle agitation for another hour at 4 ^{o}C. The two proteins were allowed to interact and any protein complexes formed were captured on the beads which were then sedimented by centrifugation at 10,000 x g for 3 min, followed by washing thrice with 3T3 lysis buffer and drained. Bound proteins were eluted by boiling in SDS-PAGE sample buffer for 10 min. Proteins were then resolved by SDS-PAGE with PKD1 protein as positive control run alongside, following by blot transfer and detection by Western blotting using an anti-PKD1 antibody.

2.7.3 Co-immunoprecipitation

Co-immunoprecipitation is an *ex vivo* method for the confirmation of interactions. Cell extracts were adjusted to equal protein amount (1 µg/µl) using 3T3 lysis buffer. After preclearing, HSP20 or PKD1 and V5 or GFP antibodies were used to immunoprecipitate (IP) endogenous and over-expressed PKD1 or HSP20, respectively. The resulting immunocomplexes were captured using Protein A beads (Invitrogen) at 4 ^{o}C overnight with shaking. The immunocomplexes were then collected by centrifugation at 13 000 rpm for 3 min and washed three times with 3T3 lysis buffer. Bound proteins were then eluted in SDS-PAGE sample buffer and subjected to SDS-PAGE and Western immuno-blotting as described previously. Negative controls using isotype-matched IgG (Jackson ImmunoResearch Laboratories, Inc.) from the same species as the antibodies were included to screen for non-specific binding.

2.7.4 SPOT synthesis of peptides and overlay experiments

Peptide arrays were produced by automatic SPOT synthesis as described by Kramer and Schneider-Mergener (1998) and Frank (2002) utilising the AutoSpot-Robot ASS 222 (Intavis Bioanalytical Instruments) followed the Fmoc (9-fluorenylmethoxycarbonyl) chemistry which based on solid phase peptide synthesis methodology (Fields and Noble, 1990). The fundamental principle of this technique is the use of the spots formed upon the dispensation of a solvent droplet on the array membrane surface which serves as a reaction vessel. These peptide arrays are able to bind purified recombinant proteins and identify biologically active motifs to understand particular cellular activities. A library of overlapping 25-mer peptides, each shifted by five amino acids was produced sequentially to increase the reliability of the screening (Fig. 2.2). The immobilised spots of peptide sequences were then directly synthesised on Whatman 50 cellulose membranes as peptide arrays.

Firstly, the arrays were activated by immersion in 100% ethanol and then washed in TBST (150 mM NaCl, 0.1% Tween20, 20 mM Tris-HCl, pH 7.6) to remove all preservative materials. This was followed by blocking with 5% milk (Marvel) dissolved in TBST for 1 h at room temperature with shaking. 10 µg/ml of recombinant fusion protein diluted in 1% milk dissolved in TBST was added onto the arrays and incubated at 4 ^{o}C overnight with shaking. The arrays were then subjected to three 10 min washes in TBST. The interaction of spotted peptides with protein of interest was detected with a specific primary antibody. After 1h incubation, the arrays were washed several times before adding secondary antibody coupled with horseradish peroxidase (HRP) diluted in 1% milk TBST solution for 1 h at room temperature. The arrays were again washed several times with TBST before subjected to enhanced chemiluminescence (ECL) Western immuno-blotting kit for autoradiography as described previously. The dark spots detected were indicative of a positive interaction of the recombinant fusion protein with the peptide array.

Scanning alanine substitution analyses was performed to determine the specific amino acid residue(s) which are important to the functionality or stability of a given protein (Morrison and Weiss, 2001). Amino acid residues were replaced with alanine (A) one at a time unless the indicated amino acid was alanine (A), when it would be substituted for aspartate (D). Control spots with known binding affinity to the protein of interest were also included for calibration purpose and comparative measurement of binding affinity. The arrays were immunolabelled and detected by autoradiography as described above

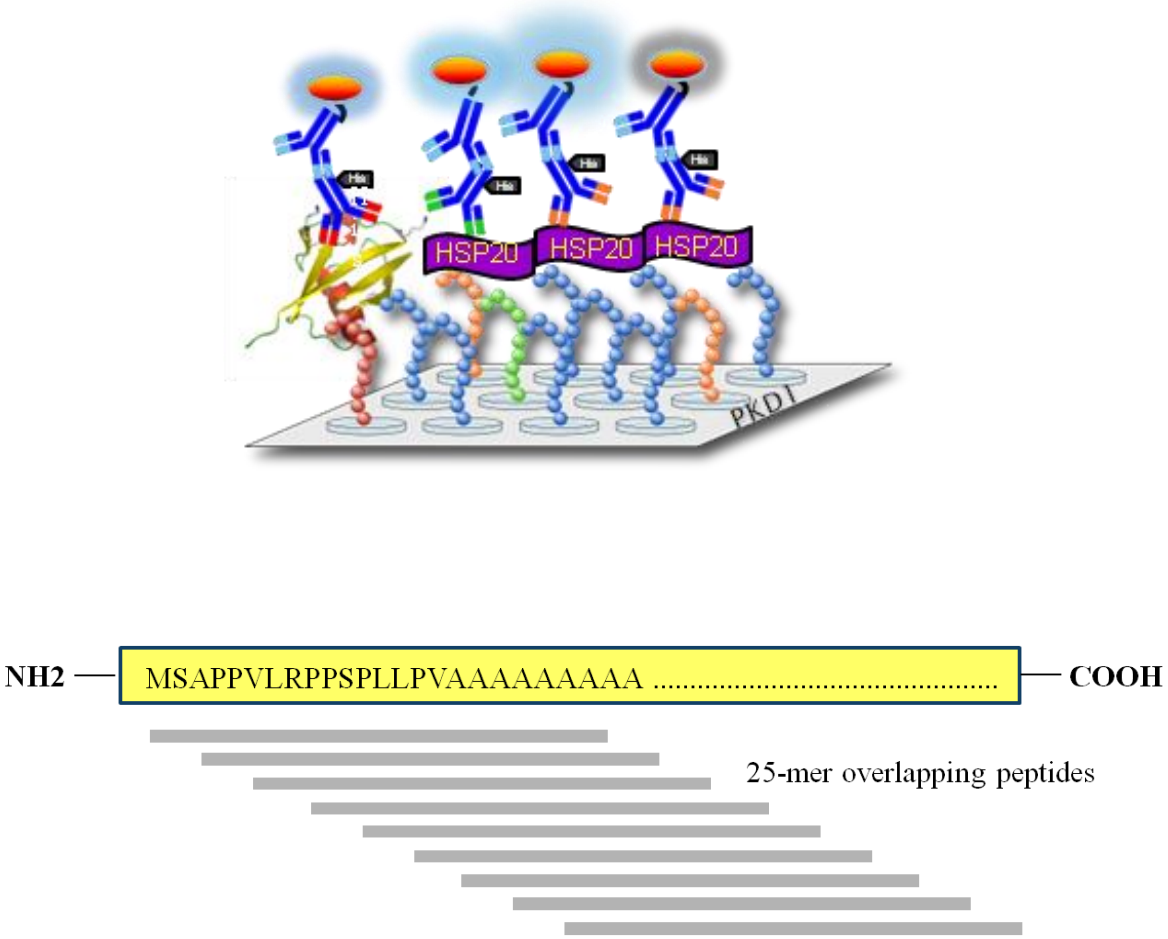

Figure 2.2. Schematic diagram showing SPOT synthesis of peptide. Immobilised peptide spots of overlapping 25-mer peptides each shifted by five amino acids across the entire PKD1 sequence were probed for interaction with a purified His-HSP20 probe and detection with anti-His antibody.

2.8 *In vitro* phosphorylation assays

2.8.1 *In vitro* phosphorylation of His-HSP20

A range of purified His-HSP20 concentration (0.5-2 µg) was incubated with 1.0 g/ml or without active PKD1 protein (Abcam) in PKD phosphorylation buffer (20 mM Tris-HCl; pH 7.5, 10 mM $MgCl_2$, 0.5 mM $CaCl_2$, 1 mM DTT, 0.2 mg/ml BSA) supplemented with 100 µM adenosine-5'-triphosphate (ATP) for 1 h at 30 ^oC with agitation. The phosphorylated protein was then subjected to SDS-PAGE and immunoblotted with an anti-phospho-HSP20 (Ser 16) antibody.

2.8.2 *In vitro* phosphorylation of peptide array

Phosphorylation of HSP20 peptide array was carried out to identify phosphorylation site(s) by PKD. Briefly, the peptide array membrane was soaked in 100% ethanol to activate it and washed with TBST, followed by overnight blocking in 5% phosphoblocker containing 0.5 mM DTT and 1 mM ATP at 4 ^oC. The membrane was then reacted with PKD phosphorylation buffer (20 mM Tris-HCl; pH 7.5, 10 mM $MgCl_2$, 0.5 mM $CaCl_2$, 1 mM DTT, 0.2 mg/ml BSA, 1 mM ATP) supplemented with 10 µg of active PKD1 (Abcam) and 5 µCi (0.185 MBq) of [γ-^{32}P] ATP EasyTides (Perkin Elmer, UK) for 30 min at 37 ^oC with gentle agitation. After the phosphorylation reaction, the membrane was washed extensively with 1 M NaCl followed by 5% H_3PO_4 and finally ethanol. The membrane was air dry and placed in intensifying screen cassette (Kodak BioMax MS, Carestream Health, Inc.) for a week before developing using the Kodak® X-Omat Model 2000 processor.

2.9 Cell-based experiments

2.9.1 Manual measurements of cell size

Cardiomyocytes were plated out on gelatin (Sigma) pre-coated 6-well plates and placed in an incubator at 37 °C and an atmosphere of 5% CO_2. After 24 h the cardiomyocytes were cultured in a serum-free condition for 48 h before experiments. The cardiomyocytes were

then challenged for 24 h with either 10 μM ISO alone or ISO following a 2 h pre-treatment with disruptor or control peptide. Thereafter, cell size was determined on a phase contrast Nikon Eclipse TE2000-S microscope (Nikon, UK) under 400× magnification. About 100 cells from several randomly chosen fields were captured digitally by a Nikon UFX-DX II camera (Nikon, Japan) and analysed. Cross-sectional area was determined by the following formula: cross-sectional area = $(\text{radius})^2 \times \pi$. Values are expressed as means ± S.E.M. of five separate culture preparations. A Student's *t*-test was performed to compare the two groups, and the *P* values are indicated.

2.9.2 Real-time xCELLigence measurements

The xCELLigence technology (Roche Applied Science) which allows a quantitative measurement of the cell size through real-time cell-electronic sensing (RT-CES) was used according to the manufacturer's instruction. As cardiomyocytes are unable to divide, they tend to increase in cell volume in respond to stress. And this method allowed us to observe the change in impedance which is automatically converted to cell index and provides quantitative measurement that reflects the nature of the cells, i.e. cell size.

Cardiomyocytes were counted using a haemocytometer and adjusted to the desired concentration. An initial population of 40,000 cardiomyocytes/well was plated out on the laminin (BD Biosciences) pre-coated E-Plate 96 (Roche) in triplicates after background measurements were taken. Briefly after 48 h of culture in the serum-free medium, cardiomyocytes were treated with either 10 μM isoprenaline alone or isoprenaline following a 30 min or 2 h pre-treatment with peptides. Controls with vehicle (DMSO alone) were also performed. The cultures were continuously monitored for up to 48 h and the impedance as reflected by cell index (CI) values was set to record every 30 min. The xCELLigence data were then analysed using the RTCA software (Roche Applied Science). The results were expressed by normalised CI, which are derived from the ratio of CIs before and after the addition of compounds.

2.9.3 Measurement of protein content

Cardiomyocytes were plated on six-well plates and cultured in a serum-free condition for 48 h before experiments. After stimulation of cardiomyocytes (2 h of compound + 24 h of ISO or 24 h of ISO alone), each well was rinsed three times with cold PBS. The cells were then scraped with 1 ml of 1× standard sodium citrate (SSC) containing 0.25% (w/v) SDS and vortexed extensively. The total cell protein and the DNA content were determined by the Ohnishi & Barr modified Lowry method and the Hoechst dye method using Total Protein Kit (Sigma #TP0200) and DNA Quantitation Kit (Sigma #DNA-QF), respectively. The protein content was normalised by the DNA amount to correct for differences in the cell number.

2.9.4 Disruptor peptide synthesis

All peptides were synthesized by Genscript and dissolved in DMSO to a stock concentration of 10 mM and then used at a final working concentration of 10 μM (Table 2.2). Based on the information gathered from peptide arrays, cell-permeable peptides which allow transport across the cell membrane were synthesised with a stearic acid group ($CH_3(CH_2)_{16}COOH$) attached to the N-terminus.

Table 2.2. Synthesised peptides used in this study.

Peptide name	Sequences
PDE4D5-HSP20 disruptor peptide 'bs906'	ENHHLAVGFKLLQEENSDIFQNLTK
scrambled peptide	KELGAINHEFDLSHNFQTQKLNLVE
PKD1-HSP20 disruptor peptide 'HJL09'	GRDVAIKIIDKLRFPTKQESQLRNE
control peptide	GAAVAIKIIAKLRFPTKQESQLRNE

2.10 Quantitative real-time PCR analysis of fetal gene expression

Real-time PCR has been widely used to determine relative gene expression. This detection method is based on the changes of fluorescence accumulation during thermocycling which can be reflected on a sigmoidal amplification plot and give a quantitative result of the amplified product (Kubista *et al*., 2006). Variability in qPCR can be influenced by steps upstream which consist of template preparation and reverse transcription.

2.10.1 RNA extraction

Total RNA was extracted using TRIzol reagent (Invitrogen) which contained phenol and guanidine thiocyanate in a procedure based on the method of Chomczynski and Sacchi (1987). Cells were first rinsed with PBS and subsequently lysed in TRI reagent for 5 min at room temperature. RNA was separated from DNA and protein by extraction with chloroform. The aqueous phase was then precipitated with ½ volume of isopropanol and spun at 12,000 x g for 15 min at 4 ^{o}C. The precipitate containing the RNA was then washed with 75% ethanol, centrifuged at 7,500 x g for 5 min, followed by air drying for 10 min at room temperature. RNA was then resuspended in Ambion® nuclease-free water (Invitrogen) and subsequently purified with the RNeasy Mini Kit (Qiagen). To remove genomic DNA contamination, the isolated RNA was subjected to RNase-free DNase I (Roche) digestion for 30 min at 37 ^{o}C. The reaction was terminated by adding 1 µl of 25 mM EDTA and incubated at 65 ^{o}C for 10 min. Total RNA was quantified using the Nanodrop 3300 spectrophotometer (Thermo Scientific).

2.10.2 Reverse transcription of PCR

One microgram of DNase-digested total RNA was reverse-transcribed to first strand complementary DNA (cDNA) using AffinityScript Multiple Temperature cDNA synthesis kit (Agilent, Edinburgh, UK) according to manufacturer's instructions. The total RNA was first incubated with 0.5 µg of oligo(dT) primer for 5 min at 65 ^{o}C to remove any secondary structures in the RNA. Oligo(dT) primer was used in this experiment as it only binds to the

poly-A tail of the RNA and only transcribes RNA. Consequently, oligo(dT) shows better specificity than other primers such as random hexamer primer, thus producing more consistent RT-PCR. The reaction was then cooled to room temperature for 10 min to allow the primers to anneal to the RNA. A reaction mixture containing 2 µl of 10x AffinityScript RT buffer, 2 µl of 100 mM DTT, 0.8 µl of 100 mM dNTP mix (25 mM each dNTP), 20 units of RNase Block Ribonuclease Inhibitor and 1 µl of reverse transcriptase (RT) was added to the RNA/oligo(dT) primer mixture mentioned above and incubated at 42 ^{o}C for 1 h. The reaction was then terminated by heating at 70 ^{o}C for 15 min and subsequently chilled on ice. The cDNA was diluted to 10 ng/µl with nuclease-free water and stored at -20 ^{o}C until use. For negative controls, 1 µl of nuclease-free water was added in place of RT.

2.10.3 TaqMan real-time PCR

Gene-specific TaqMan probes and PCR primers sets (Eurofins MWG operon) were designed assisted by the Primer 3 software (http://frodo.wi.mit.edu/primer3/) as shown in Table 2.3. If possible, the primers were designed to span an exon-intron-exon boundary to exclude amplification of genomic DNA. 18S rRNA was used as an internal control for normalising relative expression levels in the different samples. Real-time PCR was performed from reverse transcribed cDNA samples using the Platinum Quantitative PCR SuperMix-UDG with ROX (Invitrogen) following the manufacturer's instructions. Briefly, 100 ng of cDNA were added to a 96-well MicroAmp® Fast Optical Reaction Plate (applied Biosystems) with 12.5 µl TaqMan probe mix, 1 µl each of the 10 µM primer pair and 0.25 µl of 10 µM fluorogenic probe (either gene-specific inventoried assays or endogenous reference assays). Thermal cycling and fluorescent monitoring were performed using the ABI Prism 7700 Sequence Detection System (Applied Biosystems). Each PCR amplification was run in triplicate using the following conditions: initial denaturation at 95 °C for 2 min, followed by a total of 40 cycles (15 sec at 95 °C for denaturation, 15 sec at 57 °C for annealing and 1 min at 60 °C for extension). Fluorescence data were collected during the extension step of each cycle. Negative controls using RNA as template were also included in all runs to test for the presence of genomic DNA contamination.

Table 2.3. Sequences of oligonucleotide primer-probe sets used in quantitative real-time PCR assay. All assays contain sequence-specific unlabelled primers pair and a TaqMan probe labelled with a fluorophore FAM attached to the 5' end and a quencher TAMRA on the 3' end. Rat 18s rRNA was used as an endogenous control.

Gene	Oligonucleotide sequence	Accession No.
Atrial natriuretic factor (ANF)	Forward: 5'-GGATTGGAGCCCAGAGCGGAC-3' Reverse: 5'-CGCAAGGGCTTGGGATCTTTTGC-3' Probe: 5'-AGGCTGCAACAGCTTCCGGT-3'	NM_012612
Brain natriuretic peptide (BNF)	Forward: 5'-AGCCAGTCTCCAGAACAATCCACG-3' Reverse: 5'-AGGGCCTTGGTCCTTTGAGAGC-3' Probe: 5'-GCTGCTGGAGCTGATAAGAGAAAAGT-3'	NM_031545
β-myosin heavy chain (β-MHC)	Forward: 5'-CCAACACCAACCTGTCCAA-3' Reverse: 5'-CAGCTTGTTGACCTGGGACT-3' Probe: 5'-CTGGATGAGGCAGAGGAGAG-3'	NM_017240
Rat 18S rRNA	Forward: 5'-CGCGGTTCTATTTTGTTGGT-3' Reverse: 5'-CGGTCCAAGAATTTCACCTC-3' Probe: 5'-TGAGGCCATGATTAAGAGGG-3'	M11188.1

2.10.4 qPCR data analysis

Relative changes in gene expression of the three target genes (listed in Table 2.3) in different samples were quantified using the comparative Ct method (ΔΔCt) as described by Livak and Schmittgen (2001). The objective of this method is to compare the PCR signal of a target gene in a treatment group to the untreated control after normalising to an endogenous reference gene. Firstly, the point at which the PCR was detected above a set threshold in exponential phase, termed threshold cycle (Ct), was obtained from the real-time PCR instrumentation. Ct is determined from a log-linear curve where PCR signal is plotted against the cycle number. The Ct values of each sample were then imported into Microsoft Excel and the average Ct of triplicate samples was calculated. The amount detected at a certain cycle number is directly related to the initial amount of target in the

sample. Hence, to determine the quantity of gene-specific transcripts present in cDNA, Ct values for each treatment had to be normalised first to obtain ΔCt. This was accomplished by subtracting the mean Ct value of endogenous reference gene 18s rRNA of each group from the corresponding mean Ct value of gene of interest (GOI) accordingly ($\Delta Ct = Ct_{GOI} - Ct_{18s\ rRNA}$). The concentration of gene-specific mRNA in treated cells relative to untreated cells was then normalised through subtraction again to obtain ΔΔCt values (ΔΔCt = ΔCt of treated cells - ΔCt of untreated cells). Finally, the relative expression which is often termed as RQ value was determined by raising 2 to the power of the negative value of ΔΔCt ($2^{-\Delta\Delta Ct}$) for each sample (Amount of target = $2^{-\Delta\Delta Ct}$). Alteration in mRNA expression of target genes was defined as fold difference in the expression level in cells after the treatment relative to that before treatment. Samples with poor technical replicate values were excluded from analysis.

2.11 Microscopic analyses

2.11.1 Differential interference contrast microscopy

Differential interference contrast (DIC) microscopy also known as Nomarski microscopy is extremely useful for resolving individual transparent living cells. This method allows observation of unstained specimens by generation of monochromatic shadow-cast image laminin-coated contrast through different refractive index gradients. Cardiomyocytes were seeded on coverslips and placed in extracellular buffer (140 mM NaCl, 3 mM KCl, 2 mM, $MgCl_2.6H_2O$, 2 mM $CaCl_2.2H_2O$, 15 mM Glucose, 10 mM HEPES; pH 7.2). The cells were then observed under a Nikon Eclipse FN-1 microscope equipped with DIC optics. Images were captured on a CoolSNAP HQ2 monochrome camera (Photometrics, UK) using an image acquisition software (Opto-Fluor Version 7.6.3.0, Cairn Research Ltd, Kent).

2.11.2 Immunostaining and confocal microscopy

For immunofluorescent labeling, cardiomyocytes were plated onto laminin-coated 8-well chamber slides (Lab-Tek, Sigma). Cells were fixed in 95% ice-cold methanol/ 5% acetone mixture at -20 ^{o}C for 10 min and permeabilised with 0.1% Triton X-100 in PBS for 10 min at room temperature. After several washes with Tris-buffered saline (TBS) (150 mM NaCl, 20 mM Tris-HCl, pH 7.6), the cells were blocked with 10% donkey serum and 2% BSA (w/v) in TBS for 2 h followed by three washes with TBS. The primary antibodies used was diluted to the required concentration in blocking buffer diluted 1:1 with TBS and added to the cells for 2 h followed by three washes with TBS. After washing, cells were incubated with 1:400 diluted secondary antibodies Alexa Fluor 488 donkey anti-mouse IgG and Alexa Fluor 594 donkey anti-rabbit IgG (Molecular Probes) for 1 h. Following several extensive washes with TBS, the slides were dehydrated and mounted under coverslips with ProLong Gold anti-fade reagent with 4',6-diamidino-2-phenylindole (DAPI) nuclear stain (Invitrogen). Staining was visualized using a Zeiss Pascal laser-scanning confocal microscope (LSM) 510 Meta and an Axiovert 100 microscope (Carl Zeiss, UK) equipped with an oil immersion objective (63x/1.4 NA plan apochromat lens). Images were captured and processed on Zeiss LSM Image Examiner and analysed using the NIH Image J software (ImageJ, http://rsb.info.nih.gov/ij/). All incubations were carried out at room temperature unless stated otherwise.

2.11.3 Phalloidin staining of actin

Phalloidin staining was carried out for visualisation of the actin cytoskeleton. Cardiomyocytes were cultured on laminin-coated 8-well chamber slides (Lab-Tek, Sigma). Cells were maintained in serum-free media for 48 h before treated with peptides for 2 h prior to hypertrophy induction by ISO for 24 h. The cells were then washed with PBS, fixed with 3.7% methanol-free formaldehyde in PBS for 10 min at room temperature, followed by permeabilisation with 0.1% Triton X-100 in PBS for 10 min and washing twice again with PBS. Actin fibers were stained with Alexa Fluor 488 phalloidin (Molecular Probes, Invitrogen) diluted 1:500 in PBS for 30 min at room temperature and washed thrice in PBS. DAPI was used for nuclear counterstain. Finally, the slides were dried and mounted for laser scanning confocal microscopy as described previously.

2.11.4 Duolink™ proximity ligation assay

PKD1 association with HSP20 was investigated further by using a more sophisticated *in situ* analysis of protein interactions, i.e. the Duolink™ Proximity Ligation Assay (PLA) (Olink Bioscience, Uppsala, Sweden). Besides determining the subcellular localisation of the interacting complex, this method also allows the study of the dynamics of the interactions in intact living cells (Söderberg *et al*., 2008, Bellucci *et al*., 2011). After fixation, permeabilisation and blocking, slides were incubated with primary antibodies against PKD1 and HSP20 raised in two different species. Then PLA probes, which are conjugated with oligonucleotides, were introduced to recognise the primary antibodies. A solution that promotes hybridization between the PLA oligos was then added, where a hybridisation reaction only occurred if the two proteins were in close proximity (<40 nm), but not if they were far apart. This reaction was followed by ligation of the oligonucleotides and a rolling circle amplification (RCA) reaction, where a repeated sequence product was made. This product was then detected using fluorescently labeled oligonucleotides, where a PKD1-HSP20 association appeared as discrete red dots under the microscope (Fig. 2.3).

To confirm where the PKD1-HSP20 associations occur in the cardiomyocytes, cells were counterstained with α-actinin to show sarcomeric stained. Slides were finally mounted under coverslips with DUOLINK mounting media, and observed using the Zeiss Pascal laser-scanning microscope (LSM510 Meta (Carl Zeiss, UK) as described above.

2.12 Statistical analysis

Values are presented as mean ± S.E.M. from at least three independent experiments. Statistical significances between groups were determined by the use of Student's *t*-test. Values were considered significant if $p < 0.05$. Where representative immunoblots or immunocytochemistry images were shown, similar data were obtained ≥ 3 times.

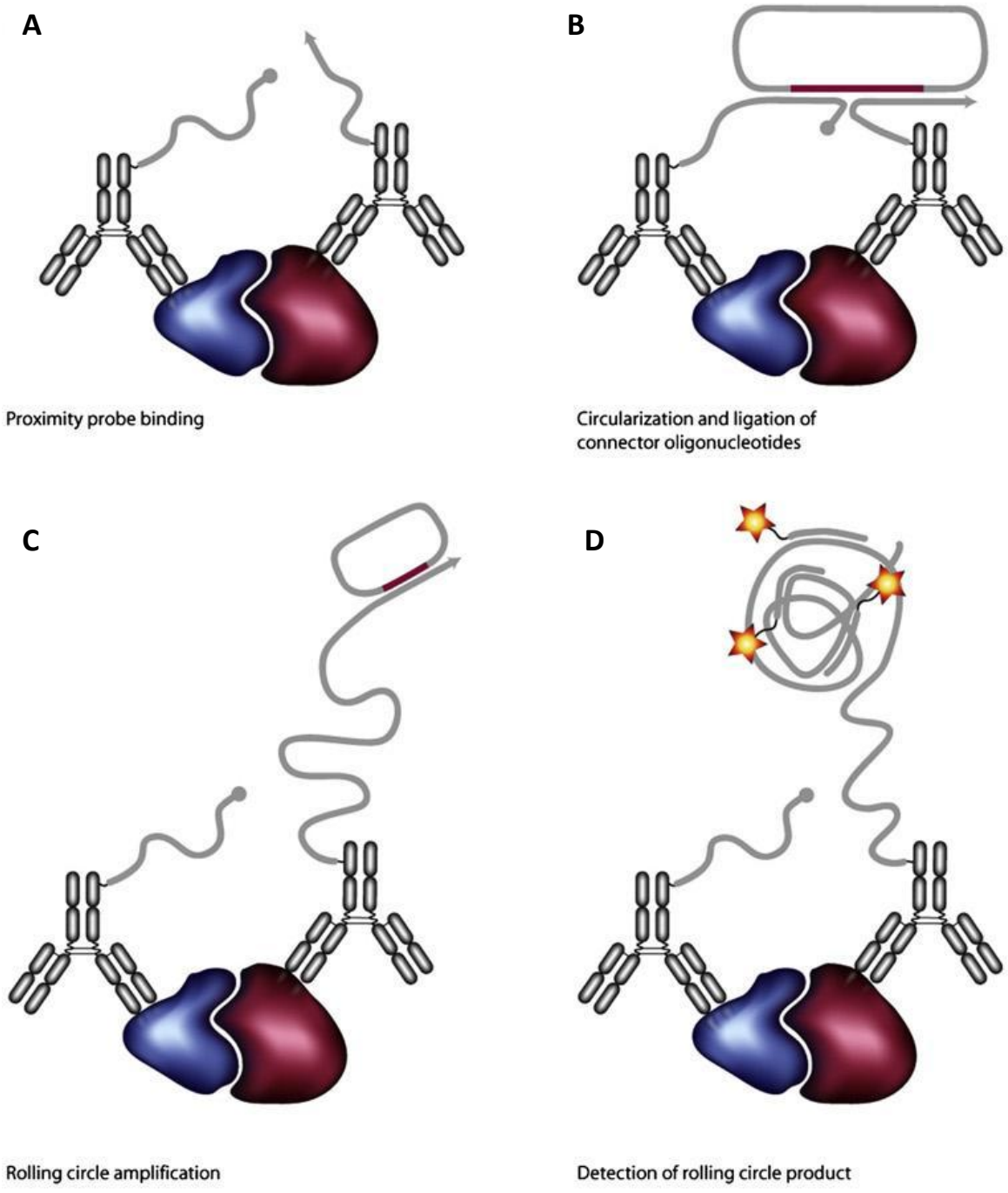

Figure 2.3. Schematic diagram of *in situ* PLA. (A) Cells are incubated with target specific primary antibodies raised in two different species. A pair of PLA probes (PLUS and MINUS) with unique DNA strand attached are added and bind their respective primary antibody. (B) When in tight nearness, the two DNA strands can interact through circle-forming DNA oligonucleotides which are then joined by enzymatic ligation. (C) and (D) Rolling-circle amplification by polymerase and fluorescent probes are hybridised to the synthesised DNA strand allowing the product to be visualised. (Adapted from Söderberg *et al*., 2008).

Chapter 3

Disruption of the cAMP PDE4D5-HSP20 complex attenuates β-agonist induced hypertrophic response in cardiomyocytes

3.1 Introduction

Cell signalling is the process by which extracellular stimuli are interpreted to elicit a specific intracellular response that acts to coordinate cell activities. The mechanisms that underpin signal transduction in cells are complex and involve many signalling components. Generally, signal transduction from the outside of a cell to its inner compartments involves three main steps: receptor activation, signal transmission and target cell response. Although the agonist action on cell surface receptors can trigger a variety of intracellular signalling events, the ligand-receptor interaction and their downstream responses are very specific. For example, signals initiated by hormones and neurotransmitters commence via activation of specialised receptors such as plasma membrane localised transmembrane G-protein-coupled receptors (GPCRs). These in turn activate intracellular messenger molecules and result in a relevant physiological response in cells. Any error in the cellular transduction cascade will thus lead to diseases. Hence, understanding of cell signalling networks are essential.

3.1.1 cAMP signalling and compartmentalisation

3',5'-cyclic adenosine monophosphate (cAMP) is a ubiquitous key second messenger, which is involved in a wide variety of intracellular signal transduction cascades that usually start with a receptor stimulation (Beavo and Brunton, 2002). cAMP is generated by adenylyl cyclases following stimulation of transmembrane receptors such as β_2-adrenergic receptors (β_2AR). GPCRs are seven transmembrane-spanning helices which interact with heterotrimeric G proteins (comprised of a GDP/GTP-binding α, β, and γ subunits) (Wheeler-Jones, 2005). Regulation of GPCR signalling involves rapid attenuation of receptor responsiveness (desensitisation) and resensitisation which alter the availability of receptors to be stimulated, and up- or down-regulate receptor expression.

The β_2AR generates signal specificity by interacting with a member of the heterotrimeric G protein family, the stimulatory G protein (G_s) (Houslay *et al.*, 2007). This causes activation of G_s via GDP-GTP exchange on the G_α subunit, follow by the release of $G_{\beta\gamma}$ subunit, thereby stimulating membrane bound adenylyl cyclase (AC) activity and leading to the production of a cAMP cloud (Cooper, 2003). The increase in intracellular levels of cAMP at the inner surface of the plasma membrane can then activate downstream effectors such

as protein kinase A (PKA), exchange protein activated by cAMP (Epac) and cyclic nucleotide gated ion channels, which in turn trigger downstream signals that lead to the regulation of various cellular processes including proliferation, differentiation and movement, apoptosis and cardiac function (Tasken and Aandahl, 2004; Houslay *et al*., 2007).

cAMP is freely diffusible within the cell and the specificity of receptor response is achieved by the generation of cAMP signalling microdomains as generally visualised using fluorescence-resonance-energy-transfer (FRET)-based approaches (Zaccolo and Pozzan, 2002; Mongillo 2004). This high temporal and spatial resolution technique is a useful tool to investigate the dynamics of molecular interactions in living cells based on the ability of a high energy fluorophore (donor) to transfer energy to a lower energy fluorophore (acceptor) particularly when the two molecules are in close proximity (<10 nm). Hence, a change in fluorescence signal strength will reflect a conformational change upon cAMP binding (Terrin *et al*., 2006). The investigations clearly showed that the gradients of cAMP are depending on the source of cAMP generation by AC located at discrete intracellular loci. It is well accepted that the compartmentalised cAMP gradient which mediates the activation of intracellular effectors, most notably PKA is regulated by PDEs. This regulation greatly depends on the degradation of cAMP to 5' AMP, thereby preventing cAMP saturation in the cell interior (Lugnier, 2006).

Using genetically encoded sensors based upon either PKA or the cAMP binding domain of EPAC, cAMP gradients were shown to be dynamically formed and shaped by tethered PDEs which provide physical barriers to free diffusion of cAMP from restricted microenvironments (Mongillo *et al*., 2004). However, later studies using siRNA-mediated knockdown of cAMP-dependent PDE4 in HEK293 cells showed that cAMP microdomains do not require impeded diffusion or diffusional barriers. In fact, cAMP degradation and intracellular gradients were actually achieved by tethered PDEs forming localised cAMP sinks (Terrin *et al*., 2006). It is thought that the PDEs regulate the magnitude and duration of cAMP gradients by acting as sinks to locally drain cAMP and preclude inappropriate activation of downstream substrates resulting from fluctuations in basal cAMP levels (Baillie, 2009). Interestingly, silencing of PDE4D was shown to disrupt cAMP microdomains, but this was not the case for silencing of PDE4B, further confirming that PDE4D is mainly responsible for the integrity and duration of cAMP microdomains. Seemingly, PDE4D decreases cAMP concentration in the cytosol more than in the submembrane region (Terrin *et al*., 2006). It was also noted that sink size greatly depends

on the tethered PDE and localised elevation in cAMP is regulated by high PDE activity. Indeed, PDE4 activity is enhanced by PKA phosphorylation since a PKA inhibitor, H89 was shown to eliminate cAMP microdomains measured using the FRET sensor, thereby suggesting a role of PKA-mediated phosphorylation of PDE on cAMP dynamics (Terrin *et al*., 2006).

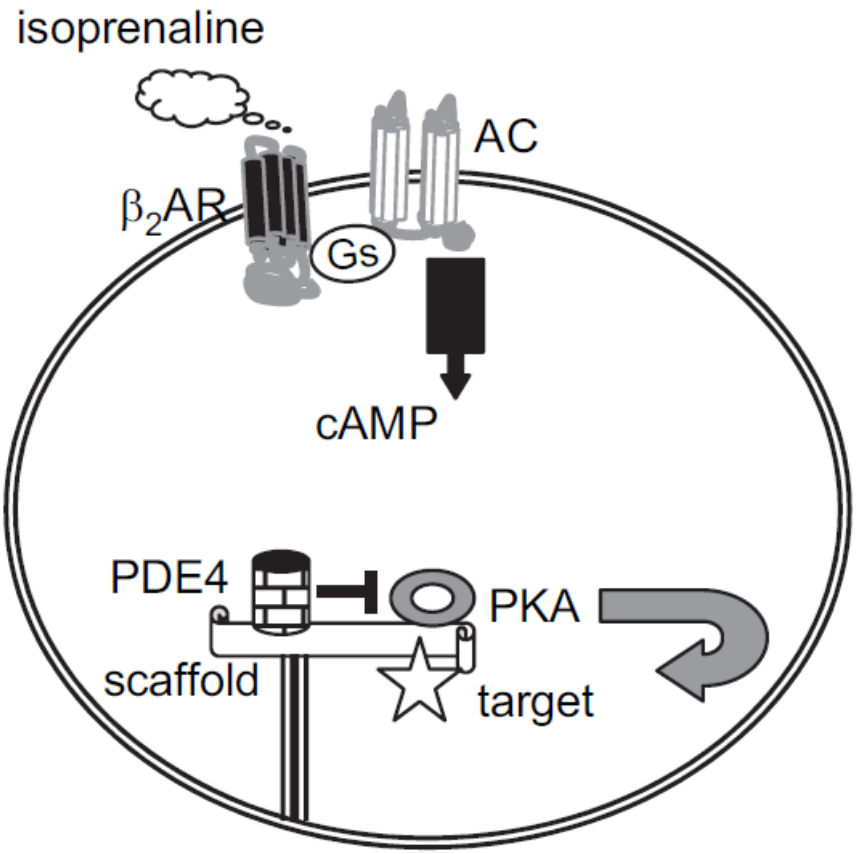

Figure 3.1. The cAMP signalling cascade. Under ISO stimulation in response to physiological stress, *β*-adrenergic transmembrane receptor couples to the stimulatory G protein (G_s), thereby activating effector protein adenylyl cyclase (AC) which are mostly embedded in the cell surface plasma membrane. AC generates intracellular cAMP which then rapidly diffuses into the cell cytosol and activates PKA that phosphorylates downstream substrates. The PDEs which anchors the AKAP scaffold modulates the intensity and duration of cAMP through hydrolysis (Adapted from Houslay, 2007).

3.1.2 PDE family

Phosphodiesterases (PDEs) serve as major regulators of cAMP signal transduction as they dynamically control localised pools of cAMP by breaking cAMP down to 5' AMP to underpin specificity of physiological responses (Houslay *et al*., 2007). There are different isoforms of PDEs that are located at distinct intracellular locations and possess different affinities for cAMP (Stangherlin and Zaccolo, 2012). Generally, the PDEs are classified into 11 gene families (PDE1-11) based on their sequence homology, substrate specificity, regulatory and kinetic characteristics. Three families specifically hydrolyse cAMP (PDE4, 7, 8), three families specifically hydrolyse cGMP (PDE5, 6, 9), and the others hydrolyse both cAMP and cGMP (PDE1, 2, 3, 10, 11). This happens in selected functional compartments upon stimulus-specific receptor activation. (Lugnier, 2006; Conti and Beavo, 2007). Within each family, PDEs can have several genes and each gene can have multiple gene products. This leads to many different isoforms within PDE families, PDE4 for example, has over 25 different isoforms. The different isoforms share identical catalytic units and are a result of alternative mRNA splicing coupled to the use of distinct promoters.

PDEs exhibit tissue- and cell-specific expression where the cAMP levels are controlled by the specific PDE isoforms in different subcellular compartments and at different times in response to different stimuli. There are nine PDE families expressed in cardiovascular system, i.e. PDE1, 2, 3, 4, 5, 6, 7, 8, and 9 (Francis *et al*., 2011). In particular, members of the PDE3 and PDE4 families play pivotal roles in modulation and compartmentation of the cAMP signal in heart, contributing about 90% of the total cAMP hydrolysis (Richter *et al*., 2005). Using genetically encoded FRET optical sensors in neonatal rat ventricular myocytes (NRVMs), β-AR stimulation was shown to generate localised increases in cAMP levels at the sarcomeric Z lines (Zaccolo and Pozzan, 2002). Further evidence showed that PDE4B is localised at the plasma membrane, whilst PDE4D is mainly distributed throughout the cytosol (Terrin *et al*., 2006). Clearly, these two isoforms are spatially organised to modulate the cAMP levels in specific subcellular compartments. Of them all, PDE4D has been studied extensively in heart. Hence, this chapter will focus on the role of PDE4D family in cAMP signal compartmentation.

3.1.3 PDE4 structure and isoforms

The PDE4 family is highly evolutionarily conserved and is encoded by four genes, namely PDE4A, PDE4B, PDE4C and PDE4D (Houslay and Adams, 2003). These four PDE4 genes further encode 25 different isoforms that are characterised by a unique N-terminal region which confers intracellular targeting of the enzymes. This isoformity is a result of alternative mRNA splicing coupled to the use of different promoters which allow cells to express numerous PDE4 enzymes (Houslay and Adams, 2003). PDE4 isoforms consist of two upstream conserved regions (UCR1 and UCR2) which are joined together by two regions known as linker region 1 (LR1) and linker region 2 (LR2) (Fig. 3.2). UCR1 and UCR2 are involved in the regulation of the PDE4 catalytic unit through phosphorylation of PKA (MacKenzie *et al*., 2000, 2002). However, the functional significance of the two linker regions is still unknown. In addition, there is a highly conserved catalytic unit common to all PDE4s and a C-terminal region, which is unique to each of the four PDE4 subfamilies. The catalytic unit contains a serine within the consensus site PQSP which allows phosphorylation by ERK to modulate PDE activity (MacKenzie *et al*., 2000). Recent findings have revealed a binding pocket for cAMP in the PDE4 catalytic unit, which contains tightly bound Zn^{2+} and loosely bound Mg^{2+} (Houslay and Adam, 2003). It is thought that PDE4 activation by PKA phosphorylation is determined by the concentration of Mg^{2+}. There is also a kinase interaction motif (KIM) docking site (VxxKKxxxxxxLL) located at the N-terminal to the target serine, and an ERK specific binding motif (FQF) at the C-terminal to the target serine.

PDE4 isoforms can be subcategorised as dead-short, super-short, short and long as indicated in Fig. 3.2 due to distinct splicing mechanisms rendering different combinations of the UCR1 and UCR2 domains (Houslay and Adams, 2003; Houslay *et al*., 2007). The long forms which are most common kind within the PDE4 subfamily, possess a full intact UCR and LR regions. These isoforms can be phosphorylated by PKA at the serine residue within the conserved RRESF motif (MacKenzie *et al*., 2002). This results in an increase in PDE activity, thereby leading to cAMP desensitisation in cells where these isoforms are selectively expressed, for example, in cardiomyocytes (Mongillo *et al*., 2004). Alternatively, PDE phosphorylation by PKA can form a feedback loop whereby localised cAMP levels are further decreased to reduce PKA activity, thereby allowing the dephosphorylation of PDE to reset the system. In contrast, the super-short and short forms lack UCR1 and LR1 but contain a truncated and intact UCR2, respectively. The dead-short isoforms do not have the regulatory and linker regions and are both N- and C- terminally

truncated. Since it is enzymatically inactive and has survived through evolution, it is speculated that it may be involved in protein scaffolding (Johnston *et al*., 2004). Interestingly, the functional outcome of ERK phosphorylation of PDE4s is dependent on the presence or absence of the two UCRs, where in long isoforms they confer inhibition but in short isoforms confer activation and in super-short isoforms, weak inhibition (MacKenzie *et al*., 2000). In other words, cAMP signalling is modulated by ERK activation depending on the types of isoform expressed. Interestingly, PKA phosphorylation can be induced by ERK-mediated PDE4 longform inhibition, which in turn leads to an increase in cAMP levels and activation of PKA (Houslay *et al*., 2007).

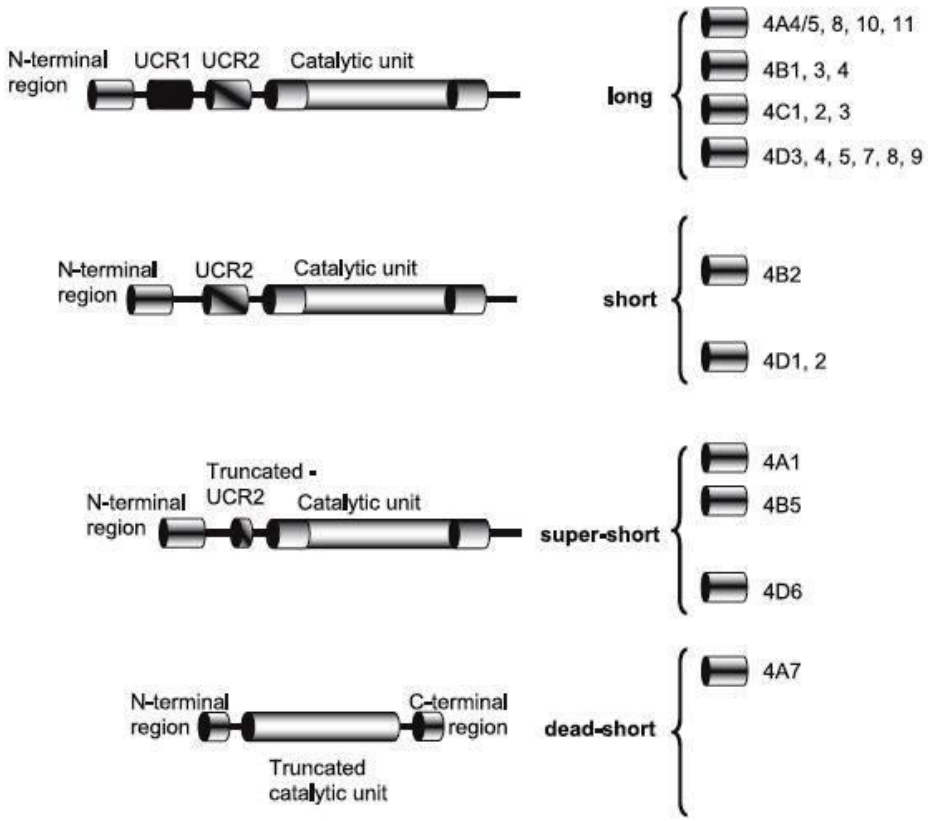

Figure 3.2. Structure and encoding of PDE4 isoforms. Different mRNA splicing resulted in the long and short of PDE4 isoforms, categorised according to their unique N-terminal targeting region. Sites for PKA-mediated phosphorylation and ERK-mediated phosphorylation are depicted as red and black circle, respectively. LR1, Linker Region 1; LR2, Linker Region 2; CTR, C-terminal region; NTR, N-terminal region. (Adapted from Houslay, 2010).

One aspect that underpins the unique functions of individual PDE4 isoforms is the complexes they form with binding partners. Each isoform has a unique set of interacting partners and binding is usually achieved via the PDE4 isoform's unique N-terminal. For example, PDE4 enzymes interact functionally with *β*-arrestins and orchestrate the dual desensitisation of β_2AR signalling (Baillie *et al*., 2003; Houslay *et al*., 2007). ISO stimulation causes *β*-arrestin to direct mainly PDE4D5 (because of its binding site within its unique N-terminus) to β_2AR upon β_2AR phosphorylation by GRK2 (G-protein-coupled-receptor kinase 2), thereby creating a localised sink for cAMP degradation in the vicinity of β_2AR and attenuating local PKA activity (Lefkowitz *et al*., 2002). In this context, PDE4D5 serves to intercede the switching between G_s-mediated activation of AC and G_i-mediated activation of ERK2 signalling. Notably, the attenuation of PKA phosphorylation of the β_2AR by PDE4D5 and the switching of *β*-adrenoceptor from G_s to G_i resulting in its signalling altered to ERK is critically dependent on the recruitment of PDE4D5 to the β_2AR-*β*-arrestin complex (Baillie *et al*., 2003).

3.1.4 cAMP-signalling modulation in the heart

The progression of cardiac disease to end-stage heart failure in particular hypertrophy, is often a consequence of long-term, signalling defects. In cardiac cells, the cAMP signalling pathway is an important regulator of myocardial function through the control of intracellular calcium concentration as a consequence of PKA-mediated phosphorylation of ryanodine receptors, phospholamban and L-type calcium channels (Stangherlin and Zaccolo, 2012). Spatial and temporal signalling dynamics of cAMP is achieved by various proteins, including PKA, PDEs and facilitated by scaffolding proteins such as A-kinase-anchoring proteins (AKAPs) (Dodge-Kafka *et al*., 2007).

The main effector of cAMP is PKA which mediates diverse cellular functions via direct phosphorylation of its substrates. PKA is a tetrameric complex, which consists of two regulatory (R) subunits with four encoded genes (RIα, RIβ, RIIα and RIIβ), and two catalytic (C) subunits with three encoded genes (Cα, Cβ and Cγ) (Skålhegg and Taskén, 1997). PKA holoenzymes are classified as type I or type II depending on the type of R subunit present (RI or RII). These two PKA types exhibit differental sensitivity to cAMP activation and have different subcellular distribution. Signalling complexes that are scaffolded by AKAPs often contain PDE4 and PKA in close proximity. Such an

arrangement vastly increases the threshold of activation of PKA, only allowing phosphorylation of PKA substrates at times of high cAMP, for example, immediately following receptor activation. Alternatively, intracellular cAMP actions can also be modulated by a newly discovered cAMP receptor, Epac (exchange proteins directly activated by cAMP) in a PKA-independent manner (de Rooij *et al*., 1998). As many receptor-mediated signalling events in cardiomyocytes are mediated via cAMP generation, alterations of the cAMP signalling pathway resulting from dysregulation of the compartmentalisation of β-AR signaling can be primary determinants in the development of cardiac remodelling and heart failure.

There are two main β-AR isoforms in the heart, namely β_1 and β_2 which are both coupled to the conventional G_s-AC-cAMP-PKA pathway, resulting in diffused signal throughout the cell. One notable distinction is that β_2AR activates both the G_s/G_i cAMP pathway and induces localised cAMP signals to regulate cardiac contractility (Xiang *et al*., 2005). It is thought that βAR signalling undergoes a time-dependent switch upon persistent stimulation (Fig. 3.3). In other words, continuous activation switches the β_1AR receptor signaling from PKA cascade to calcium/calmodulin-dependent protein kinase II pathway (CaMKII), resulting in cardiomyocyte apoptosis and maladaptive remodelling (Patterson *et al*., 2007). In addition, sustained activation of β_2AR stimulates phosphatidylinositol 3'-kinase (PI3K)-Akt mediated cardioprotection by inducing anti-apoptotic effect via the activation of inhibitory G protein (G_i) (Xiao *et al*., 2006).

Several studies have also highlighted the importance of PDEs, as well as specific roles for individual PDE isoforms in cAMP/PKA signalling in heart. Using neonatal cardiomyocytes, it was demonstrated that PDE4D is the main PDE associated with β-adrenergic regulation where it acts predominantly on β_2AR signaling (Dodge *et al*., 2001; Lehnart *et al*., 2005). There is increasing evidence to indicate that the inhibition of these PDE4s activities is associated with cardiovascular diseases. For example, PDE4D3 has been shown to bind to a striated muscle-specific AKAP (mAKAP) to regulate the trophic responses of cAMP in cardiomyocytes (Dodge *et al*., 2001). PDE4D is also associated with the ryanodine receptor 2 (RyR2) which is activated by calcium influx and mediates calcium release from sarcoplasmic reticulum (SR) (Lehnart *et al*., 2005). Notably, deficiency in this gene is associated with heart failure and arrhythmias. However, not much is known about the specific PDE isoforms which regulate PKA signalling during cardioprotective signalling mechanisms. HSP20 was identified as a substrate protein of cAMP-dependent PKA whereby PKA activation increases HSP20 phosphorylation at

Ser16 (Beall *et al*., 1997, 1999). Using cells that expressed the PKA inhibitory peptide (PKI) and phospho-HSP20 antibodies, it was reported that PKA is the sole kinase responsible for the ISO-induced HSP20 phosphorylation of HSP20 on Ser16 (Komalavilas *et al*., 2008). Furthermore, recent studies have provided evidence of HSP20's cardioprotective role through its phosphorylation on Ser16 by PKA (Fan *et al*., 2004, 2005, 2006). Importantly, HSP20 can only confer its cardioprotective ability after PKA-mediated phosphorylation upon an increase in the concentration of cAMP within cells (Fan *et al*., 2005). However, the mechanism(s) that modulates the spatiotemporal control of this modification is still unknown. Hence, it was interesting to investigate the molecular mechanism, in particular, to determine the identities of the individual PDEs that coordinate PKA activation and downstream signalling events involving HSP20 in hypertrophy.

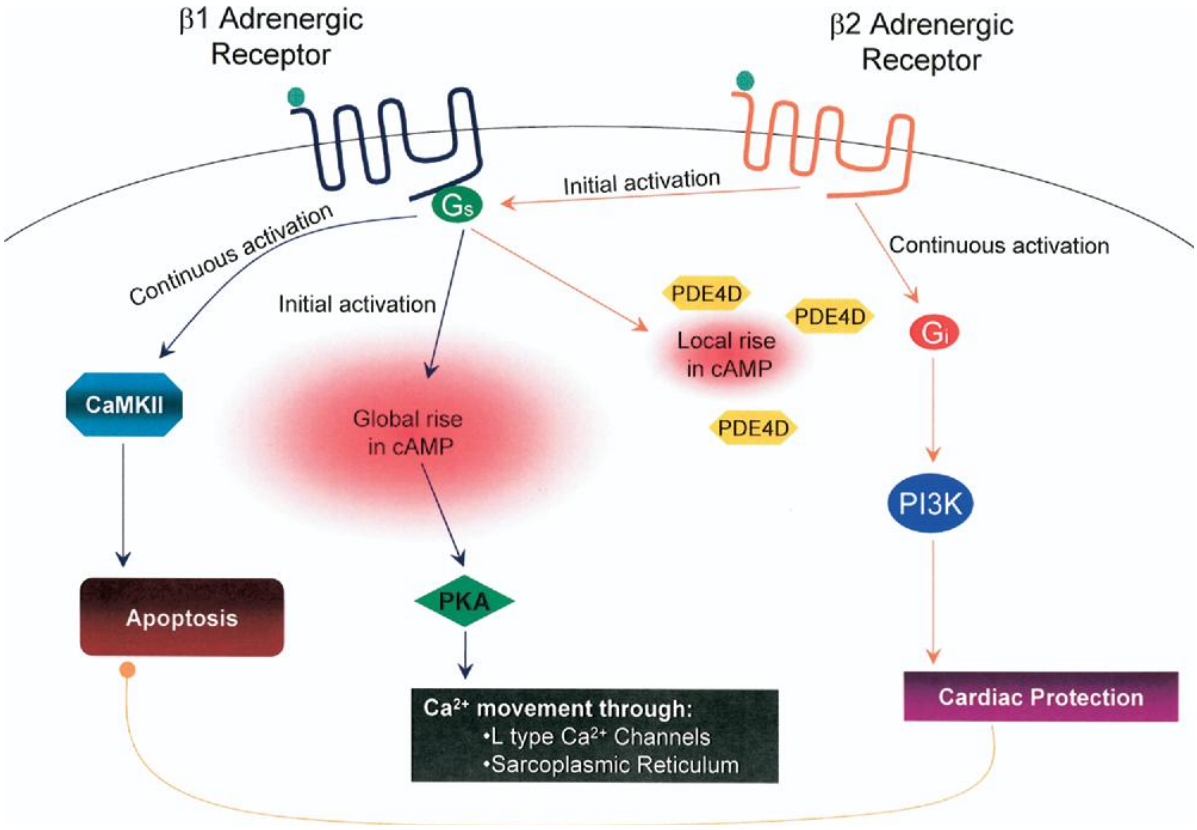

Figure 3.3. Schematic diagram showing multidimensional outline of *β*ARs signalling. *β*ARs dynamically bind to G proteins and subsequently other signalling proteins in a spatiotemporally regulated fashion. Persistent stimulation of *β*AR undergoes a time-dependent change which involves switching between two signalling pathways. (Adapted from Patterson *et al*., 2007).

3.2 Aims

Given that PDE4 isoforms play major roles in the compartmentalisation of cAMP signalling in the heart (Houslay *et al.*, 2007) and that HSP20 has been shown to be phosphorylated by cAMP-dependent PKA to confer cardioprotection (Fan *et al.*, 2005, 2006), it was hypothesised that PDE4 may be involved in the regulation of HSP20 phosphorylation to attenuate hypertrophic growth of cardiomyocytes via the control of local cAMP signals and activation of compartmentalised PKA.

The aims of this chapter are as follows:

1. to define the molecular composition of the signalling domain containing PKA, PDE4 and HSP20.

2. to address whether the spatial and temporal phosphorylation of PKA and/or HSP20 elicited by β-adrenergic receptor stimulation are influenced by PDE4 activity.

3.3 Results

3.3.1 Characterisation of neonatal rat cardiomyocytes

Most *in vitro* studies in this project were conducted in cardiomyocytes isolated from 1-3 day old Sprague-Dawley neonatal rat hearts. In order to provide reliable evaluation of the cellular response from cardiomyocytes to a given intervention, the number of contaminating non-myocardial cells such as fibroblasts was kept at a minimum. This was exceptionally important in interpreting data in order to provide reproducible results. There are several ways to eliminate non-myocardial cells, including deprivation of serum, inhibition of proliferation using cytosine-*β*-arabinofuranoside, differential attachment techniques and percoll density gradient centrifugation (reviewed in Chlopeikova *et al*., 2001). The differential attachment method is most popular and was used in this study to enrich cardiomyocyte preparations. The purity of neonatal rat cardiomyocyte cultures was determined by immunocytochemistry using an anti-α-sarcomeric actinin antibody. Immunocytochemical inspection confirmed the purity of the culture. A randomly selected microscopic field showed that the vast majority of cells were cardiomyocytes exhibiting a distinctive pattern of cross-striations stained by α-actinin. This suggests sarcomere organisation (Fig 3.4). Non-cardiomyocyte contamination 48h after isolation consisted of approximately 5% (1 out of 20 cells) of the total cell population.

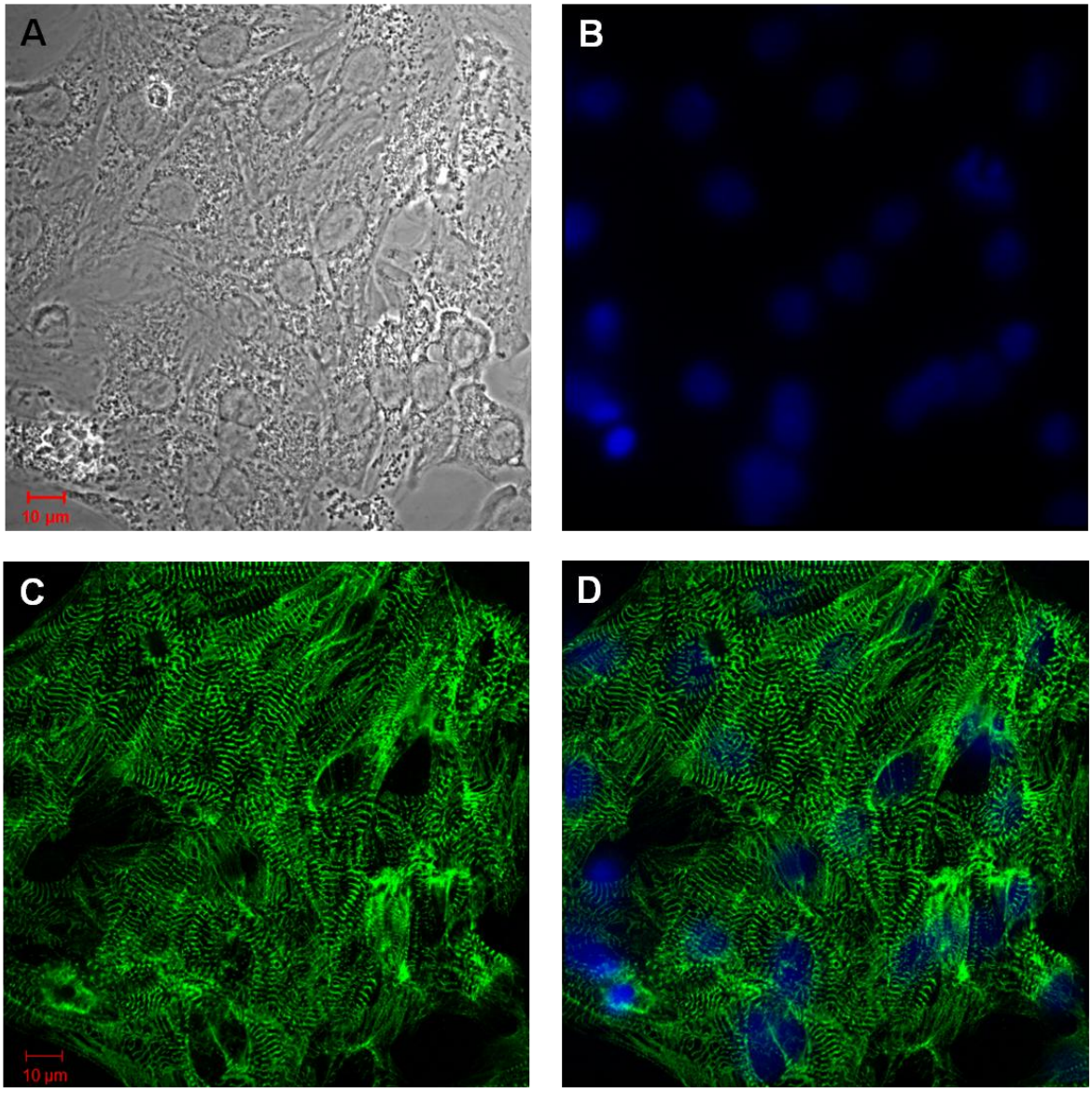

Figure 3.4. Primary culture of neonatal rat cardiomyocytes. Cells were obtained from differential plating procedure as described in 'Materials and Methods'. The cells were then assayed for α-sarcomeric actinin (green) and nuclei were detected by DAPI staining (blue), followed by laser scanning confocal microscopic visualization. Most of the cardiomyocytes interlaced with each other to form a confluent monolayer and were positive for sarcomeric staining. (A) Bright-field image, (B) DAPI-stained nuclei, (C) Actinin-stained cardiomyocytes, and (D) Composite image. Images are representatives of three separate experiments on different culture preparations.

3.3.2 Regulation of PKA-mediated HSP20 phosphorylation by PDE4

Strategically localised PDE4 isoforms underpin the compartmentalisation of cAMP signalling in the heart (Houslay *et al*., 2007). To investigate whether PDE4 isoforms regulate phospho-HSP20 levels in response to *β*-agonist treatment, cardiomyocytes that had either been pre-treated or not with the PDE4 selective inhibitor, rolipram (10 μM) were subsequently challenged with ISO (1 μM) for selected times. Upon ISO stimulation, cardiomyocytes exhibited an increase in endogenous phospho-HSP20 levels and this effect was markedly increased by rolipram pre-treatment (Fig. 3.5). Moreover, PDE4 inhibition alone in the absence of ISO sufficed to induced HSP20 phosphorylation when compared to cells under basal conditions.

To determine the role of PDE4 in modulating PKA-mediated phosphorylation of HSP20 at Ser16, cardiomyocytes were treated with ISO alone, ISO + rolipram, or pre-treated with the PKA inhibitor KT5720 prior to stimulation with ISO + rolipram. The immunoblots were then probed using the phospho-HSP20 antibody, which recognised HSP20 only when phosphorylated at Ser16. Results showed that the inhibition of PKA (Fig. 3.6) attenuated phosphorylation on HSP20 following stimulation with ISO + rolipram pre-treatment, confirming the importance of PDE4 and PKA in HSP20 phosphorylation in response to ISO treatment.

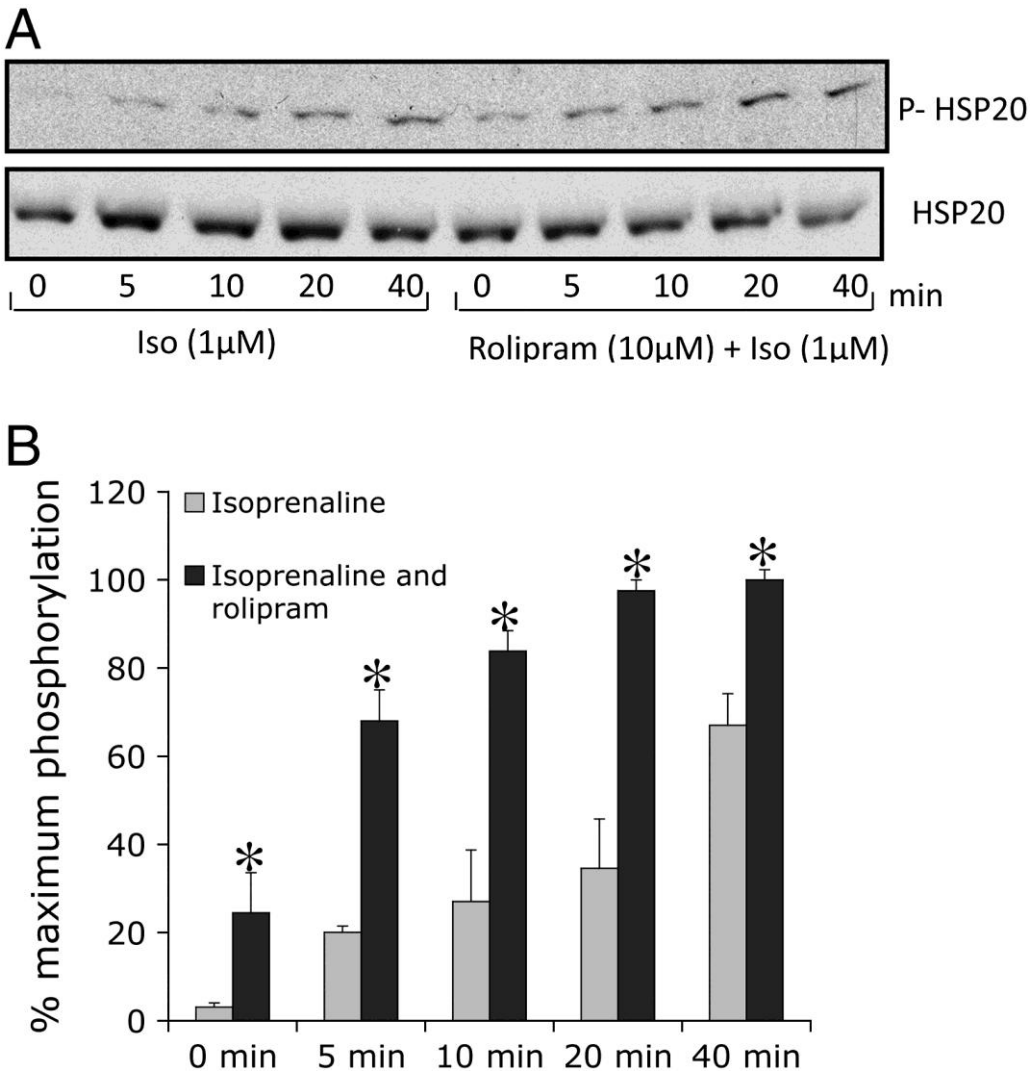

Figure 3.5. PDE4 involved in the modulation of HSP20 phosphorylation at Ser16 in cardiomyocytes. (A) Neonatal rat cardiomyocytes were treated with ISO for indicated time with or without pre-treatment with rolipram. Cells were also treated with 0.01% (v/v) DMSO as control for addition of solvent. Endogenous lysates were immunoblotted for phospho-HSP20 (Ser16) and total HSP20. (B) Densitometry analysis showed percentage of maximum HSP20 phosphorylation normalised to HSP20. Data was expressed as mean ± S.E.M. of three separate experiments. Significance level was set at $P < 0.05$ over ISO treatment.

This work was carried out by Dr Xiang Li.

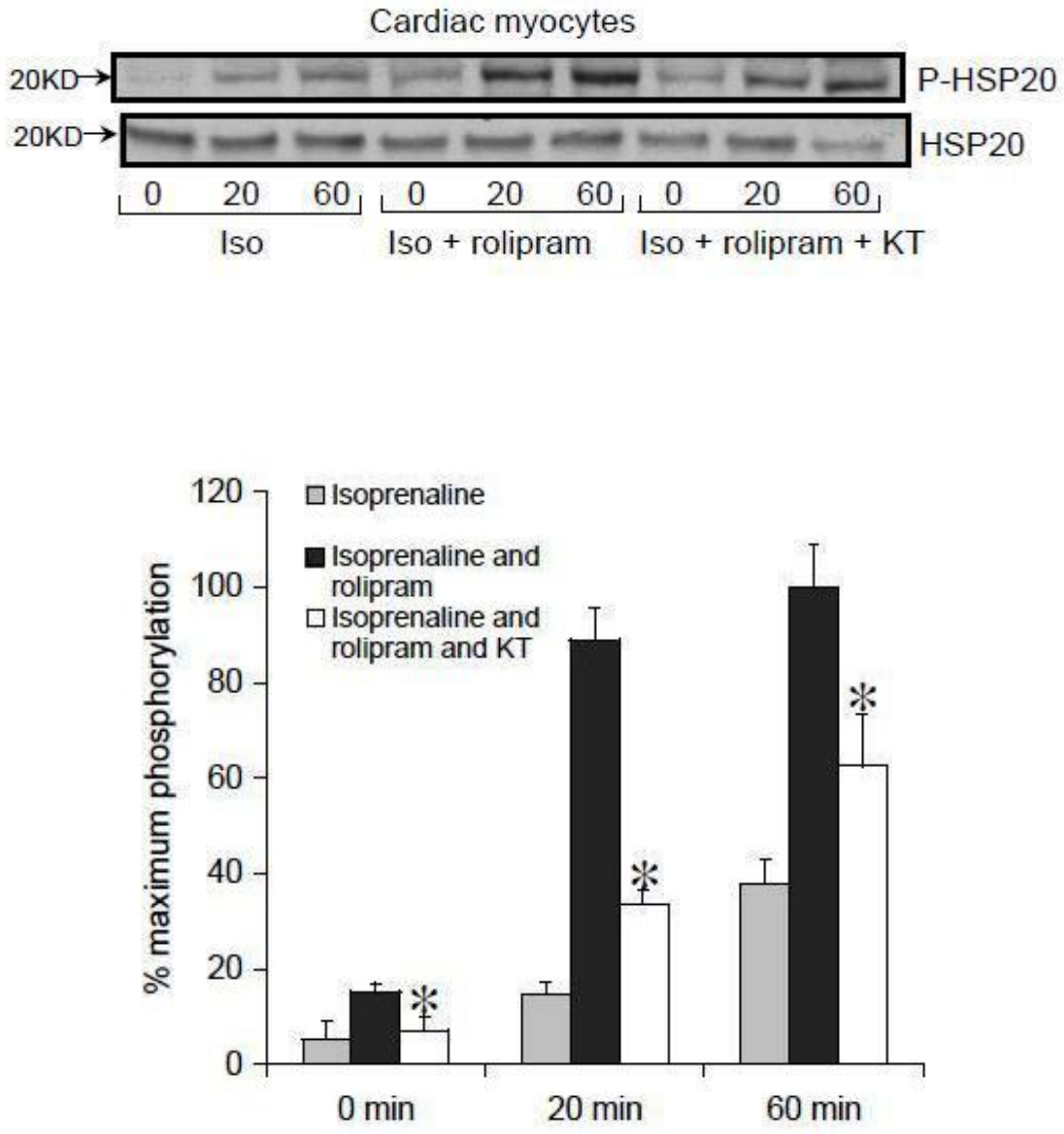

Figure 3.6. The phosphorylation of HSP20 at Ser16 is modulated by PKA. Upper panel: Cardiomyocytes were treated with ISO for indicated times with or without pre-treatment with rolipram or rolipram + KT5720. Lysates were blotted for phospho-HSP20 (Ser16) and HSP20. Lower panel: Densitometry analysis showed percentage of maximum HSP20 phosphorylation. Data was expressed as mean ± S.E.M. of three separate experiments. Significance level was set at $P < 0.05$ over ISO treatment.

This work was carried out by Dr Xiang Li.

3.3.3 HSP20 interacts directly with PDE4 isoforms

Intracellular cAMP induced by *β*AR signalling is regulated by different PDEs which are responsible for controlling local PKA activity (Conti and Beavo, 2007; Houslay *et al*., 2007). Knowing that rolipram could affect PKA-mediated HSP20 phosphorylation, it was possible that PDE4 could form a signalling complex with HSP20 to exert a phosphorylation control mechanism. Hence, biochemical studies were carried out to determine if PDE4s associate with HSP20 either dynamically in response to *β*-adrenergic agonist or constitutively under basal conditions. Co-immunoprecipitation analyses using lysates from untreated and ISO-treated cardiomyocytes showed that HSP20 immuno-complex contained PDE4D isoforms (Fig. 3.7A). In order to verify the identities of the specific PDE4D isoforms which may potentially associate with HSP20, HEK293 cells were co-transfected with HSP20 and five most common PDE4D isoforms (4D3, 4D4, 4D7, 4D8 and 4D9). Similarly, lysates were subjected to co-immunoprecipitation using anti-HSP20 antibody and then immunoblotted with anti-Pan-PDE4D antibody. Interestingly, bands corresponding to all the five PDE4D isoforms were detected in the immunoprecipitates, which may suggest the presence of common association site within the conserved region of the PDE4D family (Fig. 3.7B).

In addition, *in vitro* pull-down assays using purified species were carried out to assess the interaction between HSP20 and PDE4 family. Results showed that recombinant His-HSP20 proteins co-purified with GST-PDE4B3. GST-PDE4D3 and GST-PDE4D5 but not GST alone (Fig 3.8), suggesting direct *in vitro* interaction between these proteins. Immunocytochemical studies were also carried out to ascertain whether HSP20 and PDE4D colocalised to the same micro-compartment within cardiomyocytes. Unsurprisingly, confocal images of neonatal rat cardiomyocytes showed that both HSP20 and PDE4D localised with α-actinin in a striated pattern (Fig 3.9), suggesting that these proteins exist in the same cellular compartment. This finding is in agreement with previous studies in which localisation of PDE4D was observed at the sarcomeric Z-disk (Mongillo *et al*., 2004). It is thus postulated that the close proximity of PDE4D is likely to modulate the phosphorylation of HSP20.

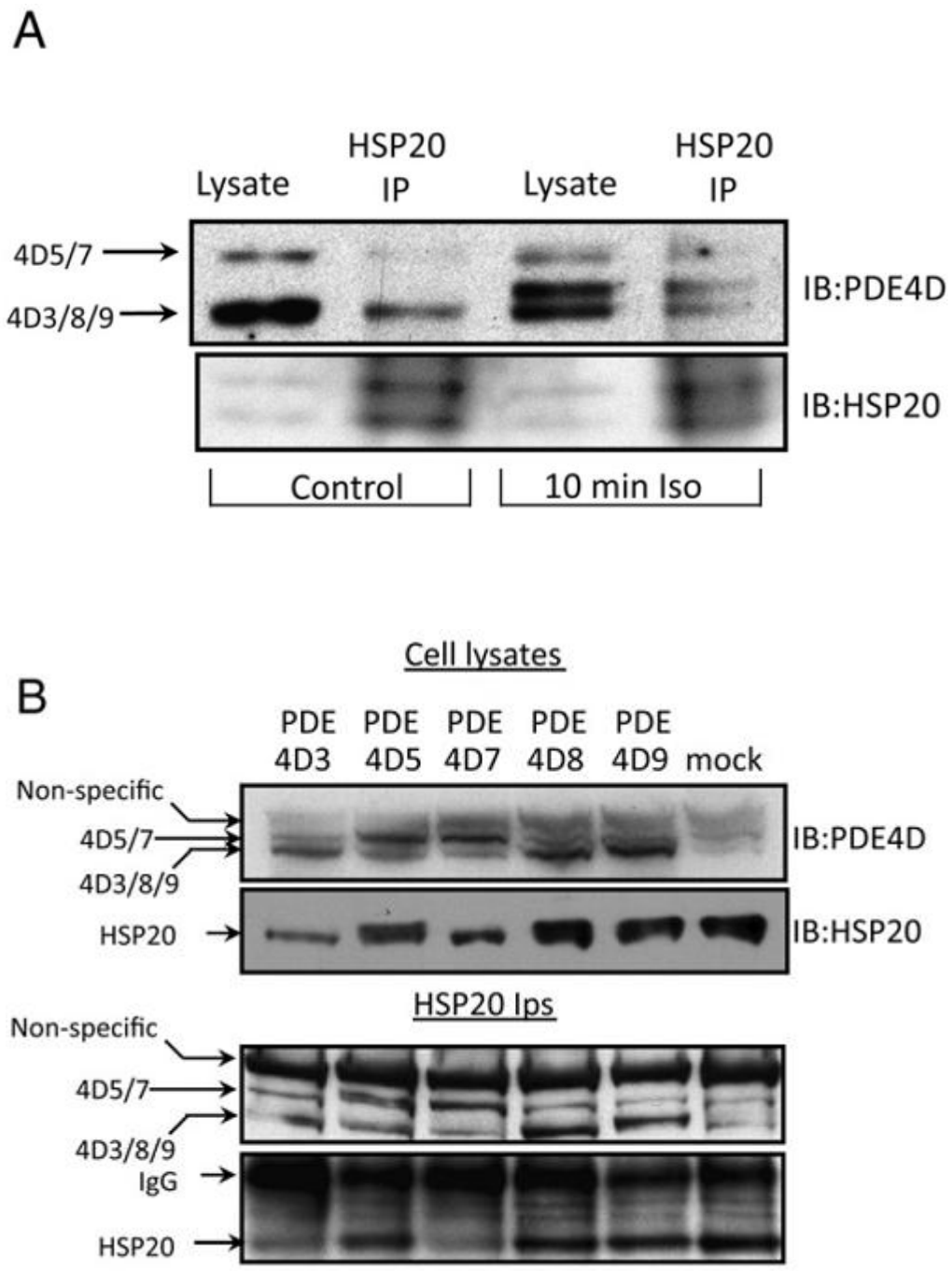

Figure 3.7. HSP20 forms a complex with PDE4D isoforms. (A) Immunoprecipitation of HSP20 from lysates extracted from cardiomyocytes following treatment with 1 μM of ISO was immunoblotted with anti-Pan-PDE4D antibody for the presence of PDE4D isoforms. (B) Five members of the PDE4D subfamily were co-expressed with HSP20 and HSP20 immuno-complex was then probed for PDE4D isoforms. Blots are representative of three separate experiments.

This work was carried out by Dr Xiang Li.

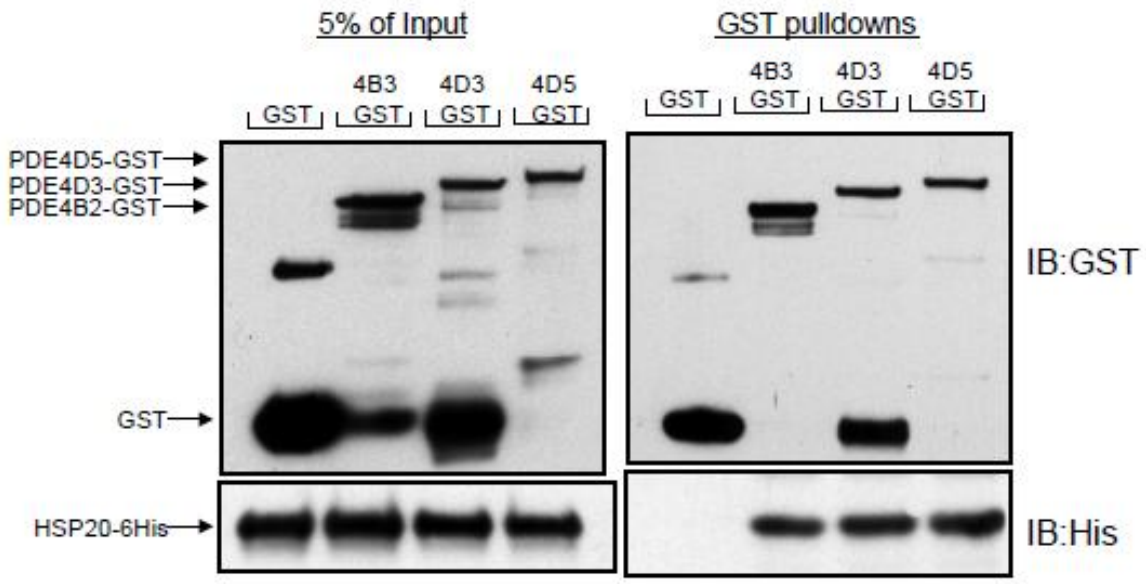

Figure 3.8. HSP20 interacts directly with PDE4 isoforms. *In vitro* pull-down assay of purified His-HSP20 and purified GST-PDE4 showed that His-HSP20 was co-precipitated in GST-pulldowns containing the PDE4 proteins.

This work was carried out by Dr Xiang Li.

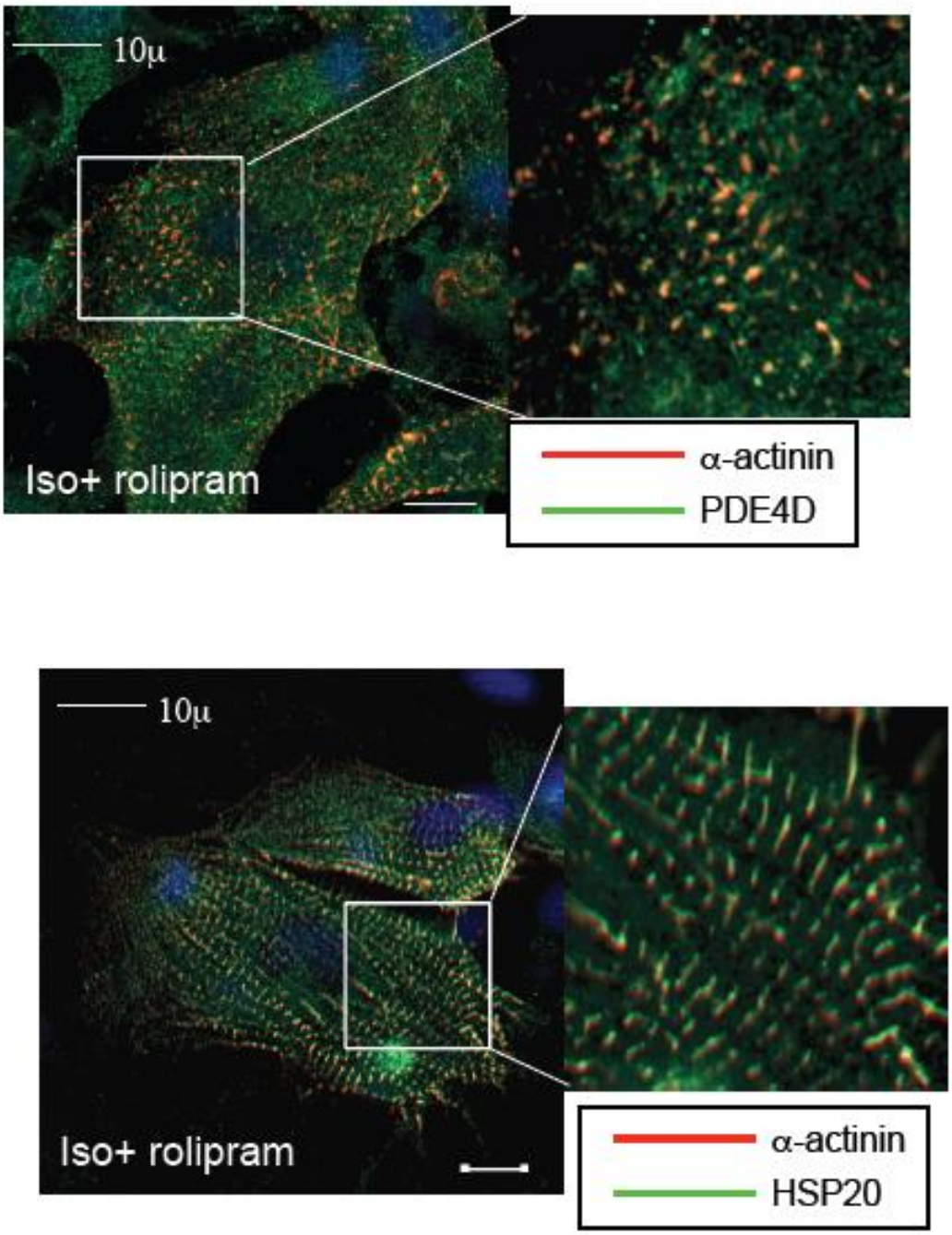

Figure 3.9. HSP20 colocalises with PDE4D. Confocal images of PDE4D and HSP20 localisation in neonatal rat cardiomyocytes. The cells were treated with ISO and rolipram for 10 min before co-staining anti-α-actinin with anti-HSP20 or anti-Pan-PDE4D antibodies. The magnification of the boxed area showed that both PDE4D and HSP20 localised into the same cellular compartment containing α-actinin. Images are representative of three independent cell culture preparations.

This work was carried out by Dr Xiang Li.

3.3.4 Mapping interaction sites between HSP20 and PDE4D5

PDE4D5 has been shown to be implicated in the interactions with diverse partners such as RACK1, *β*-arrestin and DISC1 (Millar *et al*., 2005; Bolger *et al*., 2006). In all of these cases, SPOT immobilized peptide libraries of PDE4D5 sequences were used to provide information on the molecular binding nature of these interacting proteins. This array-based method was also carried out in this study to define the HSP20 binding site within the full-length PDE4D5 sequence. Peptide array libraries of overlapping 25-mer peptides (each shifted by five amino acids) that spanned the entire sequence of PDE4D5 were probed for interaction with purified recombinant His-HSP20 protein or BSA (control). Dark spots signify positive association whereas clear spots represent no interaction. Whilst no signal was observed on control arrays overlaid with BSA, a cluster of binding spots (spots 93-96) were detected which encompassed the amino acid sequence Y^{461}-K^{500} within the conserved catalytic domain of PDE4D5 (Fig. 3.10A). Notably, this result is in agreement with the data obtained earlier, in that this region is highly conserved in all PDE4 isoforms and could represent a pan-PDE4 binding site for HSP20.

A more detailed analysis to determine the specific residues important in the protein interactions was undertaken using alanine scanning substitution arrays which focused on the E^{468}-K^{492} region of PDE4D5. The alanine scanning peptide libraries were constructed by sequentially substituting each residue to alanine or aspartate (if an alanine was the natural amino acid at that position). This approach identified a significant loss of binding ability at three regions, namely the double histidine (H^{470} and H^{471}), K^{477} and the acidic region consisting of E^{481}, E^{482} and D^{485} (Fig. 3.10A), denoting their importance in the interaction. Superimposing these six residues on the documented crystal structure of the PDE4 catalytic domain showed that all of these amino acids (except H^{471}) are surface associated, having a potential to act as docking sites for signalling proteins such as HSP20 (Fig. 3.10B).

In addition, a reciprocal scanning peptide array analysis was also carried out to identify the binding site of PDE4D5 on full-length HSP20. Results showed high-affinity binding regions in the WDPF and α-crystallin domains (Fig. 3.11). In particular, the binding region at the N-terminal encompasses a consensus sequence RRASA which serves as cAMP-dependent protein kinase A (PKA)– specific phosphorylation motif (Beall *et al*., 1997).

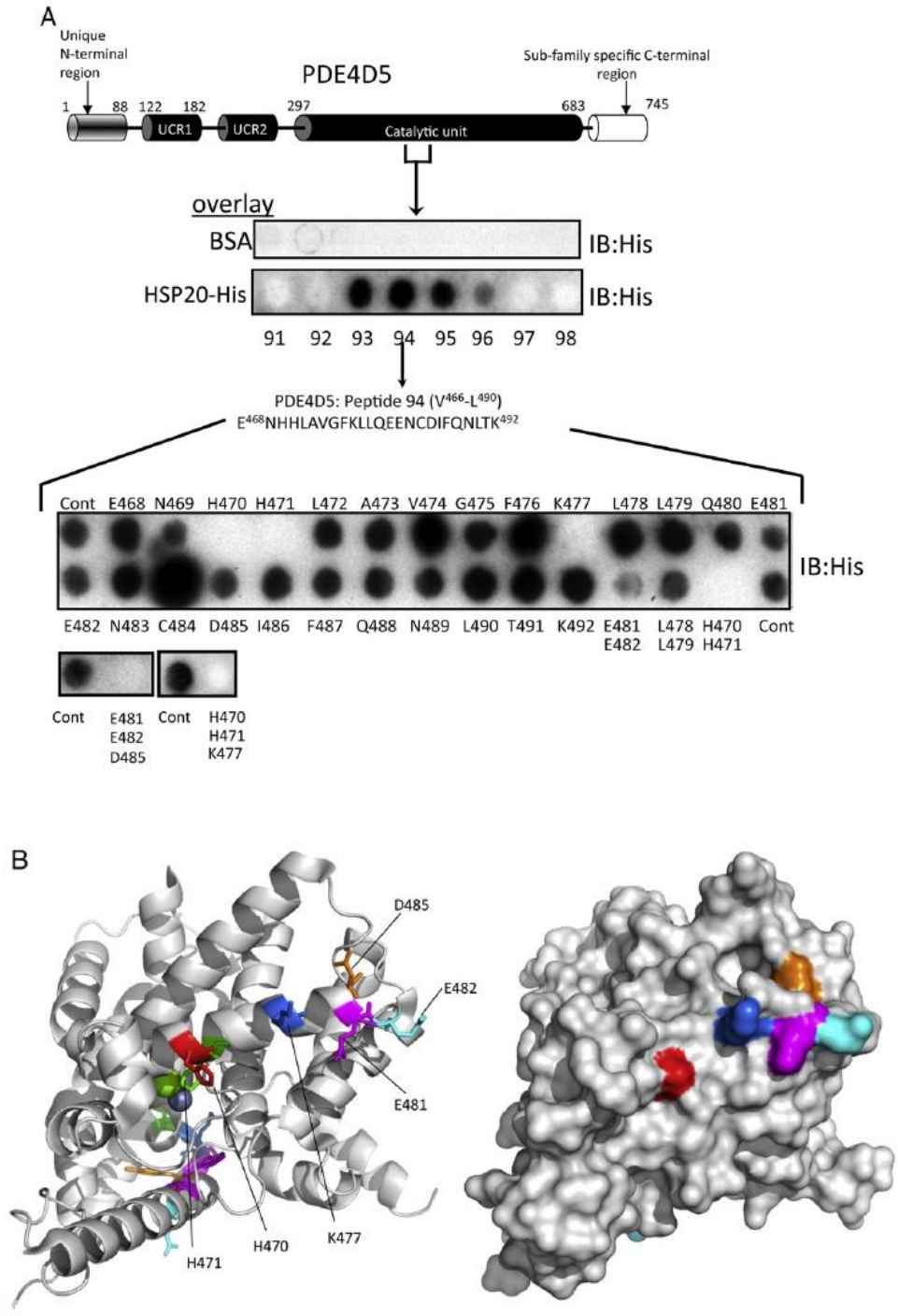

Figure 3.10. Mapping the site of HSP20 interaction on PDE4D5. (A) The disposition of the peptides is shown relative to a schematic representation of PDE4D5 structure. Peptide array analysis identified binding sites for HSP20 in the catalytic unit of PDE4D5. Binding spot numbers relate to peptides in the scanned array and whose residues position and sequences are shown. Alanine scanning analysis using the sequence covering E^{468}-K^{492} identified amino acids critical for the binding. (B) PDE4D5 residues critical for the interaction with HSP20 were superimposed on the crystal structure of the PDE4D5 catalytic unit. **This work was carried out by Dr Allan Dunlop and Prof Dave Adams.**

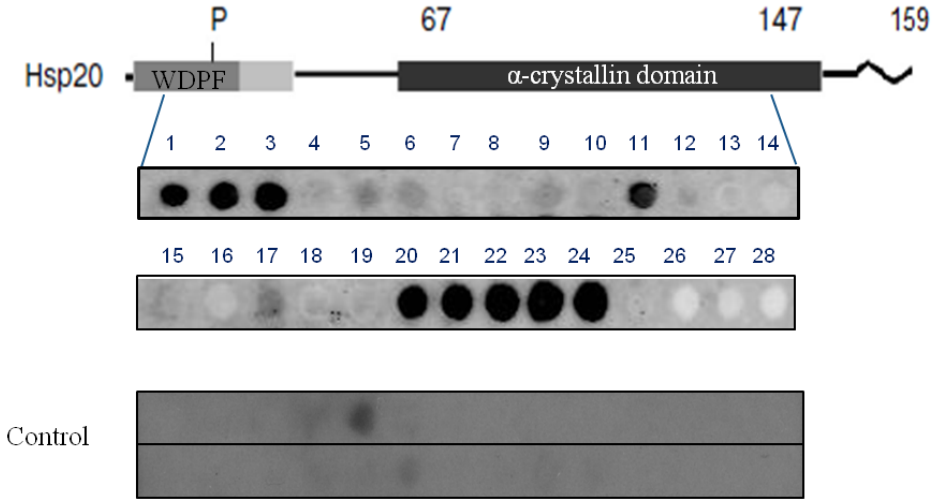

Position	Residues	25-Mer peptide sequence
1	1-25	MEIPVPVQPSWLRRASAPLPGLSAP
2	6-30	PVQPSWLRRASAPLPGLSAPGRLFD
3	11-35	WLRRASAPLPGLSAPGRLFDQRFGE
11	51-75	APYYLRAPSVALPVAQVPTDPGHFS
20	96-120	HVEVHARHEERPDEHGFVAREFHRR
21	101-125	ARHEERPDEHGFVAREFHRRYRLPP
22	106-130	RPDEHGFVAREFHRRYRLPPGVDPA
23	111-135	GFVAREFHRRYRLPPGVDPAAVTSA
24	116-140	EFHRRYRLPPGVDPAAVTSALSPEG

Figure 3.11. Mapping the site of PDE4D5 interaction on HSP20. HSP20 array was overlayed with full-length purified GST-PDE4D5 and detected by anti-GST antibody. The disposition of the peptides is shown relative to a schematic representation of HSP20 as in Gusev *et al*. (2002) with slight modifications. The dark shaded area represents the WDPF-domain, the light shaded area represents the conserved region in the N-terminal part of sHSP, the black area denotes conservative α-crystallin domain. P is the sites of phosphorylation and the zigzag denotes the flexible C-terminal region. Binding spot numbers relate to peptides in the scanned array and whose residues position and sequences are shown below.

3.3.5 Peptide disruption of PDE4D5-HSP20 complex

Based on the information gathered from peptide array analyses, cell-permeable analogues of the 25-mer peptide encompassing residues E^{468}-K^{492} (ENHHLAVGFKLLQEENSDIFQNLTK) was synthesised and named 'bs906'. At the same time, a control peptide consisted of a scrambled version of peptide 'bs906' (KELGAINHEFDLSHNFQTQKLNLVE) that had the same net charge and weight was also synthesized. Both peptides carry a C-terminal stearate group that has been shown to allow peptide transport across the cell membrane into the cells while not affecting the peptide's ability to disrupt signaling complexes (Meng *et al*., 2009). The ability of the disruptor peptide to displace PDE4D-HSP20 interaction was assessed by immunoprecipitation experiments and evaluation of the phosphorylation level of HSP20. Co-immunoprecipitation experiments using lysates from co-transfected HEK293 cells showed that the HSP20–PDE4D5 complex disruptor 'bs906' attenuated the association between PDE4D5 and HSP20 and the effect was significantly enhanced at higher concentration of disruptor peptide (Fig 3.12). However, no such disruption was evident upon use of the scrambled control peptide, hence confirming the target specificity.

3.3.6 The effect of PDE4D5-HSP20 interaction on HSP20 phosphorylation

Next, the effect of PDE4D5-HSP20 complex disruption on Ser16 phospho-levels was investigated. Co-transfected HEK293 cells treated with disruptor peptide 'bs906' but not scrambled control peptide resulted in a robust and significant increase in the phosphorylation of HSP20 at Ser16 (Fig 3.13). In particular, the maximum effect of the disruptor peptide 'bs906' was seen after 60 min. Conversely, scrambled control peptide modestly increased HSP20 phosphorylation and reached a final level of phosphorylation that was significantly lower than disruptor peptide 'bs906'. These findings suggested that the disruption of PDE4D5-HSP20 interaction is likely to alleviate PKA inhibition by preventing sequestration of PDE4D5 to the HSP20 complex. Gratifyingly, these data are in agreement with earlier studies showing that treatment with rolipram alone was sufficient to promote HSP20 phosphorylation at Ser16 (Fig 3.5). In this regard, the basal concentrations of cAMP would thus be expected to trigger PKA-mediated HSP20 phosphorylation in the absence of localised PDE4 activity, pinpointing a pivotal role of sequestered PDE4 in the regulation of HSP20 phosphorylation by PKA.

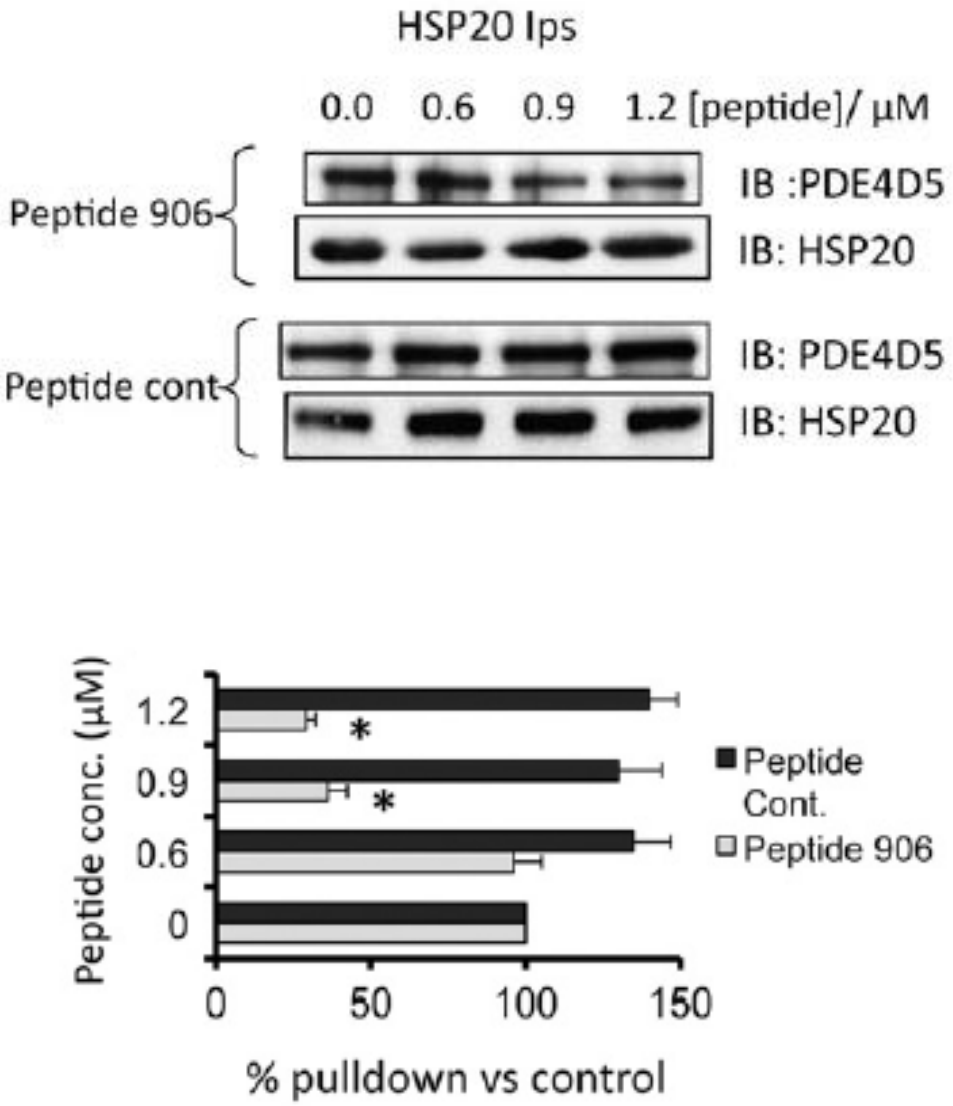

Figure 3.12. Disruption of PDE4D5-HSP20 interaction. Upper panel: HEK293 cells were co-transfected with PDE4D5 and HSP20 and subjected to increasing concentrations of disrupt peptide 'bs906' or scrambled control peptide for 2 h. Lysates were immunoprecipitated with HSP20 and then probed for PDE4D5. Anti-HSP20 antibody was used as loading control. Lower panel: Densitometric analysis of the amount of PDE4D5 in HSP20 immunoprecipitates normalised to expression level. Data are means ± S.E.M. of three separate experiments. Statistical significances between the two treatment groups were determined by the use of Student's *t*-test. **P* < 0.05 values were considered significant.

This work was carried out by Dr Frank Christian.

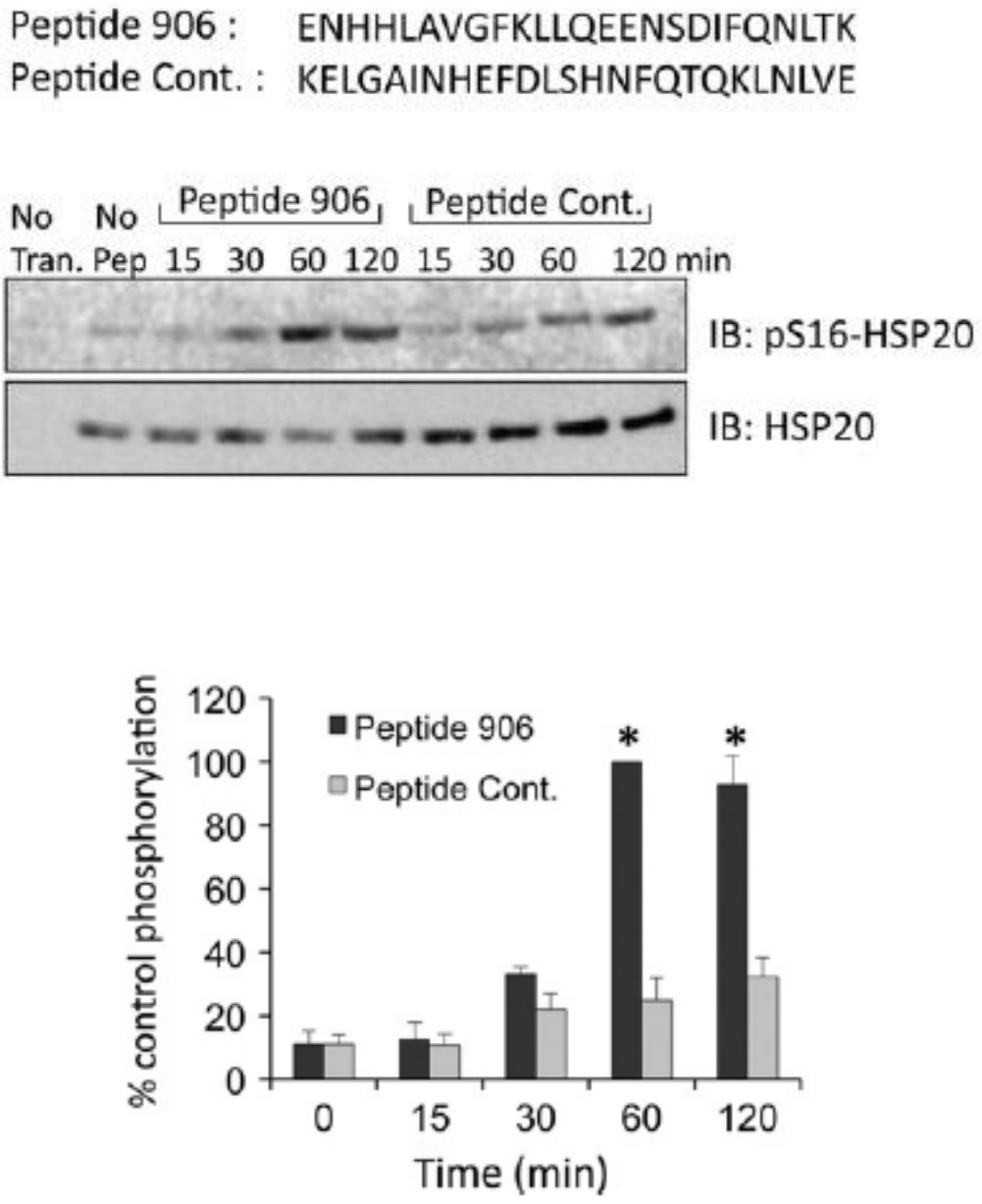

Figure 3.13. Disruption of PDE4D5-HSP20 interaction promotes HSP20 phosphorylation at Ser16. Upper panel: HEK293 cells were co-transfected with PDE4D5 and HSP20 and treated with disrupt peptide 'bs906' or scrambled control peptide for indicated times. Lysates were immunoblotted with phospho-HSP20 (Ser16) and HSP20. Lower panel: Densitometric analysis of HSP20 phosphorylation levels normalised to total HSP20. Data are means ± S.E.M. of three separate experiments. Statistical significances between the two treatment groups were determined by the use of Student's *t*-test. **P* < 0.05 values were considered significant.

3.3.7 The role of PDE4D5-HSP20 complex in hypertrophy

Recent findings have reported that prolonged treatment with ISO results in the phosphorylation of HSP20 in order to trigger its cardioprotective functions to attenuate the hypertrophic growth of cardiomyocytes *(*Fan *et al.*, 2005, 2006*)*. As shown earlier in this chapter, phosphorylation of HSP20 could be induced when the HSP20-PDE4 complex is dismantled by treating cells with disruptor peptide 'bs906'. As such, it was particularly interesting to find out if this disruptor peptide 'bs906' could also attenuate the hypertrophic response in neonatal rat cardiomyocytes following sustained *β*-agonist stimulation.

Chronic *β*-adrenergic stimulation has been implicated in the development of cardiomyocyte hypertrophy (Fan *et al*., 2004). In order to mimic hypertrophic induction in this study, cardiomyocytes were cultured under serum-free conditions for 48 h before being treated chronically with *β*-adrenergic agonist, ISO for 24 h. The role of the PDE4D5-HSP20 complex in hypertrophic growth was then evaluated by three methods: measurement of cell size, assessment of protein synthesis and real-time qPCR analysis of fetal gene expression.

3.3.7.1 Measurement of cell size

The hypertrophic phenotype was evaluated using a traditional approach where the cross-sectional areas of the cardiomyocytes were measured manually by tracing the cell perimeter on digitised images acquired on a microscope. In parallel with this traditional method, a novel approach employing xCELLigence technology was also undertaken to monitor cardiomyocytes in real-time. This method allowed quantitative measurement of cell size increases and changes in morphology through real-time cell-electronic sensing (RT-CES) (Atienza *et al*., 2006; Yu *et al*., 2006; Vistejnova *et al*., 2009). The change in electrode impedance is automatically converted to cell index (CI) values which reflect the quantitative measurement on any changes in cell morphology that alter resistance to the current, thereby allowing unbiased detection of specific cellular processes in real-time. Because cardiomyocytes are unable to divide, they tend to increase in cell size in respond to stress which can ultimately lead to thickening of the heart wall. Hence, in this context, a higher cell index value directly reflects an increase in cell cross-sectional area.

In this study, the change in cell size was monitored over time, with a special focus on changes that occurred after 24 h ISO treatment. Importantly, the reproducibility of my manual measurement was verified by the results obtained from RT-CES. Both techniques produced strikingly similar data, showing a significant 2-fold increase in cardiomyocyte size following 24 h ISO treatment. Interestingly, this hypertrophic phenotype could be rescued by pre-treatment of disruptor peptide 'bs906' but not the scrambled control peptide (Fig. 3.14). These results also provided evidences for hypertrophic responsiveness of cardiomyocytes isolated from neonatal rats to continuous β-adrenergic stimulation by ISO. Clearly, my study demonstrates that 24 hours of ISO treatment is sufficient to induce hypertrophy in cultured neonatal rat cardiomyocytes. Gratifyingly, this observation is consistent with previous reports by Morisco *et al*. (2001) who utilised ISO-stimulated hypertrophic neonatal rat cardiomyocytes to investigate the mechanism underlying induction of cardiac hypertrophy by different subtypes of *β*-adrenergic agonist receptors.

3.2.7.2 Measurement of protein content

Next, to determine the effect of PDE4D5-HSP20 complex on protein synthesis, the overall hypertrophic growth response of cardiomyocytes was determined by measuring protein/DNA ratio post-treatment. The total cell protein and the DNA content were quantified by the Ohnishi & Barr modified Lowry method, and the Hoechst dye method (see 'Materials and Methods'), respectively. As expected, the relative protein/DNA ratio in ISO-treated cardiomyocytes was significantly higher than those of the DMSO-treated controls (Fig 3.15). Clearly, ISO stimulation increased cardiomyocyte growth partially by promoting protein synthesis. In agreement with the findings reported above, increases in protein synthesis could be rescued by the disruptor peptide 'bs906', but not the scrambled control peptide.

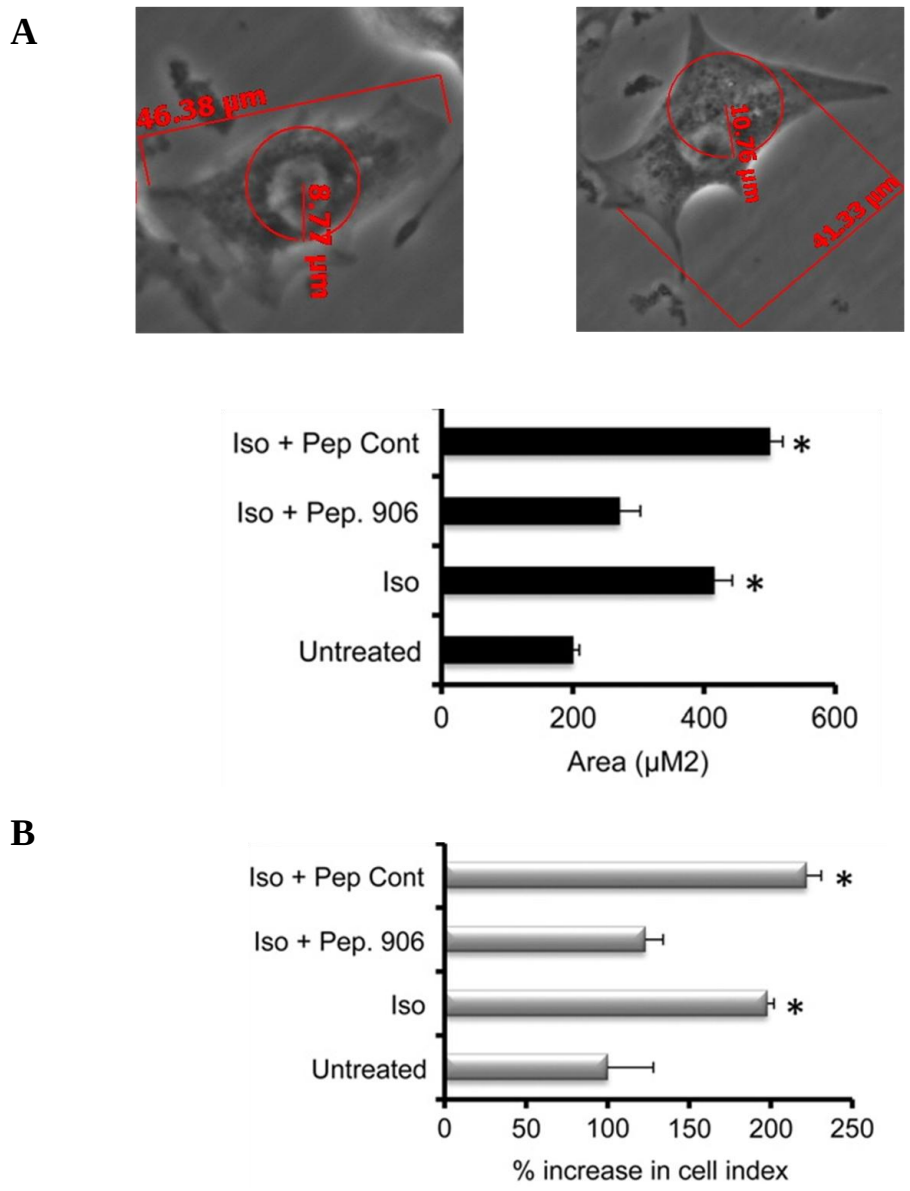

Figure 3.14. Disruption of PDE4D5-HSP20 complex inhibits cardiomyocyte enlargement. Cardiomyocytes were cultured for 48 h in a serum-free condition prior to indicated treatment. (A) Upper panel: A hundred beating cardiomyocytes from randomly selected microscope views were analysed and the cross-sectional area was measured manually. Surface areas of cardiomyocytes were calculated according to the formula stated in 'Materials and Methods'. Bottom panel: Graphical depiction of the mean areas of cells. (B) Impedance measurements were used to calculate continuous normalised cell index using RT-CES. Data were presented as a percentage of change of experimental groups compared with untreated controls. Values are expressed as means ± S.E.M of four separate experiments on different cardiomyocyte preparations. A Student's *t*-test was performed to compare untreated control with cells exposed to indicated treatment. **P* < 0.05 values denotes statistically significant.

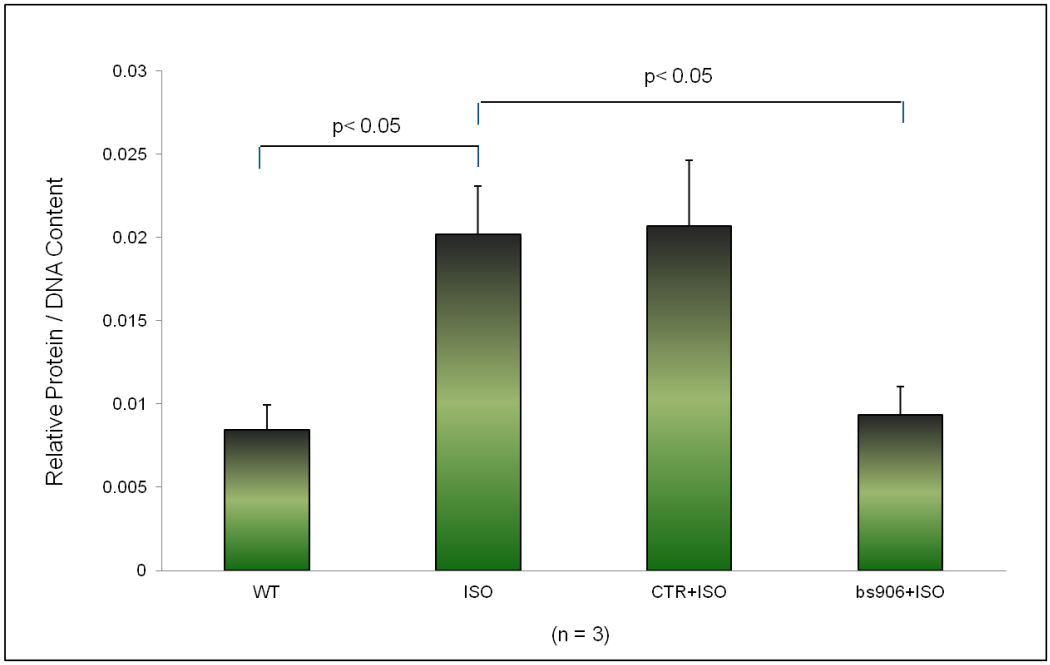

Figure 3.15 Disruption of PDE4D5-HSP20 complex inhibits protein synthesis. The protein content was normalised by the DNA amount to correct for differences in the cell number. Data are means ± S.E.M. of three experiments on different cardiomyocytes preparations. A Student's *t*-test was performed to compare the two groups as shown and statistically significance was set at $P < 0.05$.

3.2.7.3 Expression of ANF mRNA and protein expression

One of the most striking characteristics of the hypertrophic response is the phenotypic modification which leads to the re-expression of fetal genes. Atrial natriuretic factor (ANF) is a haemodynamic peptide hormone which regulates cardiovascular homeostasis. In mammals, ANF is normally produced in the atria but can be found in both atrial and ventricular cardiomyocytes during embryonic development (de Bold, 1985). As ventricular ANF expression usually ceases after birth, re-expression of ANF during hypertrophy indicates initiation of a compensatory response (Chien *et al.*, 1991; Rosenzweig and Seidman, 1991).

Hence, in addition to changes in cellular morphology and increased protein synthesis, the levels of fetal gene expression was also assessed in this study. An invariant endogenous gene, rat 18s rRNA was also included as internal control to correct for small variations in sample loading. Normalisation of target gene expression was performed to sample-to-sample and run-to-run variation (Pfaffl and Hageleit, 2001). As shown in Figure 3.16A, ISO treatment strongly enhanced the transcriptional activity of ANF, resulting in a significant 2-fold increase in ANF mRNA levels. In parallel, expression of ANF protein was increased by 1.5-fold, as detected by immunoblotting with anti-ANF antibody (Fig. 3.16B). However, the expression of α-tubulin which is expressed constitutively remained unchanged. In addition, similar changes were observed in the cardiomyocytes pre-treated with control peptide. Interestingly, disruptor peptide 'bs906' appeared to augment the increase in both ANF mRNA and protein expression triggered by ISO stimulation.

A

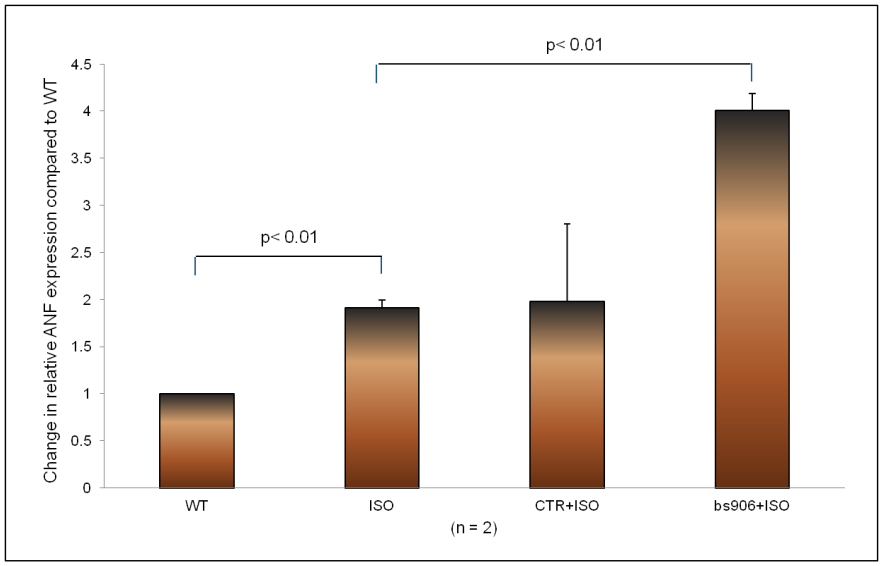

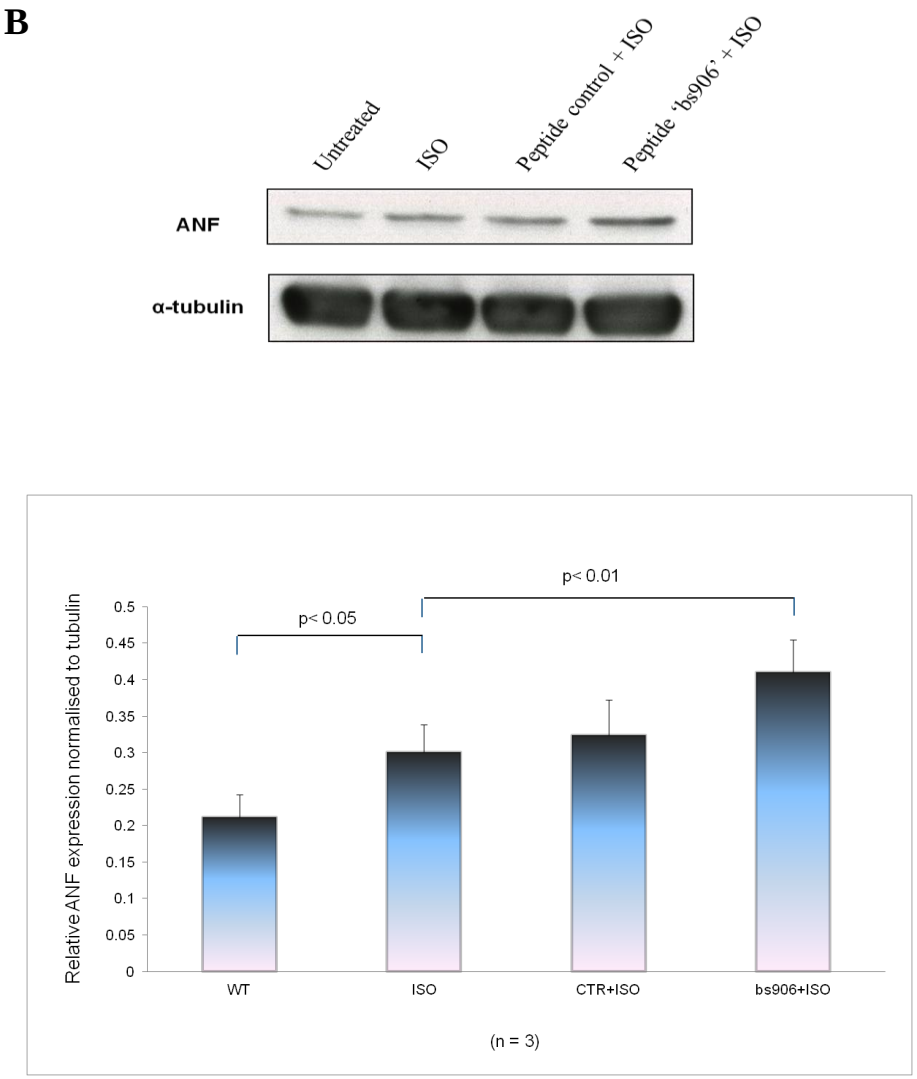

Figure 3.16. Disruption of PDE4D5-HSP20 complex enhanced transcriptional activation of hypertrophy response gene. Cardiomyocyte cultures were treated with disruptor peptide 'bs906' and control peptides prior to 24 h ISO stimulation. (A) Changes in relative ANF expression compared to wild-type. The changes in ANF mRNA transcript levels were determined by real-time qPCR analysis and normalised to reference gene rat 18s rRNA which was used as an internal control for RNA loading. Expression of each transcript was quantified and expressed as the level of expression relative to untreated cultures. (B) Upper panel: Representative immunoblot of ANF protein expression detected by an anti-ANF antibody. Lower panel: Quantitative analysis of immunoblots showing fold ratio of ANF normalised to α-tubulin. Data are mean ± S.E.M. of two or more experiments on different cardiomyocytes preparations. Statistical differences were determined using the Student's *t*-test and statistical significance was set at $P < 0.05$.

3.4 Discussion

3.4.1 Background

Despite therapeutic advances in the area of *β*-adrenergic signalling, hypertrophy leading to heart failure, remains a prime cause of death in industrialised nations. As mentioned earlier, HSP20 is known to confer cardioprotection during times of stress such as sustained *β*-adrenergic stimulation (Fan *et al*., 2004, 2005, 2006). It is well-appreciated that the mechanism underlying its protective function is greatly contingent on its phosphorylation by cAMP-dependent PKA at Ser16 (Fan *et al*., 2004; Qian *et al*., 2009; Zhu *et al*., 2011). However, little is known about the exact molecular mechanisms that link the spatial and temporal control of cAMP signalling to the post-translational modification of HSP20. The driving notion behind this present study is that PDEs contribute to the generation of intracellular cAMP microdomains which is critical for the specificity of cAMP signaling (Mongillo *et al*., 2004; Terrin *et al*., 2006). Moreover, cAMP accumulation upon extracellular hormone stimulation is highly localised in cardiomyocytes (Zaccolo and Pozzan, 2002; Mongillo *et al*., 2004). Specifically, compartmentalised PDE4 is a major regulator of cAMP gradients in the heart (Richter *et al*., 2005). With these statements in mind, we wanted to determine whether HSP20-targeted PDE4 was involved in dampening the activation of the PKA pool that directed HSP20 phosphorylation. I hypothesised that if this was true, disruption of the HSP20-PDE4 complex should attenuate hypertrophic growth of cardiomyocytes and trigger cardioprotection.

3.4.2 PDE4 modulates PKA-mediated HSP20 phosphorylation upon ISO stimulation

Part of the work in this study was carried out in transfected HEK293 cells, while most of the findings were verified in the more physiological setting of neonatal rat cardiomyocytes with endogenously expressed proteins and an established model to mimic hypertrophy (Morisco *et al*. 2001). It should be noted that in this study, all experiments with primary cultures were performed using highly purified cardiomyocytes, hence excluding possible variations attributable to other non-myocardial cells present in the heart (Fig. 3.4). The first part of this study showed that PKA-mediated phosphorylation of HSP20 was modulated by PDE4 activity in cardiomyocytes in response to ISO treatment (Fig. 3.5). The chemical ablation of PDE4 using the PDE4 specific inhibitor, rolipram could dramatically increase

ISO-induced HSP20 phosphorylation at Ser16. In addition, inhibition of PKA activity by KT5720 markedly attenuated HSP20 phosphorylation at Ser16 (Fig. 3.6). Clearly, PDE4s are highly expressed in cardiomyocytes and contribute to most PDE activities for cAMP degradation (Mongillo *et al*., 2004). Moreover, the cardioprotective mechanism triggered by HSP20 is associated with its phosphorylation on Ser16 by PKA (Fan *et al*., 2005). In this context, inhibition of PDE4 activity with rolipram which is required to achieve maximal cAMP accumulation (Thompson *et al*., 2002) is likely to result in an increase in PKA-mediated phosphorylation of HSP20. Interestingly, inhibition of PDE4 alone is enough to increase phosphorylation levels of HSP20 in resting cells, suggesting that sequestration of PDE4 may play a key role in maintaining the dephosphorylated state of HSP20 under basal condition. Seemingly, HSP20 exists in the inactive state by virtue of its association with PDE4. This enzyme is known to control cAMP dynamics by acting as 'sinks' to locally drain cAMP, thus preventing inappropriate PKA phosphorylation caused by variations in basal cAMP levels (Baillie, 2009). Intracellular cAMP levels are the result of the balance between cAMP synthesis and its exclusive hydrolysis by PDE4 (Lugnier, 2006). Presumably, PDE4 can protect HSP20 from inappropriate PKA phosphorylation due to fluctuations in basal cAMP levels. However, under conditions of elevated cAMP, the PDE4 activity associated with HSP20 is not sufficient to protect HSP20 from phosphorylation and cAMP concentration increased upon *β*-adrenergic stimulation saturate tethered PDE4 to allow PKA activation and consequently, the phosphorylation of HSP20.

3.4.3 PDE4 isoforms associate directly with HSP20

Further work using co-immunoprecipitation and *in vitro* binding assays provided evidences of direct interaction between PDE4 (in particular PDE4D) and HSP20 in cardiomyocytes (Fig. 3.7 and 3.8). Immunocytochemistry studies suggested that both HSP20 and PDE4D are likely to exist in the same cellular compartment since both proteins localised with α-actinin (Fig. 3.9). Indeed, PDE4 has been shown to be localised to the sarcomeric Z-disk in proximity to *β*AR (Mongillo *et al*., 2004). The findings outlined above support the hypothesis that PDE4 co-exists in a complex with HSP20 to modulate PKA-mediated HSP20 phosphorylation. This notion is supported by previous results showing that PDE4D isoforms are associated with *β*AR and the regulation of cAMP accumulation (Mongillo *et al*., 2004; Xiang *et al*., 2005; Richter *et al*., 2008). Using a transfected cyclic nucleotide-gated (CNG) channel sensitive to cAMP, PDE4 activity was increased upon β-adrenergic

stimulation and was shown to control the subsarcolemmal cAMP levels in cardiomyocytes (Rochais et al., 2004). Clearly, activated *β*AR couples to G_s proteins to stimulate adenylyl cyclases (ACs) for the production of cAMP and increases PKA activity for the phosphorylation of a range of substrates (Lefkowitz *et al*., 2002; Conti and Beavo, 2007; Houslay *et al*., 2007). PKA activity is greatly depending on cAMP diffusion (Saucerman *et al*., 2006). Collectively, these findings suggest a key role of PDE4 in shaping β-AR-dependent cAMP signals and thereby regulating cAMP-dependent PKA activity. In this context, PDE4 is thus considered to be particularly important in protecting HSP20 from inappropriate phosphorylation during basal cAMP oscillations and to regulate cAMP-dependent PKA phosphorylation induced by *β*-agonists.

3.4.4 HSP20 binds to the conserved catalytic region of PDE4

Peptide array technology was carried out as a rapid and informative means of determining protein-protein interaction sites (Bolger *et al*., 2006). Indeed, this method has been used in my laboratory to considerable advantage to define the binding sites on PDE4D5 for RACK1 (Bolger *et al*., 2006) and *β*-arrestin (Baillie *et al*., 2007). Here, a recombinant purified His-HSP20 was used to probe a library of overlapping, immobilized 25-mer peptides that scanned the full-length sequence of PDE4D5. An interacting peptide spanning V^{466}-L^{490} was subsequently used as a template to generate a library of progeny where individual amino acids in the 25-mer parent were each substituted with alanine (or substitute aspartate for alanine). This array-based method uncovered the interaction site of PDE4D-HSP20 within the conserved catalytic region and highlighted the critical residues involve in the binding (Fig. 3.10A). The nature of the interaction surfaces was then revealed by superimposing the key residues on a known crystal structure of PDE4D catalytic domain (Fig. 3.10B). The critical residues are mostly surface-exposed and hence available for interaction. These findings are also particularly interesting in view of the engagement of a single docking site for HSP20 on PDE4 which located within an evolutionarily conserved region. In fact, this result would contradict the notion that interacting partners of PDE4 often bind at multiple docking sites on the enzyme, as seen in RACK1-PDE4D5 (Bolger *et al*., 2006) and DISC1-PDE4B (Millar *et al*., 2005). However in this context, the binding of HSP20 to PDE4 does not require such isoform specificity. On the other hand, mapping of the interaction site of PDE4D5 on HSP20 identified a physiologically relevant phosphorylation motif RRASA within its N-terminus (Fig. 3.11),

a site which is implicated in the *β*-adrenergic/cAMP-dependent PKA signalling pathway (Beall *et al*., 1997). This region is likely to enhance the influence of PDE4D5 on the activation of PKA and the phosphorylation status of PKA-targeted HSP20. Further studies utilising site-directed mutagenesis approach together with structural information may identify other surface–associated residues of putative importance to binding.

In many cases, the biological functions of a signalling complex can be further characterised by cell-permeable analogues of 25-mer peptides that are identified from peptide array studies (Smith *et al*., 2007; Meng *et al*., 2009). Previously, my laboratory had successfully used such approach to disrupt the interactions between β-arrestin and its binding partners, PDE4D5 (Smith *et al*., 2007) and MAPK kinase, MEK1 (Meng *et al*., 2009) to study the functional consequences of these complexes. Results showed that the disruptor peptides displaced the *β*-arrestin complexes in cells and resulted in aberrant cellular signalling. Hence in this study, in order to gain insight into the functional role of the PDE4D5-HSP20 complex, the sequence information gleaned from alanine scanning array analysis was then used to generate a cell-permeable disruptor peptide 'bs906' which specifically interfered with the interaction between HSP20 and PDE4D5 (Fig. 3.12). Interestingly, the disruption of the interaction between PDE4D5 and HSP20 triggered an increase in the phosphorylation of HSP20 at Ser16 under resting conditions in HEK293 cells (Fig. 3.13). This may indicate that the association between PDE4D5 and HSP20 is required to gate the protective PKA-mediated phosphorylation of HSP20. Clearly, this peptide-mediated approach which allowed the incorporation of exogenous peptides into living cells has enhanced our understanding of the molecular mechanism behind fundamental cellular events.

3.4.5 Disruption of PDE4D5-HSP20 complex protects against hypertrophy

Given that PDE4D5 is associated with HSP20 and modulates its phosphorylation, disruption of this association is likely to have potentially beneficial effects on HSP20 phosphorylation and related function. Indeed, treatment of neonatal rat cardiomyocytes with this disruptor peptide 'bs906' resulted in hyperphosphorylated endogenous HSP20 and the induction of cardioprotective mechanisms, an outcome not seen in cells treated with scrambled control peptide. Interestingly, phospho-HSP20 was shown to attenuate ISO-mediated hypertrophic response in cultured neonatal rat cardiomyocytes as

determined by a reduction in the increase in cell size and protein synthesis (Fig. 3.14, 3.15). It is in agreement with previous results which showed increased phospho-HSP20 levels are required for cardioprotective responses during sustained *β*-agonist treatment (Fan *et al*., 2004, 2006; Nicolaou *et al*., 2008). Clearly, phosphorylation of HSP20 at Ser16 is essential to trigger the cardioprotective ability of HSP20. Hence, displacement of PDE4D5 association with HSP20 is likely to be a novel strategy for the development of cardioprotective targets.

Moreover, disruptor peptide 'bs906' appeared to augment the expression of fetal gene ANF. Despite being a marker for cardiac hypertrophy, it is noteworthy that ANF could also exert local anti-hypertrophic effects in the heart via inhibition of cell growth (Horio *et al*., 2000). Moreover, an increased in ANF expression may serve as a compensation mechanism to reduce both cardiac preload and after load via natriuretic and vasodilatory actions (Nishikimi *et al*., 2006). In this regard, the increase of ANF expression is thus likely to be part of a compensatory protective response against hypertrophy. Whether this compensatory mechanism is triggered by HSP20 hyperphosphorylation resulting from disruption of association with PDE4D5 or if other protective mechanism is involved, remains to be elucidated.

3.4.6 Conclusion

In conclusion, I present the first evidence for the specific association of PDE4D5 with HSP20 to regulate its biological function. This study also further verifies the importance of HSP20 phosphorylation and its cardioprotective role in counteracting the hypertrophic growth of cardiomyocytes in response to hypertrophic stimuli. Clearly, disruption of the PDE4D5-HSP20 interaction with the cell-permeable peptide 'bs906' that corresponds to the HSP20 docking site on PDE4D5 results in the hyperphosphorylation of HSP20. Importantly, this post-translational modification is required for cellular protection against hypertrophy. Since current conventional PDE4 inhibitors are limited by their poor selectivity which leads to serious dose-limiting side effects, such displacement strategies as that used for the selective inhibition of the PDE4D5-HSP20 signalling complex this study are likely to be a novel route for therapeutic exploitation. Observations of the effect of the disruptor peptide 'bs906' on cardiomyocytes *in vitro* are likely to provide the basis for studies to determine its *in vivo* efficacy in experimental cardiac disease models. As such,

further work may include optimisation of disruptor peptide 'bs906' to generate a small, higher affinity and metabolically stable peptide analogue for better therapeutic viability. Disruptor peptide 'bs906" could also be used in an assay to screen for small molecules that may also disrupt the HSP20-PDE4 complex. Where appropriate, these small molecule disruptors could be testing *in vivo* in animal models of cardiac hypertrophy to confirm that pharmacological manipulation of the target is therapeutically beneficial.

3.4.7 Small molecules therapies for heart disease

A growing body of evidence has demonstrated that small molecules inhibitors could be used to target intracellular signalling pathways inside the cardiac muscle cells to suppress or reverse hypertrophy. Of interest, a cGMP-specific PDE5 inhibitor, sildenafil (Viagra, Pfizer) have been shown to induce vasorelaxation of precontracted pig coronary artery in a dose-dependent manner which is accompanied by a substantial increase in the phosphorylation level of HSP20 (Tessier *et al*., 2004). Takimoto *et al*., (2005) later demonstrated that chronic inhibition of PDE5A using sildenafil hindered the progression of hypertrophy and enhanced cardiac function in mice exposed to sustained pressure overload induced by thoracic aortic banding. It was also reported that sildenafil reversed pre-existing hypertrophy by preventing contractile dysfunction and reversing pathological remodeling. In addition, ruboxistaurin (LY 333531), which is a PKCβ inhibitor has been shown to attenuate pathological fibrosis and remodeling in rats subjected to myocardial infarction (MI) (Boyle *et al*., 2005). It was proposed that the anti-hypertrophic effect may involve inhibition of PKC-mediated transforming growth factor-beta (TGF-beta) expression via the MAP kinase cascade. Clearly, there is growing promise in the use of small molecules peptides as drugs.

Chapter 4

ProtoArray analysis identifies Protein Kinase D1 (PKD1) as an interactor of HSP20

4.1. Introduction

4.1.1 The study of protein-protein interaction

Proteins need to interact with other proteins to exert their biological functions. Hence, comprehensive protein-protein interaction profiling is of immense value in providing mechanistic insight into complex regulatory networks, which underlie specific cellular function. Recently, human protein microarray (ProtoArray) technology has been established to allow rapid and robust screening of protein-protein interactions in a high-throughput manner (Schweitzer *et al*., 2003). This flexible technique can be used for a wide range of applications including characterisation of antibody specificity, identification and validation of immune response biomarkers and novel molecular targets, as well as drug profiling (Michaud *et al*., 2006; Satoh *et al*., 2006, 2009; Sumiyoshi *et al*., 2010).

The ProtoArray has many classes of highly purified, full-length, recombinant GST-tagged human proteins that are immobilised on a chip. These proteins are expressed in insect cells using the baculovirus expression system and subsequently purified under native conditions by employing glutathione affinity chromatography to ensure structural and functional stability (Satoh *et al*., 2006, 2009). The target proteins extend from the array surface via the epitope tag, which serves as a spacer to enhance binding. Interactions with the spatially accessible target proteins can then be detected by probing the array with a separate protein of interest that has been pre-purified by the user. ProtoArray chips also contain a series of built-in control spots that allow evaluation of inter- and intra-array variability.

4.1.2 Background and project aim

Previous studies have described various cardioprotective functions of HSP20 in a cardiac setting (Fan *et al*., 2005). To date, possible targets of HSP20 include cytoskeletal elements, actin and the apoptotic protein, Bax which result in the stabilisation of cytoskeleton and inhibition of apoptosis, respectively (Fan *et al*., 2004). In addition, HSP20 also alters the downregulation of apoptosis signal-regulating kinase 1 (ASK1), leading to an inhibition of isoprenaline-mediated hypertrophy (Fan *et al*., 2006). Nevertheless, the molecular mechanism that underpins HSP20-induced cardioprotection is not yet clearly defined as it

remains to be determined whether other signalling pathways are involved. As the regulation of protein function often relies on protein-protein interactions, an insight into the function of a particular protein and the regulatory signalling networks involved can be obtained if potential interaction partners are defined.

This project sought to characterise potential interactors of HSP20 using high-density ProtoArray analysis. It is anticipated that the identification of novel signalling complexes containing HSP20 will help to gain further insight into the function of HSP20 in hypertrophy signalling pathways.

4.2. Results

4.2.1 ProtoArray identified 21 HSP20 interactors

Recombinant His-HSP20 fusion protein was purified under native conditions (see 'Materials & Methods' for details). Coomassie staining of purified HSP20 sample showed a single 20-25 kDa band indicating a highly purified His-tagged HSP20 that was used to probe ProtoArray chips (Fig. 4.1). The identity of the band was further confirmed by immunoblotting using both anti-His (Fig. 4.2A) and anti-HSP20 antibodies (Fig. 4.2B). Following screening with His-HSP20 probe, the data suggested that 21 of the 8000 target proteins showed significant interaction with HSP20 (Table 4.1). Positive control spots such as Alexa Fluor 647-labelled antibody were detected, verifying the probing and detection protocols. However, no signal was detected from the negative control spots including those of BSA, GST, calmodulin, human IgG, anti-biotin antibody and buffer-only control, confirming the reliability of the data obtained.

The expression profiles of the 21 HSP20 interactors were studied using the National Center for Biotechnology Information (NCBI) website (http://www.ncbi.nlm.nih.gov). The database search suggested that most of the interactors are involved in neuronal, cardiac or immune functions. Following intensive searches for the biological implications of the putative HSP20 binders on PubMed, protein kinase D1 (PKD1) (Fig. 4.3) was found to

have physiological relevance as both it and HSP20 are known to have roles in hypertrophy signalling. Hence, PKD1 was chosen as the focus of this study. The interaction between HSP20 and PKD1 is novel and this is the first report of such an interaction.

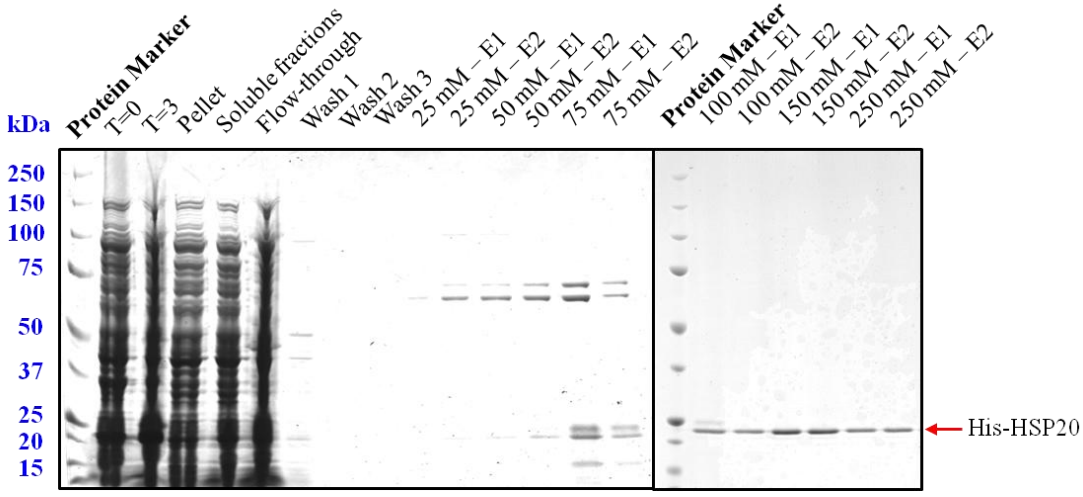

Figure 4.1. Native purification of His-tagged HSP20. The protein was purified with Ni-NTA resin as described in materials and methods. The resin with bound protein was washed with buffer containing10 mM imidazole and eluted with a linear gradient from 20 mM to 250 mM imidazole. 2x 500 µl fractions from each concentration were collected. Eluted fractions were then analysed on 4-12% SDS-PAGE gel and visualised by Coomassie staining. *T=0: before induction; T=3: after 3 h of IPTG induction; E1: first eluate; E2: second eluate.*

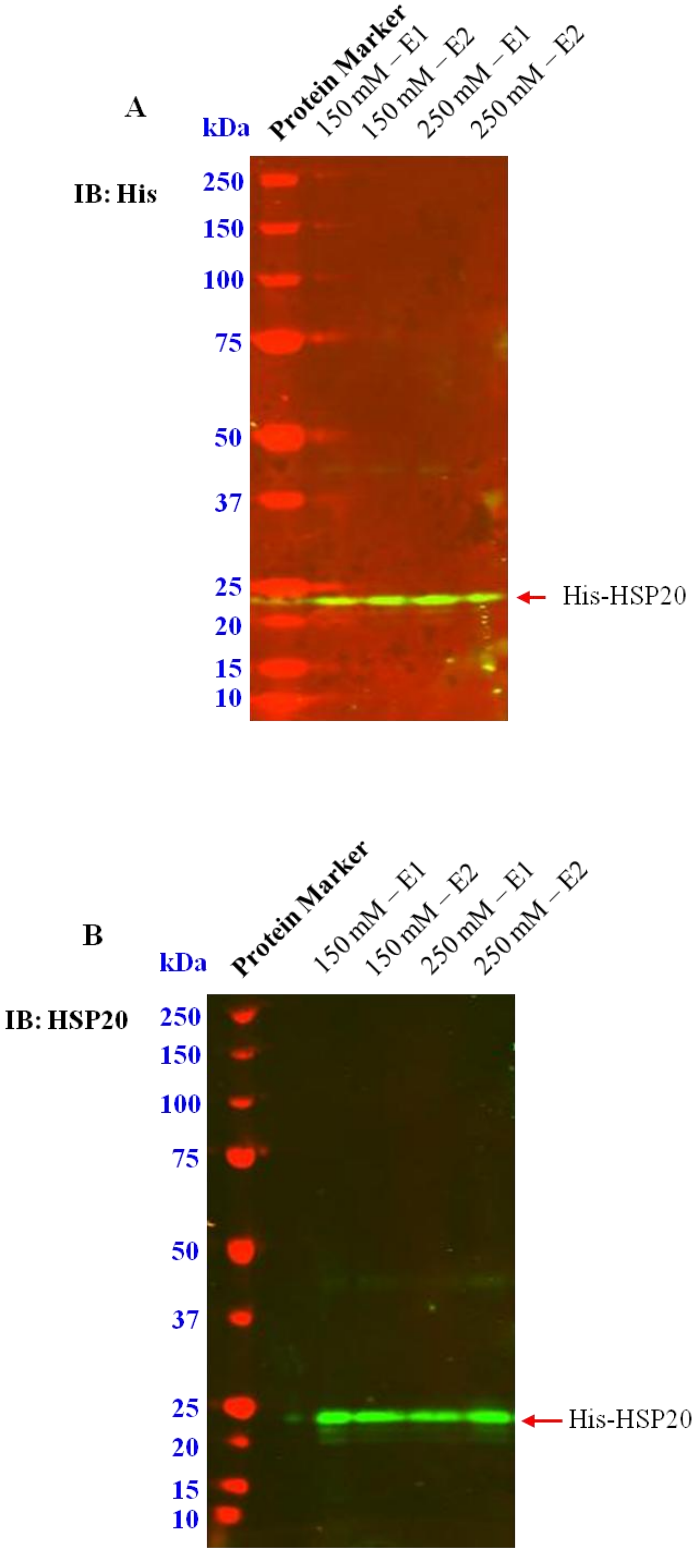

Figure 4.2. The His-tagged HSP20-specific probe utilised for ProtoArray analysis. The protein was separated by 4-12% SDS-PAGE gel. The blots were then labelled with anti-His antibody (A) and anti-HSP20 antibody (B), and detected by fluorescence secondary antibodies on Odyssey Infrared Imaging System. *IB: Immunoblotting.*

Table 4.1. The list of HSP20 interactors identified by ProtoArray.

No.	Accession No.	Name	Putative function
1	NM_002737	Protein kinase C, alpha (PRKCA)	Regulation of cardiac contractility
2	NM_002738	Protein kinase C, beta (PRKCB)	B cell activation, regulation of neuronal functions
3	NM_002739	Protein kinase C, gamma (PRKCG)	Involves in long term potentiation/depression
4	NM_002742	Protein kinase D1 (PRKD1)	Regulation of myocardial contraction and remodeling
5	NM_024482	Glucocorticoid modulatory element binding protein 1 (GMEB1)	Transactivation of gluococorticoid receptor
6	NM_004281	BCL2-associated athanogene 3 (BAG3)	Inhibition of chaperone activity by promoting substrate release
7	NM_145796	Pogo transposable element with ZNF domain (POGZ)	Interact with transcription factor SP1
8	BC012289	HLA-B associated transcript 2-like	Control of apoptosis and regulating HSP
9	BC012984	Par-3 partitioning defective 3 homolog B (C. elegans) (PARD3)	Asymmetric cell division and polarised growth
10	NM_178191	ATPase inhibitory factor 1 (ATPIF1)	Inhibition of mitochondrial ATPase to ATP hydroysis
11	NM_022101	Chromosome X open reading frame 56 (CXorf56)	Unknown
12	BC042333	F-box protein 21	Substrate-recognition component of E3 ubiquitin ligase complex

Table 4.1. *(Continued)*

No.	Accession No.	Name	Putative function
13	NM_022165	Lin-7 homolog B (C. elegans) (LIN7B)	Unknown
14	BC001709	NAD kinase	Catalyses the transfer of a phosphate group from ATP to NAD to generate NADP
15	BC034028	SHANK-associated RH domain interactor	Immune development and control of inflammation
16	NM_003161	Ribosomal protein S6 kinase, 70kDa, polypeptide 1 (RPS6KB1)	Protein synthesis and cell proliferation
17	NM_020375	Chromosome 12 open reading frame 5 (C12orf5)	Block glycolysis, protection from DNA damage-induced apoptosis
18	NM_002688	Septin 5 (SEPT5)	Regulation of cytoskeletal organisation, cytokinesis
19	NM_014321	Origin recognition complex, subunit 6 like (yeast) (ORC6L)	DNA replication and segregation with cytokinesis
20	NM_002788	Proteasome subunit, alpha type, 3 (PSMA3)	Processing of class I MHC peptides
21	NM_002609	Platelet-derived growth factor receptor, beta polypeptide (PDGFRB)	As mitogens for cells of mesenchymal origin

A

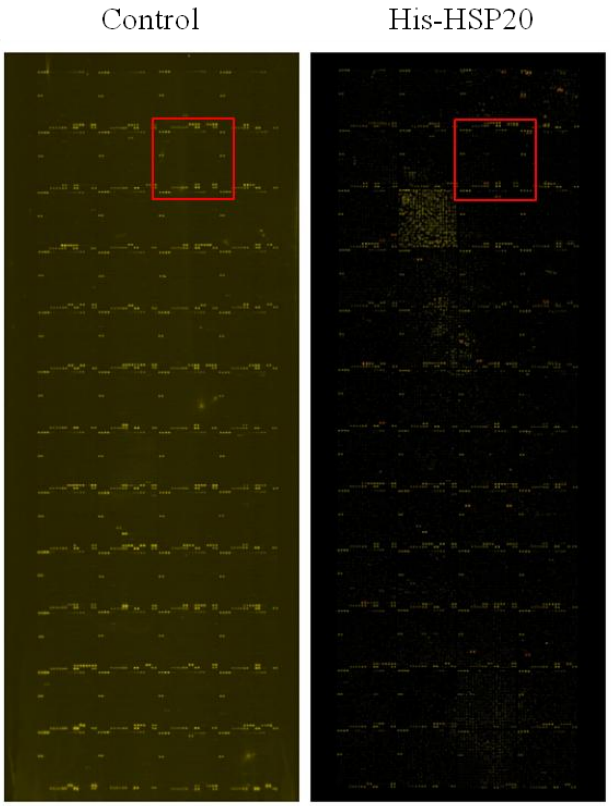

B

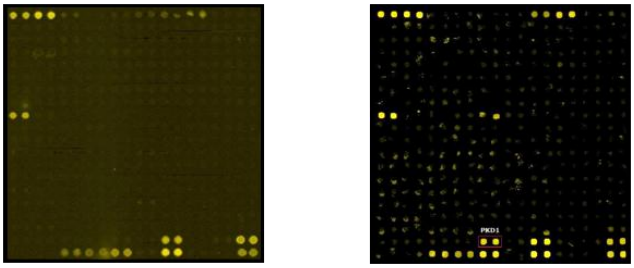

Figure 4.3. Identification of PKD1 on ProtoArray. (A) The array containing duplicate spots of more than 8000 proteins is composed of 4 x 12 sub-arrays. Each sub-array contains 20 x 20 spots composed of target proteins, control and empty spots. (B) Image showing sub-arrays (red boxes) of a control array (left) and an array probed with purified His-tagged HSP20 protein (right). A robust signal showing regular spot morphology positioned at row 19 and columns 9-10 represented PKD1. Other signals were from reference spots or proteins for which signals were not duplicated.

4.2.2 Validation of the interaction between HSP20 and PKD1

To validate the results of ProtoArray analysis, biochemical studies were carried out. The interaction between HSP20 and PKD1 was first confirmed using *in vitro* pull-down experiment where purified His-HSP20 but not purified His-tag alone acted to pull-down PKD1 (Fig. 4.4A). Co-immunoprecipitation analyses were then carried out to investigate if the interaction could also be observed *ex vivo* using endogenous and overexpressed proteins. First, an anti-PKD1 antibody was used to pull down endogenous PKD1 from lysates prepared from cardiomyocytes, while a GFP-specific antibody immunoprecipitated exogenously expressed GFP-PKD1 from lysates made from transfected HEK293 cells. The immunocomplexes were then tested for the presence of HSP20 protein using anti-HSP20 and anti-V5 antibodies, respectively. Fig. 4.4B-C shows that PKD1 and HSP20 co-immunoprecipitate in both cell lines. The interaction was detected between the endogenous and transfected proteins. Bands were also detected in reciprocal experiments where HSP20 immunoprecipitates were tested for the presence of PKD1 protein. This robust evidence suggests that a pre-formed and stable interaction exists between these interacting partners. In contrast, control experiments using mock IPs (IgG alone) recovered neither HSP20 nor PKD1, supporting the specificity of the interaction. Although co-immunoprecipitation is not evidence of direct interaction as it is possible that other proteins may be associated with the PKD1-HSP20 immunocomplex, the *in vitro* pull-down experiments suggest that there is direct contact.

ProtoArray is a useful technique for screening proteins of interest for interacting partners, however it does not provide information on whether interactions are functionally relevant. Often, the location of a protein within a cell is relevant to its function. To this end, I undertook cell imaging analyses to evaluate whether the locations of PKD1 and HSP20 showed any similarity. Confocal microscopy imaging showed that PKD1 and HSP20 localise in close proximity in both cardiomyocytes and co-transfected HEK293 cells (Fig. 4.5). These observations may suggest that interaction between PKD1 and HSP20 is likely to occur and play a functional role in cells.

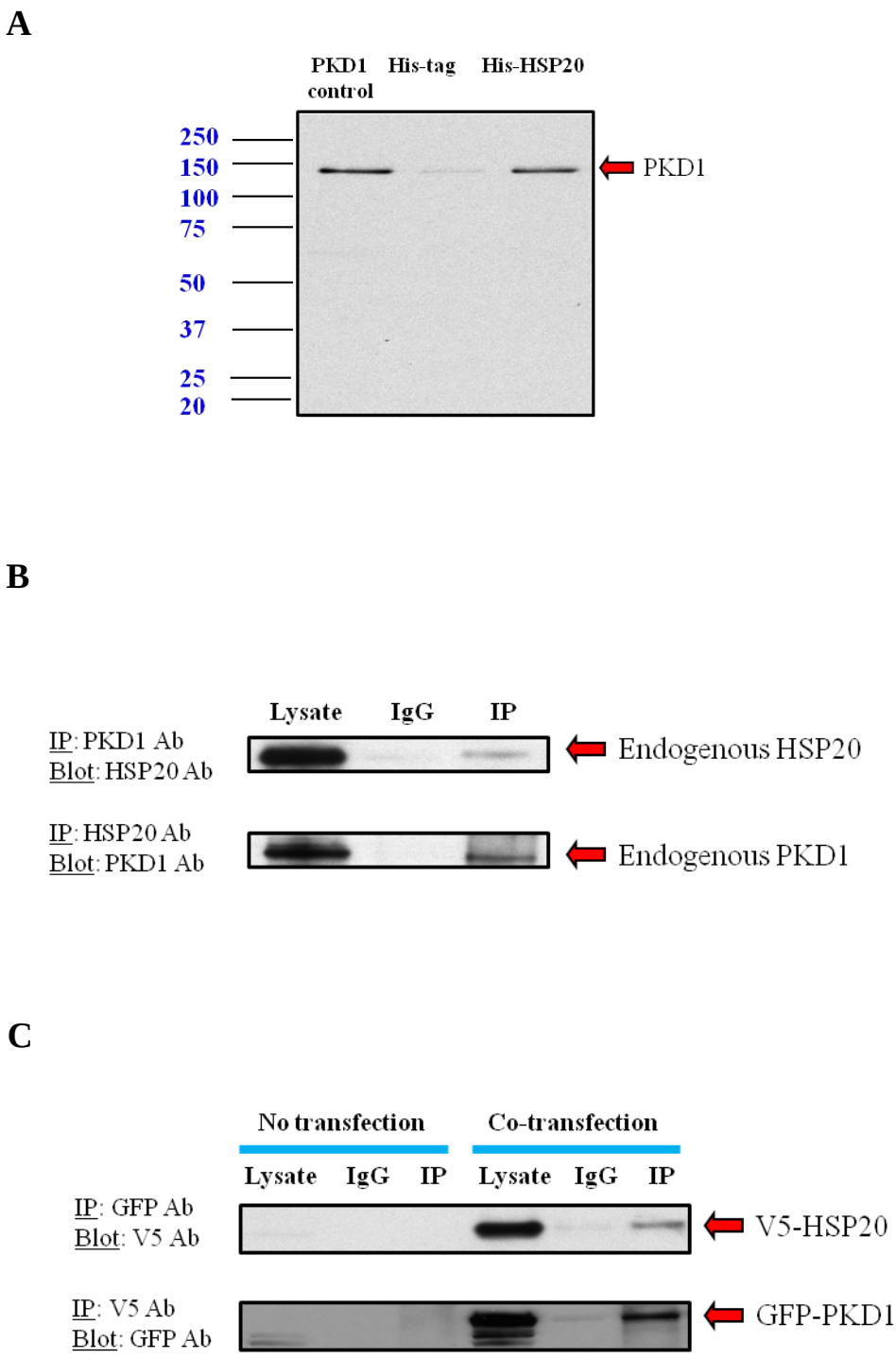

Figure 4.4. Immunoblots showing *in vitro* and *in vivo* association of HSP20 and PKD1. (A) *In vitro* pull-down: Purified His-tagged HSP20 acts as bait to pull-down PKD1. Purified PKD1 (Abcam) was used as positive control. (B) Endogenous HSP20 and PKD1 were immunoprecipitated from neonatal cardiomyocytes lysates. (C) Lysates of HEK293 cells co-expressing V5-HSP20 and GFP-PKD1 were immunoprecipitated using anti-V5 or anti-GFP antibodies. The first lanes of lysate represent input control while second lanes of IgG as negative control. Blots are representative of three separate experiments.

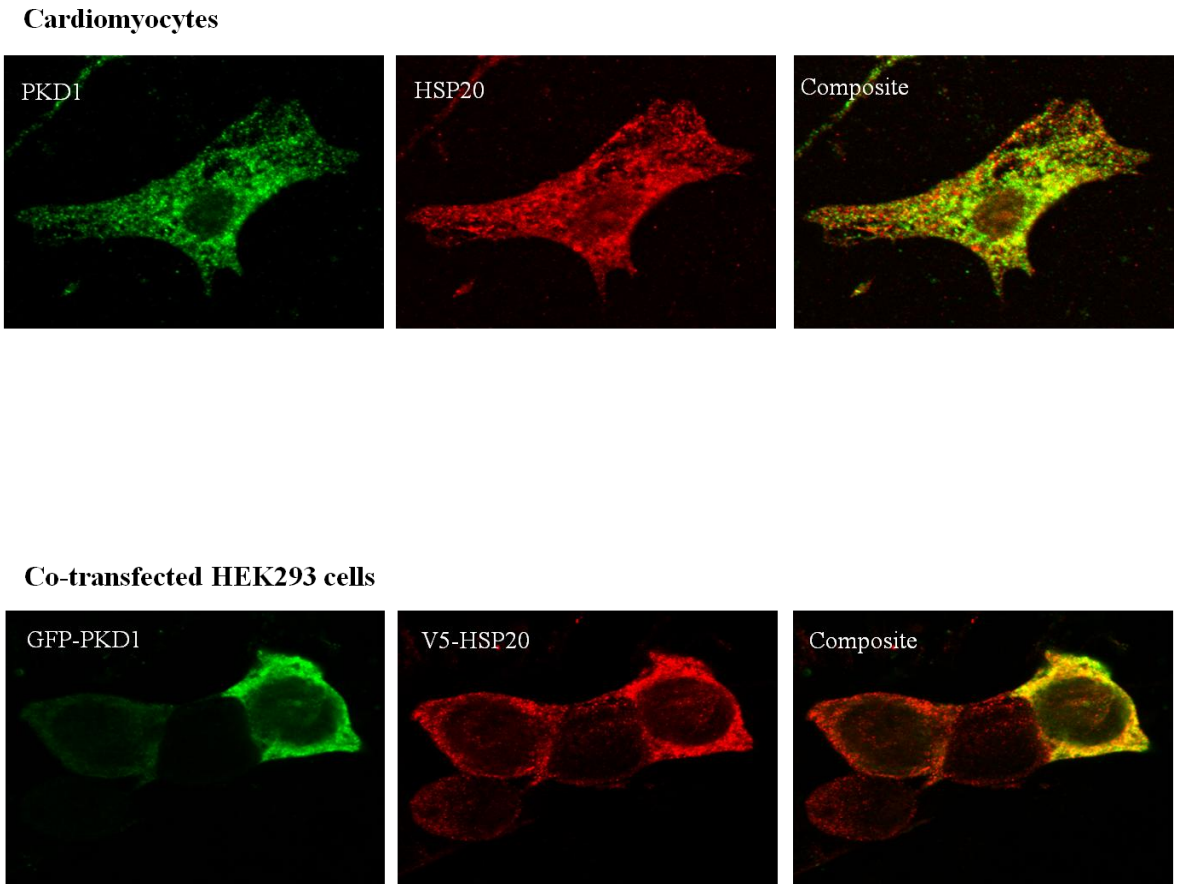

Figure 4.5. PKD1 colocalises with HSP20. Subcellular distribution of PKD1 and HSP20 assessed by immunostaining and confocal microscopic analyses using cardiomyocytes and co-transfected HEK293 cells. Cardiomyocytes were double immunolabelled with anti-PKD1 (mouse) and anti-HSP20 (rabbit) antibodies, whereas HEK293 cells were immunostained with anti-V5 (rabbit) antibody. The cells were then labelled with Alexa Fluor 488-conjugated anti-mouse IgG (green) and Alexa Fluor 594-conjugated anti-rabbit IgG (red). The merged images show the extent of overlap between PKD1 and HSP20 localisation signals. Images are representative of three separate experiments on different cell culture preparations.

4.2.3. Mapping binding region of HSP20 on PKD1

Peptide array is a rapid and flexible technique that has been used recently to map protein-protein interactions (Bolger *et al*., 2006). Peptide array libraries of overlapping 25-mer peptides (each shifted by five amino acids) that encompassed the entire sequence of PKD1 were synthesized using SPOT synthesis. The array was probed with purified recombinant His-tagged HSP20 protein and then detected with anti-His antibody. Positively interacting peptides generated dark spots whereas non-interacting peptides were left blank. Whilst no signal was observed on control array overlaid with anti-His antibody alone, five binding spots were detected when the arrays were probed with His-HSP20. These spots were located in the pleckstrin-homology (PH) and catalytic domain of PKD1 (Fig. 4.6A).

In order to gain further insight into the interaction, the optimal interacting sequence with strongest binding affinity (as shown by darkest spot) was selected for subsequent scanning alanine substitution analyses. Alanine is a non-polar, hydrophobic amino acid. It is a good substitution because it carries a relatively small methyl side chain (CH_3) and is less likely to disrupt the protein structure (Cunningham and Wells, 1989). Alanine scans of the peptide encompassing amino acids G^{606}-E^{630} (GRDVAIKIIDKLRFPTKQESQLRNE) in PKD1 clearly identified several amino acids that were essential for the direct interaction between HSP20 and PKD1. Seven residues in particular (R^{607}, D^{608}, V^{609}, I^{611}, I^{613}, D^{615}, E^{624}) appeared critical for the binding of HSP20 to PKD1 (Fig. 4.6B).

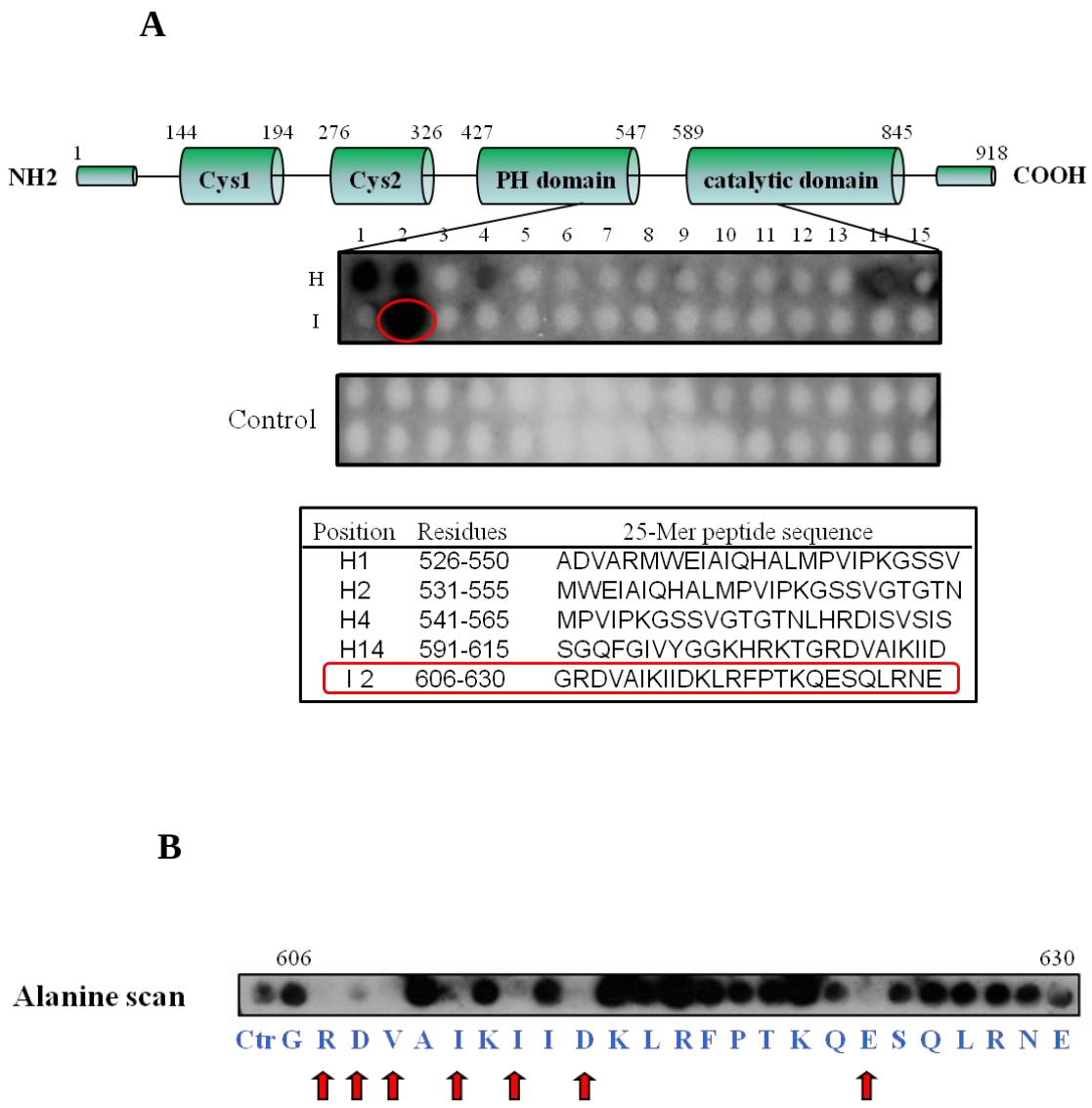

Figure 4.6. Identification of HSP20-PKD1 interaction sites. (A) The disposition of the peptides is shown relative to known regulatory regions in a schematic representation of PKD1 structure, which includes its N-terminal region, cysteine-rich domains, pleckstrin-homology (PH), catalytic domain and C-terminal region. Peptide array analysis defines binding sites for HSP20 in the pleckstrin-homology (PH) and catalytic domain of PKD1. Binding spot numbers relate to peptides in the scanned array and whose residues position and sequence are given in the table below. (B) Scanning alanine substitution analysis using the sequence showing the greatest interaction (G^{606}-E^{630}) identified key amino acids involved in HSP20 binding to the PKD1 catalytic unit (red box). Native peptide (Ctr) plus progeny with the indicated residue substituted for alanine or aspartate. Red arrow indicates ablation or severe attenuation of binding. Arrays are representative of at least three separate experiments.

4.2.4. Protein structure prediction of PKD1 catalytic domain

As the crystal structure of PKD1 structure remains unsolved, protein structure prediction was carried out to predict the three-dimensional (3D) structure of the PKD1 catalytic domain. The structural prediction was done using the Protein Homology/analogY Recognition Engine Version 2.0 (Phyre2) web server (http://www.sbg.bio.ic.ac.uk/phyre2/html/page.cgi?id=index) which implements the principles of comparative homology modeling. The modeling was undertaken by referring the protein of interest to the previously solved structure of another homologous protein (Kelley and Sternberg, 2009). Typically, the procedure for homology modeling involves four steps which consist of template selection, sequence alignment, model building, and finally analysis and evaluation. As protein structures are more likely to be evolutionally conserved than related amino acid sequences, it was expected that the two homologous kinases would share high similarity in structures.

Based on studies of local sequence alignment, a serine/threonine protein, human p21-activated kinase 6 (PAK6) (Protein Data Bank ID: 2c30) was chosen as the best template hit for modeling the structure of PKD1 catalytic domain using Phyre2 web server. Selection was based on comparison of primary sequence and alignment accuracy. Although the template shares 33% sequence identities with target sequence, confidence values were given along with the predictions as 100%, indicating high probability of homology between the two sequences. Where necessary, sequence alignment was also carried out to examine individual aligned residues and provide information on the patterns of sequence conservation, as well as secondary structure elements (Fig. 4.7). The predicted secondary structure type for each residue is the type with the highest propensity or probability.

Alternatively, structures were presented using a molecular visualisation program named Visual Molecular Dynamics (VMD) (Humphrey *et al*., 1996). Superimposing the seven residues (R^{607}, D^{608}, V^{609}, I^{611}, I^{613}, D^{615}, E^{624}) on a predicted 3D structure of PKD1 catalytic domain showed that all of these amino acids are on solvent accessible surface of the macromolecule, thereby forming a well-defined surface-exposed patch that could serve as a HSP20 docking site (Fig. 4.8).

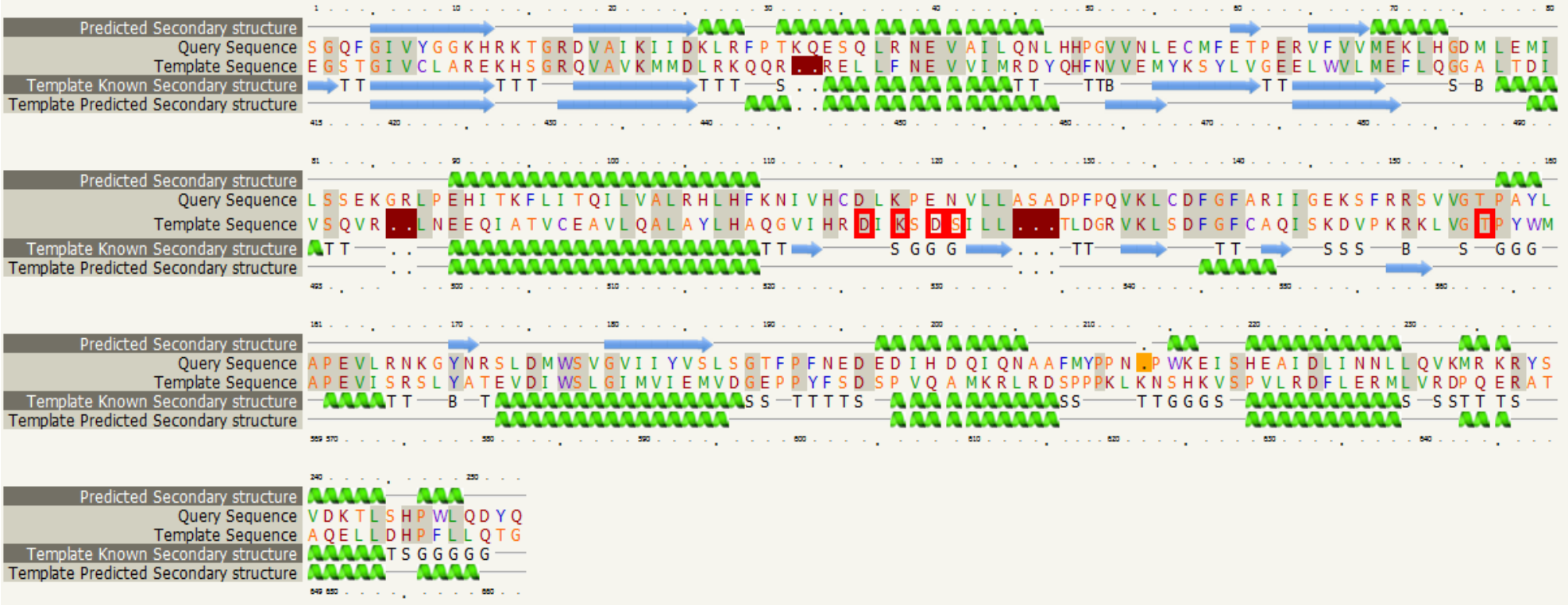

Figure 4.7. Amino acid alignment of PKD1 catalytic domain with 2c30 protein as template on Phyre2 web server. Sequence alignment and secondary structure similarity between PKD1 catalytic domain and the template used for structure prediction are shown. The amino acid sequences are represented in standard single-letter code. The polypeptide secondary structure of this domain was predicted in 3 states: α-helix, β-strand and coil. Green helices represent α-helices, whereas blue arrows indicate β-strands and straight lines indicate coil.

A

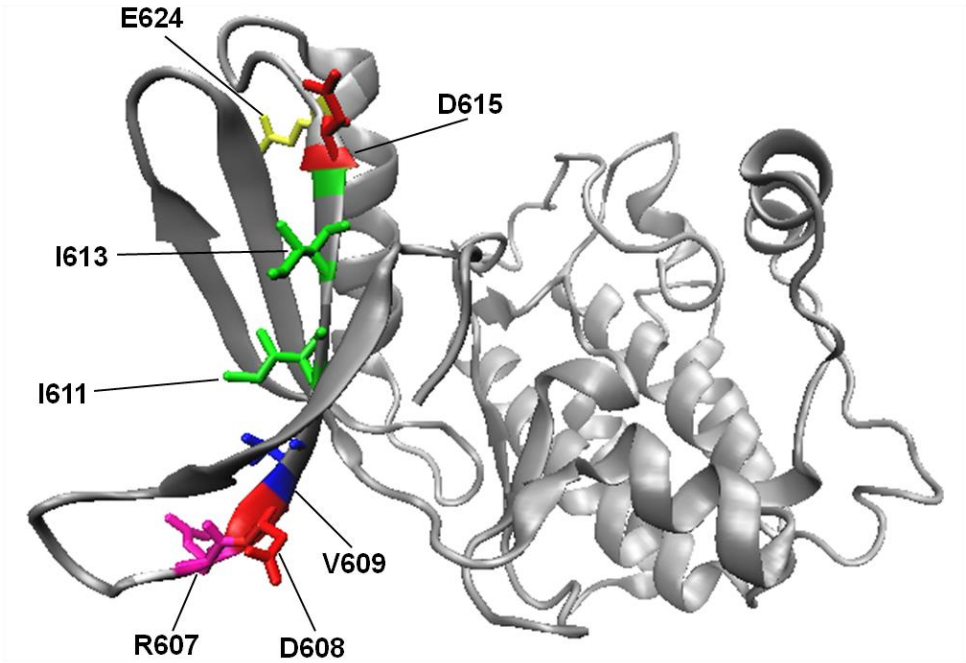

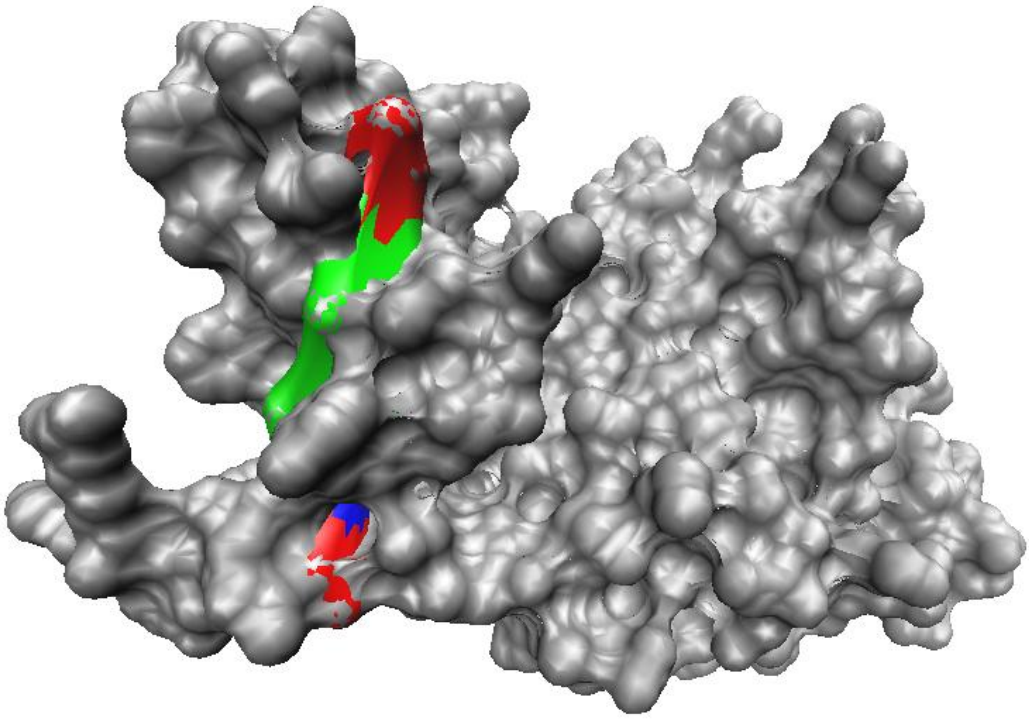

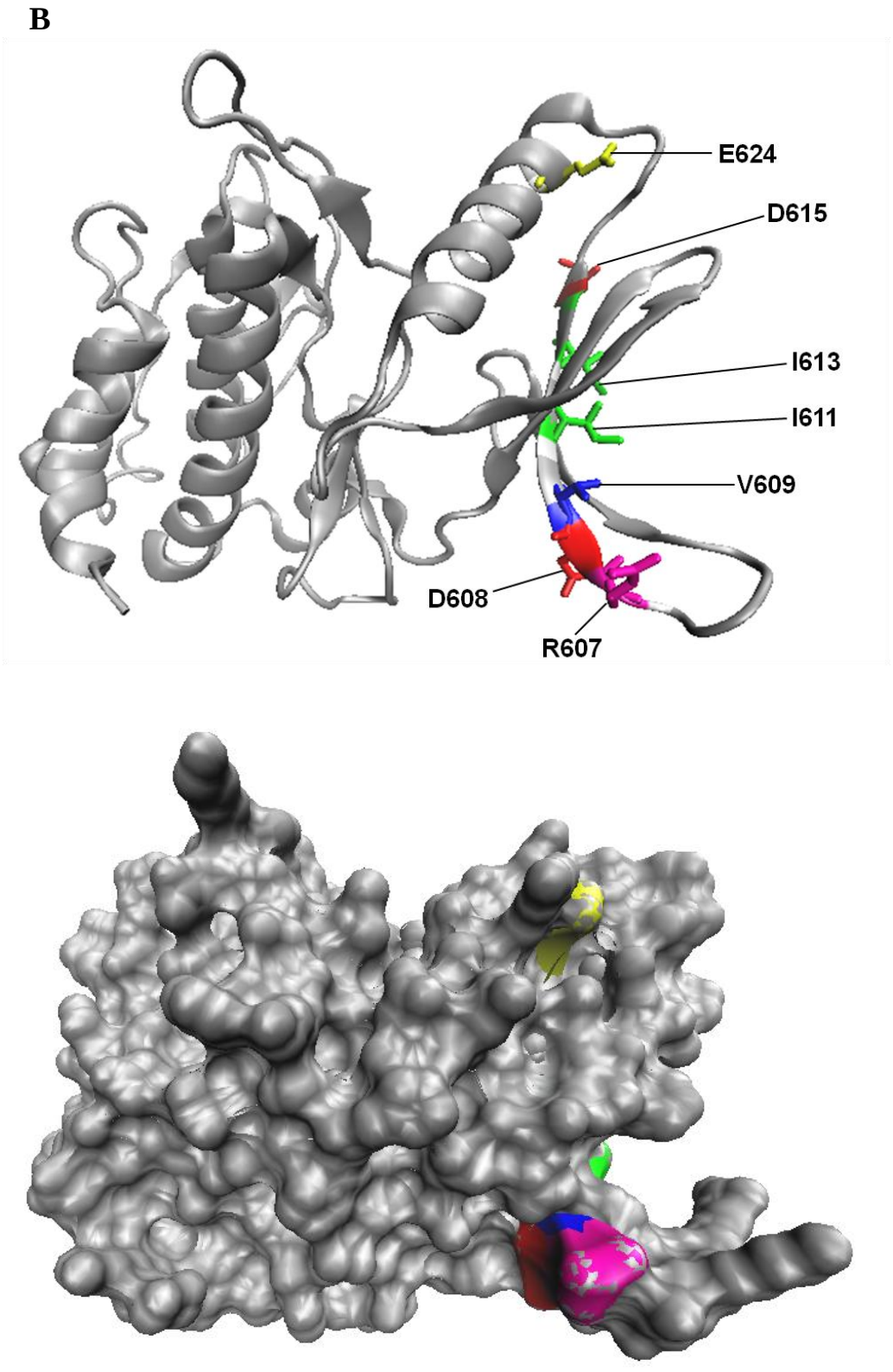

Figure 4.8. Predicted structure of PKD1 catalytic domain and location of residues implicated in HSP20 binding. PKD1 residues critical for the interaction with HSP20 were superimposed on a predicted 3D structure of PKD1 catalytic unit prepared from 2c30 structure as a template, presented in (A) front view and (B) back view, related by 180 degree rotation.

4.3. Discussion

The identification of interacting partners is one way to find clues about the functional role of a given protein. There are several methods to investigate protein-protein interactions including biochemical biophysical and computational methods. In this study, a new proteomic technology named ProtoArray was carried out as a discovery platform (Schnack *et al*., 2008; Satoh *et al*., 2009; Sumiyoshi *et al*., 2010). ProtoArray is a powerful tool to allow rapid, large-scale screening of protein-protein interactions in parallel under the same experimental conditions. The target proteins spotted on the glass slides were expressed in baculovirus expression system to promote the preservation of native conformations and post-translational modifications which often lacks in bacterially expressed proteins (Tennagels *et al*., 1999; Schweitzer *et al*., 2003). This approach has been utilised not only in basic biomedical research, but also in drug discovery research such as identification of protein kinase substrates and protein targets of small molecules (Chan *et al*., 2004; Michaud *et al*., 2003, 2006). For instance, ProtoArray substrate screen identified protein phosphatase 1, regulatory subunit 14A (PPP1R14A)/(CPI-17) as a novel substrate of a serine-threonine kinase, cyclin-dependent kinase (Cdk) 5 (Schnack *et al*., 2008), thus contributed to a better understanding of neuronal development and synaptic signalling. This array-based method was also used to characterise a comprehensive profiling of 14-3-3-interacting proteins, including those unpredicted by the Biomolecular Interaction Network Database (BIND) and PubMed database search (Satoh *et al*., 2006).

Here in this study, a comprehensive profile of human HSP20-interacting proteins was studied using high-density ProtoArray probed with recombinant purified HSP20 protein. This method was chosen over the conventional yeast two-hybrid assay because the latter requires labour-intensive steps and usually results in lower accuracy scores as it is prone to false positive and false negative interactions. Yeast two-hybrid discrepancies are commonly due to variations in bait and prey proteins levels, self-activating bait proteins, spontaneous activation of reporter transcription and alterations in yeast physiology (Knudsen *et al*., 2002; Vidalain *et al*., 2004). Moreover, the data sets obtained from yeast two-hybrid assay are often biased towards particular cellular localisation of interacting proteins, for example, the associations of tested proteins normally take place in the nucleus and not in their native cellular compartment (Fields and Song, 1989; Uetz *et al*., 2000). Hence, it is less likely to reflect the true physiological setting.

In addition, as the identity of proteins spotted on the array is known, any antibody cross-reactivity with these proteins can be further investigated to obtain information on the common sequence motifs that lead to cross-reactivity (Michaud *et al*., 2003). The fluorescent detection method used in ProtoArray analysis is also more sensitive than the commonly used chemiluminescent-based detection.

Utilising ProtoArray screening, a list of 21 proteins was identified as putative binding partners of HSP20. Among all the interactors, PKD1 was chosen for further studies because of its physiological relevance in hypertrophy. PKD1, also known as PKCμ, is an intracellular serine/threonine protein kinase which is involved in many biological functions (Lint *et al*., 2002). Being a major PKD isoform in the heart, it is involved in the regulation of myocardial contraction, hypertrophy and pathological cardiac remodeling (Harrison *et al*., 2006). Moreover, previous studies have shown that PKD1 is implicated in the phosphorylation of several myocardial proteins, such as cardiac troponin I and cardiac myosin binding protein C (cMyBP-C) (Haworth *et al*., 2004). Moreover, there is also evidence reported that PKD1 phosphorylates class II HDAC which functions as a negative regulator of cardiac remodeling through their repressive influence on myocyte enhancer factor 2 (MEF2) (Zhang *et al*., 2002). These findings suggest that PKD1 is a promising therapeutic target for a number of diseases within a cardiac setting. Nevertheless, the detailed intracellular mechanism(s) underlying cardiac hypertrophy remains to be uncovered.

Despite being a powerful tool for systematic identification of protein-protein interactions, ProtoArray has limitations that relate to the binding nature of the proteins. In fact, this method only detects direct protein-protein interaction that occurs in stable protein complexes. The protocol relies on rigorous washing steps, which may not allow weak or transient interactions to be easily detected. Indirect interactions which involve intervening molecules are also less likely to be detected. As such, it is worth noting that some other biologically important interactors could be left undetected. Nevertheless, protein microarray technology has been reported to be reliable and reproducible (Huang *et al*., 2004; Michaud *et al*., 2006; Satoh *et al*., 2006, 2009; Sumiyoshi *et al*., 2010).

The molecular interaction between HSP20 and PKD1 were investigated by biochemical and immunocytochemical studies. *In vitro* pull-down assay and co-immunoprecipitation experiments provided further evidence of a direct physical interaction and *in vivo* association of these two proteins. Additionally, scanning confocal imaging showed some

degree of overlapping punctuate staining of PKD1 and HSP20 which is primarily in the cytoplasm, suggesting that they are likely to localise to the same cellular compartment. Thus, it is speculated that the PKD1-HSP20 interaction is likely to be biologically relevant. Interestingly, this study was the first to show that PKD1 is a binding partner of HSP20. As both proteins are involved in hypertrophy signalling pathways, these observations may suggest a potential role of PKD1-HSP20 complex in regulating the hypertrophic response. Peptide array analyses were carried out to map the interaction sites of HSP20 on PKD1. This method provides valuable information to inform predictions of binding events of proteins with peptide ligands (Bolger *et al*., 2006). Results showed that HSP20 binds mainly in the PH and catalytic domain of PKD1, having stronger binding affinity with the latter.

Previous studies have performed yeast two-hybrid screens of human cardiac libraries to identify myocardial substrates of PKD1 by using the PKD catalytic domain as bait (Haworth *et al.,* 2004). This work has highlighted several myofilament proteins such as cardiac troponin (cTnI), cardiac myosin-binding protein C (cMyBP-C) and telethonin as forming complexes with PKD. My findings represent another demonstration that the PKD catalytic domain is likely to be responsible for the regulation of cardiac function via its association with HSP20.

Sequence alignment using the Basic Local Alignment Search Tool (BLAST) at the NCBI website (http://www.ncbi.nlm.nih.gov/blast) was undertaken to compare the 25-mer sequence spanning G^{606}-E^{630} (which yielded the strongest binding signal) to the whole human protein component database for sequence similarity and profiling. It is apparent that this sequence has a high degree of specificity for the PKD family (Table. 4.2). Interestingly, homology studies performed to investigate evolutionary relationships revealed that this 25-mer sequence is highly conserved in eukaryotic PKD, providing evidence for sequence and structural conservation (Table. 4.3). Hence, it is postulated that this region may have functional importance.

Subsequent alanine scanning analysis of the conserved sequence (G^{606}-E^{630}) highlighted seven amino acid residues which are potentially involved in PKD1-HSP20 interaction, namely the basic (R^{607}), non-polar (V^{609}, I^{611}, I^{613}) and acidic region consisting of D^{608}, D^{615} and E^{624} which formed a motif of **R^{607}DV**x**I**x**I**x**D**xxxxxxxx**E^{624}** (where x is not a key amino acid). This 25-mer peptide sequence could then serve as a basis for the design of cell-permeable disruptor peptide to inhibit PKD1-HSP20 interaction.

In summary, using a novel array-based approach, PKD1 was identified as a new interactor of HSP20. The present study provides validation of the interaction between PKD1 and HSP20, as proved by *in vitro* pull-down assay, co-immunoprecipitation and immunocytochemical studies. Furthermore, probing the PKD1 peptide array with His-HSP20 not only identified the binding sites, but also highlighted seven surface-exposed amino acid residues critical for the interaction. In combination with structural superposition analysis of the predicted 3D model of the PKD1 catalytic domain, the putative location of interaction sites was suggested. Interestingly, sequence alignment analyses showed high sequence homology between species suggesting a ubiquitous complex between PKD1 and HSP20.

Taken together, the data presented in this chapter suggests that HSP20 binds directly to PKD1 within the conserved catalytic region to form a highly specific complex. The integration of ProtoArray data with protein biochemical and immunocytochemical studies may lead to the discovery of a novel hypertrophy signalling complex with functional significance. Further studies were carried out to investigate the role(s) of PKD1-HSP20 complex in hypertrophic response. This will be discussed in Chapter 5.

Table 4.2. Sequence alignment of G^{606}-E^{630} of PKD1. Analysis was done using the Basic Local Alignment Search Tool (BLAST) at the NCBI website (http://www.ncbi.nlm.nih.gov/blast).

Accession	Description	Max score	Total score	Query coverage
NP_002733.2	serine/threonine-protein kinase D1 [Homo sapiens]	82.9	82.9	100%
NP_001073351.1	serine/threonine-protein kinase D2 isoform B [Homo sapiens]	77.8	77.8	100%
NP_005804.1	serine/threonine-protein kinase D3 [Homo sapiens]	77.8	77.8	100%
NP_057541.2	serine/threonine-protein kinase D2 isoform A [Homo sapiens]	77.8	77.8	100%
NP_001122392.1	MAP/microtubule affinity-regulating kinase 3 isoform d [Homo sapiens]	35.0	35.0	44%
NP_001122391.1	MAP/microtubule affinity-regulating kinase 3 isoform b [Homo sapiens]	35.0	35.0	44%
NP_001122390.1	MAP/microtubule affinity-regulating kinase 3 isoform a [Homo sapiens]	35.0	35.0	44%
NP_002367.4	MAP/microtubule affinity-regulating kinase 3 isoform c [Homo sapiens]	35.0	35.0	44%

Table 4.3. Amino acid homology showing comparison of G^{606}-E^{630} between species. Homology analysis was done using the Basic Local Alignment Search Tool (BLAST) at the NCBI website (http://www.ncbi.nlm.nih.gov/blast).

Species	Sequence	NCBI Reference
Homo sapiens	GRDVAIKIIDKLRFPTKQESQLRNE	NP_002733
Mus musculus	GRDVAIKIIDKLRFPTKQESQLRNE	NP_032884
Rattus norvegicus	GRDVAIKIIDKLRFPTKQESQLRNE	NP_001019434
Xenopus laevis	GRDVAIKIIDKLRFPTKQESQLRNE	NP_001087707
Bos taurus	GRDVAIKIIDKLRFPTKQESQLRNE	NP_001192467
Gallus gallus	GRDVAIKIIDKLRFPTKQESQLRNE	NP_001026372
Drosophila melanogaster	QREVAIKVIDKLRFPTKQEAQLKNE	NP_650710

Chapter 5

The role of the PKD1-HSP20 complex in hypertrophy signalling

5.1 Introduction

Protein phosphorylation is a fundamental mechanism that has the ability to regulate a myriad of cellular processes. This post-translational modification is catalysed by various protein kinases in response to different stimuli (Edelman *et al*., 1987; Yarden and Ullrich, 1988). By adding phosphate groups from a nucleoside triphosphate to substrate proteins, kinases act as regulators of receptor-mediated signal transduction that are central to cellular growth, metabolism, apoptosis and gene transcription (Hunter and Karin, 1992). Human protein kinase families can be divided into seven main groups. They consist of cyclic nucleotide regulated protein kinases, calcium-calmodulin-dependent protein kinases (CaMK), casein kinase 1 group (CK1), CMGC group (including cyclin-dependent kinases (CDKs), mitogen-activated protein kinases (MAPK), glycogen synthase kinases (GSK) and CDK-like kinases), yeast sterile-phenotype kinases (STE), tyrosine kinases (TK) and tyrosine-kinase like group (TKL). This chapter will focus on protein kinase D1 (PKD1) and review current understanding of its structure and function, as well as its role in cardiac hypertrophy.

5.1.1 Background and structure of PKD

PKD was first discovered in 1994 (Johannes *et al*., 1994; Valverde *et al*., 1994) and characterises a family of stress-activated ubiquitous serine/threonine intracellular kinases which phosphorylates the OH group of serine or threonine amino acids. There are three isoforms known in mammals, namely, PKD1 (formerly protein kinase Cμ (PKCμ), PKD2 and PKD3 (also named PKCν), sharing similar structure and exhibiting high degree of homology. Although similar, these three isoforms execute independent biological functions due to different expression patterns in distinct tissues and different subcellular distribution (Rozengurt *et al*., 2005). Of the three isoforms, PKD1 has been most extensively studied and is also referred to as PRKD1 to differentiate it from polycystic kidney disease (PKD).

PKD1 is evolutionarily well-conserved, spanning 912 amino acids long and having a molecular mass of 115 kDa. It contains an N-terminal regulatory domain (containing two zinc finger-like cysteine-rich domains (CRD) that bind both diacylglycerol (DAG) and DAG analog phorbol esters with high affinity), an internal pleckstrin homology (PH)

domain which maintains its inactive state by inhibiting catalytic domain, and a C-terminal serine/threonine kinase catalytic domain (Fig. 5.1). PKD1 was previously classified as a member of the PKC family due to its resemblance to the DAG-binding domains of PKC. However, it was later shown that PKD1 has distinct structural and enzymatic properties, and does not phosphorylate a variety of substrates targeted by PKC (Van Lint *et al*., 1995). In fact, based on the sequence homology of catalytic domain and substrate specificity, PKD1 is now thought to be distinct from PKC isoforms, being classified into the calcium/calmodulin-dependent kinase (CaMK) group in the human kinome (Manning *et al*., 2002). Nevertheless, recent evidence has shown that PKD1 is activated in living cells through a PKC-dependent pathway, suggesting that PKD1 can function either downstream of or in parallel with PKC (Zugaza *et al*., 1996). Indeed, in many cases, PKD1 activation is known to be attenuated by PKC inhibition (Harrison *et al*., 2006; Haworth *et al*., 2007).

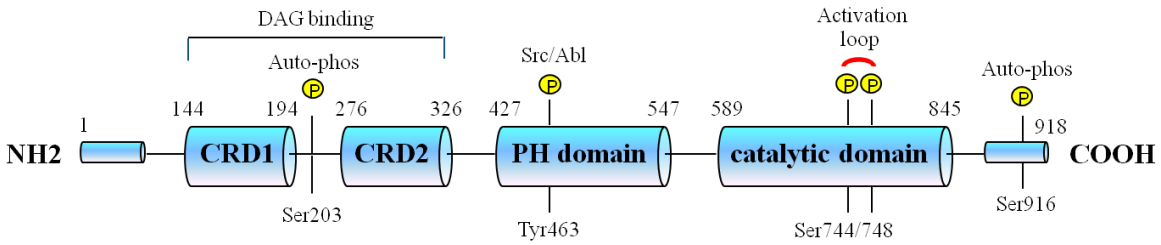

Figure 5.1. Functional domains and conserved phosphorylation sites of PKD1. PKD1 is composed of two N-terminal cystein-rich regulatory domains which mediate binding to diacylglycerol (DAG), an internal pleckstrin homology domain with auto-inhibitory functions and a C-terminal catalytic domain. Distribution of phosphorylation sites and the kinases that phosphorylate these sites are indicated. CRD1/CRD2 indicates cysteine-rich domain; PH, pleckstrin homology domain.

5.1.2 PKD1 phosphorylation

PKD1 is a kinase that can be phosphorylated on a number of different sites and its activation requires distinct regulatory mechanisms. Mass spectrometry, phosphopeptide mapping and mutational analyses showed that DAG stimulation is not sufficient to activate PKD1. In fact, PKD1 activation requires the phosphorylation of Ser744 and Ser748 in mouse (human Ser738 and Ser742) within the activation loop of the catalytic domain, along with alleviation on the inhibitory effect of the PH domain via a PKC-dependent signalling pathway (Iglesias *et al*., 1998; Vertommen *et al*., 2000; Waldron *et al*., 2001; 2003; Rykx *et al*., 2003). Notably, PKD1 can also be targeted by tyrosine kinases and activated via a PKC-independent pathway. For instance, in response to oxidative stress, the phosphorylation of PKD1 at Tyr463 in the PH domain is activated through a Src/Abl pathway that excludes the involvement of PKC (Storz *et al*., 2003). This leads to a derepression of PKD1 activity and initiation of NFκB transcription activity (Storz and Toker, 2003). In addition to the two activation loop sites, PKD1 also contains two autophosphorylation sites at Ser203 and Ser916 in the regulatory domain and carboxy-terminal, respectively, which is not *trans*-phosphorylated by other upstream kinases (Matthews *et al*., 1999; Vertommen *et al*., 2000).

5.1.3 PKD1 substrates in heart

Several recent advances in PKD research have provided insights into its functions. Being a major PKD isoform in the heart, PKD1 has been a focus of interest for cardiovascular research. Previous studies have reported that PKD1 is involved in cardiac pathogenesis, as seen in the regulation of myocardial contractile function. It is also linked with hypertrophy and pathological cardiac remodelling in response to neurohormonal stimuli (Avkiran *et al*., 2008; Fielitz *et al*., 2008). To date, PKD1 has been implicated in the phosphorylation of several sarcomeric proteins, such as cardiac troponin I, cMyBP-C and telethonin (Haworth et al., 2004) to regulate myocardial contractility. Additionally, PKD1 also regulates class II histone deacetylases (HDACs) proteins which are known as pro-hypertrophy transcription regulators (Vega *et al*., 2004). The pro-hypertrophy action of class II HDACs is exerted by repressing transcriptional activity as opposed to the function of histone acetyltransferases which initiate acetylation of nucleosomal histones to promote transcription (Kuo and Allis,

1998). Interestingly, these putative PKD1 substrates commonly contain a well defined phosphorylation motif in their sequence (LXRXXS/T), where an aliphatic amino acid (Ile/Leu/Val) and a basic amino acid (Arg) are located at the -5 and -3 positions relative to the serine target site, respectively (Nishikawa *et al*., 1997; Doppler *et al*., 2005).

5.1.4 Subcellular distribution of PKD1

In the basal state, the majority of PKD1 localises to the cytosol, while a subpopulation is found in various organelles, such as the nucleus, plasma membrane, mitochondria and trans Golgi network (Van Lint *et al*., 2002). Interestingly, PKD1 has previously been shown to translocate to the nucleus in response to G protein-coupled receptors (GPCR) stimulation. Notably, PKD1 is bound by DAG at its cystein-rich domain and followed by phosphorylation on serine residues in the activation loop by PKC and the release of PH-mediated PKD1 inhibition, thereby promoting PKD1 activation and redistribution (Rey *et al*., 2001). These observations strongly suggest a pertinent role for PKD1 as a signalling mediator that has two major sites of action. First, PKD1 resides mainly in the cytosol during basal conditions and then it moves into the nucleus upon receptor activation via an as yet not well-defined mechanism. As such, the subcellular localisation of PKD is likely to be associated with its activation status resulting in different biological responses. Further work is required to elucidate the precise mechanisms which control PKD1 localisation and translocation.

5.1.5 The roles of PKD1 in hypertrophy

Previous studies have shown that siRNA-mediated knockdown of endogenous PKD1 expression attenuates hypertrophy (Harrison *et al*., 2006), whereas over-expression of active PKD1 promotes hypertrophy in cultured neonatal rat cardiomyocytes (Iwata *et al*., 2005). In addition, the role of PKD in cardiac pathogenesis was also confirmed *in vivo* using ventricular tissue from rodent models of hypertrophy. Hence, it is thought that PKD1 signalling is closely associated with hypertrophic agonists through both PKC-dependent and PKC-independent mechanisms, resulting in a robust hypertrophic phenotype. Such a notion suggests a key role for PKD1 as a regulator of cardiac signalling. Indeed, there is

accumulating evidence to show that PKD1 and its upstream activator PKC, in particular PKCε, are implicated in the control of pathological remodelling of the heart (Haworth *et al*., 2000). These kinases have been shown to phosphorylate HDAC proteins, in particular HDAC5, creating docking sites for 14-3-3 proteins that facilitate nuclear efflux of HDAC5 in a chromosome region maintenance 1 (CRM1)-dependent manner (McKinsey *et al*., 2001; Vega *et al*., 2004). MEF2 activity is stimulated by dissociation from HDAC5, thereby promoting transcriptional derepression (Zhang *et al*., 2002). Consequently, the activation of MEF2 transcription factors evoke a reprogramming of cardiac gene expression that promotes a fetal gene response, resulting in hypertrophic growth (Chang *et al*., 2005). Indeed, mutant mice lacking HDAC5 have been shown to develop extremely enlarged hearts in response to hypertrophic agonists (Zhang et al., 2002). Specifically, when MEF2 is bound to the promoters of cardiac muscle differentiation genes, it elicits a shift in expression of the two myosin heavy chain (MHC) isoforms. As a result, the α-myosin heavy chain (α-MHC) is switched to β-myosin heavy chain (β-MHC), resulting in reorganisation of putative contractile units and this in turn leads to cardiac remodelling and hypertrophic phenotype (Chien *et al*., 1991).

Another kinase that impinges on PKD1's actions is PKA. PKA activity can impose a block on α_1-adrenergic stimulation and suppress PKD1 phosphorylation (Haworth *et al*., 2007). In this context, PKA may act as a counter-regulator to modulate PKD1 activation. This notion has been supported by ground breaking work, showing that acute *β*-adrenergic stimulation and activation of PKA inhibits phosphorylation of not only PKD1, but also HDAC5, highlighting its critical role in the induction of hypertrophy-associated genes (Sucharov *et al*., 2011). PKD1 activity has also been shown to undergo stimulation by G protein-coupled receptors (GPCR), which couple to the $G_{q\alpha}$ subunit of heterotrimeric G proteins in response to PKC activation, suggesting a causal relationship between PKC and PKD1 in the regulation of myocardial responses (Haworth *et al*., 2000). Interestingly, it has recently been reported that cardiac A-Kinase Anchoring Protein (AKAP)-Lbc functions as a scaffolding protein for PKA and PKC to mediate activation of PKD1 (Carnegie *et al*., 2004; 2008). Upon neurohormonal stimuli such as endothelin-1 (ET-1) or phenylephrine (PE), upregulation of AKAP-Lbc facilitates PKD/HDAC5/MEF2 signalling and enhances the transduction of hypertrophic response. Conversely, reduced AKAP-Lbc expression prevents the translocation of HDAC5, thereby hindering the progression of hypertrophy. Since PKA and PKC are components of AKAP-Lbc anchoring complex, this may suggest the involvement of both cyclic AMP (cAMP) and phospholipid signalling

pathways in the regulation of PKD1 activation. Indeed, recent findings have revealed the roles of compartmentalised phosphodiesterases (PDEs) in cAMP-dependent PKA-mediated PKD1 activation. It was reported that the combined inhibition of PDE3 and PDE4 is required to achieve substantial attenuation of ET1-induced PKD1 activation through increased PKA activity (Haworth *et al*., 2011). Based on these findings, it is tempting to postulate that AKAP-Lbc serves as a connector, providing a locus for signaling crosstalk between the kinases in a stimulus-dependent manner within the hypertrophy signaling cascades (Fig. 5.2). In addition, it is increasingly apparent that PKD1 is a key player in the regulation of cardiac hypertrophy, most likely through its effect on the transcriptional regulation of fetal gene programming via the phosphorylation of HDAC5.

In summary, the function of PKD1 depends upon (1) its phosphorylation state, either directly activated by neurohormonal stimuli or by an upstream regulator and (2) its localisation within the cell. These findings open new routes for the investigation into the role of PKD1 as a potential target for novel therapeutic intervention in the treatment of cardiac hypertrophy. Nevertheless, the detailed intracellular mechanism(s) underlying fetal gene reprogramming remains to be determined. Novel insights may be gleaned from further exploration of the signalling network involving AKAP-Lbc and its scaffold partners. Further work is also required to clarify the mechanistic details underpinning the crosstalk between different signal transduction pathways which contribute to the induction of the hypertrophic response, with a particular emphasis on understanding the upstream regulators and downstream functional consequences of PKD activation.

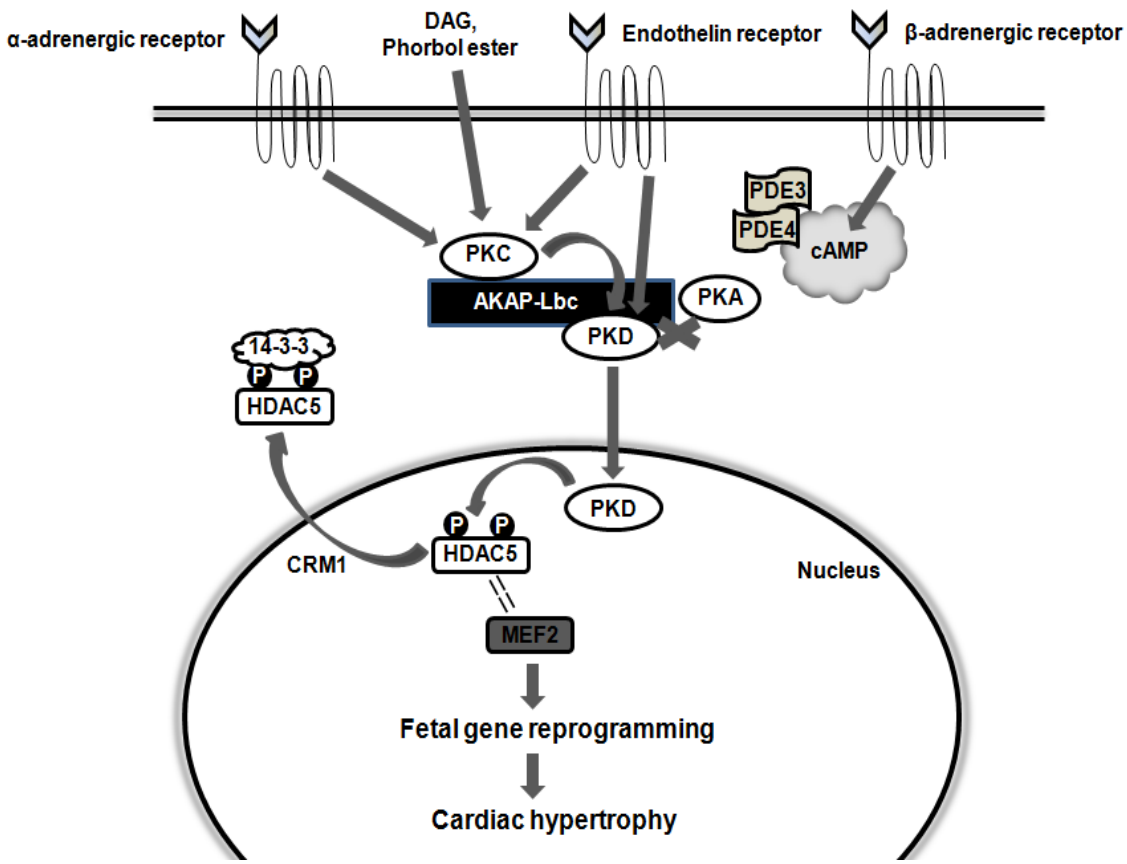

Figure 5.2. Schematic diagram depicting the hypertrophic signalling cascades. *α*-adrenergic, phorbol ester and ET receptors stimulate the nuclear export of HDAC5 via activation of PKC and the downstream effector PKD1. PKD1 can also be activated by ET receptor via a PKC independent pathway. Phospho-HDAC5 binds 14-3-3 proteins, resulting in nuclear export of HDAC5 and upregulation of MEF2, thereby triggering the induction of hypertrophic fetal gene program. PDE3 and PDE4 regulate β-adrenergic receptor stimulation and activation of PKA, hence preventing phosphorylation of PKD1 and HDAC5.

5.1.6 Aims of Chapter 5

The experimental evidence presented in Chapter 4 describes the molecular interaction between PKD1 and HSP20. Using peptide array technology, the molecular docking sites of HSP20 on PKD1 were mapped and critical residues for the interaction determined. The apparent importance of HSP20 in cardioprotective mechanisms and PKD1 in cardiac remodelling, coupled with the interaction between these proteins, led to the hypothesis that PKD1-HSP20 complex may affect the induction of hypertrophy. Here, the role(s) of the PKD1-HSP20 complex in hypertrophic signalling are studied *in vitro*. Neonatal rat cardiomyocytes were chosen as the model system of choice.

Hence, the aims of this chapter were:

1. to use the molecular information from peptide array analysis to develop cell-permeable peptides for the disruption of the PKD1-HSP20 complex.

2. to examine the functional implications of PKD1-HSP20 complex in hypertrophic cardiomyocytes.

3. to identify putative phosphorylation sites on HSP20 that are modified by PKD1.

5.2 Results

5.2.1 Disruption of PKD1-HSP20 interaction

Previous work from my laboratory has shown that stearoylated, cell-permeable analogues of 25-mer peptides identified in peptide array analyses, could be used to disrupt signalling complexes within cells to affect cellular functions such as protein phosphorylation (Smith *et al*., 2007; Meng *et al*., 2009). In this study, the docking site of HSP20 on PKD1 encompassing residues G^{606}-E^{630} (GRDVAIKIIDKLRFPTKQESQLRNE) was used to manufacture a disruptor peptide named 'HJL09'. A control peptide with three of the seven key residues replaced by alanine (GAAVAIKIIAKLRFPTKQESQLRNE) was also synthesised. More specifically, both peptides were synthesised with a C-terminal stearate group to facilitate cell-permeability, thereby allowing peptides transport across the cell membrane. Due to a stronger affinity towards PKD1, the disruptor peptide is likely to compete with the binding of HSP20 on the docking site. The effectiveness of the peptides to disrupt the HSP20-PKD complex was then evaluated by co-immunoprecipitation experiments. Gratifyingly, these experiments showed that the disruptor peptide could successfully hinder the association of the two endogenous proteins in cardiac myocytes. However, this was not true for the control peptide (Fig. 5.3). In addition, a reciprocal co-immunoprecipitation study using an HSP20-antibody also showed similar results whereby the peptide but not the peptide control could attenuate PKD1-HSP20 association. These findings verified the peptide array data and showed that the peptides were cell permeable. Thus, these peptides could now be utilised in functional experiments.

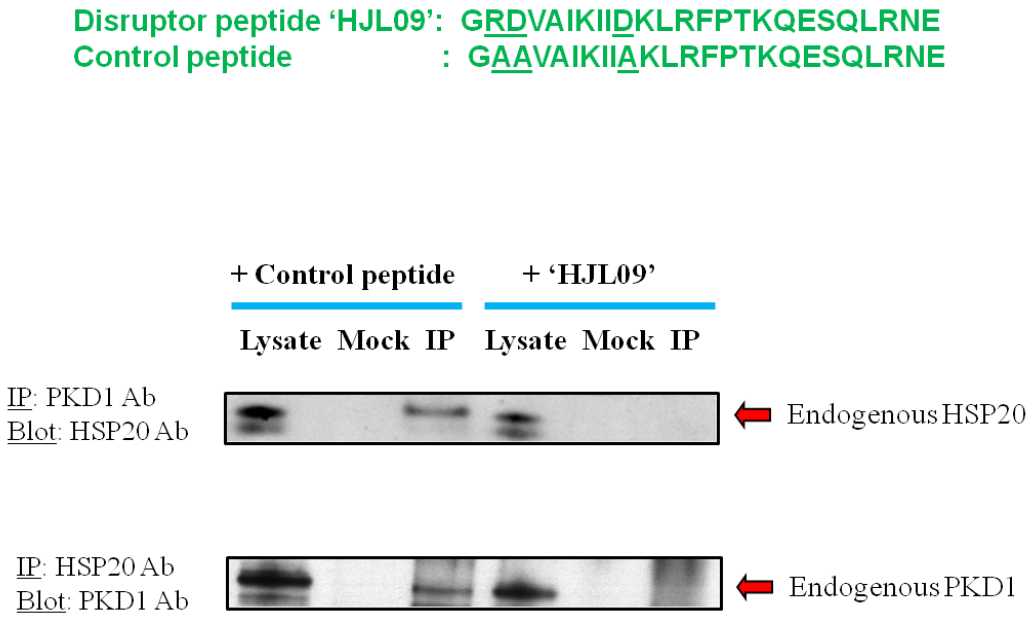

Figure 5.3. Disruption of PKD1-HSP20 interaction. Cardiomyocytes were treated with 10 µM of control peptide or 10 µM of PKD-disruptor peptide 'HJL09' for 2 h. The same amount of lysates was then co-immunoprecipitated with anti-PKD1 (upper panel) or anti-HSP20 (lower panel) antibody. Cellular lysates were then blotted for HSP20 or PKD1, respectively. Pre-cleared lysates was used as positive control and immunoprecipitate without antibody added (only IgG) was used as negative control. All results are typical of three independent experiments.

5.2.2 Peptide disruption of PKD1-HSP20 complex protects against hypertrophy in cardiomyocytes

As previous studies have demonstrated the cardioprotective roles of HSP20 during hypertrophy, it was interesting to study the role of the PKD1-HSP20 complex in this context. In order to address the possible functions of this complex on the hypertrophic response in cultured neonatal rat cardiomyocytes, the consequences of disruption of this signalling node was examined by use of the disruptor peptide. Experimentation was done using an *in vitro* cell model of cardiomyocyte hypertrophy that was set up as described in 'Materials & Methods' and Chapter 3. In this chapter, five separate methods were performed to evaluate the role of the PKD1-HSP20 complex in the hypertrophic response in cardiomyocytes.

5.2.2.1 Measurement of cell size

As cardiac hypertrophy is characterised by enlargement in cell size, the influence of the PKD1-HSP20 interaction on the surface area of cardiomyocytes was examined. Firstly, real-time xCELLigence RT-CES analysis was undertaken to monitor cell size change in response to ISO stimulation in cultured neonatal rat cardiomyocytes. Real-time analysis provides constant monitoring and permits continuous observations of different conditions. The impedance recorded on the surface of the electrode-embedded 96-well plates was automatically converted to cell index (CI) to provide quantitative assessment. As cardiomyocytes are terminally differentiated and have limited proliferative capacity, a higher CI would represent an increase in impedance that could only be a result of a corresponding increase of cell cross-sectional area. Here, ISO stimulation resulted in an increase in the cell index, with incremental increases evident between 10-35 h. These increases started to level out at 38 h after treatment (Fig. 5.4). For a clearer interpretation, cell index values were normalized after 24 h of the indicated treatments. In contrast to the control cells, which were treated with DMSO (vehicle) alone, the normalised cell index was increased nearly 1.5x fold in ISO- and control peptide + ISO-treated cells, suggesting a relative increase in cell size. Excitingly, pre-treatment with PKD-disruptor peptide 'HJL09' reversed this effect, preventing the enlargement in cell size despite hypertrophic

stimulus. These initial experiments were the first indication that disruption of PKD1's association with HSP20 was a beneficial mechanism during hypertrophy.

5.2.2.2 Effect on cell morphology and actin cytoskeleton dynamics

The next step was to examine the impact of ISO stimulation and disruption of the PKD1-HSP20 interaction on cardiomyocyte morphology. There was an easily detectable increase in ISO-stimulated cardiomyocyte area as seen under the differential interference contrast (DIC) microscope (Fig. 5.5). Remarkably, 24 h of ISO treatment triggered dramatic morphological changes in the cells. Treated cells differed from control untreated cells as they seemed stretched and enlarged to double their normal size. Similar morphological changes were also observed in cells treated with control peptide + 24 h ISO. However, cells treated with PKD-disruptor peptide 'HJL09' had no discernible ISO induced effects on morphology. I propose that such a blunted hypertrophic response is due to the disruption of PKD1-HSP20 interaction.

Reorganisation of actin filaments is another important characteristic of hypertrophy (Frey and Olson, 2003). To determine the effect on the actin cytoskeleton, cultured cells were subjected to indicated treatments and Alexa Fluor 488-conjugated phalloidin staining. Confocal microscopic images showed that actin cytoskeletal rearrangement was substantially stimulated by hypertrophy induction and was reduced in cells pre-treated with PKD-disruptor peptide 'HJL09' (Fig. 5.6). Seemingly, untreated cardiomyocytes exhibited poorly organised actin, which was characterised by a punctate pattern. ISO-stimulated cells, in contrast, displayed robust stress fibres, showing extensive parallel actin alignment. This was also true for cells pre-treated with control peptide prior to ISO addition. Interestingly, cells pre-treated with disruptor peptide 'HJL09' were partially resistant to the actin reorganising effects of ISO, displaying a somewhat disorganised myofibril network. In addition to its role in the prevention of cell enlargement, the PKD1-HSP20 association is also likely to have the capacity to regulate the integrity of cellular actin filaments. This notion is supported by previous work showing that in cultured neonatal cardiomyocytes, some weak cytoskeletal staining was visible under basal conditions, whereas ISO treatment resulted in HSP20 redistribution to the cytoskeleton (Fan *et al*., 2004). Notably, these results may suggest that the disruption of PKD1-HSP20 complex is required to confer cardioprotection in cultured neonatal rat cardiomyocytes from prolonged β-adrenergic stimulation.

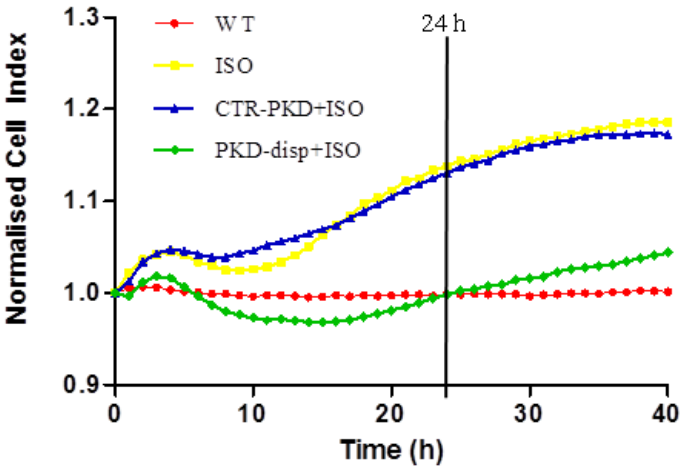

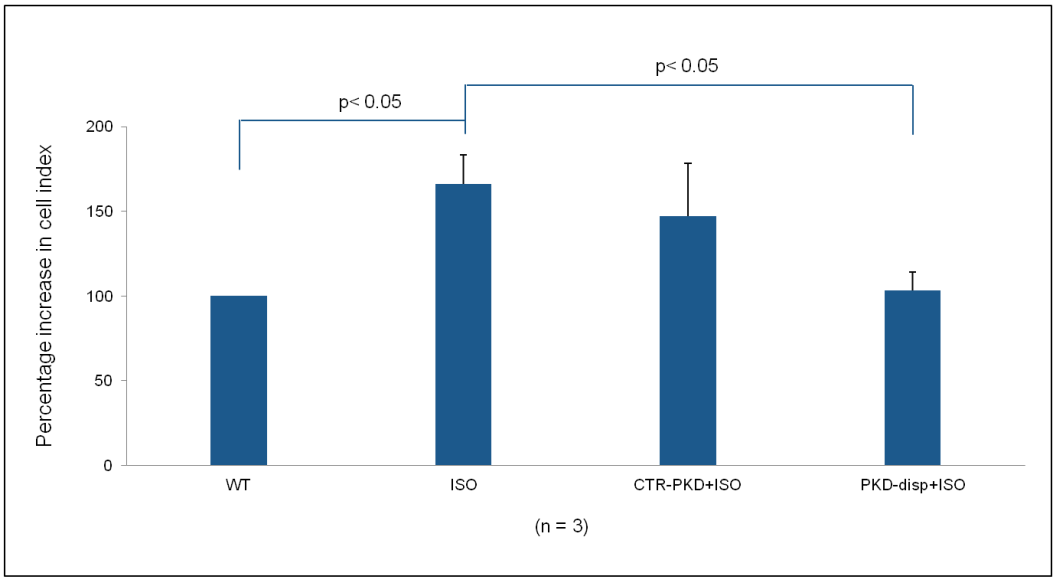

Figure 5.4. The effect of PKD1-HSP20 interaction on cell size. Upper panel: Quantitative measurement of neonatal rat cardiomyocyte cell size by real-time cell-electronic sensing (RT-CES). Continuous impedance measurement displayed as normalised cell index were recorded using RT-CES instrument. Bottom panel: Average cell indexes were taken and normalised after 24 h of indicated treatments. Neonatal cardiomyocytes were pre-incubated with PKD-disruptor peptide 'HJL09' or control peptide in the presence of 24 h ISO stimulation. Data are means ± S.E.M. of 3 experiments on different cardiomyocytes preparations. Statistical significances between groups were determined by the use of Student's *t*-test. Values were considered significant if $p < 0.05$.

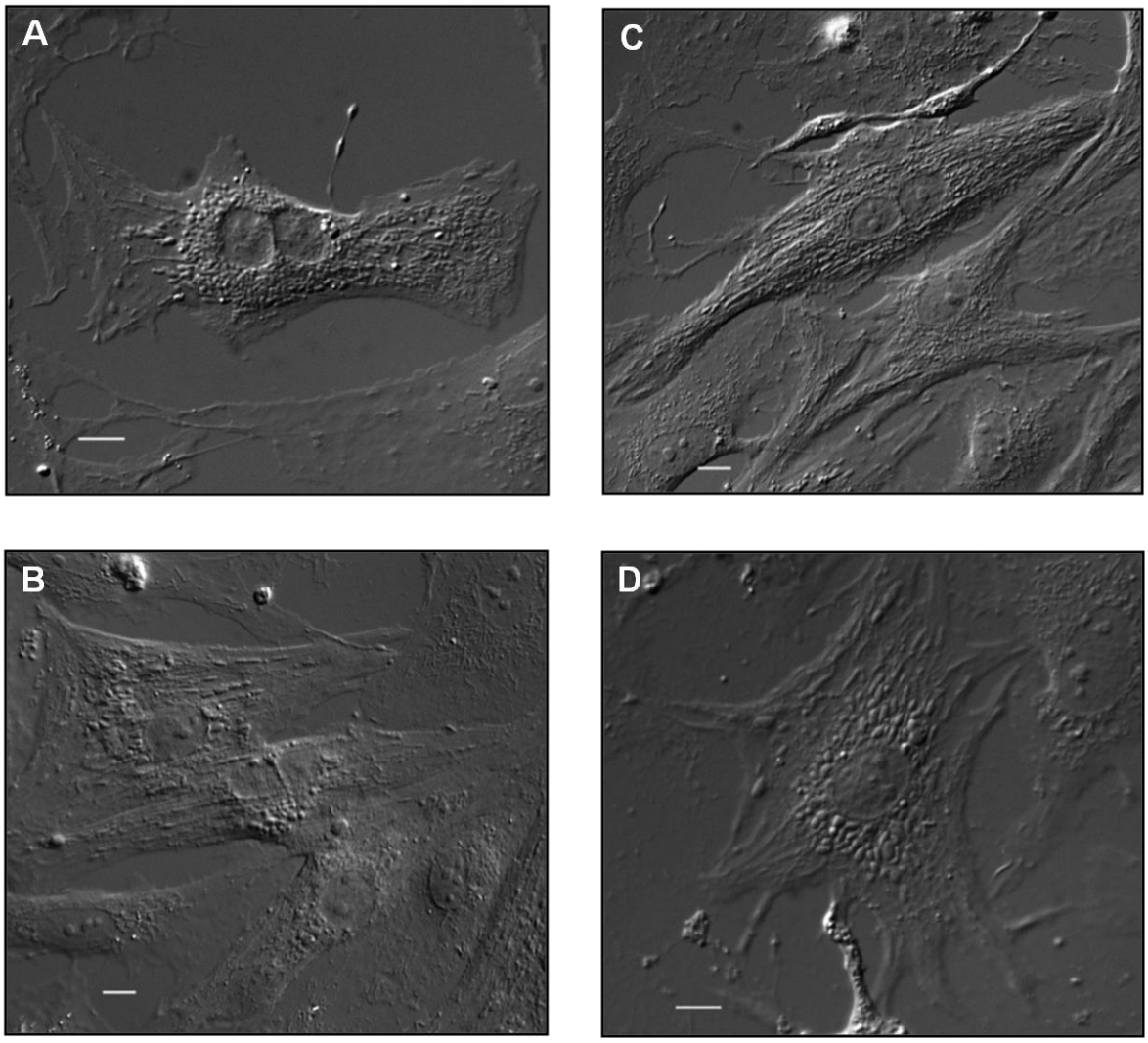

Figure 5.5. The effect of PKD1-HSP20 interaction on cell morphology. Cardiomyocytes were cultured on coverslips and subjected to different treatments as indicated. Differential interference contrast (DIC) imaging was employed to examine morphological change in cardiomyocytes. (A) Wild-type, (B) 24 h ISO treatment, (C) Control-peptide + 24 h ISO treatment, (D) PKD-disruptor peptide 'HJL09' + 24 h ISO treatment. Images shown are representative of three separate experiments on different cardiomyocytes preparations. Scale bars = 10 μm.

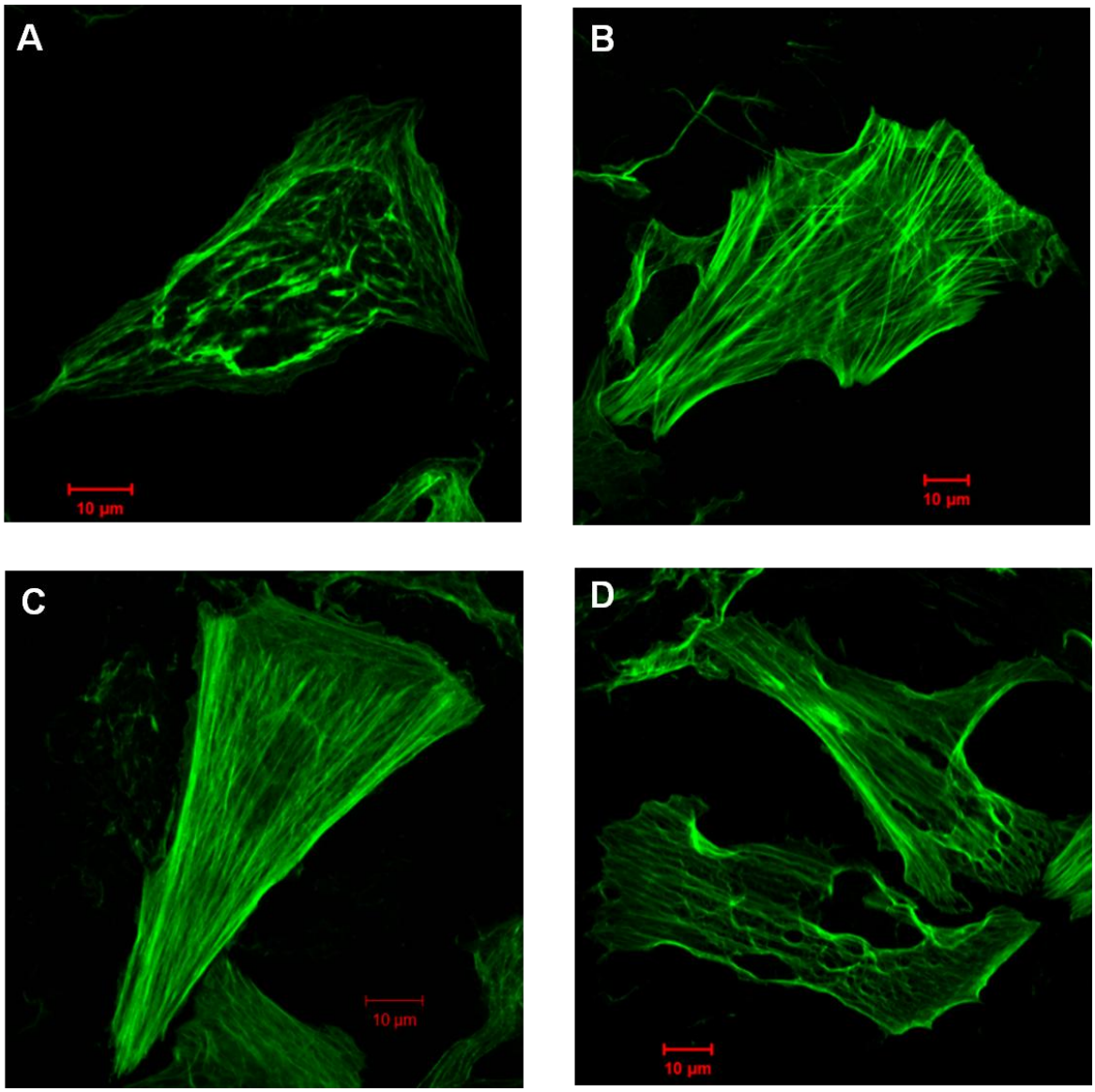

Figure 5.6. The effect of PKD1-HSP20 interaction on actin organisation. Cells were fixed and actin was visualised by immunostaining with actin-phalloidin. (A) Wild-type, (B) 24 h ISO treatment, (C) Control-peptide + 24 h ISO treatment, (D) PKD-disruptor peptide 'HJL09' + 24 h ISO treatment. Wild-type cardiomyocyte exhibited poorly organised actin which was visualised by a punctate pattern as detected by phalloidin staining. Stimulation of cardiomyocytes with 24h ISO alone or with control peptide significantly induced reorganisation of actin, showing long symmetrically spaced filaments. In contrast, disruption of PKD1-HSP20 interaction resulted in reduced actin assembly and organisation. Images shown are representative of three separate experiments. Scale bars = 10 µm.

5.2.2.3 Measurement of protein content

Cytoplasmic protein synthesis was measured and expressed relative to DNA content as described in 'Materials & Methods' (Fig. 5.7). Following hypertrophic stimulation, there was a considerable increase (nearly 2-fold) in the total protein content of ISO- and control peptide + ISO- treated cells compared to untreated wild-type cells. In contrast, the PKD disruptor peptide 'HJL09' treated cells had a 'normal' level of protein synthesis.

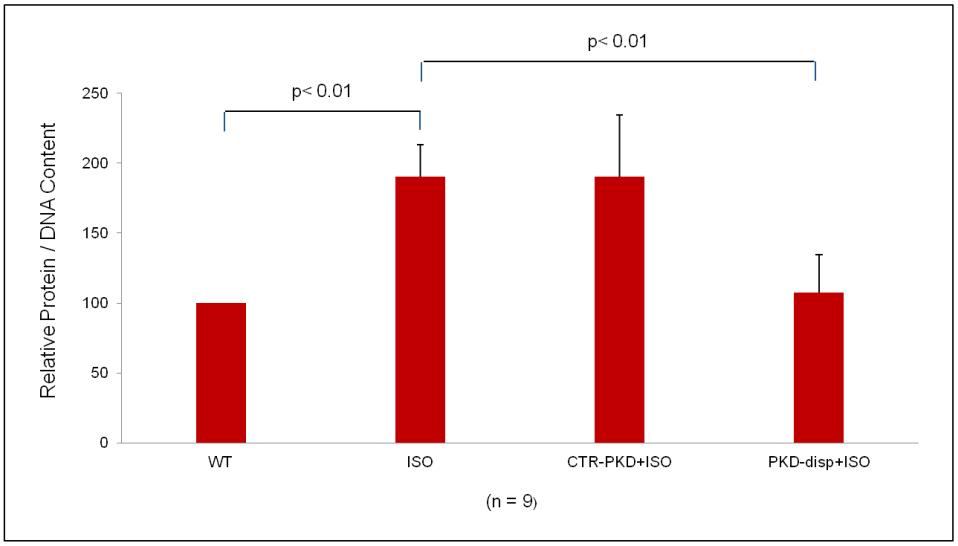

Figure 5.7. The effect of PKD1-HSP20 interaction on protein synthesis. The total cell protein and DNA content were determined by the Lowry and the Hoechst dye method. The protein content was then normalised to the DNA amount to correct for differences in the cell number. Data are means ± S.E.M. of nine experiments on different cardiomyocyte preparations. A Student's *t*-test was performed to compare the two groups as shown and *P* values are indicated.

5.2.2.4 Quantification of fetal gene expression

As mentioned earlier, cardiac hypertrophy is associated with reactivation of the fetal gene program, which may initially serve as a compensatory mechanism to reduce both cardiac preload and load by natriuretic, diuretic and vasodilatory actions, but eventually resulting in the loss of cardiac function. In this study, real-time qPCR analyses were carried out to determine whether the PKD1-HSP20 interaction influenced the transcriptional activity of genes (ANF, BNF and β-MHC) known to be re-expressed as part of the hypertrophic response. The expression level was then normalised to a reference gene rat 18s rRNA to correct for differences in RNA loading. This allowed evaluation of alterations in hypertrophic gene expression that may have occured upon disruption of PKD1-HSP20 interaction. This information would suggest the participation of this signalling complex in regulation of hypertrophic gene expression.

ISO-induced hypertrophic signaling events have been shown to culminate in gene expression changes in the nucleus (Izumo *et al*., 1988; Chien *et al*., 1991; Rosenzweig and Seidman, 1991). Indeed, the data in this chapter shows that cells pre-treated with either ISO or the combination of control peptide and ISO, had dramatically elevated expression of fetal genes, particularly BNF, as compared to wild-type (Fig. 5.8). However, treatment of cells with disruptor peptide 'HJL09' markedly reduced the expression of fetal gene mRNA transcripts despite application of hypertrophy stimulating conditions. In fact, the disruption has initiated an anti-hypertrophic effect, resulting in the suppression of fetal gene reactivation that drives cardiomyocyte hypertrophic growth. This effect may be the result of peptide blocking the nuclear translocation of PKD1 where the PKD-disruptor peptide 'HJL09' displaces HSP20 from its binding site on PKD1. It is postulated that such displacement hinders PKD1 from entering the nucleus, which in turn disfavours the phosphorylation of HDAC5. The above results not only confirm that 24 h ISO stimulation can activate hypertrophic gene expression, but also indicates a close relationship between PKD1-HSP20 interaction and fetal gene re-expression. The interaction between these two proteins is likely to contribute to agonist-mediated cardiomyocyte hypertrophy.

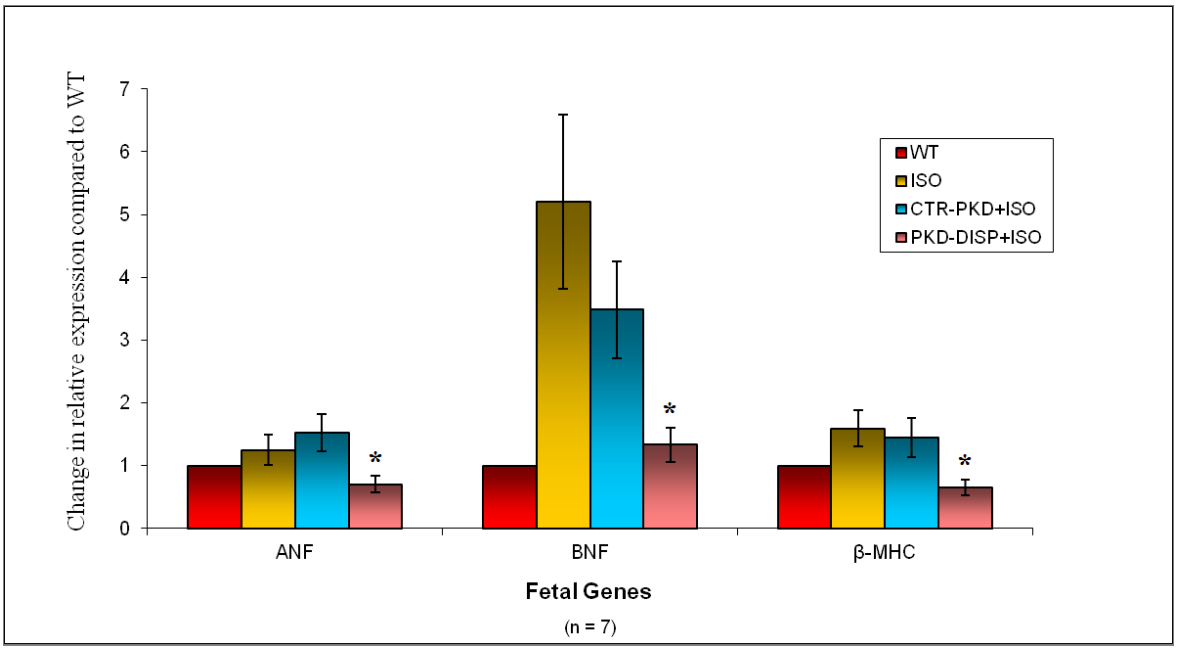

Figure 5.8. The effect of PKD1-HSP20 interaction on fetal gene expression. Total RNAs were isolated and the expression of ANF, BNF and β-MHC were examined by real-time qPCR. Rat 18s rRNA was used to serve as an internal control. All data are presented as mean ± S.E.M. of seven experiments on different cardiomyocytes preparations. A Student *t*-test was performed to compare PKD-disruptor peptide 'HJL09'+ISO and ISO-treated cells. * $P < 0.05$ value was based on comparison with cells treated with 24 h ISO.

5.2.3 Mapping binding region of PKD1on HSP20

Molecular information on the binding site of PKD1 on full-length HSP20 was obtained by scanning peptide array analysis. Results revealed overlapping high-affinity binding regions which mainly locate in the WDPF and α-crystallin domains (Fig. 5.9A). In addition, alanine scanning peptide arrays of residues 6-30 and 96-120 identified a number of key amino acids that are potentially involved in the HSP20-PKD1 interaction (Fig. 5.9B). Specifically, in an alanine substituted peptide array encompassing amino acids P^{6}-D^{30} of HSP20, a loss of binding upon substitution of $Arg^{11,12}$ with alanine and $Ala^{13,15}$ with aspartic acid was observed. Interestingly, these amino acids form the domain surrounding serine 16 (RRApSAP), a site which is phosphorylated by both cAMP-dependent protein kinase A (PKA) and cGMP-dependent protein kinase G (PKG) (Beall *et al*., 1997).

Taken together all overlay studies so far, it is apparent that PKD1 and PDE4D5 shared common binding sites within the WDPF domain (Met^{1}-Glu^{35}) and α-crystallin domain (His^{96}-Gly^{140}) of HSP20. Interestingly, there were also exclusive PDE4D5 binding to Ala^{51}-Leu^{55} (Fig. 3.11) and exclusive PKD1 binding to Val^{76}-Val^{80} (Fig. 5.9) of HSP20. These distinct but proximal sites may suggest that PDE4D5 and PKD1 interact with HSP20 in a mutually exclusive manner which could be potentially regulatory.

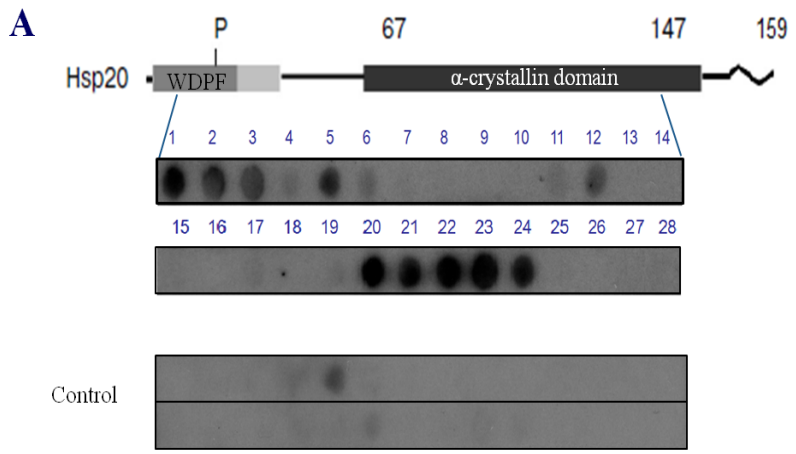

Position	Residues	25-Mer peptide sequence
1	1-25	MEIPVPVQPSWLRRASAPLPGLSAP
2	6-30	PVQPSWLRRASAPLPGLSAPGRLFD
3	11-35	WLRRASAPLPGLSAPGRLFDQRFGE
5	21-45	GLSAPGRLFDQRFGEGLLEAELAAL
12	56-80	RAPSVALPVAQVPTDPGHFSVLLDV
20	96-120	HVEVHARHEERPDEHGFVAREFHRR
21	101-125	ARHEERPDEHGFVAREFHRRYRLPP
22	106-130	RPDEHGFVAREFHRRYRLPPGVDPA
23	111-135	GFVAREFHRRYRLPPGVDPAAVTSA
24	116-140	EFHRRYRLPPGVDPAAVTSALSPEG

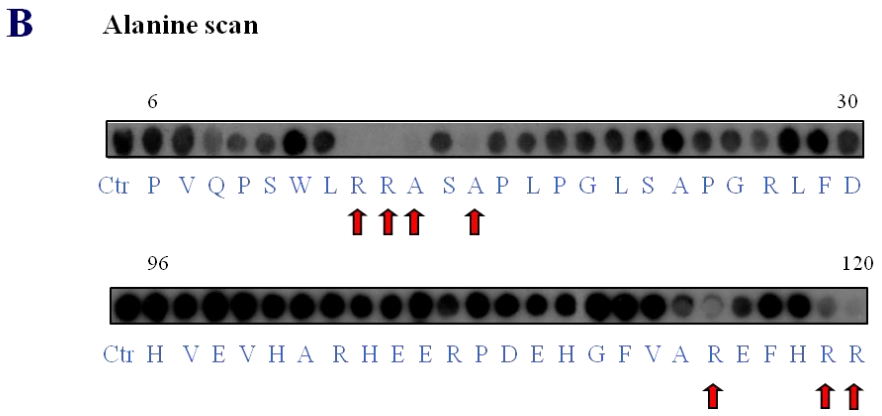

Figure 5.9. Identification of PKD1-HSP20 interaction sites. (A) HSP20 is shown schematically as in Gusev *et al*. (2002) with slight modifications. The dark shaded area represents the WDPF-domain, the light shaded area represents the conserved region in the N-terminal part of sHSP, the black area denotes conservative α-crystallin domain. P is the sites of phosphorylation and the zigzag denotes the flexible C-terminal region. Binding spot numbers relate to peptides in the scanned array whose residue position and sequence are given in the table below. (B) Scanning alanine substitution analysis using spots 1 and 20. Native peptide (Ctr) plus progeny with the indicated residue substituted for alanine or aspartate. Red arrow indicates ablation or severely reduced interaction. Arrays are representative of at least three separate experiments.

5.2.4 Identification of PKD1 phosphorylation site on HSP20

Protein phosphorylation is a ubiquitous post-translational modification (PTM), which is important for signal transduction and regulation of biological function. Hence, identification of kinase-specific phosphorylation sites is critical for molecular delineation of a diverse array of cellular processes. Initially, prediction of HSP20 phosphorylation sites by PKD1 was performed using an online computational software named GPS (Group-based Prediction System, ver 2.0) (http://gps.biocuckoo.org/online.php). The prediction is based on similarity found in query sequences with respect to the known phosphorylation sites in at least one kinase group in the same hierarchy.

The search consistently showed one possible phosphorylation site at Ser16 of HSP20 with the highest score as PKD-phosphorylated amino acid residue. Figure 5.10 depicts the online user interface of GPS, showing that the domain surrounding the predicted PKD-phosphorylated HSP20 site at serine 16 contains a sequence (RRA**S**^{16}AP). Interestingly, this site is similar to the phospho-motif of the AGC kinase subfamily (PKA, PKG and PKC) (Beall *et al*., 1997). More interestingly, it has also been shown that serine 16 is the phosphorylation site for sustained *β*-adrenergic signaling which leads to expression and phosphorylation of cardiac HSP20 (Chu *et al*., 2004). Hence, it is highly likely that this PKD1-HSP20 phosphorylation motif is physiologically significant. Nevertheless, the prediction is speculative and requires experimental verification.

An *in vitro* phosphorylation assay was then carried out on HSP20 peptide arrays using [γ-^{32}P-ATP] to validate the predicted phosphorylation site. As predicted, analysis of the HSP20 amino acid sequence reveals an optimal putative PKD phosphorylation site at Ser16. Importantly, Ser16 is part of the docking site that allows complex formation between PKD1 and HSP20. More interestingly, this site falls within the minimal PKD recognition motif of RxxS, where an arginine is normally located at the -3 position (Fig. 5.11 Upper panel). As reported previously, well-known substrates of PKD such as HSP27, HDAC5 and cTnI commonly conform perfectly to this phosphorylation motif as identified through combinatorial peptide libraries (Haworth *et al*., 2004; Vega *et al*., 2004; Döppler *et al*., 2005; Huynh and McKinsey, 2006) (Fig. 5.11 Lower panel)

Predicted Sites

Position	Code	Kinase	Peptide	Score	Cutoff
16	S	AGC/PKA	PSWLRRASAPLPGLS	5.084	2.77
16	S	AGC/PKG	PSWLRRASAPLPGLS	7.952	5.095
16	S	CAMK/PKD	PSWLRRASAPLPGLS	8	6.7
16	S	AGC/PKC/Delta	PSWLRRASAPLPGLS	3.839	3.806
16	S	AGC/PKC/Delta/PKCd	PSWLRRASAPLPGLS	3.478	3.478

Figure 5.10. Predicted phosphorylation site of HSP20 by PKD1. GPS software (Group-based Prediction System, ver 2.0) was used for predicting kinase-specific phosphorylation sites. One potential phosphorylation site on HSP20 by PKD was identified at Ser16.

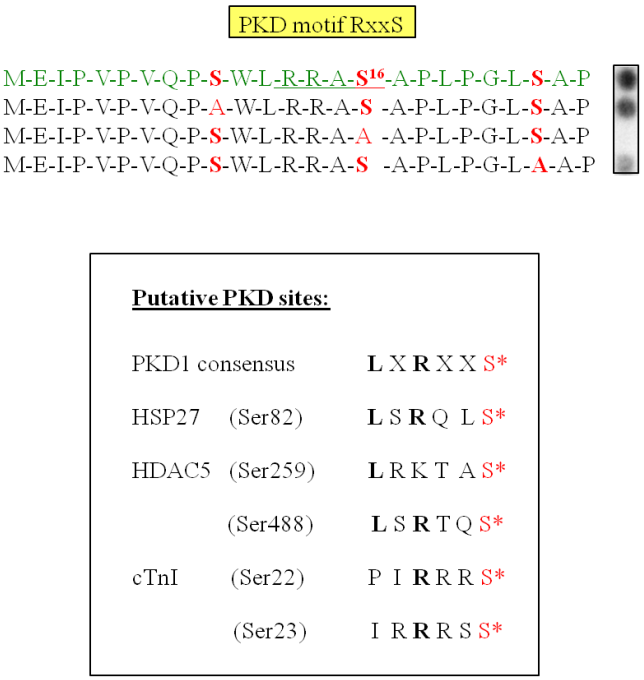

Figure 5.11. PKD1 phosphorylates HSP20 at Ser16. Upper panel: *In vitro* phosphorylation assay using [γ-^{32}P-ATP] on alanine scanning peptide array of residues 1-25 of HSP20 revealed that HSP20 is phosphorylated at Ser16 by PKD1. Lower panel: Shown for comparisons are the minimal PKD1 consensus phosphorylation sequence and the PKD1 phosphorylation sites in HSP27, HDAC5 and cTnI. The amino acid residues in red with asterisks denote serine phosphorylation sites.

In order to verify that it is specifically HSP20 being phosphorylated by PKD1 at Ser16, a cold *in vitro* kinase assay was carried out using recombinant purified His-HSP20 protein and PKD1 active protein. The immunoblots were then probed with phospho-HSP20 antibody which recognises HSP20 only when phosphorylated at Ser16 (Fig 5.12). Phosphobands were detected when active PKD1 was added. No appreciable immunoreactivity was evident when the assay mix was devoid of PKD1. These results clearly demonstrated that: (1) HSP20 can be directly phosphorylated by PKD1 *in vitro*, and that (2) the specificity of the phosphorylation site at Ser16 was validated by using phospho-Ser16 anti-sera. Taken together, it is thus concluded that HSP20 is a novel PKD1 substrate.

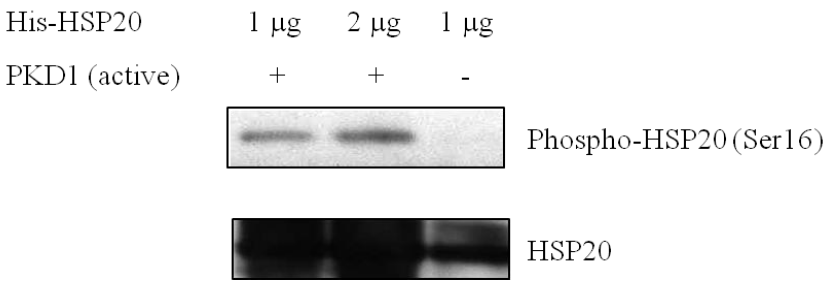

Figure 5.12. Ser16 is the site phosphorylated on HSP20 by PKD1. Purified His-HSP20 was incubated in a cold i*n vitro* kinase assay with PKD active protein and resolved by SDS-PAGE. HSP20 phosphorylation was determined by immunoblotting with anti-phospho-HSP20 (Ser16). Lysates were also immunoblotted with anti-HSP20 as loading control. The immunoblots shown are representative of two independent experiments.

5.2.5 The effect of PKD1 activation on HSP20 phosphorylation

As active PKD triggered recognition by a ser16 phospho-specific antibody, it is proposed that PKD1 activation may lead to the subsequent phosphorylation of HSP20. The effect of PKD1 activation on the phosphorylation level of HSP20 was examined in co-transfected HEK293 cells using commercially available activator bryostatin (10 nM) (Matthews *et al*., 1997) and inhibitor Gö6976 (20 nM) (Gschwendt *et al*., 1996). PKD1 activation was then assessed using an anti-phospho-PKD1 (Ser916) antibody that detects only the active form of the kinase (Matthews *et al*., 1999). Using PKD1 and HSP20 co-transfected HEK293 cells, the results show that PKD1 activation was elevated following stimulation with activator bryostatin, but decreased considerably after treatment with Gö6976. Interestingly, the phosphorylation of HSP20 increased along with activation of PKD1 and conversely inhibition of PKD1 decreased HSP20 phosphorylation (Fig. 5.13).

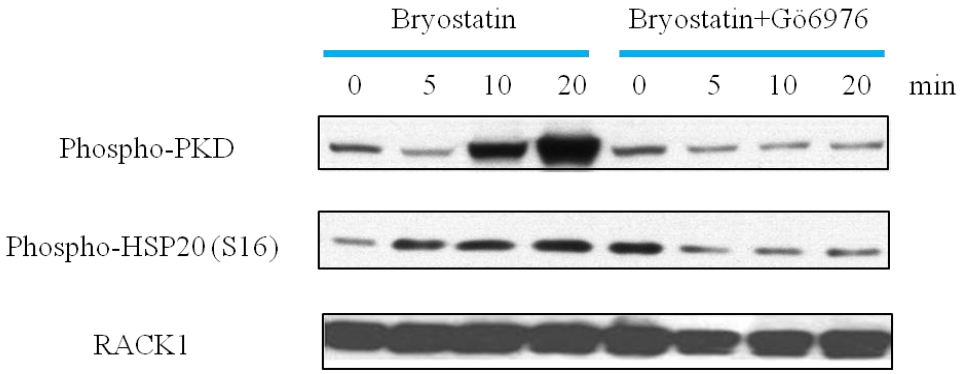

Figure 5.13. The effect of PKD1 activity on HSP20 phosphorylation. PKD1 and HSP20 co-transfected HEK293 cells were treated with bryostatin (PKD activator) alone or with Gö6976 (a potent PKD inhibitor) for the indicated times. PKD1 activation, HSP20 phosphorylation and total HSP20 were monitored via immunoblotting with anti-phospho-PKD1 (Ser916), anti-phospho-HSP20 (Ser16) and anti-HSP20 antibodies, respectively. Anti-RACK1 antibody was used as loading control. Representative immunoblots from three independent experiments are shown.

In addition, a loss-of-function approach was employed to further probe the functional role of PKD1 on HSP20 phosphorylation in intact cell systems. To confirm gene silencing, the level of PKD1 expression was assessed by immunoblotting. Figure 5.14 depicts the level of siRNA-mediated PKD1 knockdown in neonatal rat cardiomyocytes. Clearly, the transfection of cardiomyocytes with PKD1 siRNA markedly suppresses endogenous PKD1 expression, whereas non-specific control siRNA had no effect. Notably, there was a profound reduction in the phosphorylation level of HSP20 as detected by immunoblotting total cell lysates with anti-phospho-HSP20 (Ser16). However, this knockdown had no evident effect on total HSP20 expression. α-tubulin, which is expressed constitutively was also unchanged. Decreasing PKD1 expression by siRNA knockdown significantly inhibited HSP20 phosphorylation. To our knowledge, this is the first direct demonstration that PKD1 is involved in the regulation of HSP20 phosphorylation. Because HSP20 plays a major role in cardioprotection against hypertrophy, it is thus speculated that HSP20 phosphorylation by PKD1 may play a pertinent role in this cellular response.

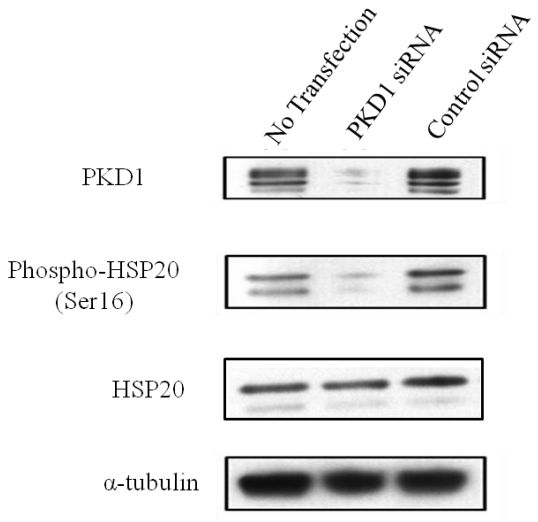

Figure 5.14. siRNA-mediated knockdown of PKD1 blunt phosphorylation of HSP20. Cells were transfected with rat PKD1 siRNA or control siRNA for 48 h to investigate the role of PKD1 in intact cell system. PKD1 expression levels were evaluated by immunoblotting with an anti-PKD1 antibody to confirm the level of knockdown. Phosphorylation of HSP20 and total HSP20 were monitored by immunoblotting with anti-phospho-HSP20 (Ser16) and anti-HSP20 antibodies, respectively. Anti-α-tubulin antibody was used as loading control. Representative immunoblots from three independent experiments are shown.

5.2.6 The effect of PKD1-HSP20 interaction on HSP20 phosphorylation

The regulation of protein function through protein phosphorylation is critical for the modulation of cellular activities. Hence, I investigated further the notion that disruption of PKD1-HSP20 interaction would be associated with changes in levels of HSP20 phosphorylation. Indeed, as shown in Figure 5.15, HSP20 phosphorylation was greatly reduced upon disruption of the PKD1-HSP20 interaction, however, no evident effect was observed on total PKD activity (as measured by phospho-PKD (Ser916)). This indicates that PKD1 and HSP20 association is required for HSP20 phosphorylation.

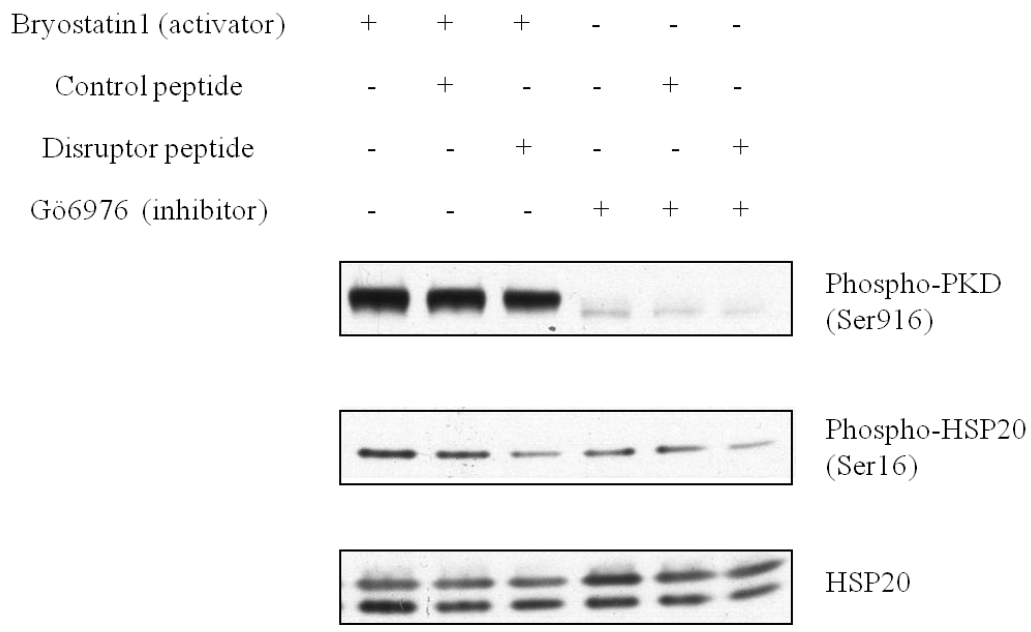

Figure 5.15. The effect of PKD-disruptor peptide 'HJL09' on HSP20 phosphorylation. Cardiomyocytes were subjected to compound treatment as indicated. Protein lysates were subjected to immunoblotting with antibodies that recognise phospho-PKD (Ser916) and phospho-HSP20 (Ser16). Anti-HSP20 antibody was used as loading control. Representative immunoblots from three independent experiments are shown.

In addition, earlier studies have shown that sustained β-adrenergic stimulation results in phosphorylation of cardiac HSP20 on Ser16 and that this can trigger cardioprotective functions and attenuate hypertrophic growth of cardiomyocytes (Fan *et al*., 2005, 2006). In light of the involvement of HSP20 phosphorylation in mediating cardiac responses in cultured cardiomyocytes, it was an exciting prospect to study the effect of PKD1 and HSP20 association on HSP20 phosphorylation in ISO-mediated hypertrophic cardiomyocytes. Here, cells were pre-treated with control or PKD-disruptor peptide 'HJL09' prior to 24 h ISO stimulation. In agreement with earlier results in this chapter, the disruption of PKD1-HSP20 complex initiated decreases in the phosphorylation level of HSP20 (Fig. 5.16). This finding is in contrast with earlier data that researched the role of PKA-regulated HSP20 phosphorylation that facilitated the cardioprotective mechanism. In this regard, the functional consequence of PKD1 phosphorylation on serine 16 appears to be different from that of PKA phosphorylation at the same site. One could speculate that HSP20 phosphorylation may have dual anti- and pro-hypertrophic functions in the cardiovascular system in a kinase-dependent manner. It is also possible that different pools of HSP20 control different functions depending on which kinase (PKA or PKD1) they are associated with.

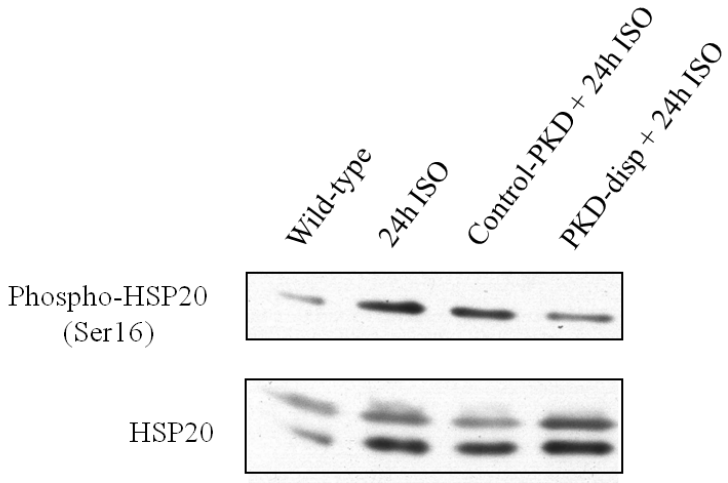

Figure 5.16. The effect of PKD-disruptor peptide 'HJL09' on HSP20 phosphorylation in ISO-induced hypertrophic cardiomyocytes. HSP20 phosphorylation was determined by immunoblotting with anti-phospho-HSP20 (Ser16). Lysates were also immunoblotted with anti-HSP20 as loading control. The blots shown are representative of three independent experiments.

5.2.7 Use of a novel PLA to assess PKD1 association with HSP20

Previous studies have shown that PKD1 translocates into the nucleus upon agonist-dependent hypertrophic response (Vega *et al*., 2004). However, the mechanism of this nuclear influx has not been investigated. To address this issue and at the same time to further elucidate the mechanism underlying the role of PKD1-HSP20 interaction in hypertrophic response, a possible change in subcellular distribution was monitored in cardiomyocytes treated with the panel of compound described. Here, a novel *in situ* proximity ligation assay (PLA) was utilised to characterise patterns of protein interaction within cells (Söderberg *et al*., 2008, Bellucci *et al*., 2011). This method studied the occurrence of alterations in the distribution of PKD1-HSP20 complexes by providing highly specific and better resolution for the observation of the association between PKD1 and HSP20. Specifically, a discrete fluorescent signal (red spot) would only appear when PKD1 and HSP20 form a complex. The proteins need to be less than 40 nm apart before association is detected. In order to detect all PLA signals, images were taken throughout the entire thickness of the cells using Z stacking.

Under non-stimulated condition, diffuse cytoplasmic staining of PKD1-HSP20 complexes was observed and there was less PLA signal in the nuclei, suggesting that the PKD1-HSP20 complex is cytosolic under basal conditions and generally excluded from the nuclei. (Fig. 5.17). In contrast, PKD1-HSP20 complexes were enriched and mostly confined to the nuclei of ISO-treated cardiomyocytes, with a small subpopulation remaining in the cytoplasm. A similar distribution pattern was also observed in cells treated with control peptide + ISO. However, treatment of the cells with PKD-disruptor peptide 'HJL09' triggered a profound change in the intracellular localisation of PKD1-HSP20. Seemingly, the interaction of the two proteins was perturbed, less PKD1-HSP20 complex was visible and complexes that were observed, were scattered in all directions throughout the cells. Parallel samples incubated only with the secondary antibody were also included to confirm that the observed fluorescence pattern could not be attributed to artifacts (data not shown).

My results herein not only further verify that PKD1 exists in a complex with HSP20, but also suggest a spatial relationship between these two proteins. Clearly, the nuclear accumulation of the PKD1-HSP20 complex occurred in cells treated with ISO, whereas disruption of the interaction seemed to hinder nuclear entry of PKD1. These observations strongly suggest a role for HSP20 in mediating translocation of PKD1. Excitingly, the data

reported here provide first evidence for the role of HSP20 in mediating nuclear/cytoplasmic trafficking of PKD1 in response to prolonged *β*-adrenergic stimulation.

5.2.8 Cell fractionation shows PKD1 and HSP20 localisation

Next, cell fractionation studies were performed to extend the above findings and evaluate the degree of PKD1-HSP20 complex distribution. Cells were fractionated after drug treatment as described in 'Materials and Methods'. Cellular proteins were fractionated into cytosolic, membrane and nuclear fractions before being subjected to immunoblotting to detect the protein levels of the PKD1 and HSP20 (Fig. 5.18 Upper panel). The purity of each fraction was validated by using specific markers such as cytosol (HSP90), membrane (GM130) and nuclear (Lamin A/C). The amount of protein recovered in each fraction was then quantified by densitometry and expressed as the percentage of the total protein content (Fig. 5.18 Lower panel). As expected, the cell fractionation results were consistent with the PLA data, showing that both proteins were predominantly in the cytosolic fraction under basal conditions and after treatment with PKD-disruptor peptide 'HJL09'. However, in response to ISO alone and control peptide + ISO treatment, the nuclear pools of the proteins were more abundant than in unstimulated cells. These results underpin the notion that HSP20 has a potential role in mediating PKD1 nuclear translocation. Indeed, PKD1 nuclear translocation during hypertrophic stimulus has been characterised previously by others (Rey *et al*., 2001; Vega *et al*., 2004). Interestingly, this is the first indication that the said dynamic movement of PKD1 is mediated by another protein (in this case HSP20).

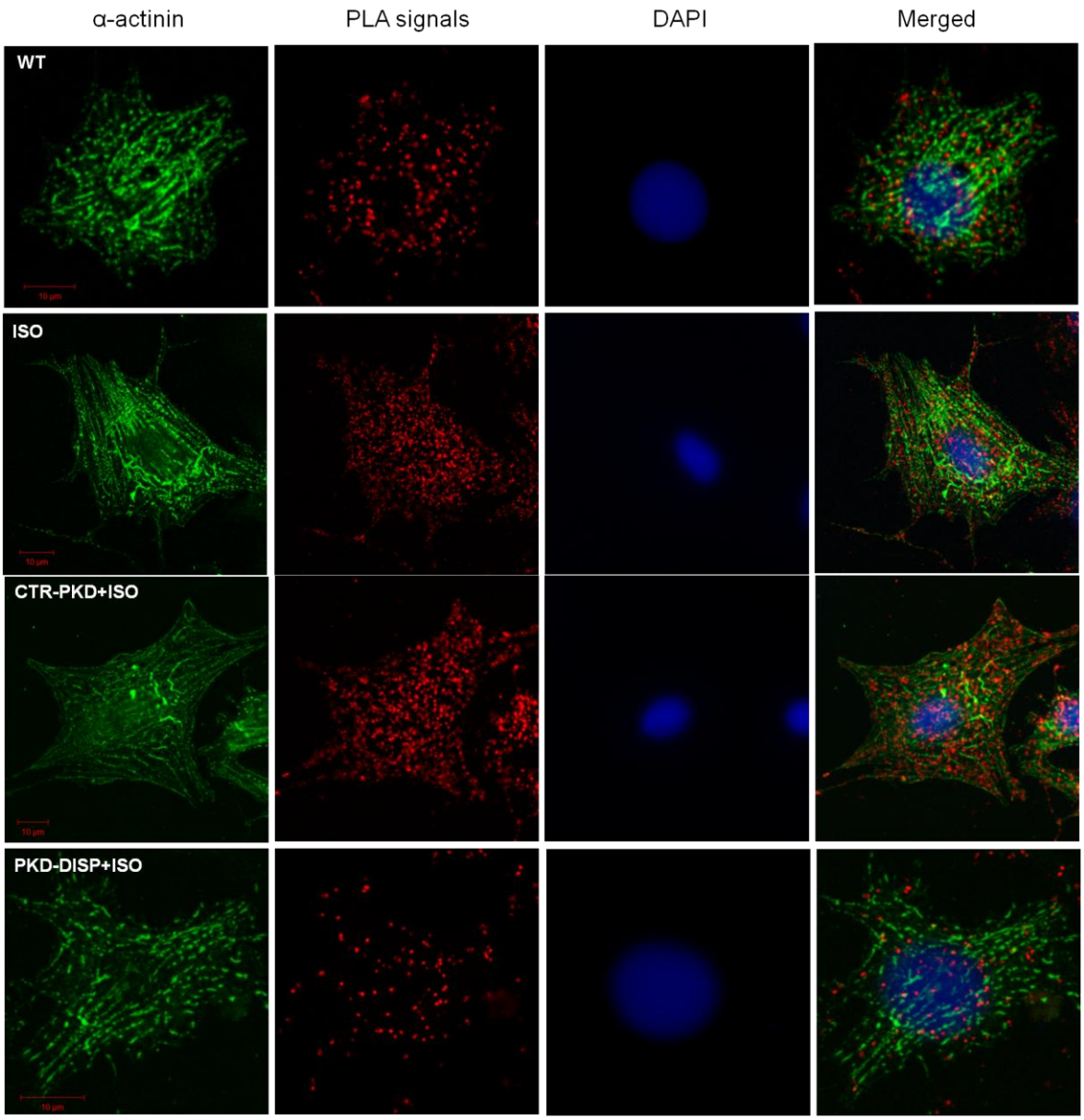

Figure 5.17. The effect of PKD-disruptor peptide 'HJL09' on subcellular distribution of PKD1-HSP20 complex. PKD1-HSP20 associations were recognised with PLA as described in 'Materials and Methods'. PLA signal (red) is only shown in cases where PKD1 forms a complex with HSP20. Cardiomyocytes were counterstained with α-actinin to show sarcomeric staining. DAPI staining was used to mark nuclei. Results showed that the distribution of PKD1-HSP20 complex between cytoplasmic and nuclear compartments could potentially be affected by disrupting the interaction of these two proteins. Images shown are representative of three separate experiments on different cardiomyocytes preparations. Scale bars = 10 μm.

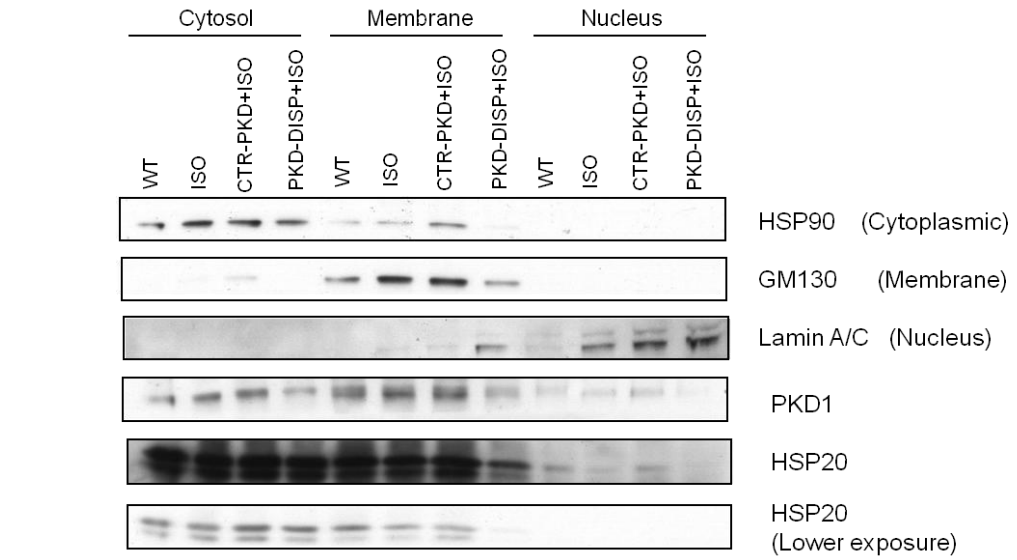

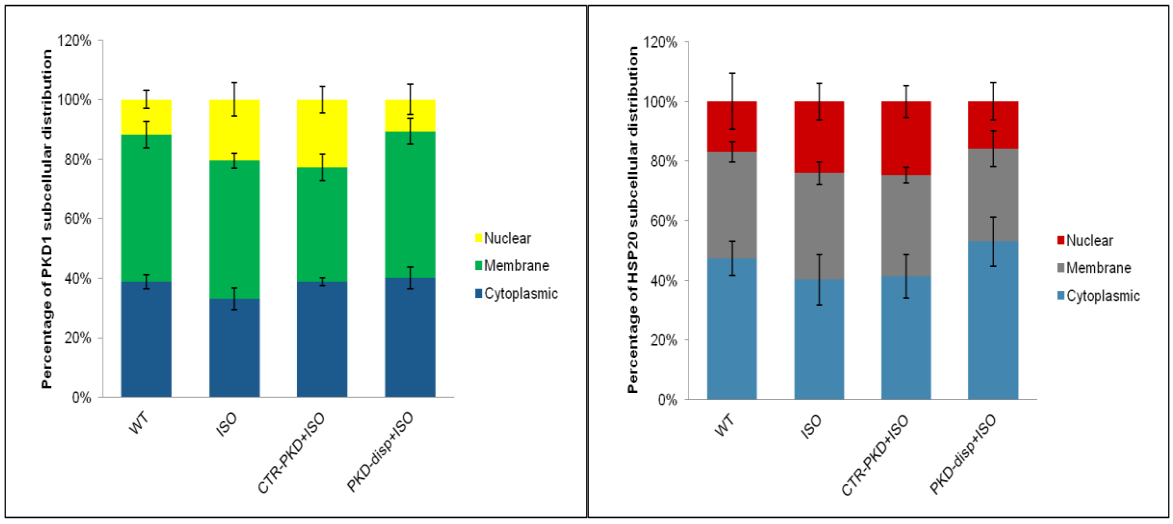

Figure 5.18. Cell fractionation experiments showing PKD1 and HSP20 localisations. Upper panel: A representative Western blot showing protein levels of PKD1 and HSP20 in each fraction with respect to different treatments. Specific markers such as cytosolic (HSP90), membrane (GM130) and nuclear (Lamin A/C) were included to establish fraction purity. Lower panel: Quantification of immunoband intensities was determined by densitometry and was presented as mean percentage of the total protein content ± S.E.M. of three experiments on different cardiomyocytes preparations.

5.2.9 HSP20 phosphorylation : PKA vs PKD1

The abovementioned contradictory findings that PKA- and PKD1-mediated HSP20 phosphorylation at the same site (serine 16) have opposite effects on the hypertrophic response prompted me to carry out further biochemical studies. Because HSP20 can be phosphorylated by PKA, the next step was to determine whether it also affects PKD1-mediated phosphorylation. As expected, treatment with the PKA-selective inhibitor, KT5720 greatly reduced HSP20 phosphorylation in hypertrophic cardiomyocytes. Interestingly, the combined effect of PKA inhibition and disruption of PKD1-HSP20 complex was additive suggesting that both kinases can phosphorylate the global pool of HSP20 at the same time (Fig. 5.19). Based on these findings, it is tempted to suggest that there are different pools of HSP20 regulated by different kinases at specific times and places within cells. In other words, the functional roles of HSP20 are likely to be associated with its phospho-ser16 status resulting from different kinase activation within sub-pools of HSP20. Seemingly, HSP20 may also exert pro-hypertrophic effects depending on the cellular context. These results could have important implications for interpreting the findings of other potential role(s) of HSP20 in heart.

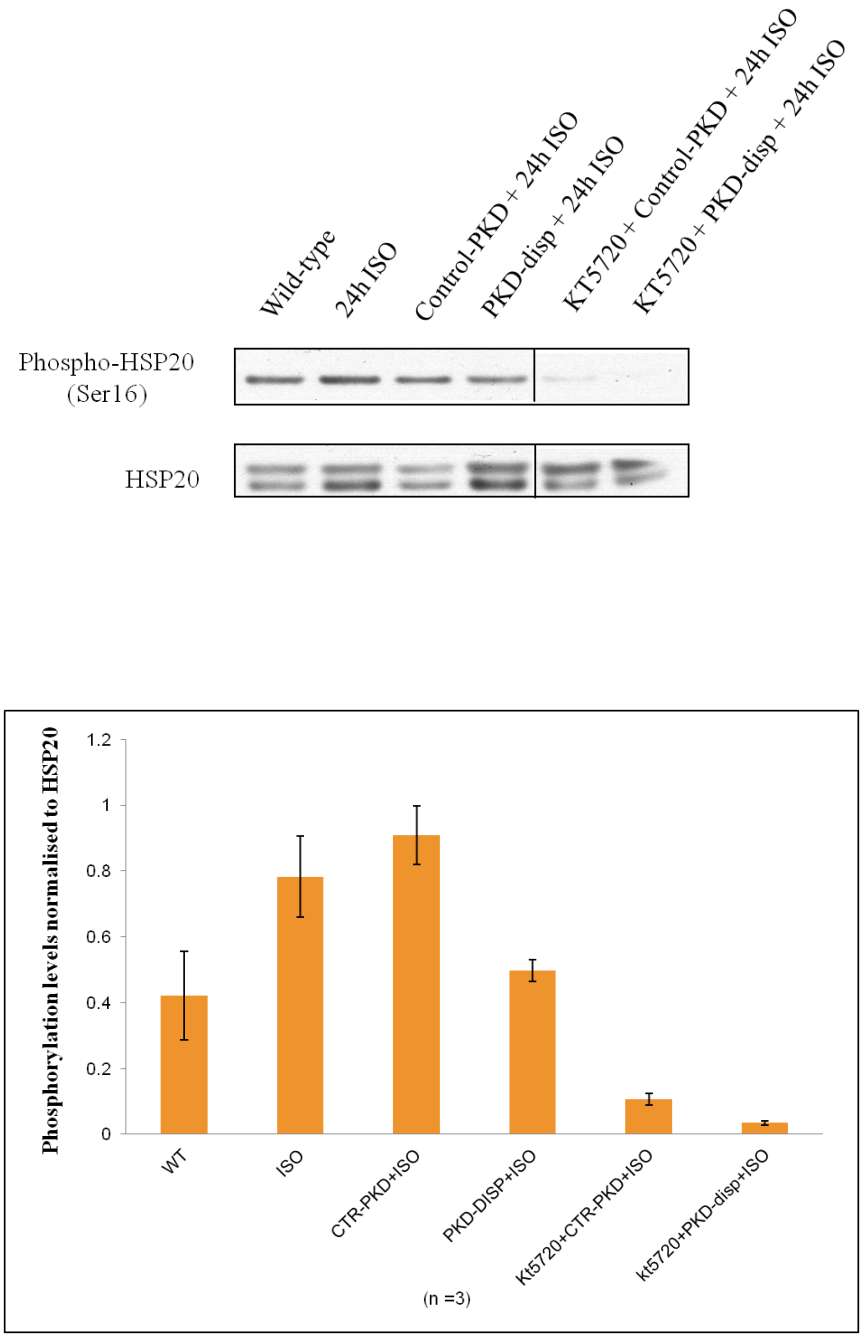

Figure 5.19. PKA and PKD1 modulate HSP20 phosphorylation under prolonged *β*-adrenergic stimulation. The combination of both PKA inhibitor and PKD1-HSP20 disruptor peptide greatly decreased HSP20 phosphorylation**.** Upper panel: Immunoblots showing HSP20 phosphorylation level with respect to different treatments. Total HSP20 protein was used as loading control. Lower panel: Quantification of immunoband intensities was determined by densitometry and was presented as fold ratio of phosphorylation level normalised to HSP20 ± S.E.M. of three experiments on different cardiomyocytes preparations.

5.3 Discussion

Peptide array technology has provided detailed information on the putative docking site for HSP20 on PKD1 and also highlighted several key residues within the conserved catalytic unit of PKD1 (Fig. 4.6). Although insight into the properties and mechanism of the intermolecular interactions of PKD1-HSP20 complex is hampered by the lack of structural information, advanced prediction methods on amino acid sequences have helped to reveal some major structural features of the key residues (Fig. 4.8). In trying to understand the functional role of the PKD1-HSP20 complex in hypertrophic cardiomyocytes, the sequence encompassing G^{606}-E^{630} (GRDVAIKIIDKLRFPTKQESQLRNE) was utilised to develop a cell-permeable disruptor peptide. The stearate group which allows cell insertion is added to the N-terminal end of the peptide, so as not to cause any possible steric interference. Through displacement experiments in neonatal rat cardiomyocytes (Fig. 5.3), the functional relationship between HSP20 and PKD1, and the role for HSP20 in coordinating hypertrophic responses was studied.

5.3.1 PKD1- HSP20 interaction in hypertrophic response

Hypertrophy is characterised by the increase in cardiomyocyte size (in length and/or width), protein synthesis and cytoskeletal remodeling, which represent part of the compensatory mechanism that develops in response to hypertrophic stimuli (reviewed in Frey and Olson, 2003). Consistent with earlier studies (Morisco *et al*. 2001), 24 h sustained ISO-stimulation induced hypertrophy in neonatal rat cardiomyocytes. Subsequently, cardiomyocytes displayed an increase in cell size (Fig. 5.4) and actin filament assembly (Fig. 5.5) upon onset of the hypertrophic response. Interestingly, pharmacological disruption of the PKD1-HSP20 interaction altered ISO-induced morphological changes and actin organisation, indicating that PKD1 and HSP20 association is required for cellular enlargement and actin realignment in hypertrophic cardiomyocytes. As HSP20 has been shown to bind actin and regulate heart function through stabilisation of the cytoskeleton (Brophy *et al*., 1999; Fan *et al*., 2004), PKD1-HSP20 association is likely to be functionally significance to this process.

Apart from the changes in cellular morphology and actin reorganisation, a significant increase in total cellular protein was also observed (Fig. 5.7). It is thought that this is

required for cellular increased growth, a typical cellular feature of pathological hypertrophy (Frey and Olson, 2003). In accordance, real-time qPCR results showed that ISO- and control peptide + ISO- treatment markedly increased the mRNA levels of the fetal genes: ANF, BNF and *β*-MHC (Fig. 5.8), which are pathological hallmarks of hypertrophy (Chien *et al*., 1991; Rosenzweig and Seidman, 1991). The reactivation of these fetal genes may indicate a redeployment of the transcriptional program that governs fetal gene expression to regulate hypertrophic growth. Interestingly, the PKD-disruptor peptide 'HJL09' suppressed the transcriptional activation of the three hypertrophy response genes, returning levels to that of untreated cells. These data are consistent with the hypothesis that PKD1 association with HSP20 is involved in the regulation of the hypertrophic response. Indeed, my data strongly suggests that cardioprotection is conferred upon disruption of the PKD1-HSP20 interaction. Seemingly, this disruption favours cardioprotective mechanisms by repressing expression of fetal cardiac genes. From a biological standpoint, it is likely to be an important mechanism to hinder the progression of hypertrophic phenotype. Hence, it is purported that the PKD1-HSP20 interaction plays important roles in cardiac development and in hypertrophic growth in response to *β*-adrenergic stimulation. Nevertheless, these findings lead to two important questions: (1) how does the disruption of PKD1-HSP20 interaction confer cardioprotection? (2) what is the role(s) of HSP20 in this signalling pathway?

5.3.2 PKD1 regulates HSP20 phosphorylation

Multiple approaches were applied to assess the molecular role of PKD1 in regulating the biological function of HSP20. Firstly, mapping of the phosphorylation site on HSP20 using peptide array identified a physiologically relevant phosphorylation site at Ser16 (Fig. 5.10), a site which is implicated in the sustained *β*-adrenergic/PKA signalling (Beall *et al*., 1997; Chu *et al*., 2004). As previous studies have shown that PKD1 phosphorylates the same sites on TnI as PKA (Haworth *et al*., 2004; Cuello *et al*., 2007), it is therefore no surprise that PKD1 is also capable of phosphorylating other PKA targets such as HSP20 as seen in this study.

In vitro validation by direct kinase assay and immunoblotting using phospho-HSP20 antibodies (Ser16) showed that PKD1 activation corresponded to increases in the phosphorylation of HSP20, further confirming HSP20 as a newly identified PKD1

substrate (Fig. 5.11, 5.12). In addition, pharmacological inhibition of PKD1 activation significantly diminished phosphorylation of HSP20 (Fig. 5.13). It should be noted that selective pharmacological inhibitors of PKD were unavailable at the time when these experiments were conducted. The indolocarbazole compound Gö6976 used in this study is a PKC inhibitor that at nanomolar concentrations inhibits isozymes PKCα, PKCβ, PKCγ and PKCμ/PKD (Moore *et al*., 1999). Although Gö6976 was previously used to inhibit PKD activity *in vitro* (Vega *et al*., 2004), it may not be a perfect model to infer cellular functions of PKD1 especially since PKD1 can be activated through either a PKC-dependent or PKC-independent pathway (Zugaza *et al*., 1996). Unless PKD1 is activated through a PKC-dependent pathway, PKC inhibition could neither inhibit PKC-independent PKD activation effectively nor lead to an outcome similar to that achieved by direct PKD inhibition. Hence in this context, a parallel loss-of-function approach was undertaken to evaluate a possible direct effect of PKD1 activation on HSP20 phosphorylation. Gratifyingly, genetic ablation using siRNA-mediated knockdown of PKD1 reinforced earlier results that showed a diminished HSP20 phosphorylation (Fig. 5.14). These results confirmed a direct relationship between PKD1 activation and phosphorylation of HSP20 at Ser16. Collectively, my study demonstrates for the first time that PKD1 is a novel kinase for HSP20 that modulates its phosphorylation at Ser16. As HSP20 phosphorylation is involved in cardioprotection against hypertrophy [as described in Chapter 3 and by other investigators (Fan *et al*., 2004, 2005, 2006; Qian *et al*., 2009)], I speculated that PKD1-mediated HSP20 phosphorylation may also play a key role in this response. Further work may be required to assess the functional implications of PKD1 knockdown on hypertrophic responses. Also, PKD1 kinase-dead mutants should be used to examine whether kinase activity is essential for HSP20 phosphorylation in hypertrophic cardiomyocytes.

As previous findings have shown that sustained β-adrenergic stimulation results in phosphorylation of cardiac HSP20 on Ser16 by PKA and that this action attenuates hypertrophic growth of cardiomyocytes and triggers cardioprotective functions (Fan *et al*., 2004, 2005), it was interesting to study the effect of a PKD-disruptor peptide on HSP20 phosphorylation. However, early observations on the potential role(s) of the PKD1-HSP20 complex revealed unexpected findings. It turned out that disruption of the PKD1-HSP20 interaction decreased the phosphorylation level of HSP20 in hypertrophic cardiomyocytes without affecting PKD1 activity (Fig. 5.16). In other words, the cardioprotection conferred by the PKD-disruptor peptide ‘HJL09’ occurred when a lower level of HSP20 phosphorylation was evident. Clearly, this is in stark contrast with PKA-regulated HSP20

phosphorylation. So, what are the functional implications of HSP20 phosphorylation in this context? It is tempting to speculate that HSP20 may have both anti- and pro-hypertrophic functions in the cardiovascular system. Seemingly, HSP20 facilitates hypertrophic response in a kinase-dependent manner. The notion is supported by studies demonstrating that opposite function of cyclin-dependent kinases (CDKs), CDK1 and CDK2 which phosphorylate the same site on forkhead box O (FoxO) transcription factor, FoxO1 at Ser249. Similar to HSP20, FoxO1 shuttles between the cytoplasm and nucleus, whereby its subcellular localisation and biological function (its transcriptional activity) is regulated by intracellular kinases. Specifically, the phosphorylation of FoxO1 by CDK1 promotes nuclear accumulation of FoxO1 and triggers apoptosis in neurons (Yuan *et al*., 2008), whereas CDK2 phosphorylates FoxO1 results in cytoplasmic localisation and inhibition of FoxO1 (Huang *et al*., 2006). However, the mechanism underlying the opposite function of both CDK1 and CDK2 on Fox01 phosphorylation remains incompletely defined. Clearly, different kinases can elicit opposite effects despite phosphorylating the same residue.

5.3.3 HSP20 is the 'molecular escort' of PKD1

These apparently contradictory findings prompted me to carry out immunocytochemical studies to investigate the effect of PKD-disruptor peptide 'HJL09' on intracellular distribution of PKD1 and HSP20 proteins. The novel technology involved *in situ* PLA analyses holds great potential for shedding light on the function of PKD1 and HSP20 by positioning them within a functional signalling complex. This highly specific and sensitive method allowed direct observation of endogenous protein complexes without any need for genetic modification of target cells, such as cells with overexpressed fusion-tagged target proteins (Söderberg *et al*., 2008, Bellucci *et al*., 2011). It is based on the use of two primary antibodies raised in different species and a pair of fluorophore-labelled oligonucleotide PLA probes (priming and non-priming secondary antibodies). Dot-like positive signal is generated only when the two PLA probes bind in close proximity to each other. It is thought that the PLA signal is proportional to protein associations. Conversely, immunofluorescence (IF)-based methods which have lower sensitivity with scarce proteins and is likely to exhibit poor target selectivity, cannot be used to study protein-protein interactions (Pradidarcheep *et al*., 2008). Moreover, *in situ* PLA results which exhibit higher signal to noise ratio, are shown as discrete fluorescent spots and not by measuring the total fluorescence intensity. It is thus less likely to encounter fluorescence

photobleaching which may complicate the observation of fluorescent signal compared with IF-based methods. Indeed, a number of studies have indicated that in situ PLA generated more accurate predictions of *in vivo* effects in primary cells than the regular IF detection methods, in particular for drug-induced perturbations of protein-protein interactions. For example, *in situ* PLA was used to examine the effects of small molecule kinase inhibitors on platelet-derived growth factor receptor (PDGFR) β signalling in primary human fibroblasts (Leuchowius *et al*., 2010). This method has also been used to study the redistribution of dopamine transporter (DAT)/α-synuclein complexes in the Parkinson's disease brain of transgenic mice (Bellucci *et al*., 2011). Interestingly, my PLA results showed that the PKD1-HSP20 complex underwent dynamic intercellular redistribution from the cytoplasm under basal conditions, to the nucleus in response to 24 h ISO stimulation. Notably, similar observations were also obtained in biochemical fractionation experiments, confirming the reproducibility of *in situ* PLA.

Pathological cardiac remodeling involves reactivation of the fetal gene program, which encodes proteins to regulate cardiac functions such as contractility (Frey and Olson, 2003). Previous studies have demonstrated that PKD1 phosphorylates HDAC5 leading to its export from the nucleus to the cytoplasm, resulting in a pro-hypertrophic phenotype through MEF2 transcriptional activity (Zhang *et al*., 2002; Chang *et al*., 2005; Vega *et al*., 2004). However, none of these reports have provided an adequate explanation concerning the mechanism behind the nuclear import of PKD1 and subsequent regulation of HDAC5 pro-hypertrophic properties. As such, one possible explanation for the dynamic cellular localisation of PKD1-HSP20 complex seen in present study is that HSP20 serves as a 'molecular escort' for facilitating nuclear translocation of PKD1. Given that PKD1 is required to be translocated into the nucleus to trigger fetal gene expression (Harrison *et al*., 2006), it is thus likely that the induction of hypertrophy is also a consequence of the PKD1-HSP20 interaction. Moreover, it is plausible that disruption of the complex halts translocation and this action may be protective against the hypertrophic response. Additionally, because PKD1 regulates the pathological remodelling of the heart via its ability to modulate phosphorylation and nucleocytoplasmic shuttling of HDAC5 (Zhang *et al*., 2002), it is thus speculated that the suppression of fetal gene expression resulting from the disruption of PKD1 nuclear translocation involves dephosphorylation of HDAC5. Further experimentation is needed to prove this idea. Clearly, these findings support a role for PKD1-HSP20 interaction in the modulation of the repressive influence of HDAC5 on hypertrophic cardiomyocyte via its ability on nuclear influx.

Gratifyingly, results from PLA shed new light on the incomplete mechanism underlying the nuclear translocation of PKD1 following hypertrophic onset. As deduced from the results gathered in the second part of this project, a testable model is proposed to explain this series of molecular events (Fig. 5.20). Seemingly, the association of PKD1 and HSP20 and the consequent effects on fetal gene program are primarily a β-adrenergic-mediated hypertrophic response. HSP20-mediated PKD1 nuclear translocation may account for the induction of fetal gene expression. In contrast, disruption of PKD1-HSP20 complex leads to downregulation of fetal gene program, thereby hindering the development of hypertrophy and cardiac failure. Although it is reasonable to suggest that the disruptor peptide inhibits fetal gene expression by inhibition of PKD1 nuclear translocation, it should be noted that other HSPs or proteins may also play compensatory roles in the effects exerted by HSP20. Future studies may require clarifying the specificity of this response to HSP20 using inducible or conditional knockout models.

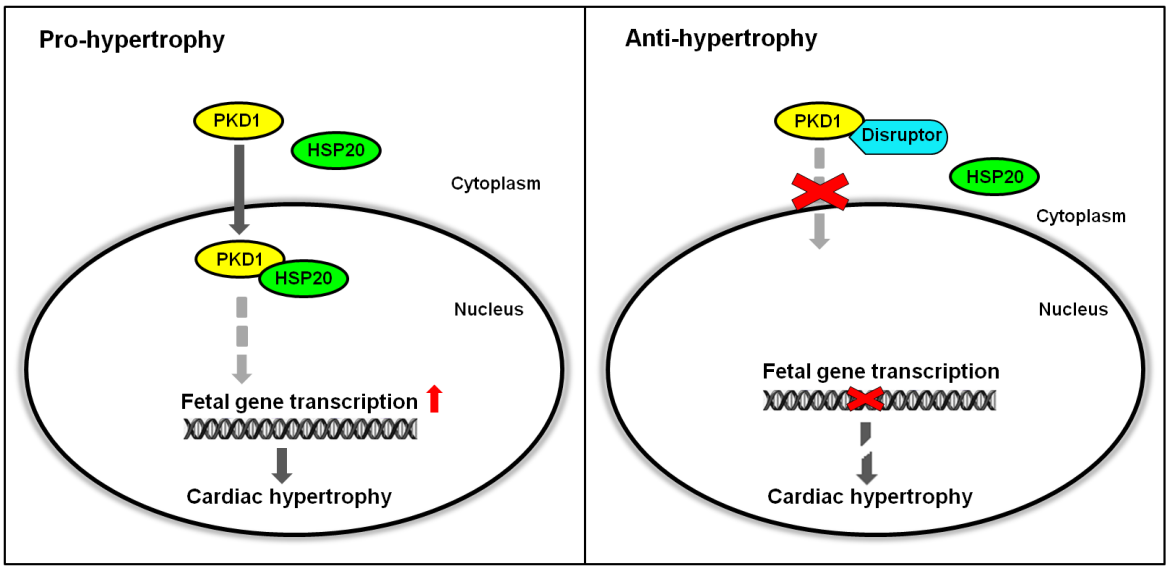

Figure 5.20. Proposed models for the role of HSP20 in PKD1 nuclear translocation. Upon prolonged β-adrenergic stimulation, HSP20 binds to PKD1 and mediates PKD1 transport into the nucleus. This action leads to the activation of fetal gene program which promotes cardiac hypertrophy. Conversely, disruption of the PKD1-HSP20 complex results in the downregulation of fetal gene expression, thereby hindering the progression of cardiomyopathy. The PKD1-HSP20 complex may serve as a promising therapeutic target as they indirectly facilitate the hypertrophic growth response.

This study has mainly focused on the PKD1-HSP20 interaction, and has examined the regulation of HSP20 phosphorylation by PKD1, where phosphorylation actually induces a pro-hypertrophy response. Again, it should be noted that HSP20 can also be phosphorylated by PKA and conversely, increase PKA-mediated phosphorylation of HSP20 has been shown earlier to initiate anti-hypertrophy response (see Chapter 3). The differences in hypertrophic responsiveness between PKA- and PKD1-mediated HSP20 phosphorylation may also suggest that although they share a similar phosphorylation site at Ser16, they serve different functions. As such, we cannot rule out the possibility that PKA regulates redundantly or in concert with PKD1 to control HSP20 phosphorylation. Indeed, phosphorylation assays showed that PKA inhibitor, KT5720 resulted in nearly 80% reduction in the level of HSP20 phosphorylation and this could be further diminished upon disruption of PKD1-HSP20 interaction. It is thus hypothesised that there are different pools of HSP20 which are regulated by different kinases in response to specific stress stimuli. The mechanism behind this discrepancy is still unclear, but it is likely to involve crosstalk between kinases and downstream targets in the hypertrophy signalling pathway. This will be discussed in more detail in Chapter 6.

5.3.4 Conclusions

In conclusion, the integration of ProtoArray data with biochemical and immunocytochemical studies have led to a new hypothesis for cardioprotective mechanism, which has provided a deeper insight into hypertrophy signalling. These cumulative observations, for the first time, reveal a novel role of PKD1 and HSP20 in ISO-mediated hypertrophy in neonatal rat cardiomyocytes. I strongly feel that this represents an important mechanism, which underpins sustained β-adrenergic effects on pathological cardiac growth and cardiac remodeling. In fact, my findings herein have established that the PKD1-HSP20 complex acts as a nuclear effector of hypertrophy signalling pathways, which is causally involved in the induction of fetal gene program. Importantly, my present findings have identified the PKD1-HSP20 complex as a new component in the hypertrophy signalling pathway. However, the important question remains: what is the mechanism(s) underlying the role of HSP20 in PKD1-mediated hypertrophy signalling? Overall, it is thought that at least four mechanisms are involved: (1) activation of PKD1 in response to a stress signal or upstream regulator; (2) HSP20 interaction with PKD1 to form a complex; (3) HSP20 mediation of PKD1 nuclear translocation, most likely through a post-

translational modification such as phosphorylation; and (4) attenuation of PKD1-triggered fetal gene program through the disruption of PKD1-HSP20 complex. This latter point is particularly pertinent when considering the blockade of hypertrophic signalling in response to sustained β-adrenergic stimulation, thereby hindering the progress of hypertrophy and cardiac failure. Clearly, the stimulatory actions of the PKD1-HSP20 interaction on cardiomyocyte hypertrophic progression, further confirms that HSP20 is an intracardiac modulator of cardiomyocyte function. In other words, HSP20 serves as a pro-hypertrophic regulator by mediating nuclear transport of PKD1. Because cardiac hypertrophy often involves the nuclear export of PKD1-phosphorylated class II HDAC5 into the cytoplasm which derepresses hypertrophic genes (McKinsey *et al*., 2001; Zhang *et al*., 2002; Vega *et al*., 2004), it is thus postulated that PKD-disruptor peptide 'HJL09' derived from this study may ameliorate the hypertrophic effects by barring PKD1 from entering the nucleus to regulate repressive activities of HDAC5, thereby inhibiting MEF2-dependent fetal gene transcriptional activation. In this regard, PKD1 and HSP20 may emerge as promising therapeutic targets to hinder the hypertrophic phenotype.

Further studies to define the functional role of PKD1 and HSP20 in experimental animal models would provide exciting new information on the role of the PKD-HSP20 complex on pathological cardiac hypertrophy. Moreover, there would be value in studies to investigate whether HSP20, in addition to serving as 'transport mediator' for PKD1, is also involved in the regulation of various PKD1 substrates in the hypertrophy signalling pathway.

5.4 Further work

Using information derived from the peptide array analyses described above, further work was also carried out to examine whether PDE4D5-HSP20 and PKD1-HSP20 interactions interfere with each other in the presence of all three interacting proteins. To do this, I simultaneously probed HSP20 peptide array with equimolar amounts of full-length purified PKD1 and PDE4D5 proteins. Simultaneous detection of equimolar PKD1 and PDE4D5 binding was carried out on the Odyssey system using rabbit-anti-PKD1 and sheep anti-PDE4D antibodies, each linked to distinct secondary antibodies labelled with different wavelength probes (anti-rabbit IRDye800 (green channel) and Alexa Fluor 680-conjugated

anti-rabbit IgG (red channel)). This independently identified PKD1 (green) and PDE4D5 (red) associated with specific peptide spots in single channel analyses. The signals were then merged to identify peptide spots with solely PKD1-HSP20 complexes (green), solely PDE4D5-HSP20 (red) and those with mixed populations of PKD1-HSP20 and PDE4D5-HSP20 (yellow) (Fig. 5.21). Overlay studies showed that PKD1 and PDE4D5 mainly interact at multiple overlapping sites within the WDPF domain (Met^{1}-Glu^{35}) and α-crystallin domain (His^{96}-Gly^{140}) of HSP20 which may suggest competitive binding in these regions. In fact, PKD1 was able to bind to amino acids covering a broader part within the N-terminal of the α-crystallin domain extending from Glu^{41}-Ser^{75}, unlike a more localised PDE4D5 binding site spanning only Ala^{51}-Ser^{75}. Notably, this also pinpointed exclusive PKD1 binding (green) to the region Glu^{41}-Asp^{50} of HSP20. Alternatively, superimposing the binding sites on a predicted 3D structure of HSP20 revealed common surface-accessible region of both PKD1 and PDE4D5 and well-defined surface-exposed patch of PKD1 exclusive binding site (Fig. 5.22).

Interestingly, the binding site of PKD1 on HSP20 showed by 2-protein simultaneous detection method here was inconsistent with that showed earlier in Figure 5.9 using 1-protein overlaying approach. Seemingly, PKD1 was able to bind to the α-crystallin domain of HSP20 more extensively in the presence of PDE4D5. This may due to steric interaction caused by PDE4D5 which is likely to induce changes in conformation and binding properties of PKD1. Despite competing for docking site on HSP20, PDE4D5 may also facilitate mutual interaction of PKD1 with HSP20. However, the underlying mechanism is still unclear. Nevertheless, these findings may highlight, to some extent, an additional degree of functional complexity associated with a crucial role of PDE4D5 on PKD1-HSP20 interaction. It is speculated that such consequence of PDE4D5 binding is likely to exert a functional effect on the regulation of PKD1 on HSP20.

Further studies using yeast two-hybrid assay with HSP20 expressed as ‘bait’, PKD1 as ‘prey’ and PDE4D5 as a ‘competitor’ and co-immunoprecipitation may help to verify whether PDE4D5 can enhance the binding of PKD1 to HSP20. Moreover, siRNA-mediated knockdown of cAMP-specific PDE4D5 is required to examine explicitly whether the alterations in the level of PDE4D5 expression could act to modulate PKD1-mediated phosphorylation of HSP20.

On the other hand, the restriction of PKD1 nuclear entry is clearly a potential route to attenuate the pathologic hypertrophic response. Previous studies have shown that

biologically active peptides can be efficaciously delivered into organs of intact animals via the blood vessels (Chen *et al*., 2001). It is thought to be more effective compared to gene delivery, as adaptations to any modifications induced by signal transduction modulator are less likely to occur. However, there are several factors regarding peptide-based therapy that need to be taken into consideration. These include the synthesis and solubility of peptide, target specificity, maintenance of peptide activity and stability, as well as degradation of unwanted peptide products (Mason, 2010). As such, it will be necessary to take further steps to translate the PKD-disruptor peptide 'HJL09' into small molecules for easy manipulation in drug development. This could be done by identifying the smallest active fragment required for its biological activity. Optimisation of peptide array is a fundamental approach to identify the minimum high affinity binding sequence of the interaction motif (Hummel *et al*., 2006). Using progressive stepwise truncations from either N- or C-terminal or both termini, my preliminary data suggest that peptide sequences as short as six amino acid residues ($R^{607}DVAIK^{612}$) may be effective for such disruption. Short peptides are more "drug like" and can be therapeutically viable (Fig. 5.22A). While alanine scanning highlights the contribution made by the functional group of each side chain, positional scanning of sequential substitution with other naturally occurring amino acids offers a route to the enhancement of peptide activity (Fig. 5.22B). Nevertheless, it should be noted that small length peptides does not take into account the steric chemistry of proteins and therefore could represent false positives. Peptide array also has the drawback that it will miss binding events involving a number of amino acids that are far separated in the linear sequence but coalesce to form a complex binding site within the 3-D protein structure. As such, biological techniques such as co-immunoprecipitation and site-directed mutagenesis are needed in parallel. Nevertheless, the development of a selective disruptor of PKD1-HSP20 for use in proof-of-concept studies using animal models of cardiac hypertrophic is likely to advance our current understanding on hypertrophy signalling.

Further experimentation should also be undertaken into the molecular mechanism of PKD1 nuclear influx, for instance, whether the binding of PKD1 and HSP20 affects the phosphorylation of HDAC5. Additional work is required to establish the underlying molecular requirements, for example, whether PKD1-HSP20 complex crosstalks with other signalling systems to regulate hypertrophic response upon β-adrenergic stimulation. It would also be interesting to see if the subcellular distribution of phospho-HSP20 is different from the non-phospho form via immunocytochemical studies. In addition, using *in situ* PLA analysis to investigate whether the binding nature of the complex is affected by

phospho-HSP20 may also provide valuable information on the possible function of HSP20 phosphorylation on PKD1 translocation. I would also have liked more time to prove that there are different pools of HSP20 that are modified by different kinases as this would help to explain the obvious contradiction that both kinases (PKA and PKD1) phosphorylate HSP20 at the same site but have opposing actions. These experiments would have been carried out utilising *in situ* PLA which allows subcellular localisation and quantification of the relative amounts of endogenous PKA-HSP20 and PKD1-HSP20 complexes in cells based on the use of three primary antibodies (anti-PKA, anti-PKD1 and anti-HSP20), all raised in different species. For example, a rabbit antibody directed against HSP20 would be used together with a mouse PKD1 antibody and a goat PKA antibody, follow by secondary PLA probes directed against mouse, rabbit and goat IgG. The products would then be detected using two different fluorescently labelled oligonucleotides, where PKA-HSP20 and PKD1-HSP20 associations will appear as discrete spots of two different colours (eg. green and red), thereby showing the subcellular localisation of these heteromeric complexes. To investigate if *in situ* PLA will be suitable for monitoring such interactions, perturbations of interactions between these proteins would also be studied in cells treated with inhibitors and/or disruptor peptides.

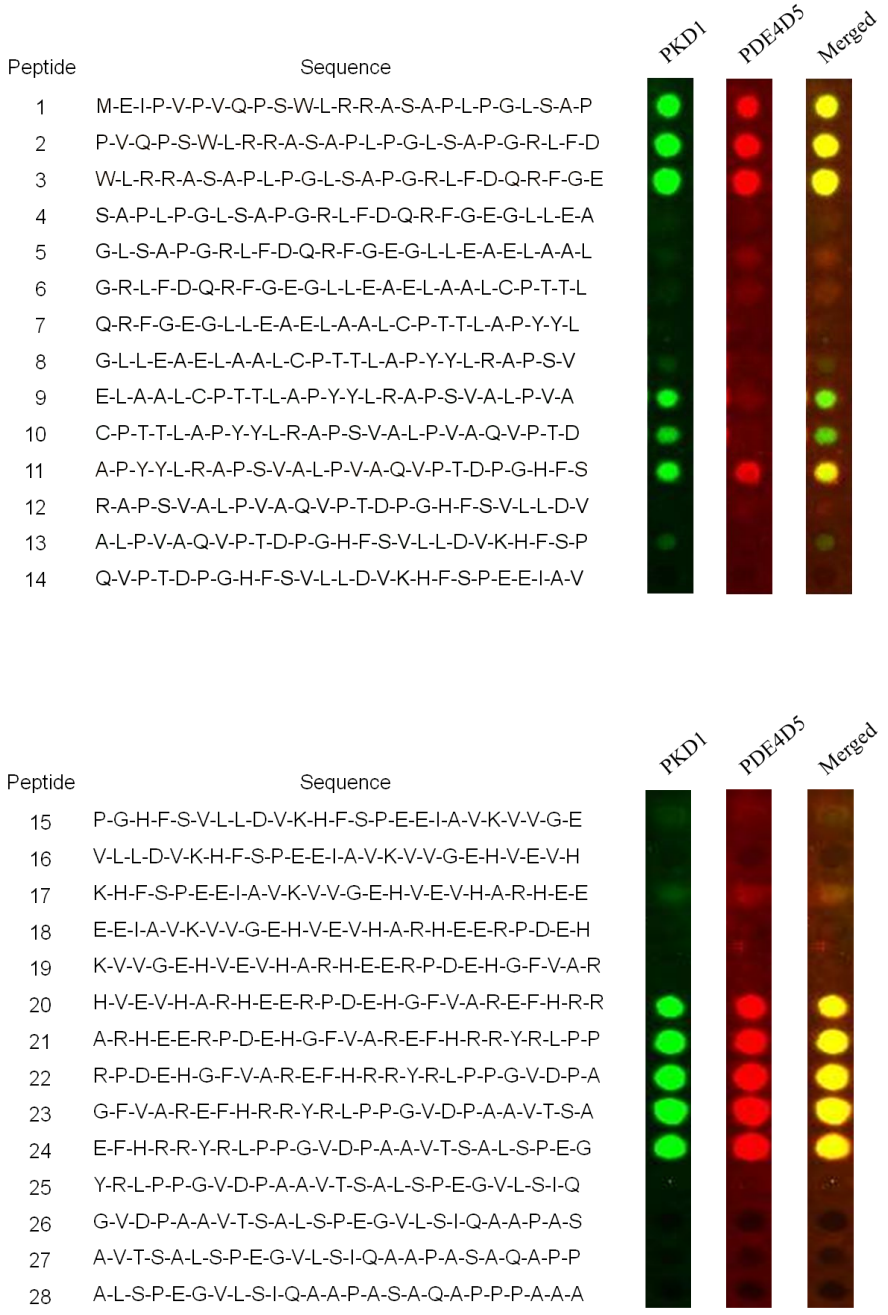

Figure 5.21. Simultaneous detection of PKD1 and PDE4D5 interactions on HSP20. Odyssey analysis of HSP20 peptide array incubated with equimolar (3.8 nM) PKD1 and PDE4D5, followed by blotting with anti-PKD1 (rabbit) and anti-PDE4D5 (sheep). PKD1 (green) and PDE4D5 (red) binding were detected simultaneously with dual binding (yellow) shown in the combined channels (overlay) using fluorescence secondary antibodies. Null binding is black. Data are typical of those obtained using three separately synthesised arrays.

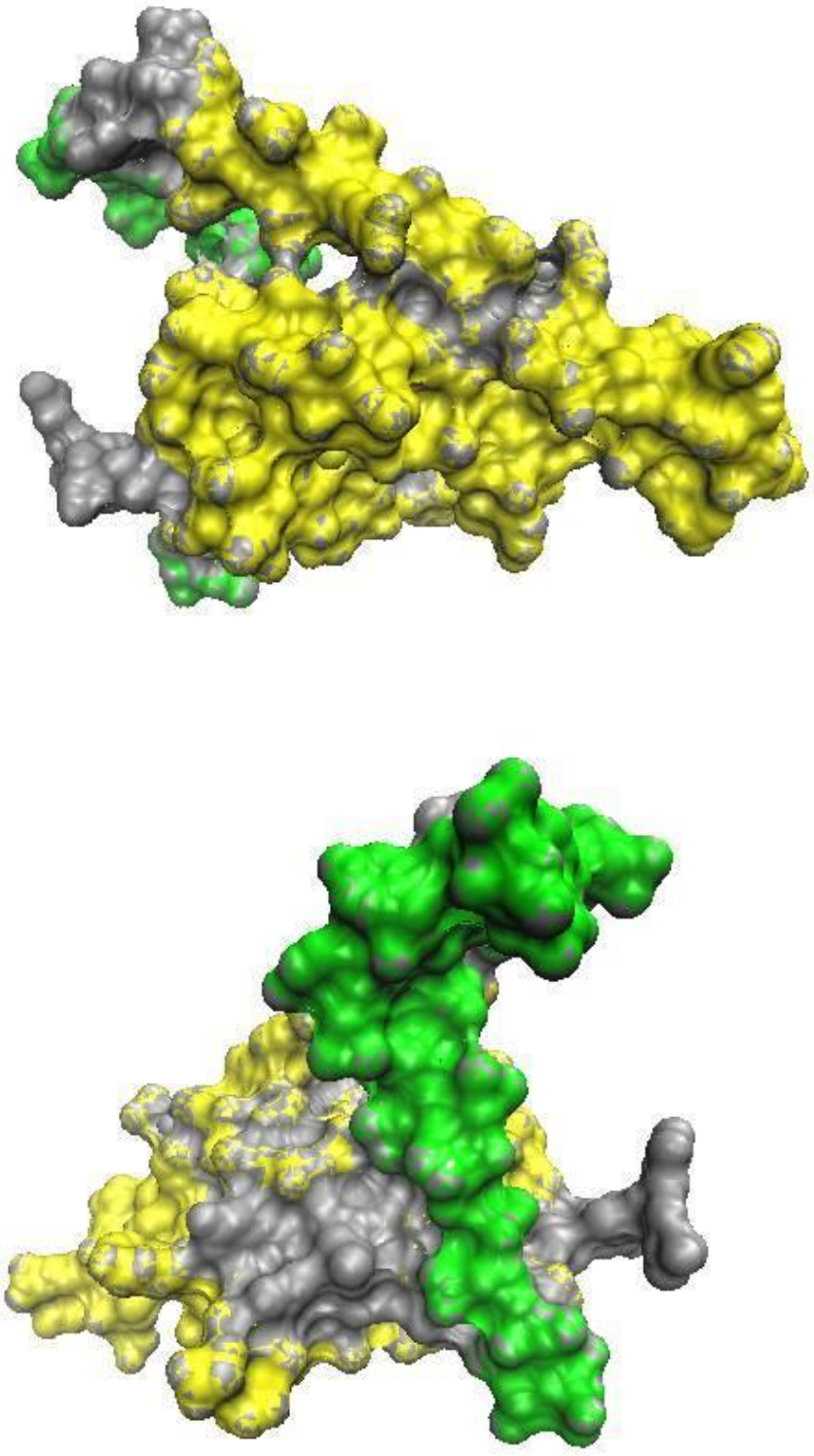

Figure 5.22. Predicted structure of HSP20 and location of binding sites with PKD1 and PDE4D5. Interaction sites with HSP20 were superimposed on a predicted 3D structure of HSP20, presented in front view (upper) and back view (lower), related by 180 degree rotation. Yellow region represents common binding sites of PKD1-HSP20 and PDE4D5-HSP20 whereas green patch depicts PKD1 exclusive binding region on HSP20.

A

B

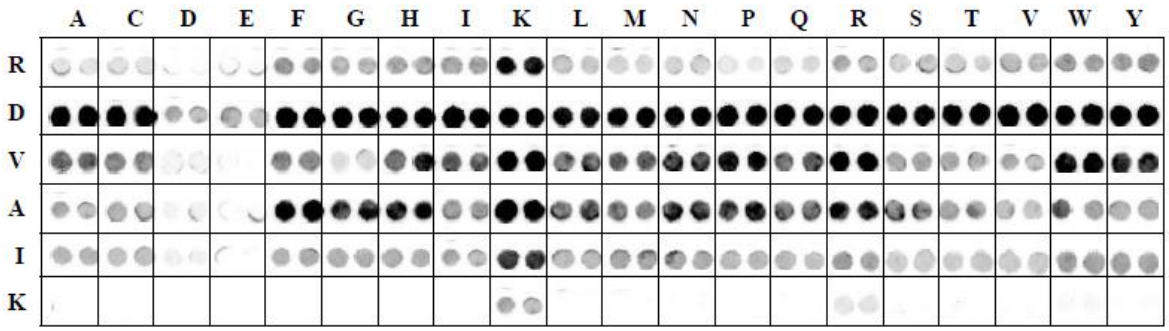

Figure 5.23. Optimisation of peptide length and substitutional analysis. (A) Truncation studies omitting one or more amino acids from the amino, carboxyl or both termini. (B) Positional scanning shows all possible combinations of the most active amino acids at each position, hence identifying potential more favourable residues for enhanced peptide activity.

Chapter 6

Final Discussion

6.1 Background

HSP20 and its phosphorylation have been implicated in many protective processes in heart. In particular, the role of PKA in directing HSP20 phosphorylation to trigger cardioprotective mechanisms has attracted much interest from research groups. My PhD project herein aimed to further elucidate the molecular mechanism behind HSP20 induced cardioprotection, in particular against hypertrophy. This project was divided into two parts: (1) to investigate the role of PDE4-HSP20 complex in hypertrophy; (2) to identify novel signalling complexes containing HSP20 in the hypertrophic signalling pathway.

6.2 The association of PDE4D and HSP20

Initial studies involved setting up an *in vitro* cell-based model for hypertrophy using sustained β-adrenergic agonist, ISO-stimulated neonatal rat cardiomyocytes. Hypertrophic growth was evaluated by manual microscopic measurement of cell size, quantitative measurements of cell size using RT-CES, protein synthesis and real-time qPCR analysis of fetal gene expression. The first section of my work showed that (1) members of the cAMP-specific PDE4 family can form signalling complexes with HSP20 and (2) the PKA-mediated phosphorylation of HSP20 can be controlled by PDE4. The selective disruption of PDE4D5-HSP20 complex using a competing peptide 'bs906' based on PDE4D5 sequence could specifically dissociate these proteins, resulting in a local increase in cAMP levels in the vicinity of HSP20 that resulted in hyperphosphorylation of HSP20 at Ser16. In contrast, intact PDE4D5-HSP20 complexes lower the cAMP concentration in the vicinity of HSP20, thereby preventing activation of localised PKA and consequently reducing HSP20 phosphorylation. Interestingly, disruption of the HSP20-PDE4 complex attenuated the hypertrophic response in cultured cardiomyocytes, as shown by a reduction of the increase in cell size and protein content. Seemingly, peptide 'bs906' augmented the increase in ANF expression. In summary, the protective mechanism conferred by HSP20 in this context depends on it phosphorylation at Ser16 by cAMP-dependent PDE4D5-regulated PKA phosphorylation. Because HSP20 is versatile and has multiple protective roles, it is important to further explore the target network of HSP20, which may be involved in cardioprotective mechanism.

6.3 The association of PKD1 and HSP20

The second part of my work identified PKD1 as a novel binding partner for HSP20 using proteomic analysis as described in Chapter 4. The interaction was then validated by biochemical means, immunocytochemistry and array-based analysis, which provided the first evidence of the direct association between HSP20 and PKD1. My work also revealed that HSP20 not only interact with PKD1 but is also substrate for PKD1 *in vitro*. Ser 16 (also the PKA site) was identified as the PKD1-mediated phosphorylation site in HSP20. Furthermore, displacement studies using PKD-disruptor peptide 'HJL09' derived from PKD1 peptide array data provided a novel functional insight into the role of HSP20 in hypertrophy. My experiments showed that disruption of the PKD1-HSP20 complex protected against hypertrophy (as shown by a reduction in the increase in cell size and protein content, as well as actin reorganisation and fetal gene expression).

In addition, PLA analysis suggested a pivotal role of HSP20 in directing nuclear translocation of PKD1, in which disruption of the PKD1-HSP20 interaction consequently suppressed activation of fetal genes. My results also demonstrated that cardioprotection can be induced by disruption of the PKD1-HSP20 complex which results in a decrease in HSP20 phosphorylation at Ser16. This is in contrast to the findings from the first part of my work (see Chapter 3) and previous studies (Fan *et al*., 2004, 2005, 2006) which showed that increased (PKA-mediated) phosphorylation of HSP20 at serine 16 is required to trigger cardioprotective mechanisms. Seemingly, PKD1 phosphorylates HSP20 at the same phosphorylation site, yet induces an opposite effect to PKA-mediated HSP20 phosphorylation. These opposing functions of PKA and PKD1 on HSP20 may be a feature of multi-stationarity which involves mechanism of cellular decision-making. Whether the binding of these proteins is mutually exclusive or competitive is still unknown. Nevertheless, the disruption of PDE4D5-HSP20 and PKD1-HSP20 complexes with consequent upregulation and downregulation of fetal gene expression, respectively, strongly suggest that these two signalling complexes are differentially regulated in hypertrophic cardiomyocytes. Seemingly, PKA-mediated HSP20 phosphorylation could complement the function of PKD1-mediated HSP20 phosphorylation in cardioprotective mechanism. In this regard, cross-phosphorylation of PKA and PKD1 on HSP20 appears possible and interplay between these two kinases is likely, hence pinpointing the complexity of control mechanism in maladaptive signalling in the heart.

6.4 Antagonistic actions of PKA and PKD1on HSP20

The paradoxical findings here suggested that PKA could function in concert with PKD1 to elicit signalling changes in response to hypertrophic stimuli. Notably, in cardiomyocytes, the molecular fingerprint of PKD-mediated phosphorylation differs from that of PKA, with only the latter targeting sites such as Ser282 in cardiac myosin-binding protein C, Ser16 in phospholamban, and Ser68 in phospholamban (Cuello *et al*., 2007). Thus, the functional outcome of PKD activation would be expected to be different from those of PKA activation. In line with my findings, there is evidence to suggest the existence of PKA-independent mechanisms of calcium-dependent protein kinases which act in an opposing manner (Backs *et al*., 2011). The report from Backs *et al.* (2011), identified class II histone deacetylases HDAC4 as common targets of both PKA and calcium/calmodulin-dependent protein kinase II (CaMKII), where both docking sites lie in close proximity. It was reported that PKA induced proteolysis of HDAC4 and repressed MEF2 activity, thereby antagonising the pro-hypertrophic actions of CaMKII signalling. Clearly, HDAC4 in this regard, functions as an integrator of the two opposing signaling cues that regulate fetal gene expression. Likewise, my findings show that PKA and PKD1 signals converge on HSP20 phosphorylation to modulate its activity. This may imply a role of HSP20 as a 'regulatory hotspot' in the control of cardiac hypertrophy. Clearly, the balance between PKA and PKD1 activation prescribes the consequence of hypertrophic response. However, how HSP20 discriminates between PKA and PKD1 in different settings remains unclear. There are several questions to address: (1) what factors determine which kinase phosphorylates HSP20? (2) are PKA- and PKD1-mediated HSP20 phosphorylations independently regulated or are these phosphorylation events controlled in an interdependent fashion? (3) does it involve a negative feedback system that regulates the equilibrium between these kinases and if balance shifts upon specific receptor stimulation? (4) do HSP20 exist in different "pools" that are differentially regulated by separate kinase types?

PKA is a well-known downstream effector of cardiac β-AR signalling where an increase PKA activity promotes phosphorylation of various substrates such as myofibrillar proteins and phospholamban which are involved in the excitation-contraction coupling (Dzimiri, 1999; Johnson *et al*., 2001). However, β-AR does not activate PKD1 *in vitro* or *in vivo* (Harrison *et al*., 2006). Although β-AR signaling fails to activate PKD1, it should be noted that PKA, a major downstream effector of β-ARs, has been reported to regulate PKD1 signaling. Of particular interest, are contradictory reports concerning the effect of PKA on

the function of PKD1. The controversy has arisen around the duration of stress stimuli and mechanisms involved. For example, recent studies have demonstrated that acute β-adrenergic stimulation and activation of PKA inhibits PKD1 phosphorylation and downstream HDAC5 activation, thereby repressing transcriptional activity (Haworth *et al*., 2007; Sucharov *et al*., 2011). In contrast, an opposing effect of PKA on PKD1 was reported by Carnegie *et al*. (2004). This research group revealed the existence of a multi-protein complex containing PKD1, PKCη, PKA and the PKA anchoring protein, AKAP-Lbc in adult rat heart. In this study, PKA-mediated phosphorylation of AKAP-Lbc in response to hypertrophic stimuli was shown to result in the release of PKC activated PKD1 from the complex, and this action initiated the nuclear export of HDAC5 and the consequent reexpression of hypertrophic genes. So, *β*-AR signalling seemed to alter PKD1 signaling by controlling its subcellular distribution rather than through direct effects on its catalytic activity. How do these various pathways communicate with one another to execute their biological functions? It is evident that AKAP-Lbc serves as a connector to mediate crosstalk between different pathways by providing a platform for the assembly of signalling complexes (Carnegie *et al*., 2004, 2008). Clearly, signal responsiveness is underpinned by AKAP-Lbc through the presence of both upstream activators and downstream effectors. Nevertheless, additional studies are required to elucidate the interconnectivity between this signalling complex and other intracellular signaling pathways to gain a greater understanding of the coordinated regulation of AKAP-Lbc in cardiac hypertrophy.

Growing evidence pinpoints crosstalk among adrenoceptor (AR) subtypes, in particular *β*-AR and *α*-AR that regulate contractility, as a fundamental mechanism in regulating cardiovascular function via second messengers and protein kinases as intermediate mediators (Dzimiri, 2002). In addition to cooperativity, it should also be noted that inhibitory interaction between distinct signalling pathways can occur at the post-receptor level to counter potentially detrimental effects resulting from malfunctional signal transduction. For instance, it was found that signals from *α*-AR can directly inhibit *β*-AR-mediated cAMP accumulation in neonatal rat cardiomyocytes, thereby regulating downstream signalling components of the *β*-AR pathway (Barrett *et al*., 1993). The upregulation of α-AR was associated with downregulation of *β*-AR and increased Gi protein levels (Dzimiri, 1999). It was proposed that the convergence of these two receptor pathways was a consequence of their cross regulation via G_s or G_i coupling and that any malfunction or change in transduction of these signalling routes may contribute to the

manifestations of cardiac disease (Barrett *et al*., 1993; Lemier *et al*., 1998). Moreover, negative feedback system may involve in the regulation of the equilibrium between two signalling mechanisms such as the reciprocal regulation of vascular tone by endothelin-1 (ET-1) and nitric oxide (NO) (Rossi *et al*., 2001). A downregulated NO was shown to be associated with enhanced synthesis of ET-1 and vice versa, suggesting a key role of ET-1 and NO interplay in the regulation of vasodilation and vasoconstriction.

Alternatively, crosstalk-type cardiovascular signalling can also be excuted by two types of cellular responses, i.e. short- and long-term receptor activations. It is thought that continuous receptor stimulation will trigger a time-dependent switch to alter receptor signalling pathway. For instance, short-term actions normally involve the activation of Ca^{2+} to stimulate contractile components and increase cardiac performance. However, long-term effects are implicated in the regulation of gene transcriptional activity, which is often seen as an adaptive mechanism of hypertrophy (Calil *et al*., 2007). In fact, long term hypertrophic stimulation could lead to maladaptive of PDE activity and loss of cAMP compartmentation, causing unrestricted diffusion of cAMP and chronic activation of PKA, thereby leading to desensitization of βAR/cAMP/PKA pathway (Frey and Olson, 2003). In this regard, it is likely that PKD1-mediated phosphorylation assumes greater functional significance in settings where the cAMP-dependent PKA pathway is downregulated. This notion is in agreement with the data of Xiang *et al*., (2005) who concluded that sustained stimulation of β1-AR switches the receptor signaling from a PKA activation pathway to calcium/calmodulin-dependent pathway. Indeed, neurohormonal stimulation of PKD1 activity has been shown to be enhanced under conditions where PKA activity is downregulated, which is a hallmark of heart failure (Lohse *et al*., 2003; Haworth *et al*., 2007). Whether these regulations involve a feedback loop or equilibrium of steady state in which the balance shifts upon specific receptor stimulation is an unanswered question.

6.5 Conclusions

The findings presented in my thesis suggest that HSP20 plays a dual but antagonistic role in the regulation of the hypertrophic response and this depends on (1) the type of kinase-mediating the phosphorylation, (2) the localisation of PKA, PKD1 and HSP20 within the cell and (3) the time or duration of the stress stimuli. Excitingly, my findings have led to the novel idea that hypertrophy signalling does not result from the sequential activation of

a linear signalling pathway of proteins, but may rather involves crosstalk between complex interactions of multiple signalling networks. The hypertrophic response generated by PKA and PKD1 mediated signals in this study are likely to involve the synchronisation and integration of multiple hypertrophic pathways in the heart. Collectively, these studies highlighted the multifactorial nature of hypertrophic signaling pathways in cardiomyocytes, indicating that different regulatory pathways are required to work in concert to underpin functional responsiveness. Clearly, crosstalk between anti-hypertrophic and pro-hypertrophic signalling routes is an important conduit of the regulation of cardiac size, protein turnover and gene expression patterns. It is anticipated that such crosstalk will provide vital insight into the role of HSP20 in heart and may provide a basis for the development of drug targets for cardiac hypertrophy.

6.6 Future directions

The cumulative evidence provided in this study offers possible new routes for the therapeutic manipulation of cardiac hypertrophy. More is required to validate the experimental results described in this thesis and to clarify the mechanistic details underpinning the crosstalk between different signal transduction pathways which contribute to the induction of the hypertrophic response. Special emphasis should be placed on gaining more understanding of the upstream regulators and downstream functional consequences of PKD1 activation, including identification of other possible mechanisms involving HSP20's mode of action. Novel insights may also be gleaned from further exploration of the signalling network involving of AKAP-Lbc and its scaffold partners. Future work may include the use of inducible overexpression and cardiac-specific knockout or transgenic animal models of cardiac hypertrophy to further characterise the specific molecular pathways that mediate the anti-hypertrophic effects. It is anticipated that these findings will provide deeper insight into molecular and cellular mechanisms at the tissue and organ levels.

6.7 Limitations of this work

My work has identified new aspects of the roles of HSP20 in cardiac hypertrophy with further insight into how this protein may function when regulated by different upstream kinases. In the present study, the power of analysing protein-protein interactions was exemplified through array-based methods. It has allowed the identification and definition of binding sites between PDE4D5-HSP20 and PKD1-HSP20, thereby provide molecular information to generate two structurally distinct disruptor peptides, i.e. 'bs906' and 'HJL09' (based on PDE4D5 and PKD1 sequences, respectively) that selectively disrupt their interactions with HSP20. Nevertheless, the precise mechanism of action appears to be far more complicated than previously thought. Small molecules targeted to disrupt individual protein-protein interaction could provide a highly specific therapeutic means for the treatment of cardiac hypertrophy. It is anticipated that such approach is less likely to have potential side effects as seen in drugs nowadays. However, it should be taken into consideration that disruptor peptides that are proven to be effective *in vitro* may not be equally effective *in vivo* due to issues associated with toxicity towards the organism albeit efficient peptide delivery and tissue targeting. It is possible that the results presented here using an *in vitro* system may not be a true reflection of the phenotype seen in intact organisms. As is the case for most primary isolations, primary cells are more prone to batch-to-batch variability in quality which may provide substantial challenges for the reproducibility of some experimental results. For example, the inconsistent degree of hypertrophy induction (ISO-treated cells) as showed here in Fig 3.16 and Fig. 5.8.

Another limitation to the work presented here is the lack of data bridging the gap between the molecular mechanisms of cAMP-specific PDE4D5, cAMP-dependent PKA and PKD1, particularly the functional outcomes of these interacting proteins in regulating the roles of HSP20 in cardioprotection. A great deal of research into this study still needs to be carried out. For instance, in this study, the effects of PKD1, its potent inhibitors and PKD-disruptor peptide on the levels of phospho-Ser16 of HSP20 were shown (Fig. 5.14-Fig. 5.16) but not the direct functional consequences on hypertrophy phenotype, including any changes in HSP20-mediated nuclear import of PKD1 which may contribute to the induction of fetal gene program. In addition to the short-term future work discussed in Chapters 3, 4 and 5, it would also be interesting to further investigate if (1) PKA- and PKD1- mediated HSP20 phosphorylation and (2) phosphorylations or activation of PKA and PKD1 can be modulated by disrupting PKD1-HSP20 and PDE4D5-HSP20 interactions selectively or a combinatorial effect of both.

Ahuja, P., Sdek, P., MacLellan, W.R. (2007) Cardiac myocyte cell cycle control in development, disease, and regeneration. *Physiol Rev*. **87**: 521-544.

Amin, J., Ananthan, J., Voellmy, R. (1988) Key features of heat shock regulatory elements. *Mol Cell Biol*. **8**: 3761-3769.

Atienza, J.M., Yu, N., Kirstein, S.L., Xi, B., Wang, X., Xu ,X., Abassi, Y.A. (2006) Dynamic and label-free cell-based assays using the real-time cell electronic sensing system. *Assay Drug Dev Technol*. **4**: 597-607.

Avkiran, M., Rowland, A.J., Cuello, F., Haworth, R.S. (2008) Protein kinase D in the cardiovascular system: emerging roles in health and disease. *Circ Res*. **102**: 157-163.

Backs, J., Worst, B.C., Lehmann, L.H., Patrick, D.M., Jebessa, Z., Kreusser, M.M., Sun, Q., Chen, L., Heft, C., Katus, H.A., Olson, E.N. (2011) Selective repression of MEF2 activity by PKA-dependent proteolysis of HDAC4. *J Cell Biol*. **195**: 403-415.

Bagneris, C., Bateman, O.A., Naylor, C.E., Cronin, N., Boelens, W.C., Keep, N.H., Slingsby, C. (2009) Crystal structures of alpha-crystallin domain dimers of alphaB-crystallin and Hsp20. *J Mol Biol*. **392**: 1242-1252.

Baillie, G. S., Sood, A., McPhee, I., Gall, I., Perry, S. J., Lefkowitz, R. J., Houslay, M. D. (2003) *β*-arrestin-mediated PDE4 cAMP phosphodiesterase recruitment regulates beta-adrenoceptor switching from Gs to Gi. *Proc Natl Acad Sci. USA* **100**: 940-945.

Baillie, G.S., Adams, D.R., Bhari, N., Houslay, T.M., Vadrevu, S., Meng, D., Li, X., Dunlop, A., Milligan, G., Bolger, G.B., Klussmann, E., Houslay, M.D. (2007) Mapping binding sites for the PDE4D5 cAMP-specific phosphodiesterase to the N- and C-domains of β-arrestin using spot-immobilized peptide arrays. *Biochem J*. **404**: 71-80.

Baillie, G.S. (2009) Compartmentalized signalling: spatial regulation of cAMP by the action of compartmentalized phosphodiesterases. *FEBS J*. **276**: 1790-1799.

Barrett, S., Honbo, N., Karliner, J.S. (1993) α_1-Adrenoceptor mediated inhibition of cellular cAMP accumulation in neonatal rat ventricular myocytes. *Naunyn Schmiedebergs Arch Pharmacol*. **347**: 384-393.

Beall, A.C., Kato, K., Goldenring, J.R., Rasmussen, H., Brophy, C.M. (1997) Cyclic nucleotide-dependent vasorelaxation is associated with the phosphorylation of a small heat shock-related protein. *J Biol Chem*. **272**: 11283-11287.

Beall, A., Bagwell, D., Woodrum, D., Stoming, T.A., Kato, K., Suzuki, A., Rasmussen, H., Brophy, C.M. (1999) The small heat shock-related protein, HSP20, is phosphorylated on serine 16 during cyclic nucleotide-dependent relaxation. *J Biol Chem.* **274**: 11344-11351

Beavo, J.A. and Brunton, L.L (2002) Cyclic nucleotide research - still expanding after half a century. *Nat Rev Mol Cell Biol.* **3**: 710-718.

Becker, J. and Craig, E.A. (1994) Heat-shock proteins as molecular chaperones. *Eur J Biochem*. **219**: 11-23.

Bellucci, A., Navarria, L., Falarti, E., Zaltieri, M., Bono, F., Collo, G., Grazia, M., Missale, C., Spano, P. (2011) Redistribution of DAT/a-Synuclein Complexes Visualized by ‘‘In Situ’’ Proximity Ligation Assay in Transgenic Mice Modelling Early Parkinson’s Disease. *PLoS One*. **6**: e27959.

Benjamin, I.J. and McMillan, D.R. (1998) Stress (heat shock) proteins: molecular chaperones in cardiovascular biology and disease. *Circ Res.* **83**: 117-132.

Bishopric, N.H., Andreka, P., Slepak, T., Webster, K.A. (2001) Molecular mechanisms of apoptosis in the cardiac myocyte. *Curr Opin Pharmacol*. **1**: 141-50.

Bogoyevitch, M. A., Clerk, A., Sugden, P. H. (1995) Activation of the mitogen activated protein kinase cascade by pertussis toxin-sensitive and -insensitive pathways in cultured ventricular cardiomyocytes. *Biochem J.* **309**: 437-443.

Bolger, G.B., Baillie, G.S., Li, X., Lynch, M.J., Herzyk, P., Mohamed, A., Mitchell, L.H., McCahill, A., Hundsrucker, C., Klussmann, E., Adams, D.R., Houslay, M.D. (2006) Scanning peptide array analyses identify overlapping binding sites for the signalling scaffold proteins, beta-arrestin and RACK1, in cAMP-specific phosphodiesterase PDE4D5. *Biochem J*. **398**: 23-36.

Boyle, A. J., Kelly, D.J., Zhang, Y., Cox, A.J., Gow, R.M., Way, K., Itescu, S., Krum, H., Gilbert, R.E. (2005) Inhibition of protein kinase C reduces left ventricular fibrosis and dysfunction following myocardial infarction. *J Mol Cell Cardiol.* **39**: 213-221.

Bradford, M.M. (1976) A rapid and sensitive method for the quantitation of microgram quantities of protein utilizing the principle of protein-dye binding. *Ana. Biochem*. **72**: 248-254.

Brophy, C.M., Lamb, S., Graham, A. (1999) The small heat shock-related protein-20 is an actin-associated protein. *J Vasc Surg*. **29**: 326-333.

Bukach, O.V., Seit-Nebi, A.S., Marston, S.B., Gusev, N.B. (2004) Some properties of human small heat shock protein Hsp20 (HspB6). *Eur J Biochem*. **271**: 291-302.

Bukach, O.V., Glukhova, A.E., Seit-Nebi, A.S., Gusev, N.B (2009) Heterooligomeric complexes formed by human small heat shock protein HspB1 (Hsp27) and HspB6 (Hsp20). *Biochim Biophys Acta.* **1794**: 486-495.

Calil, l., Tineli, R.A., Vicente, W.V., Rodrigues, A.J., Evora, P.R. (2007) The concept of crosstalk and its implications for cardiovascular function and disease. *Arg Bras Cardiol.* **88**: e26-31.

Carnegie, G.K., Smith, F.D., McConnachie, G., Langeberg, L.K., Scott, J.D. (2004) AKAP-Lbc nucleates a protein kinase D activation scaffold. *Mol Cell*. **15**: 889-899.

Carnegie, G.K., Soughayer, J., Smith, F.D., Pedroja, B.S., Zhang, F., Diviani, D., Bristow, M.R., Kunkel, M.T., Newton, A.C., Langeberg, L.K., Scott, J.D. (2008) AKAP-Lbc mobilizes a cardiac hypertrophy signaling pathway. *Mol Cell*. **32**: 169-179.

Caspers, G-J., Leunissen, J.A.M., de Jong, W.W. (1995) The expanding small heat-shock protein family, and structure predictions of the conserved "α-crystallin domain". *J. Mol. Evol.* **40**: 238-248.

Chan, S.M., Ermann, J., Su, L., Fathman, C.G., Utz, P.J. (2004) Protein microarrays for multiplex analysis of signal transduction pathways. *Nat Med*. **10**: 1390–1396.

Chang, S., Bezprozvannaya, S., Li, S., Olson, E.N. (2005) An expression screen reveals modulators of class II histone deacetylase phosphorylation. *Proc Natl Acad Sci USA* **102**: 8120-8125.

Chen, L., Hahn, H., Wu, G.Y., Chen, C.H., Liron, T., Schechtman, D., Cavallaro, G., Banci, L., Guo, Y.R., Bolli, R., Dorn II, G.W., Mochly-Rosen, D. (2001) Opposing cardioprotective actions and parallel hypertrophic effects of δPKC and εPKC. *Proc Natl Acad Sci. USA* **98**: 11114–11119.

Chiang, H.L., Terlecky, S.R., Plant, C.P., Dice, J.F. (1989) A role for a 70-kilodalton heat shock protein in lysosomal degradation of intracellular proteins. *Science*. **246**: 382–385.

Chien, K.R., Knowlton, K.U., Zhu, H., Chien, S. (1991) Regulation of cardiac gene expression during myocardial growth and hypertrophy: Molecular studies of an adaptive physiologic response. *FASEB J.* **5**: 3037–3046.

Chlopeikova, S., Psotova, J., Miketova, P. (2001) Neonatal rat cardiomyocytes – a model for the study of morphological, biochemical and electrophysiological characteristics of the heart. *Biomed. Papers* **145**: 49-55.

Chomczynski, P. and Sacchi, N. (1987) Single step method of RNA isolation by acid guanidinium thiocyanate-phenol-chloroform extraction. *Anal Biochem*. **162**: 156-159.

Chu, G., Egnaczyk, G.F., Zhao, W., Jo, S.H., Fan, G.C., Maggio, J.E., Xiao, R.P., Kranias, E.G. (2004) Phosphoproteome analysis of cardiomyocytes subjected to *β*-adrenergic stimulation: Identification and characterization of a cardiac heat shock protein p20. *Circ Res*. **94**: 184-193.

Conti, M. and Beavo, J. (2007). Biochemistry and physiology of cyclic nucleotide phosphodiesterases: essential components in cyclic nucleotide signaling. *Annu Rev Biochem*. **76:** 481-511.

Cooper, D.M. (2003) Regulation and organization of adenylyl cyclases and cAMP. *Biochem J*. **375**: 517–529.

Cuello, F., Bardswell, S.C., Haworth, R.S., Yin, X., Lutz, S., Wieland, T., Mayr, M., Kentish, J.C., Avkiran, M. (2007) Protein kinase D selectively targets cardiac troponin I and regulates myofilament Ca^{2+} sensitivity in ventricular myocytes. *Circ Res*. **100**: 864-873.

Cunningham, C., and J. A. Wells. (1989) High-resolution epitope mapping of hGH-receptor interactions by alanine-scanning mutagenesis. *Science* **244:** 1081-1085.

de Bold, A. J. (1985) Atrial natriuretic factor: a hormone produced by the heart. *Science* **230**: 767-770.

de Jong, W.W., Leunissen, J.A., Voorter, C.E. (1993) Evolution of the alpha-crystallin/small heat-shock protein family. *Mol Biol Evol*. **10**: 103-126.

de Rooij, J., Zwartkruis, F.J., Verheijen, M.H., Cool, R.H., Nijman, S.M., Wittinghofer, A., Bos, J.L. (1998) Epac is a Rap1 guanine-nucleotide-exchange factor directly activated by cyclic AMP. *Nature* **396**: 474-477.

Dodge, K.L., Khouangsathiene, S., Kapiloff, M.S., Mouton, R., Hill, E.V., Houslay, M.D., Langeberg, L.K., Scott, J.D. (2001) mAKAP assembles a protein kinase A/PDE4 phosphodiesterase cAMP signaling module. *EMBO J*. **20**: 1921-1930.

Dodge-Kafka, K.L., Langeberg, L., Scott, J.D. (2006) Compartmentation of cyclic nucleotide signaling in the heart: The role of A-kinase anchoring proteins. *Circ Res*. **98**: 993-1001.

Döppler, H., Storz, P., Li, J., Comb, M.J., Toker, A. (2005) A phosphorylation state-specific antibody recognizes Hsp27, a novel substrate of protein kinase D. *J Biol Chem*. **280**: 15013-15019.

Dreiza, C.M., Brophy, C.M., Komalavilas, P., Furnish, E.J., Joshi, L., Pallero, M.A., Murphy-Ullrich, J.E., von Rechenberg, M., Ho, Y.S., Richardson, B., Xu, N., Zhen, Y., Peltier, J.M., Panitch, A. (2005) Transducible heat shock protein 20 (Hsp20) phosphopeptide alters cytoskeletal dynamics. *FASEB J* **19**: 261-263.

Dzimiri,N. (1999) Regulation of β-adrenoceptor signaling in cardiac function and disease. *Pharmacol Rev*. **51**: 465-502.

Dzimiri, N. (2002) Receptor crosstalk. Implications for cardiovascular function, disease and therapy. *Eur J Biochem*. **269**: 4713-4730.

Edelman, A.M., Blumenthal, D.K., Krebs. E.G. (1987) Protein serine/threonine kinase. *Annu Rev Biochem.* **56**: 567-613.

Eefting, F., Rensing, B., Wigman, J., Pannekoek, W.J., Liu, W.M., Cramer, M.J., Lips, D.J., Doevendans, P.A. (2004) Role of apoptosis in reperfusion injury. *Cardiovasc Res*. **61**: 414-426.

Fan, G.C., Chu, G., Mitton, B., Song, Q., Yuan, Q., Kranias, E.G. (2004) Small heat-shock protein HSP20 phosphorylation inhibits beta-agonist-induced cardiac apoptosis. *Circ Res.* **94**: 1474-1482.

Fan, G.C., Chu, G., Kranias E.G. (2005) Hsp20 and its cardioprotection. *Trends Cardiovasc Med.* **15** : 138-141.

Fan, G.C., Ren, X., Qian, J., Yuan, Q., Nicolaou, P., Wang, Y., Jones, W.K., Chu, G., Kranias, E.G. (2005) Novel cardioprotective role of a small heat-shock protein, HSP20, against ischemia/reperfusion injury. *Circulation.* **111**: 1792-1799.

Fan, G.C., Yuan, Q., Song, G., Wang, Y., Chen, G., Qian, J., Zhou, X., Lee, Y.J., Ashraf, M., Kranias, E.G. (2006) Small heat-shock protein HSP20 attenuates beta-agonist-mediated cardiac remodeling through apoptosis signal-regulating kinase 1. *Circ Res*. **99**: 1233-1242.

Fan, G.C., Zhou , X., Wang, X., Song, G., Qian, J., Nicolaou, P., Chen, G., Ren, X., Kranias, E.G. (2008) Heat shock protein 20 interacting with phosphorylated Akt reduces doxorubicin-triggered oxidative stress and cardiotoxicity. *Circ Res*. **103**: 1270-1279.

Fan, G.C. and Kranias, E.G. (2011) Small heat shock protein 20 (HspB6) in cardiac hypertrophy and failure. *J Mol Cell Cardiol*. **51**: 574-577.

Feder, M.E. and Hofmann, G.E. (1999) Heat-shock proteins, molecular chaperones, and the stress response: Evolutionary and ecological physiology. *Annu Rev Physiol.* **61**: 243-282.

Fields, S. and Song, O. (1989) A novel genetic system to detect protein–protein interactions. *Nature* **340**: 245-246.

Fields, G.B. and Noble, R.L. (1990) Solid phase peptide synthesis utilizing 9-fluorenylmethoxycarbonyl amino acids. *Int J Pept Protein Res*. **35**: 161-214.

Fielitz, J., Kim, M.S., Shelton, J.M., Qi, X., Hill, J.A., Richardson, J.A., Bassel-Duby, R., Olson, E.N. (2008) Requirement of protein kinase D1 for pathological cardiac remodeling. *Proc Natl Acad Sci. USA* **105**: 3059-3063.

Fink, K., and Zeuther, E. (1978) Heat shock proteins in Tetrahymena. ICN-UCLA Symposium. *Mol Cell Biol*. **12**: 103-115.

Fishelson, Z., Hochman, I., Greene, L.E., Eisenberg, E. (2001) Contribution of heat shock proteins to cell protection from complement lysis. *Int Immunol.* **13**: 983-991.

Francis, S.H., Blount, M.A., Corbin, J.D. (2011) Mammalian cyclic nucleotide phosphodiesterases: molecular mechanisms and physiological functions. *Physiol Rev* **91**: 651-690.

Frank, R. (2002) The SPOT-synthesis technique. Synthetic peptide arrays on membrane supports–principles and applications. *J Immunol. Methods* **267**: 13-26.

Frey, N. and Olson E.J. (2003) Cardiac hypertrophy: the good, the bad, and the ugly. *Annu Rev Physiol*. **65**: 45-79.

Gething, M.J. and Sambrook, J. (1992) Protein folding in the cell. *Nature* **355**: 33-45.

Ghayour-Mobarhan, M., Rahsepar, A. A., Tavallaie, S., Rahsepar, S., Ferns, G. A. (2009) The potential role of heat shock proteins in cardiovascular disease: evidence from in vitro and in vivo studies. *Adv Clin Chem.* **48**: 27-72.

Gschwendt, M., Dieterich, S., Rennecke, J., Kittstein, W., Mueller, H., Johannes, F. (1996) Inhibition of protein kinase Cμ by various inhibitors. Differentiation from protein kinase C isoenzymes. *FEBS Lett*. **392**: 77-80.

Gusev, N.B., Bogatcheva, N.V., Marston, S.B. (2002) Structure and properties of small heat shock proteins (sHsp) and their interaction with cytoskeleton proteins. *Biochemistry. (Moscow)* **67**: 511-519.

Harrison, B.C., Kim, M.S., van Rooij, E., Plato CF, Papst, P.J., Vega, R.B., McAnally, J.A., Richardson, J.A., Bassel-Duby, R., Olson, E.N., McKinsey, T.A. (2006) Regulation of cardiac stress signaling by protein kinaseD1. *Mol Cell Biol*. **26**: 3875-3888.

Hartl, F. (1996) Molecular chaperones in cellular protein folding. *Nature* **381**: 571–579.

Haworth, R.S., Goss, M.W., Rozengurt, E., Avkiran, M. (2000) Expression and activity of protein kinase D/protein kinase Cμ in myocardium: evidence for α_1-adrenergic receptor- and protein kinase C-mediated regulation. *J Mol Cell Cardiol*. **32:** 1013-1023.

Haworth, R.S., Cuello, F., Herron, T.J., Franzen, G., Kentish, J.C., Gautel, M., Avkiran, M. (2004) Protein Kinase D Is a Novel Mediator of Cardiac Troponin I Phosphorylation and Regulates Myofilament Function. *Circ Res.* **95**: 1091-1099.

Haworth, R.S., Robers, N.A., Cuello, F., Avkiran, M. (2007) Regulation of protein kinase D activity in adult myocardium: novel counter-regulatory roles for protein kinase Cε and protein kinase A. *J Mol Cell Cardiol*. **43:** 686-695.

Haworth, R.S., Cuello, F., Avkiran, M. (2011) Regulation by phosphodiesterase isoforms of protein kinase A-mediated attenuation of myocardial protein kinase D activation. *Basic Res Cardiol*. **106**: 51-63.

Hendrick, J.P. and Hartl, F.U. (1993) Molecular chaperone functions of heat-shock proteins. *Annu Rev Biochem.* **62**: 349-384.

Hightower LE. (1991) Heat shock, stress proteins, chaperones, and proteotoxicity. *Cell* **66**: 191-197.

Hirotani, S., Otsu, K., Nishida, K., Higuchi, Y., Morita, T., Nakayama, H., Yamaguchi, O., Mano, T., Matsumura, Y., Ueno, H., Tada, M., Hori, M. (2002) Involvement of nuclear factor-kappaB and apoptosis signal-regulating kinase 1 in G-protein-coupled receptor agonist-induced cardiomyocyte hypertrophy. *Circulation*. **105**: 509-515.

Horio, T., Nishikimi, T., Yoshihara, F., Matsuo, H., Takishita, S., Kangawa, K. (2000) Inhibitory regulation of hypertrophy by endogenous atrial natriuretic peptide in cultured cardiac myocytes. *Hypertension* **35**: 19-24.

Houslay, M.D. and Adams, D.R. (2003) PDE4 cAMP phosphodiesterases: modular enzymes that orchestrate signalling cross-talk, desensitization and compartmentalization. *Biochem J.* **370:** 1-18.

Houslay, M.D., Baillie, G.S., Maurice, D.H. (2007) cAMP-specific phosphodiesterase-4 enzymes in the cardiovascular system: a molecular toolbox for generating compartmentalized cAMP signaling. *Circ Res.* **100**: 950-966.

Houslay, M.D. (2010) Underpinning compartmentalised cAMP signalling through targeted cAMP breakdown. *Trends Biochem Sci.* **35:** 91-100.

Huang, H., Regan, K.M., Lou, Z., Chen, J., Tindall, D.J. (2006) CDK2-dependent phosphorylation of FOXO1 as an apoptotic response to DNA damage. *Science* **314**: 294-297.

Hummel, G., Reineke, U., Reimer, U. (2006) Exploiting chemical diversity for drug discovery. *Mol BioSyst*. **2**: 499-508.

Humphrey, W., Dalke, A., Schulten, K., (1996) VMD - Visual Molecular Dynamics. *J Molec. Graphics* **14**: 33-38.

Hunter, T. and Karin, M. (1992) The regulation of transcription by phosphorylation. *Cell* **70:** 375-387.

Huynh, Q.K., McKinsey, T.A. (2006) Protein kinase D directly phosphorylates histone deacetylase 5 via a random sequential kinetic mechanism. *Arch Biochem Biophys*. **450**: 141-148.

Iglesias, T., Waldron, R.T., Rozengurt, E. (1998) Identification of in vivo phosphorylation sites required for protein kinase D activation. *J Biol Chem*. **273:** 27662-27667.

Iwata, M., Maturana, A., Hoshijima, M., Tatematsu, K., Okajima, T., Vandenheede, J.R., Van Lint, J., Tanizawa, K., Kuroda, S. (2005) PKCepsilon-PKD1 signaling complex at Z-discs plays a pivotal role in the cardiac hypertrophy induced by G-protein coupling receptor agonists. *Biochem Biophys Res Commun.* **327**: 1105-1113.

Izumo, S., Nadal-Ginard, B., Mahdavi, V. (1988) Proto-oncogene induction and reprogramming of cardiac gene expression produced by pressure overload. *Proc Natl Acad Sci. USA* **85**: 339-343.

Jiang, J., Prasad, K., Lafer, E.M., Sousa, R. (2005) Structural basis of interdomain communication in the Hsc70 chaperone. *Mol Cell.* **20**: 513-524.

Johannes, F.J., Prestle, J., Eis, S., Oberhagemann, P., Pfizenmanier, K. (1994) PKCμ is a novel, atypical member of the protein kinase C family. *J Biol Chem.* **269**: 6140-6148.

Johnson, D. A., Akamine, P., Radzio-Andzelm, E., Madhusudan, M., Taylor, S. S. (2001) Dynamics of cAMP-dependent protein kinase. *Chem. Rev.* **101**: 2243-2270.

Johnston, L.A., Erdogan, S., Cheung, Y.F., Sullivan, M., Barber, R., Lynch, M.J., Baillie, G.S., Van Heeke, G., Adams, D.R., Huston, E., Houslay, M.D. (2004) Expression, intracellular distribution and basis for lack of catalytic activity of the PDE4A7 isoform encoded by the human PDE4A cAMP-specific phosphodiesterase gene. *Biochem J.* **380:** 371-84.

Kappe, G., Franck, E., Verschuure, P., Boelens, W.C., Leunissen, J.A., de Jong W.W. (2003) The human genome encodes 10 alpha-crystallin-related small heat shock proteins: HspB1-10. *Cell Stress Chaperones* **8**: 53-61.

Kato, K., Goto, S., Inaguma, Y., Hasegawa, K., Morishita, R., Asano, T. (1994) Purification and characterization of a 20 kDa protein that is highly homologous to α-B-crystallin. *J Biol Chem.* **269**: 15302-15309.

Kelley, L.A. and Sternberg, M.J.E. (2009) A case study using the Phyre server. *Nature Protocols* **4**: 363-371.

Knudsen, C.R., Jadidi, M., Friis, I., Mansilla, F. (2002) Application of the yeast two-hybrid system in molecular gerontology. *Biogerontology* **3**: 243-256.

Komalavilas, P., Penn, R.B., Flynn, C.R., Thresher, J., Lopes, L.B., Furnish, E.J., Guo, M., Pallero, M.A., Murphy-Ullrich, J.E., Brophy, C.M. (2008) The small heat shock-related protein, HSP20, is a cAMP-dependent protein kinase substrate that is involved in airway smooth muscle relaxation. *Am J Physiol Lung Cell Mol Physiol*. **294**: L69-78.

Kozawa, O., Matsuno, H., Niwa, M., Hatakeyama, D., Oiso, Y., Kato, K., Uematsu, T. (2002) Hsp20, low-molecular-weight heat shock related protein, acts extracellularly as a regulator of platelet functions: a novel defense mechanism. *Life Sci.* **72**: 113-124.

Kubista, M., Andrade, J.M., Bengtsson, M., Forootan, A., Jonak, J., Lind, K., Sindelka, R., Sjoback, R., Sjogreen, B., Strombom, L., Stahlberg, A., Zoric, N. (2006) The real-time polymerase chain reaction. *Mol Aspects Med*. **27**: 95-125.

Kuo, M. H. and Allis, C.D. (1998) Roles of histone acetyltransferases and deacetylases in gene regulation. *Bioessays* **20:** 615-626.

Kramer, A. and Schneider-Mergener, J. (1998) Synthesis and screening of peptide libraries on continuous cellulose membrane supports. *Methods Mol Biol.* **87**: 25-39.

Labarca, C. and Paigen, K. (1980) A simple, rapid, and sensitive DNA assay procedure. *Anal Biochem.* **102**: 344-352.

Latronico, M.V., Catalucci, D., Condorelli, G. (2007) Emerging role of microRNAs in cardiovascular biology. *Circ Res.* **101**: 1225-1236.

Layland, J., Solaro, R.J., Shah, A.M. (2005) Regulation of cardiac contractile function by troponin I phosphorylation. *Cardiovasc Res*. **66**: 12-21.

Lee, S., Carson, K., Rice-Ficht, A., Good, T. (2005) Hsp20, a novel α-crystallin, prevents Aβ fibril formation and toxicity. *Protein Sci.* **14**: 527-533.

Lee, S., Carson, K., Rice-Ficht, A., Good, T. (2006) Small heat shock proteins differentially affect Aβ aggregation and toxicity. *Biochem Biophys Res Commun.* **347**: 527-533.

Lefkowitz, R. J., Pierce, K. L., Luttrell, L. M. (2002) Dancing with different partners: protein kinase A phosphorylation of seven membrane-spanning receptors regulates their G protein-coupling specificity. *Mol Pharmacol.* **62**: 971-974.

Lehnart, S.E., Wehrens, X.H.T., Reiken, S., Warrier, S., Belevych, A.E., Harvey, R.D., Richter, W., Jin, S.L.C. (2005) Phosphodiesterase 4D deficiency in the ryanodine-receptor complex promotes heart failure and arrhythmias. *Cell* **123**: 25-35.

Lemire, I., Allen, B.G., Rindt, H., Hebert, T.E. (1998) Cardiacspecific overexpression of α1B-AR regulates β-AR activity via molecular crosstalk. *J Mol Cell Cardiol*. **30**: 1827-1839.

Leuchowius, K.J., Jarvius, M., Wickström, M., Rickardson, L., Landegren, U., Larsson, R., Söderberg, O., Fryknäs, M., Jarvius, J. (2010) High content screening for inhibitors of protein interactions and post-translational modifications in primary cells by proximity ligation. *Mol Cell Proteomics*. **9**: 178-183.

Lindquist, S. 1986. The heat-shock response. *Annu Rev Biochem.* **55**: 1151-1191.

Lint, J., Rykx, An., Maeda, Y., Vantus, T., Sturany, S., Malhotra, V., Vandenheede, J., SeuVerlein, T. (2002) Protein kinase D: an intracellular traffic regulator on the move. *TRENDS Cell Biol.* **12**: 193-200.

Livak, K.J., and Schmittgen, T.D. (2001) Analysis of Relative Gene Expression Data Using Real-Time Quantitative PCR and the 2-[Delta][Delta]CT Method. *Methods* **25**: 402 - 408.

Lohse, M.J., Engelhardt, S., Eschenhagen, T. (2003) What is the role of β-adrenergic signaling in heart failure? *Circ Res*. **93**: 896-906.

Lugnier, C. (2006) Cyclic nucleotide phosphodiesterase (PDE) superfamily: a new target for the development of specific therapeutic agents. *Pharmacol Ther*. **109:** 366-398.

MacKenzie, S.J., Baillie, G.S., McPhee, I., Bolger, G.B., Houslay, M.D. (2000) ERK2 MAP kinase binding, phosphorylation and regulation of PDE4D cAMP specific phosphodiesterases: the involvement of C-terminal docking sites and N-terminal UCR regions. *J Biol Chem*. **275**: 16609-16617.

MacKenzie, S.J., Baillie, G.S., McPhee, I., MacKenzie, C., Seamons, R., McSorley, T., Millen, J., Beard, M.B., van Heeke, G., Houslay, M.D. (2002) Long PDE4 cAMP specific phosphodiesterases are activated by protein kinase A-mediated phosphorylation of a single serine residue in upstream conserved region 1 (UCR1). *Br J Pharmacol*. **136**: 421-433.

Manning, G., Whyte, D.B., Martinez, R., Hunter, T., Sydarsanam, S. (2002) The protein kinase complement of the human genome. *Science* **298:** 1912-1934.

Mason, J.M. (2010) Design and development of peptides and peptide mimetics as antagonists for therapeutic intervention. *Future Med Chem*. **2**: 1813-1822.

Matsuno, H., Ishisaki, A., Nakajima, K., Kato, K., Kozawa, O. (2003) A peptide isolated from alpha B-crystallin is a novel and potent inhibitor of platelet aggregation via dual prevention of PAR-1 and GPIb/V/IX. *J Thromb Haemost.* **1**: 2636-2642.

Matsushima-Nishiwaki, R., Adachi, S., Yoshioka, T., Yasuda, E., Yamagishi, Y., Matsuura, J., Muko, M., Iwamura, R., Noda, T., Toyoda, H., Kaneoka, Y., Okano, Y., Kumada, T., Kozawa, O. (2011) Suppression by heat shock protein 20 of hepatocellular carcinoma cell proliferation via inhibition of the mitogen-activated protein kinases and AKT pathways. *J Cell Biochem*. **112**: 3430-3439.

Matthews, S.A., Pettit, G.R., Rozengurt, E. (1997) Bryostatin 1 induces biphasic activation of protein kinase D in intact cells. *J Biol Chem*. **272**: 20425-20250.

Matthews, S.A., Rozengurt, E., Cantrell, D. (1999) Characterization of serine 916 as an in vivo autophosphorylation site for protein kinase D/Protein kinase Cμ. *J Biol Chem.* **274:** 26543-26549.

McKinsey, T.A., Zhang, C.L., Olson, E.N. (2001) Identification of a signal-responsive nuclear export sequence in class II histone deacetylases. *Mol Cell Biol*. **21:** 6312-6321.

McMillan, D.R., Xiao, X.Y., Graves, K., Benjamin, I.J. (1998) Targeted disruption of heat shock transcription factor 1 abolishes thermotolerance and protection against heat-inducible apoptosis. *J Biol Chem.* **273**: 7523-7528.

Meng, D., Lynch, M.J., Huston, E., Beyermann, M., Eichhorst, J., Adams, D.R., Klussmann, E., Houslay, M.D., Baillie, G.S. (2009) MEK1 binds directly to β-arrestin1, influencing both its phosphorylation by ERK and the timing of its isoprenaline-stimulated internalization. *J Biol Chem*. **284**: 11425-11435.

Michaud, G. A., Salcius, M., Zhou, F., Bangham, R., Bonin, J., Snyder, M., Predki, P.F., Schweitzer, B.I. (2003) Analyzing antibody specificity with whole proteome microarrays. *Nat Biotechnol.* **21**: 1509-1512.

Michaud, G.A., Samuels, M.L., Schweitzer, B. (2006) Functional protein arrays to facilitate drug discovery and development. *IDrugs* **9**: 266-272.

Millar, J.K., Pickard, B.S., Mackie, S., James, R., Christie, S., Buchanan, S.R., Malloy, M.P., Chubb, J.E., Huston, E., Baillie, G.S., Thomson, P.A., Hill, E.V., Brandon, N.J., Rain, J-C., Camargo, L.M., Whiting, P.J., Houslay, M.D., Blackwood, D.H.R., Muir, W.J., Porteous, D.J. (2005) DISC1 and PDE4B are interacting genetic factors in schizophrenia that regulate cAMP signaling. *Science* **310**: 1187-1191.

Mongillo, M., McSorley, T., Evellin, S., Sood, A., Lissandron, V., Terrin, A., Huston, E., Hannawacker, A., Lohse, M.J., Pozzan, T., Houslay, M.D., Zaccolo, M. (2004) Fluorescence Resonance Energy Transfer–Based Analysis of cAMP Dynamics in Live Neonatal Rat Cardiac Myocytes Reveals Distinct Functions of Compartmentalized Phosphodiesterases. *Circ Res*. **95**: 67-75.

Moore, E.D.W., Ring, M., Scriven, D.R.L., Smith, V.C., Meloche, R.M., Buchan, A.M.J. (1999) The role of protein kinase C isozymes in bombesin-stimulated gastric release from human antral gastrin cells. *J Biol Chem*. **274**: 22493-22501.

Morisco, C., Zebrowski, D.C., Vatner, D.E., Vatner, S.F., Sadoshima, J. (2001) β-adrenergic cardiac hypertrophy is mediated primarily by the β_1-subtype in the rat heart. *J Mol Cell Cardiol.* **33**: 561-573.

Morrison, K.L. and Weiss, G.A. (2001) Combinatorial alanine-scanning. *Curr Opin Chem Biol.* **5**: 302-307.

Nicolaou, P., Knöll, R., Haghighi, K., Fan, G.C., Dorn, G.W. 2nd., Hasenfub, G., Kranias, E.G. (2008) Human mutation in the anti-apoptotic heat shock protein 20 abrogates its cardioprotective effects. *J Biol Chem*. **283**: 33465-33471.

Nishikawa, K., Toker, A., Johannes, F-J., Songyang, Z., Cantley, L.C. (1997) Determination of the specific substrate sequence motifs of protein kinase C isozymes. *J Biol Chem*. **272:** 952-960.

Nishikimi, T., Maeda, N., Matsuoka, H. (2006) The role of natriuretic peptides in cardioprotection. *Cardiovasc Res*. **69**: 318-28.

Noda, T., Kumada, T., Takai, S., Matsushima-Nishiwaki, R., Yoshimi, N., Yasuda, E., Kato, K., Toyoda, H., Kaneoka, Y., Yamaguchi, A., Kozawa, O. (2007) Expression levels of heat shock protein 20 decrease in parallel with tumor progression in patients with hepatocellular carcinoma. *Oncol Rep.* **17**: 1309-1314.

Ohnishi, S.T. and Barr, J.K. (1978) A simplified method of quantitating proteins using the biuret and phenol reagents. *Anal. Biochem.* **86**: 193-200.

Patterson, A.J., Pearl, N., Chang, C. (2007) Impact of phosphodiesterase 4D on cardiac β2 adrenergic receptor signaling. *Sem Anesth Periop Med Pain.* **26**: 22-27.

Pfaffl, M.W., and Hageleit, M. (2001) Validities of mRNA qualification using recombinant RNA and recombinant DNA external calibration curves in real-time RT-PCR. *Biotechnology Letters* **23**: 275-282.

Pipkin, W., Johnson, J.A., Creazzo, T.L., Burch, J., Komalavilas, P., Brophy, C. (2003) Localization, macromolecular associations, and function of the small heat shock-related protein HSP20 in rat heart. *Circulation* **107**: 469-476.

Pradidarcheep, W., Labruye` re, W. T., Dabhoiwala, N. F., Lamers, W. H. (2008) Lack of specificity of commercially available antisera: better specifications needed. *J Histochem Cytochem.* **56**: 1099-1111.

Qian, J., Ren, X., Wang, X., Zhang, P., Jones, W.K., Molkentin, J.D., Fan, G.C., Kranias, E.G. (2009) Blockade of Hsp20 phosphorylation exacerbates cardiac ischemia/reperfusion injury by suppressed autophagy and increased cell death. *Circ Res.* **105**: 1223-1231.

Rabe, K.F., Bateman, E.D., O'Donnell, D., Witte, S., Bredenbroker, D., Bethke, T.D. (2005) Roflumilast-an oral anti-inflammatory treatment for chronic obstructive pulmonary disease: a randomised controlled trial. *Lancet.* **9485**: 563-571.

Raboy, B., Sharon, G., Parag, H.A., Shochat, Y., Kulka, R.G. (1991) Effect of stress on protein degradation: role of the ubiquitin system. *Acta biologica Hungarica.* **42**: 3-20.

Rakonczay, Z. Jr., Takacs, T., Boros, I., Lonovics, J. (2003) Heat shock proteins and the pancreas. *J Cell Physiol.* **195**: 383-391.

Rembold, C.M., Foster, D.B., Strauss, J.D., Wingard, C.J., Van Eyk, J.E. (2000) cGMP-mediated phosphorylation of heat shock protein 20 may cause smooth muscle relaxation without myosin light chain dephosphorylation in swine carotid artery. *J Physiol*. **52**4: 865-878.

Ren, X.P., Wu, J., Wang, X., Sartor, M.A. , Qian, J., Jones, K., Nicolaou, P., Pritchard, T.J., Fan, G.C. (2009) MicroRNA-320 is involved in the regulation of cardiac ischemiareperfusion injury by targeting heat-shock protein 20. *Circulation* **119**: 2357-2366.

Rennard, S.I., Schachter, N., Strek, M., Rickard, K., Amit, O. (2006) Cilomilast for COPD: results of a 6-month, placebo-controlled study of a potent, selective inhibitor of phosphodiesterase 4. *Chest.* **1**: 56-66.

Rey, O., Sinnett-Smith, J., Zhukova, E., Rozengurt, E. (2001) Regulated nucleocytoplasmic transport of protein kinase D in response to G protein-coupled receptor activation. *J Biol Chem*. **276**: 49228-49235.

Richter, W., Jin, S.L.C., Conti, M. (2005) Splice variants of the cyclic nucleotide phosphodiesterase PDE4D are differentially expressed and regulated in rat tissue. *Biochem J*. **388**: 803-811.

Ritossa, F. (1962) A new puffing pattern induced by temperature shock and DNP in Drosophila. *Experentia* **18**: 571-573.

Rochais, F., Vandecasteele, G., Lefebvre, F., Lugnier, C., Lum, H., Mazet, J. L., Cooper, D.M., Fischmeister, R. (2004) Negative feedback exerted by cAMP-dependent protein kinase and cAMP phosphodiesterase on subsarcolemmal cAMP signals in intact cardiac myocytes: an in vivo study using adenovirus-mediated expression of CNG channels. *J Biol Chem*. **279**: 52095-520105.

Rosenzweig, A. and Seidman, C. E. (1991) Atrial natriuretic factor and related peptide hormones. *Annu Rev Biochem*. **60**: 229-255.

Rossi, G.P., Seccia, T.M., Nussdorfer, G.G. (2001) Reciprocal regulation of endothelin-1 and nitric oxide: relevance in the physiology and pathology of the cardiovascular system. *Int Rev Cytol.* **209**: 241-272.

Rozengurt, E., Rey, O., Waldron, R.T. (2005) Protein kinase D signaling. *J Biol Chem.* **280**: 13205-13208.

Rudiger, S., Buchberger, A., Bukau, B. (1997) Interaction of Hsp70 chaperones with substrates. *Nat Struct Biol.* **4**: 342-349.

Rykx, A., De Kimpe, L., Mikhalap, S., Vantus, T., Seufferlein, T., Vandenheede, J.R., Van Lint, J. (2003) Protein kinase D: a family affair. *FEBS lett.* **546**: 81-86.

Sambrook, J., Fritsh, E.F., Maniatis, T. (1989) Molecular Cloning: A Laboratory Manual, 2nd ed, Vol.1, Cold Spring Harbor Laboratory Press, Cold Spring Harbor.

Satoh, J., Nanri, Y., Yamamura, T. (2006) Rapid identification of 14-3-3-binding proteins by protein microarray analysis. *J Neurosci Methods.* **152**: 278-288.

Satoh, J., Obayashi, S., Misawa, T., Sumiyoshi, K., Oosumi, K., Tabunoki, H. (2009) Protein microarray analysis identifies human cellular prion protein interactors. *Neuropathol Appl Neurobiol.* **35**: 16-35.

Saucerman, J.J., Zhang, J., Martin, J.C., Peng, L.X., Stenbit, A.E., Tsien, R.Y., McCulloch, A.D. (2006) Systems analysis of PKA-mediated phosphorylation gradients in live cardiac myocytes. *Proc Natl Acad Sci. USA* **103:** 12923-12928.

Schlesinger, M. (1986) Heat shock proteins: The search for functions. *J Cell Biol.* **103**: 321-325.

Schnack, C., Hengere, B., Gillardon, F. (2008) Identification of novel substrates for Cdk5 and new targets for Cdk5 inhibitors using high-density protein microarrays. *Proteomics* **8**: 1980-1986.

Schweitzer, B., Predki, P., Snyder, M. (2003) Microarrays to characterize protein interactions on a whole-proteome scale. *Proteomics* **3**: 2190-2199.

Seit-Nebi, A.S. and Gusev, N.B. (2010) Versatility of the small heat shock protein HSPB6 (Hsp20). *Cell Stress Chaperone*s **15**: 233-236.

Skålhegg,B.S. and Taskén,K. (1997) Specificity in the cAMP/PKA signalling pathway. Differential expression, regulation and subcellular localization of subunits of PKA. *Front Biosci.* **2**: D331–D342.

Smith, K.J., Baillie, G.S., Hyde, E.I., Li, X., Houslay, T.M., McCahill, A., Dunlop, A.J., Bolger, G.B., Klussmann, E., Adams, D.R., Houslay, M.D. (2007) 1 H NMR structural and functional characterisation of a cAMP-specific phosphodiesterase-4D5 (PDE4D5) N-terminal region peptide that disrupts PDE4D5 interaction with the signalling scaffold proteins, beta-arrestin and RACK1. *Cell Signal.* **19**: 2612-2624.

Söderberg, O., Leuchowius, K.J., Gullberg, M., Jarvius, M., Weibrecht, I., Larsson, L.G., Landegren, U. (2008) Characterizing proteins and their interactions in cells and tissues using the in situ proximity ligation assay. *Methods* **45**: 227-232.

Solaro, R.J., Rosevear, P., Kobayashi, T. (2008) The unique functions of cardiac troponin I in the control of cardiac muscle contraction and relaxation. *Biochem Biophys Res Commun*. **369**: 82-87.

Stangherlin, A. and Zaccolo, M. (2012) Phosphodiesterases and subcellular compartmentalized cAMP signaling in the cardiovascular system. *Am J Physiol Heart Circ Physiol*. **302**: H379-390.

Storz, P., Döppler, H., Johannes, F-J., Toker, A. (2003) Tyrosine phosphorylation of protein kinase D in the pleckstrin homology domain leads to activation. *J Biol Chem*. **278**: 17969-17976.

Storz, P., Toker, A. (2003) Protein kinase D mediates a stress-induced NFkappaB activation and survival pathway. *EMBO J*. **22**: 109-20.

Sucharov, C.C., Dockstader, K., Nunley, K., Mckinsey, T.A., Bristow, M. (2011) ß-adrenergic receptor stimulation and activation of protein kinase A protect against α_1-adrenergic-mediated phosphorylation of protein kinase D and histone deacetylase 5. *J Card Fail.* **17**: 592-600.

Sugden G. P. (1999) Signaling in myocardial hypertrophy: Life after calcineurin? *Circ Res* **84**: 633-646.

Sumiyoshi, K., Obayshi, S., Tabunoki, H., Arima, K., Satoh, J. (2010) Protein microarray analysis identifies cyclic nucleotide phosphodiesterase as an interactor of Nogo-A. *Neuropathology* **30**: 7–14.

Takimoto, E., Champion, H.C., Li, M., Belardi, D., Ren, S., Rodriquez, E.R., Bedja, D., Gabrielson, K.L., Wang, Y., Kass, D.A. (2005) Chronic inhibition of cyclic GMP phosphodiesterase 5A prevents and reverses cardiac hypertrophy. *Nature Med.* **11**: 214-222.

Tasken, K., and Aandahl, E.M. (2004) Localized effects of cAMP mediated by distinct routes of protein kinase A. *Physiol Rev.* **84**: 137-167.

Taylor, R.P and Benjamin, I.J. (2005) Small heat shock proteins: a new classification scheme in mammals. *J Mol Cell Cardiol.* **38**: 433-444.

Tennagels, N., Hube-Magg, C., Wirth, A., Noelle, V., Klein, H.W. (1999) Expression, purification, and characterization of the cytoplasmic domain of the human IGF-1 receptor using a baculovirus expression system. *Biochem Biophys Res Commun.* **260**: 724-728.

Terrin, A., Di Benedetto, G., Pertegato, V., Cheung, Y.F., Baillie, G., Lynch, M.J., Elvassore, N., Prinz, A., Herberg, F.W., Houslay, M.D., Zaccolo, M. (2006) PGE1 stimulation of HEK293 cells generates multiple contiguous domains with different [cAMP]: role of compartmentalized phosphodiesterases. *J Cell Biol*. **175**: 441-451.

Tessier, D.J., Komalavilas, P., Panitch, A., Joshi, L., Brophy, C.M. (2003) The small heat shock protein (HSP) 20 is dynamically associated with the actin cross-linking protein actinin. *J Surg Res*. **111**: 152-157.

Tessier, D.J., Komalavilas, P., McLemore, E., Thresher, J., Brophy, C.M. (2004b) Sildenafil-induced vasorelaxation is associated with increases in the phosphorylation of the heat shock related protein 20 (HSP20). *J Surg Res*. **118**: 21-25

Tevaearai, H.T., Koch, W.J. (2004) Molecular restoration of beta-adrenergic receptor signaling improves contractile function of failing hearts. *Trends Cardiovasc Med*. **14**: 252-256.

Thompson, W.J., Ashikaga, T., Kelly, J.J., Liu, L., Zhu, B., Vemavarapu, L., Strada, S.J. (2002) Regulation of cyclic AMP in rat pulmonary microvascular endothelial cells by rolipram-sensitive cyclic AMP phosphodiesterase (PDE4). *Biochem Pharmacol*. **63**: 797-807.

Tissieres, A., Mitchell, H.K., Tracy, U.M. (1974) Protein synthesis in salivary glands of Drosophila melanogaster: Relation to chromosome puffs. *J Mol Biol*. **85**: 389-398.

Uetz, P., Giot, L., Cagney, G., Mansfield, T.A., Judson, R.S., Knight, J.R., Lockshon, D., Narayan, V., Srinivasan, M., Pochart, P., Qureshi-Emili, A., Li, Y., Godwin, B., Conover, D., Kalbfleisch, T., Vijayadamodar, G., Yang, M., Johnston, M., Fields S, Rothberg, J.M. (2000) A comprehensive analysis of protein-protein interactions in Saccharomyces cerevisias. *Nature* **403**: 623-627.

Valverde, A.M., Sinnett-Smith, J., Van Lint, J., Rozengurt, E. (1994) Molecular cloning and characterization of protein kinase D: a target for diacylglycerol and phorbol esters with a distinctive catalytic domain. *Proc. Natl. Acad. Sci. USA* **91**: 8572-8576.

Van de Klundert, F. A., Smulders, R.H., Gijsen, M.L., Lindner R.A., Jaenicke, R., Carver, J.A., de Jong W.W. (1998) The mammalian small heat-shock protein Hsp20 forms dimers and is a poor chaperone. *Eur J Biochem*. **258**: 1014-1021.

Van de Klundert, F.A. and de Jong, W.W. (1999) The small heat shock proteins Hsp20 and alphaB-crystallin in cultured cardiac myocytes: differences in cellular localization and solubilization after heat stress. *Eur J Cell Biol*. **78**: 567-572.

Van Lint, J., Sinnett-Smith, J., Rozengurt, E. (1995) Expression and characterization of PKD, a phorbol ester and diacylglycerol-stimulated serine protein kinase. *J Biol Chem*. **270**: 1455-1461.

Van Lint, J., Rykx, A., Maeda, Y., Vantus, T., Sturany, S., Malhotra, V., Vandenheede, J.R., Seufferlein, T. (2002) Protein kinase D: an intracellular traffic regulator on the move. *Trends Cell Biol.* **12**: 193-200.

Vega, R.B., Harrison, B.C., Meadows, E., Roberts, C.R., Papst, P.J., Olson, E.N., McKinsey, T.A. (2004) Protein kinase C and D mediate agonist-dependent cardiac hypertrophy through nuclear export of histone deacetylase 5. *Mol Cell Biol*. **24**: 8374-8385.

Vertommen, D., Rider, M., Ni, Y., Waelkens, E., Merlevede, W., Vandenheede, J. R., Van Lint, J. (2000) Regulation of protein kinase D by multisite phosphorylation. Identification of phosphorylation sites by mass spectrometry and characterization by site-directed mutagenesis. *J Biol Chem.* **275:** 19567-19576.

Vidalain, P.O., Boxem, M., Ge, H., Li, S., Vidal, M. (2004) Increasing specificity in high-throughput yeast two-hybrid experiments. *Methods* **32**: 363-370.

Visick, J.E. and Clarke, S. (1995) Repair, refold, recycle: how bacteria can deal with spontaneous and environmental damage to proteins. *Mol Microbiol*. **16**: 835-845.

Vistejnova, L., Dvorakova, J., Hasova, M., Muthny, T., Velebny, V., Soucek, K., Kubala, L. (2009) The comparison of impedance-based method of cell proliferation monitoring with commonly usedmetabolic-based techniques. *Neuro Endocrinol Lett*. **30**: 121-127.

Waldron, R.T., Rey, O., Iglesias, T., Tugal, T., Cantrell, D., Rozengurt, E. (2001) Activation loop Ser744 and Ser748 in protein kinase D are transphosphorylated in vivo. *J Biol Chem*. **276**: 32606-32615.

Waldron, R.T. and Rozengurt, E. (2003) Protein kinase C phosphorylates protein kinase D activation loop Ser744 and Ser748 and releases autoinhibition by the pleckstrin homology domain. *J Biol Chem*. **278**: 154-163.

Wang, Y., Su, B., Sah, V.P., Brown, J.H., Han, J., Chien, K.R. (1998) Cardiac hypertrophy induced by mitogen-activated protein kinase kinase 7, a specific activator for c-Jun NH2-terminal kinase in ventricular muscle cells. *J Biol Chem*. **273**: 5423-5426.

Wang, Y., Xu, A., Pearson, R.B., Cooper, G.J. (1999) Insulin and insulin antagonists evoke phosphorylation of P20 at serine 157 and serine 16 respectively in rat skeletal muscle. *FEBS Lett*. **462**: 25-30.

Wang, K. and Spector, A. (2001) ATP causes small heat shock proteins to release denatured protein. *Eur J Biochem.* **268**: 6335-6345.

Wang, H., Peng, M.S., Chen, Y., Geng, J., Robinson, H., Houslay, M.D., Cai, J., Ke, H. (2007) Structures of the four subfamilies of phosphodiesterase-4 provide insight into the selectivity of their inhibitors. *Biochem J*. **408**: 193-201.

Wang, X, Zingarelli, B., O'Connor, M., Zhang, P., Adeyemo, A., Kranias, E.G., Wang, Y., Fan, G.C. (2009) Overexpression of Hsp20 prevents endotoxin-induced myocardial dysfunction and apoptosis via inhibition of NF-κB activation. *J Mol Cell Cardiol*. **47**: 382-390.

Wheeler-Jones, C.P.D. (2005) Cell signalling in the cardiovascular system: an overview. *Heart* **91**: 1366-1374.

Woodrum, D.A., Brophy, C.M., Wingard, C.J., Beall, A., Rasmussen, H. (1999) Phosphorylation events associated with cyclic nucleotide-dependent inhibition of smooth muscle contraction. *Am J Physiol*. **277**: H931-H939.

Xiang, Y., Naro, F., Zoudilova, M., Catherine Jin, S-L., Conti, M., Kobilka, B. (2005) Phosphodiesterase 4D is required for β_2 adrenoceptor subtype-specific signaling in cardiac myocytes. *Proc Natl Acad Sci USA*. **102**: 909-914.

Xiao, R.P., Zhu, W., Zheng, M., Cao, C., Zhang, Y., Lakatta, E.G., Han, Q. (2006) Subtype-specific α_1- and β-adrenoceptor signaling in the heart. *Trends Pharmacol Sci* **27**: 330-337.

Xue, Y., Ren, J., Gao, X.J., Jin, C.J., Wen, L.P., Yao, X.B. (2008) GPS 2.0, a Tool to Predict Kinase-specific Phosphorylation Sites in Hierarchy *Mol Cell Proteomics*. **7**: 1598-1608.

Yamamori, T., Ito, K., Nakamura, Y., Yura, T. (1978) Transient regulation of protein synthesis in Escherichia coli upon shift-up of growth temperature. *J Bacteriol*. **134**: 1133-1140.

Yamashita, N., Nishida, M., Hoshida, S., Kuzuya, T., Hori, M., Taniguchi, N., Kamada, T., Tada, M. (1994) Induction of manganese superoxide dismutase in rat cardiac myocytes increases tolerance to hypoxia 24 hours after preconditioning. *J Clin Invest.* **94:** 2193-2199.

Yarden, Y. and Ullrich, A. (1988) Growth factor receptor tyrosine kinases. *Annu Rev Biochem.* **57**: 443-478.

Yu, N., Atienza, J.M., Bernard, J., Blanc, S., Zhu, J., Wang, X., Xu, X., Abassi, Y.A. (2006) Real-time monitoring of morphological changes in living cells by electronic cell sensor arrays: an approach to study G protein-coupled receptors. *Anal Chem.* **78**: 35-43.

Yuan, Z., Becker, E.B., Merlo, P., Yamada, T., DiBacco, S., Konishi, Y., Schaefer, E.M., Bonni, A. (2008) Activation of FOXO1 by Cdk1 in cycling cells and postmitotic neurons. *Science* **319**: 1665-1668.

Zaccolo, M. and Pozzan, T. (2002) Discrete microdomains with high concentration of cAMP in stimulated rat neonatal cardiac myocytes. *Science* **295**: 1711-1715.

Zaugg, M., Xu, W., Lucchinetti, E., Shafiq, S.A., Jamali, N.Z., Siddiqui, M.A. (2000) Beta-adrenergic receptor subtypes differentially affect apoptosis in adult rat ventricular myocytes. *Circulation* **102**: 344-350.

Zhang, C.L., McKinsey, T.A., Chang, S., Antos, C.L., Hill, J.A., Olson, E.N. (2002) Class II histone deacetylases act as signal-responsive repressors of cardiac hypertrophy. *Cell* **110**: 479-488.

Zhu, Y.H., Ma, T.M., Wang, X. (2005) Gene transfer of heat-shock protein 20 protects against ischemia/reperfusion injury in rat hearts. *Acta Pharmacol Sin*. **26**: 1193-1200.

Zhu, H., Wang, X., Zhang, X., Kranias, E.G., Liang, Q., Fan, G.C. (2011) Hsp20 promotes cardiac autophagy via interaction with Beclin-1. *Circ Res.* **109**: AP046.

Zugaza, J.L., Sinnett-Smith, J., Rozengurt, E. (1996) Protein kinase D (PKD) activation in intact cells through a protein kinase C-dependent signal transduction pathway. *EMBO J.* **15:** 6220-6230.